CHARACTERIZATION, MECHANISM AND KINETICS OF PHASE – SEPARATION OF MIXED LANGMUIR – BLODGETT FILMS

A Thesis Submitted to the College of
Graduate Studies and Research
In Partial Fulfillment of the Requirements
For the Degree of Doctor of Philosophy
In the Department of Chemistry
University of Saskatchewan
Saskatoon

By

SHATHA EID QAQISH

PERMISSION TO USE

In presenting this thesis in partial fulfilment of the requirements for a Postgraduate degree from the University of Saskatchewan, I agree that the Libraries of this University may make it freely available for inspection. I further agree that permission for copying of this thesis in any manner, in whole or in part, for scholarly purposes may be granted by the professor or professors who supervised my thesis work or, in their absence, by the Head of the Department or the Dean of the College in which my thesis work was done. It is understood that any copying or publication or use of this thesis or parts thereof for financial gain shall not be allowed without my written permission. It is also understood that due recognition shall be given to me and to the University of Saskatchewan in any scholarly use which may be made of any material in my thesis.

Requests for permission to copy or to make other use of material in this thesis in whole or part should be addressed to:

Head of the Department of Chemistry

University of Saskatchewan

110 Science Place

Saskatoon, Saskatchewan (S7N 5C9)

ABSTRACT

The phase – separation of mixed Langmuir-Blodgett (LB) monolayers was investigated using a combination of atomic force microscopy (AFM), X-ray photoelectron emission microscopy (X-PEEM) and confocal fluorescent microscopy measurements. Shapes of phase-separated domains that formed on solid substrate surfaces depended on a competition between line tension and dipole-dipole interactions. In the mixed LB film of arachidic acid ($C_{19}H_{39}COOH$) (C20) and perfluorotetradecanoic acid ($C_{13}F_{27}COOH$) (F14), the components phase – separated into elevated hexagonal domains of C20 surrounded by a continuous domain primarily consisting of F14. The underlying molecular arrangement of C20 was found to be an oblique packing. The domains in this system grew via Ostwald ripening and the kinetics of their growth was modeled by two–dimensional Lifshitz–Slyozov equation. In the stearic acid ($C_{17}H_{35}COOH$) (C18) and F14 mixed films, the C18 domains formed a linear pattern where the F14 molecules filled the areas in between the lines occupied by C18. For the mixed film of palmitic acid ($C_{15}H_{31}COOH$) (C16) and perfluorooctadecanoic acid ($C_{17}F_{35}COOH$) (F18), the surfactants phase–separated into elevated hexagonal domains with hairy extensions radiating from them. These domains were composed of F18 and surrounded by C16. Ostwald ripening was found to be the mechanism of domain growth. Phase – separation was controlled by different forces such as line tension and dipole interactions, as well as the diffusion of the molecules, solubility of the surfactant in the sub-phase, temperature and surface pressure. Simple mechanisms regarding phase –separation and pattern formation were discussed in these mixed systems. It was observed that all fatty acid / F14 systems in this study were immiscible at all

molar fractions examined. The fatty acid / F18 systems were immiscible at short chains of fatty acids (myristic acid ($C_{13}H_{27}COOH$) C14, C16, C18), whereas at longer fatty acid chains (C20, C22 behenic acid ($C_{21}H_{43}COOH$)) the components of the mixed system became miscible. When perfluorocarboxylic acid chain combined with fatty acids, the domains changed from large hexagonal domains into narrow lines as the fatty acid chain decreased in length.

ACKNOWLEDGEMENTS

I would like to express my gratitude to all whose guidance and advice allowed me to grow, and without whom this work would have never been possible. I had the good fortune of working under the supervision of Dr. Matthew F. Paige, whose guidance, patience and advice were invaluable throughout my studies. I will always consider the learning experience provided by Dr. Paige as an asset to my future career.

I would also like to thank my committee members, Dr. A. Baranski, Dr. R. W. J. Scott, Dr. Y. Pan, Dr. B. H. Kraatz, and Dr. M. McDermott for their constructive discussions, genuine advice, and imparted experience. I am grateful to Dr. S. G. Urquhart for all his effort in measuring and analyzing X-PEEM data, and Dr. S. Brunet for confocal fluorescent microscopy measurements. I would like to acknowledge the Department of Chemistry and the Hertzberg Fund for financial support.

Without the support of my friends and colleagues, obstacles would never have been overcome. I would like to thank all the wonderful members of Dr. Paige's group; Jahangir Valiani, Jaclyn O'Brien, Stephen Christensen, Yin Lu, Sunish Sugnan, Terri Thunder, Adam Leontowich, Zahid Islam and Sangram Bagh. Jimena Larraguivel Espejo and Lana Nelson deserve much credit for their wonderful and supportive friendship that I will never forget.

I am most grateful to my parents for all the sacrifice, and the support that they have provided me. I would also like to thank my brother, Ma'en, my sister, Dimah, and my nieces and nephew: Nour, Diana and Muheeb for all their encouragement throughout the hard times.

To my parents, Eid and Ra’eda, with love.

TABLE OF CONTENTS

LIST OF TABLES

LIST OF FIGURES

LIST OF ABBREVIATIONS

AA: Arachidic acid, $C_{19}H_{39}COOH$

AFM: Atomic Force Microscopy

BAM: Brewster Angle Microscopy

CFM: Chemical Force Microscopy

C22: Behenic acid, $C_{21}H_{43}COOH$

C20: Arachidic acid, $C_{19}H_{39}COOH$

C18: Stearic acid, $C_{17}H_{35}COOH$

C16: Palmitic acid, $C_{15}H_{31}COOH$

C14: Myristic acid, $C_{13}H_{27}COOH$

F14: Perfluorotetradecanoic acid, $C_{13}F_{27}COOH$

F18: Perfluorooctadecanoic acid, $C_{17}F_{35}COOH$

IR: Infra-Red

LB: Langmuir-Blodgett

LS Equation: Lifshitz-Slyozov Equation

LFM: Lateral Force Microscopy

NEXAFS: Near Edge X-Ray Absorption Fine Structure

PA: Perfluorotetradecanoic acid, $C_{13}F_{27}COOH$

SA: Stearic acid, $C_{17}H_{35}COOH$

STM: Scanning Tunneling Microscopy

THF: Tetrahydrofuran

X-PEEM: X-Ray Photoelectron Emission Microscopy

XPS: X-Ray Photoabsorption spectroscopy

2D: Two-dimensional

3D: Three-dimensional

CHAPTER 1
INTRODUCTION

"Today … I propose to tell you of a real two-dimensional world in which phenomena occur that are analogous to those described in 'Flatland'. I plan to tell you about the behavior of molecules and atoms that are held at the surface of solids and liquids."[1, 2]

Irving Langmuir, *Science* **1936**,84,379

1.1 The gas-liquid interface

Surface active agents (surfactants) are molecules that possess a hydrophobic "tail" region and a hydrophilic "head" region. They reduce the surface tension of water when used in low concentrations. At the air / water interface, surfactants can orient themselves such that their polar heads are on the water surface whereas their hydrophobic tail is pointed away from the water surface. Dipole-dipole interactions between the water molecules and the head group of the surfactants are responsible for keeping the hydrophilic head immersed in water. However because of the strong hydrogen bonding between the water molecules and the strong hydrophobic interactions between the hydrocarbon chains, the hydrocarbon tail is forced away from the water. Under suitable conditions, surfactant molecules can align themselves at the air / water interface forming a layer that is one molecule thick. This layer is often called a monomolecular layer or a monolayer[3].

To study the stability of the molecules in the monolayer, dynamic molecular motion is applied. Dynamic molecular motion is the microscopic model of an interface where molecules diffuse in and out of it[4]. At equilibrium, the number of molecules diffusing from the surface into

the bulk of the liquid per unit time should equal the number of molecules moving from the bulk to the surface. The molecules on the surface are surrounded by less number of adjacent molecules compared to those in the bulk. This results in an initial diffusion of the molecules from the surface into the bulk, and a difficult movement of the molecules from the bulk to the surface since the latter increases the internal energy. The energy per molecule in the bulk $E_{A,\,bulk}$ is given by equation (1-1):

$$E_{A,bulk} = \frac{z_b}{2} W_{AA} \qquad (1\text{-}1)$$

where z_b is the number of the nearest-neighbor molecules in the bulk phase, and W_{AA} is the pair energy of interaction of a molecule in the bulk which represents the work of adhesion. The energy per molecule on the surface is given by equation (1-2) where z_s represents the number of neighboring molecules for the surface molecule[5].

$$E_{A,S} = \frac{z_s}{2} W_{AA} \qquad (1\text{-}2)$$

Since $z_b > z_s$ as discussed previously, the process of bringing the molecule to the surface is energetically costly and work should be done. The energy required to create the new surface, which results from the unbalanced intermolecular interactions between molecules in the surface and those in the bulk, is called the surface tension γ[6].

Since the surface tension is defined in terms of the work (W) needed to create a surface (ΔA), it can be written as follows:

$$\gamma = \frac{W}{\Delta A} \qquad (1\text{-}3)$$

However, the surface tension can also be considered as a force (F) acting on a unit length (l). Figure 1-1 represents a schematic diagram of the forces acting on a thin liquid film. If the film is

at rest, the downward force (F) that acts to increase the length of the film is balanced by the opposite force that shrinks the film (the surface tension, γ), generating equation (1-4)[5].

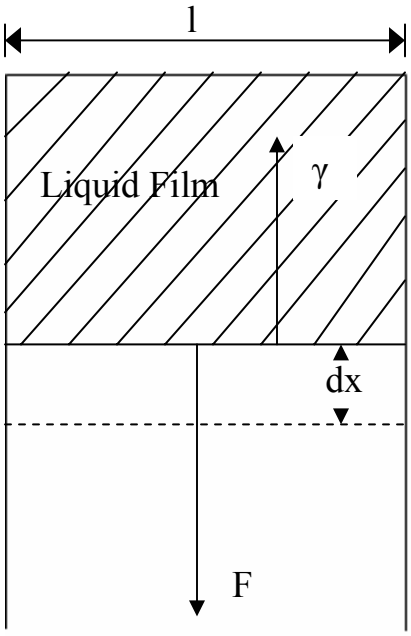

Figure 1-1. A sketch that shows a liquid film stretched by an applied force[5].

$$\gamma = \frac{F}{2l} \qquad (1\text{-}4)$$

The length is multiplied by 2 as the film (surface) has two sides.

At thermodynamic equilibrium for a plane interface, equation (1-5) is applicable[7]:

$$dG = VdP - SdT + \sum_i \mu_i dn_i + \gamma dA \qquad (1\text{-}5)$$

where G is the free energy, V is the volume, P is the pressure, S is the entropy, T is temperature, μ is the chemical potential and n is the number of moles. The surface tension in equation (1-6) is the partial derivative of the Gibbs free energy of the system for a plane interface at constant temperature, pressure and composition:

$$\gamma = \left(\frac{\partial G}{\partial A}\right)_{T,P,n_i} \qquad (1\text{-}6)$$

In monolayer studies, surface tension is one of the main measurable parameters that can provide insight into the structure and the composition of the film. When surface tension is measured as a function of the area occupied by the molecule on the surface, important information can be revealed including the miscibility and the degree of interactions between components of the films. Rather than surface tension alone, it is customary to measure the surface pressure, $\prod$, of the liquid-air interface. Surface pressure is defined as the difference between the surface tension of pure liquid (γ_0) and that of the liquid when the monolayer is added (γ) as follows:

$$\Pi = \gamma_0 - \gamma \qquad (1\text{-}7)$$

1.2 Phase transformation of a monolayer

Phases of monolayers are similar to those of the bulk. As the monolayer is compressed on the air / water interface, the molecules move closer to each other. They begin to interact and can undergo phase transitions. The mean molecular area (A), defined as the area occupied by a single molecule of surfactant on the surface, decreases and the surface pressure increases upon compression. This generates a surface pressure – area isotherm. The mean molecular area is given by equation (1-8):

$$A = \frac{A_{tot} M}{C N_A V} = \frac{A_{tot}}{c N_A V} \qquad (1\text{-}8)$$

where A_{tot} is the overall film area in cm^2, M is the molar mass of the surfactant in g/mol, C is the concentration of the surfactant solution in mg/mL, c is the concentration in mol/L, N_A is Avogadro's number and V is the volume of the solution spread in the monolayer. Surface pressure - area isotherms are important measurements that provide useful information about

monolayers. They give insight into the stability of the monolayer at the air / liquid interface, phase transition, conformational transformation and reorientation of the molecules[2].

When surfactant molecules are spread on the air-water interface, they exhibit low surface pressure. The molecules are far apart from each other and they move freely. Low intermolecular interactions exist between them, and they lie nearly flat on the sub-phase. This is called the gas phase as shown in Figure 1-2G. This phase is characterized by a surface pressure that approaches zero asymptotically when the mean molecular area increases[6]. The molecules in this phase obey a thermodynamic equation of state in two-dimensions (2D) (equation 1-9)[2, 4]. By assuming that the molecules have an average translational kinetic energy of ½ kT for each degree of freedom, the 2D total kinetic energy will be kT, where k is Boltzmann constant and T is temperature. This yields the following equation:

$$\Pi A = kT \qquad (1\text{-}9)$$

Upon compression, the surfactant molecules move closer to each other. Each molecule occupies a smaller mean molecular area compared to the gas phase. The interactions between molecules increase as the surface pressure increases. This represents the liquid expanded phase (Figure 1-2E). The hydrocarbon chains of the molecules in the film are in a less random orientation and are pointing away from the water sub-phase. The mean molecular area is two to three times larger than the cross section of the single chain[6]. Unsaturated fatty acid chains favor the liquid expanded phase. This is related to the repulsion in the electronic clouds of the double bonds upon further compression[6]. Theoretical models were developed for the 2D transition similar to that for the gaseous phase. Langmuir assumed that the upper surface of the film behaves as a bulk liquid and that the interactions between the head group could be represented by

an ideal gas law[8]. Equation (1-10) is generated by taking into account the correction for finite molecular size[8].

$$(\Pi - \Pi_0)(A - A_0) - kT \qquad (1\text{-}10)$$

where A_0 is the correction of the area for the finite size polar group, and $\prod_0$ corresponds to the spreading coefficient for the hydrocarbon part on water and is given as follows:

$$\Pi_0 = \gamma_{water} - \gamma_{oil} - \gamma_{water-oil} \qquad (1\text{-}11)$$

where γ_{water} and γ_{oil} are the surface tensions of liquid water and oil, respectively, whereas $\gamma_{water\text{-}oil}$ is the interfacial tension between the two liquids. Van der Waals' forces between the hydrocarbon chains are assumed to be responsible for the transition in fatty acids[4].

Further compression causes the molecules to arrange themselves with parallel hydrocarbon chains pointing away from the interface (Figure 1-2C). The molecules are closely packed because of the strong hydrophobic interactions between the chains. This phase is called the liquid condensed phase. Measurements revealed that the molecules are primarily aligned perpendicular to the surface. The area occupied by the molecule in this region is called the molecular footprint and is equivalent to the horizontal cross section of a cylindrical hydrocarbon chain. The molecular footprint for fatty acids at room temperature is ~ 20 $Å^2$. $molecule^{-1}$ [9].

It was observed that the mean molecular area slightly increases as the length of the hydrocarbon chain decreases, which is attributed to the shorter chain-length compounds' tendency to form expanded monolayers[4, 10]. This results from the lower hydrophobic (van der Waals') interactions between the chains producing a less condensed phase. A decrease in temperature has the opposite effect to a decrease in chain length. The former decreases the mobility of the molecules leading to a condensed film. In general, an increase in temperature by 5 – 10 K is equivalent to a decrease in the length of the hydrocarbon chain of a fatty acid by one methyl group[4].

Because of the differences in behavior between monolayers of different compounds, a number of surface states or phases were introduced by authors to explain these monolayers under the general category of condensed phase. The term 'solid phase' corresponds to a highly incompressible, closely packed film[11]. Liquid condensed or mesomorphous[11] refers to the most compressible, lower pressure condensed phase. Super liquid is associated with abnormal surface viscosity which leads to less pronounced surface pressure increase as the compressibility increases[12]. At temperatures below 10 ºC, fatty acids have a compact phase called the close-packed solid[13].

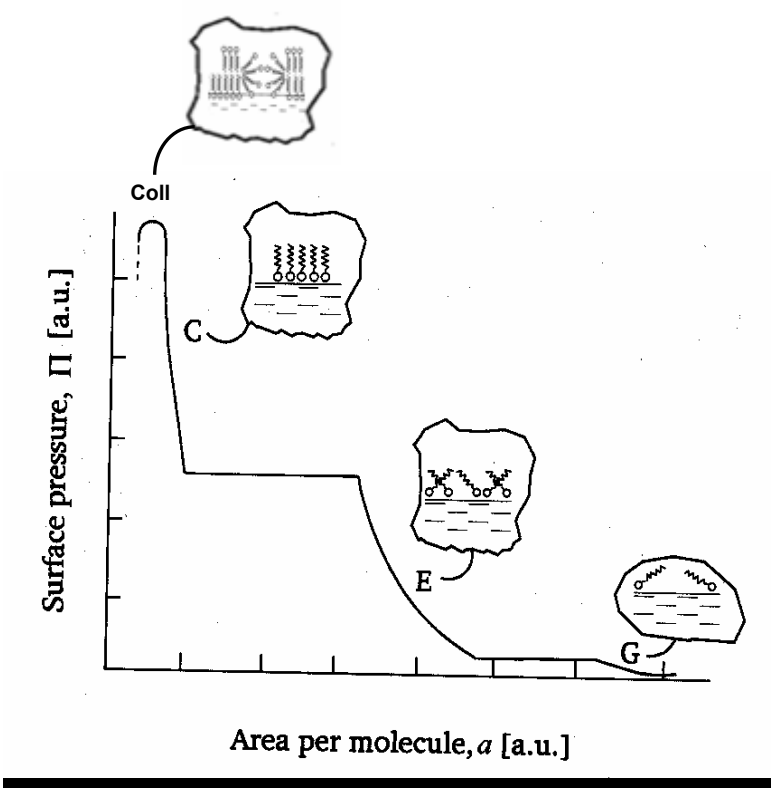

Figure 1-2. Surface pressure – area isotherm of a monolayer showing the different phases. G: gaseous; E: Liquid expanded; C: liquid condensed; Coll: collapse[4]. Reprinted by permission of Cambridge University Press, (Langmuir-Blodgett Films An Introduction, Michael C. Petty), (copyright 1996).

The different regions (phases) in the isotherm are associated with a change in enthalpy of the monolayer[4]. Surface pressure continues to increase as the mean molecular area decreases upon film compression, until reaching a collapse pressure (Figure 1-2). The collapse pressure is observed when the decrease in the area is followed by a sharp decrease in the surface pressure.

At the collapse pressure, the mechanical instability of the film[2] is related to the formation of a second layer, micelles or vesicles as shown in Figure (1-3). If the head group interactions are strong enough and the concentration is above the critical micelle concentration, micelles form. Vesicles form if the hydrophobic interactions of the chains are stronger than the head group interactions as in phospholipids. At the collapse pressure, molecules are lost in the bulk of the sub-phase[4]. The collapse pressure is a function of numerous variables including temperature, pH of the sub-phase, the speed of film compression and the material of the monolayer[2].

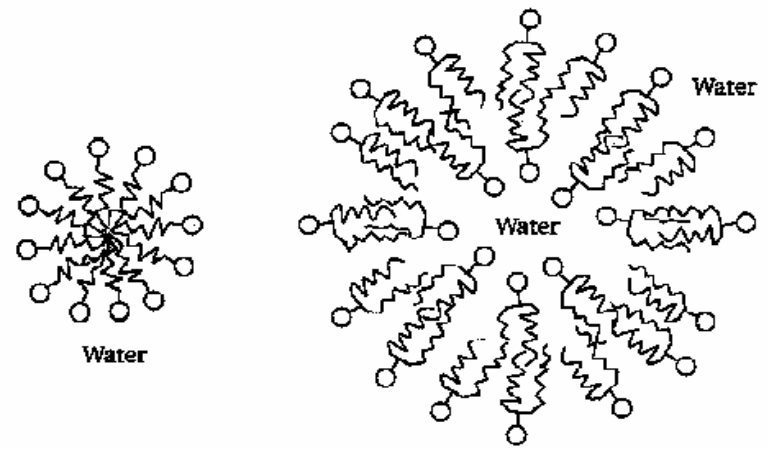

Figure 1-3. Left, a sketch of a micelle; right, sketch of a vesicle made of surfactants[4]. Reprinted by permission of Cambridge University Press, (Langmuir-Blodgett Films An Introduction, Michael C. Petty), (copyright 1996).

1.3 Miscibility and mixing in multi-component monolayer

1.3.1 Free energy of mixing

The thermodynamic stability of a mixed monolayer can be estimated using the excess free energy of mixing. For a film of two components that are immiscible, the excess free energy (ΔG^{ex}) at a specific surface pressure is given as follows:

$$\Delta G^{ex} = G_{12} - \chi_1 G_1 - \chi_2 G_2 \qquad (1\text{-}12)$$

where G_{12} is the Gibbs free energy of the system containing the mixed monolayer, χ_1 and χ_2 are the molar fractions of component 1 and 2 in the mixed monolayer, respectively, and G_1 and G_2 are the free energy of the pure monolayer containing one component. The excess free energy of mixing equals the difference between the energy of mixing of the mixed monolayer and that of the same system containing two pure films separately. Gibbs free energy as a function of surface pressure can be rewritten from equation (1-6) as follows:

$$dG = -Ad\Pi \qquad (1\text{-}13)$$

The excess free energy of mixing can be written as in the following equation:

$$\Delta G^{ex} = \int_0^{\pi} [A_{12} - (\chi_1 A_1 + \chi_2 A_2)] d\Pi \qquad (1\text{-}14)$$

This means that the excess free energy of mixing can be found experimentally by integrating the area of the surface pressure – area isotherm of the mixtures at each molar fraction up to the desired surface pressure. This value is compared to the integrated values of the isotherms of the pure components at the same surface pressure multiplied by the corresponding molar ratio[6]. These equations were first derived by Goodrich[14]. A negative value of the free energy of mixing indicates that the mixed film has greater thermodynamic stability than the pure component films

and shows some type of attraction within the film components. A positive free energy of mixing indicates that the components in the monolayer repel each other and are immiscible.

In general, ΔG^{ex} depends on the sub-phase and it might change by changing the sub-phase composition, such as by adding salt to the water sub-phase[6]. ΔG^{ex} is lower in the presence of cations in the sub-phase compared to pure water. It depends also on the charge of the cation. A high cation charge leads to a lower value of ΔG^{ex} and more thermodynamic stability of the film[15]. For the interactions of phospholipids and fatty alcohols in a monolayer, it was observed that ΔG^{ex} is negative at low molar fractions of fatty alcohols, and positive at higher molar fractions of the alcohols[15].

From the free energy of mixing, the interaction parameter (α) can be calculated as in equation (1-15)[16]:

$$\alpha = \frac{\Delta G^{ex}}{RT(\chi_1 \chi_2^2 + \chi_2 \chi_1^2)} \qquad (1\text{-}15)$$

The negative value of α represents strong interactions between different types of molecules in the mixed monolayer. The positive value of α suggests that the interactions between the different types of molecules are repulsive or less attractive than between the same type of molecules[16].

It was observed that the interaction parameter α for partially fluorinated alkyl chains and fatty alcohols is negative. This indicates a strong interaction between the components. Upon reaching a specific molar ratio, α is independent on the concentration and its value is close to zero. This means that the interactions between the different types of molecules are of similar strength to those between the same types of molecules. However when the fatty alcohol was replaced by partially fluorinated fatty alcohol, the interactions between the unlike molecules are unfavorable and the components are immiscible[16].

1.3.2 Ideal mixing

In an ideal mixture, the enthalpy of mixing is zero and the chemical interactions between the two components are equal. The adhesive forces between the same type of molecules are equal to the cohesive forces between different types of molecules. Regardless of the type of neighboring molecules, the interactions are similar. This is applicable to the miscible components in the film which are ideally mixed[17]. If the cohesive forces are repulsive, the components phase-separate and the monolayer is considered as two separate films in equilibrium with each other[6]. In this case, the components are immiscible and the system follows the additivity rule. For a two-component system that is ideally mixed, a variation of Raoult's law or the additivity rule (equation 1-16) applies.

$$A_{12} = \chi_1 A_1 + \chi_2 A_2 \qquad (1\text{-}16)$$

A_{12} is the area per molecule in the mixed monolayer, χ_1 and χ_2 are the molar fractions of component 1 and 2, respectively in the mixed film, A_1 and A_2 is the mean molecular area of component 1 and 2, respectively in their pure films.

To check if a system follows the additivity rule, the above equation is used and the data are analyzed at a constant surface pressure. If the experimental trend derived from the surface pressure – area isotherm experiments and the theoretical ideal behavior are consistent, the additivity rule applies to the system. This indicates that the components of the films are either ideally mixed or completely immiscible[18]. In other words, the area occupied by the components in the mixed film is the sum of the areas occupied by the separate components in their pure films[6]. To confirm whether the components of the monolayer are completely immiscible or ideally mixed, further measurements should be performed such as Brewster angle microscopy or atomic force microscopy.

Any deviation from the additivity rule indicates the presence of different interactions between the two components. The cohesive interactions can be repulsive, resulting in positive deviation in the additivity rule. In this case, an expansion in the monolayer and a larger mean molecular area, compared to what is expected in the ideal mixture, are observed. These repulsive interactions could be attributed to the tilt in chains or to the difference in height between the adjacent molecules, resulting in fewer interactions. When the cohesive interactions are attractive such as more hydrophobic interactions between the different chains, a negative deviation occurs and the molecules occupy smaller mean molecular area than expected[19].

1.3.3 Two-dimensional phase rule

Surface pressure – area isotherms can reveal the miscibility in mixed monolayers and directly represent phase diagrams. Other phase diagrams can be generated from the surface pressure - area isotherm measurements when performed at different temperatures. By plotting the surface pressure at which the transition between phases occurs as a function of temperature, a 2D phase diagram can be constructed. The information derived from the phase diagram can be used to select the deposition conditions of the film on solid substrates. For example if the deposition conditions were set close to the phase boundary, minor fluctuations in the temperature or surface pressure might cause a transition from one phase to another affecting the characteristics of the film deposited[4].

Other types of phase diagrams can be generated from the isotherms by plotting the transition pressure as a function of molar fraction. This type of phase diagram reveals the miscibility of the components in the case of mixed films. Depending on the regions of the phase diagram, the number of phases and the miscibility of the mixed monolayer are revealed[10, 20].

To better understand the phase diagrams, a surface phase rule, analogous to Gibbs' three dimensional (3D) phase rule, can be derived for a 2D system. At constant temperature, surface tension and varied external pressure, equation (1-17) is applied[6]:

$$F = (C^b + C^s) - (P^b + P^s) + 3 \qquad (1\text{-}17)$$

where F is the number of degrees of freedom, C^b and C^s are the number of components in the bulk and on the surface, respectively, P^b is the number of phases in the bulk, P^s is the number of surface phases in equilibrium with each other.

For a single component monolayer at the interface between a pure liquid and a pure gas, $C^b = 2$ referring to the liquid and the gas, $C^s = 1$ referring to a single component layer, $P^b = 2$ referring to a gas phase and liquid phase, and $P^s = 1$ referring to one phase of the monolayer. This means that there are three degrees of freedom; the temperature, the external pressure and the surface pressure should vary as a function of mean molecular area.

For a monolayer of two components that are miscible, $C^b = 2$, $C^s = 2$, $P^b = 2$ and $P^s = 1$. This means that there are four degrees of freedom: temperature, pressure, surface pressure and the composition of the mixed film. This indicates that by changing the composition of the film, the phase of the monolayer does not change. If the two components are immiscible, $P^s = 2$, and the degrees of freedom will be three. In this case the composition of the film should be constant in terms of the molar fractions of the components. Any change in this term will change the phase of the monolayer[6].

If the two-component monolayer is compressed until it collapses, an additional bulk phase is added, so the number of phases in the bulk increases to three. If the components are miscible in the monolayer then there is one surface phase and three degrees of freedom; temperature, pressure, and surface pressure should vary with the film composition (Figure 1-6).

This surface pressure represents the surface pressure at which the monolayer is in equilibrium with the bulk (collapse pressure or equilibrium spreading pressure). However, if the components are immiscible in the monolayer, then the number of surface phases is two and the number of degrees of freedom is two; temperature and pressure. The surface pressure does not depend on the monolayer composition and should be constant (Figure 1-4). In this case, the less stable component with the lower equilibrium spreading pressure should escape from the monolayer into the bulk at the same collapse pressure regardless to the film composition[4, 6]. As shown in Figure 1-4, when the components of the monolayer are immiscible, each component retains its collapse pressure constant regardless to the molar fraction. However if the components are miscible, the collapse pressure changes as a function of the molar fraction.

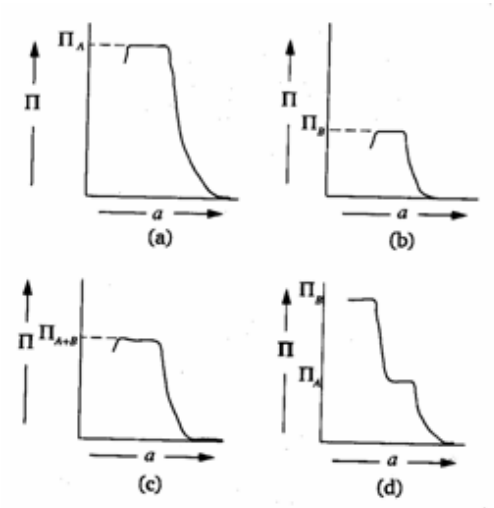

Figure 1-4. Surface pressure – area isotherms of a monolayer of a: pure component A; b: pure component B; c: miscible components A and B; d, immiscible components A and B[4]. Reprinted by permission of Cambridge University Press, (Langmuir-Blodgett Films An Introduction, Michael C. Petty), (copyright 1996).

The phase rule and the equilibrium spreading pressure provide a useful tool to detect the miscibility of the monolayer in terms of number of phases on the surface. It gives insight into the conditions at which the experiment should be performed to obtain desirable and reproducible monolayers. The phase rule determines the miscibility of the components at the equilibrium spreading pressure. However, some of the components of the monolayer might be miscible at low surface pressure and become immiscible upon compression[6].

1.4 Langmuir-Blodgett (LB) film deposition

Langmuir-Blodgett (LB) deposition has been successfully used to create monolayers and patterned films. LB deposition was first introduced by Irving Langmuir[21] and applied extensively by Katherine Blodgett[22]. Since the development of the thin film concept by Langmuir and the design of the LB trough that produces thin films on liquid (Langmuir films) and solid surfaces (Langmuir-Blodgett films), monolayers have been the subject of numerous studies. Their importance arises from the fact that surface films that are one molecule thick can be formed and the molecules in the film are often highly oriented. This orientation allows the molecules to interact in a specific way that might be unlikely in 3D systems.

Langmuir and LB films composed of multiple components are extensively used to study 2D phenomena such as miscibility, phase-separation, pattern formation and ideal behavior of different systems. Mixed Langmuir and LB films were studied to generate 2D phase diagrams for different surfactants. These films helped in understanding intermolecular interactions in terms of dispersive forces and dipole interactions and their effect on the pattern formed as discussed later in section 1.8. Langmuir and LB films have numerous applications in different fields. In biological studies, the preparation of phospholipid bilayers using LB deposition creates a model for biological membranes[4]. In materials studies, the fabrication of patterned surfaces helps

understanding the interaction between different compounds[6]. Langmuir films can detect the presence of trace elements such as aluminium in a monolayer of stearic acid. This is because of the interaction between the ions and the fatty acid on the subphase. The change in the isotherm of the pure fatty acid is an indication of the presence of the ions. This technique can detect concentrations as low as 10^{-8} M[23].

1.4.1 LB film apparatus

Figure 1-5 is an image of the LB apparatus. It consists of a trough filled with a sub-phase liquid (usually water); on top of it on each side is a compressing barrier. The trough and the barriers are usually made of teflon to minimize adhesion of the surfactants. A substrate is dipped vertically in the sub-phase by a dipper, and a Wilhelmy plate is used to measure the surface pressure. The trough can be attached to a thermostat through water circulation in the external jacket of the trough in order to regulate the temperature. The temperature of the sub-phase is monitored by a thermocouple that is immersed in the sub-phase closer to the surface.

Figure 1-5. LB trough and its components[24].

1.4.2 Experimental details

The monolayer components are spread on the sub-phase surface using a volatile, water insoluble solvent with good spreading properties such as chloroform and hexane. The solution is spread on the water sub-phase using a microsyringe by depositing very small droplets (~3 μL) of solution onto the sub-phase. Time is given for the solvent to evaporate before compressing the film. The spreading solvent should be inert and does not react with the components of the trough. The choice of the spreading solvent used can alter the isotherms obtained as well as the structure of the monolayer produced[6]. In a study of arachidic acid and perfluorotetradecanoic acid system, when chloroform was used as the spreading solvent, the isotherms obtained were scattered and did not follow the additivity rule[25]. When the spreading solvent was changed into hexane:tetrahydrofuran (9:1) for the same system, the isotherms were found to follow the additivity rule. The reason for this discrepancy is not known[18].

The sub-phase is usually pure water. For some unstable films, low concentration of divalent cations can be added such as in the case of some fatty acids[26]. The cation can interact with the head groups making the molecules more rigid. A buffer can be added to the sub-phase to perform the measurements at specific pH. A low pH sub-phase is used in the case of shorter chains of surfactants in order to reduce the ionization of the head groups of the acid. For example a better monolayer of lauric acid ($CH_3(CH_2)_{10}COOH$) is obtained upon the use of acidic sub-phase of low pH. This decreases the ionization of the fatty acid molecules so it decreases their solubility in the sub-phase[4]. A low pH helps in stabilizing the perfluorinated carboxylic acid as well. Shibata et al. obtained a stable monolayer of perfluorodecanoic acid when the experiment was performed at pH=1.0 using HCl[20]. It was found that monolayers cannot be formed of fatty acid chains that have less than 12 carbon atoms even under low sub-phase pH[4].

Once the solution is spread and the solvent evaporates, the barriers move toward each other from both sides at a specific speed to compress the monolayer until reaching the desired surface pressure. The speed of the barrier compression can be varied. When the barrier compressing speed is low, the film formed is more stable.

For the preparation of LB films on solid substrates, the substrate should be cleaned prior to use. Some typical types of solid substrates used in LB deposition include mica, silicon, glass and gold. The choice of the substrate used depends on the measurement that needs to be carried out on these films and the desired data. For measurements where conductive surface is needed, such as scanning tunneling microscopy (STM) and near edge x-ray absorption fine structure (NEXAFS), silicon or gold is used. For fluorescence study, glass is preferred whose thickness is related to the refractive index of the lens of the microscope. For infra-red studies, gold is the substrate needed as it enhances the signal[2]. The other factor that determines the substrate chosen is its hydrophilicity.

The substrate can be dipped in the sub-phase before the spreading of the solution or after reaching the desired surface pressure. This depends on the hydrophilicity of the substrate. In the case of a hydrophilic substrate, the substrate should be dipped in the sub-phase before spreading the solution. Upon reaching the desired pressure, the substrate is withdrawn so that the hydrophilic head groups of the surfactants are in contact with the substrate (Figure 1-6). If the substrate is hydrophobic, it should be dipped upon reaching the desired surface pressure so that the hydrophobic chains of the surfactants are attached to the substrate.

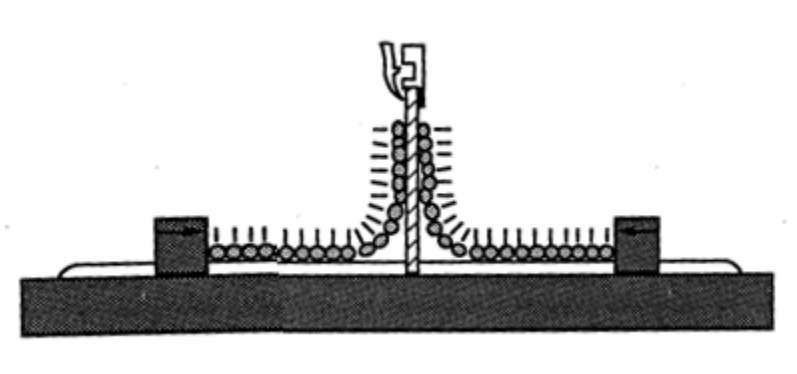

Figure 1-6. Schematic representation of the deposition of a monolayer from the air water interface to a vertical susbstrate[2].

Surface pressure is often measured and monitored by a Wilhelmy plate. The Wilhelmy plate is a solid plate that is suspended in the surface of the sub-phase. The plate forms a meniscus with the sub-phase at a contact angle = θ as shown in Figure 1-7. The forces acting on the plate are the gravitational force and the surface tension pulling downward, opposed by the buoyancy upward because of the weight of the water displaced. The net downward force acting on the surface can be written as:

$$F = \rho_p glwt + 2\gamma(t + w)\cos\theta - \rho_l gtwh \qquad (1\text{-}18)$$

where ρ_p and ρ_l are the density of the plate and water, respectively, t , l and w are the dimensions of the plate, g is the gravitational constant, h is the immersed depth of the plate in the sub-phase. The first term in the equation represents the gravitational force acting on the plate; the second term is the weight of the meniscus defined in terms of the surface tension. The last term in the equation represents the buoyancy related to the density of the liquid (sub-phase). This equation neglects the other phase which is air.

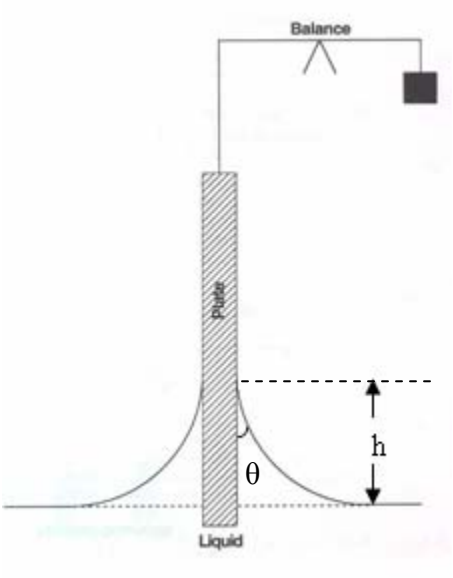

Figure 1-7. The Wilhelmy plate used to measure the meniscus and the change in the height of water level[5].

One of the drawbacks of this method is that the wetting angle (θ) changes with the change of the surface pressure. Some of the surfactants might adhere to the balance especially while moving upward, thus affecting the contact angle[6]. To avoid the difficulty in measuring θ, the change in the weight of water raised on the plate is monitored (equation 1-19). This is achieved by keeping the plate completely wetted by the liquid so cosθ = 1. When the surface pressure increases, the plate moves upward, both h and γ change,

$$\Pi = -\Delta\gamma = -[\Delta F / 2(t + w)] \qquad (1\text{-}19)$$

where the surface pressure is the force acting on unit length as shown in equation (1-4). During compression, the surface tension downward and the buoyancy upward are the only forces that change since the weight of the plate is constant. Accordingly the overall change in force ΔF is zero and these two forces (surface tension and buoyancy) are equal in value but opposite in direction. This results in Equation (1-20).

$$\Pi = -\Delta\gamma = -[\rho_l gtw / 2(t + w)]\Delta h \qquad (1\text{-}20)$$

If the thickness of the plate is small compared to its width (w), and by measuring the change in h as shown in Figure 1-7, this yields the following equation:

$$\Pi = -\Delta\gamma = -\frac{1}{2}\rho_t gt\Delta h \qquad (1\text{-}21)$$

The deposition can be performed at any desired surface pressure. Film transfer is often characterized by the transfer ratio (τ) which represents the ratio of the decrease of the area occupied by the film on the water sub-phase (A_L) to the coated area of the solid substrate (A_S) as in equation (1-22).

$$\tau = \frac{A_L}{A_S} \qquad (1\text{-}22)$$

The complete coverage of the monolayer on the solid substrate indicates a good homogeneity of the film and τ equals to one[4]. It is preferable that the withdrawal rate of the substrate from the sub-phase being comparable to that of the water draining from the substrate. The rate of the water coming out of the film represents the rate of the adhesion of the surfactants to the substrate thus expelling water out[4].

1.5 Characterization of Langmuir and LB films

Different techniques have been used to characterize Langmuir and LB films such as Brewster angle microscopy (BAM)[10], infrared spectroscopy[18], Near edge x-ray fine structure (NEXAFS) spectroscopy and x-ray photoabsorption spectroscopy (XPS)[27], fluorescence microscopy[28,29], and atomic force microscopy (AFM)[25, 30]. Among all the techniques mentioned, AFM is one of the most widely used for characterizing LB films. It is a non-destructive technique which measures in different environment (air, liquid and vacuum). AFM does not need

a conductive surface as in NEXAFS, nor does it need a fluorescent molecule to dope the samples as in fluorescence microscopy.

1.5.1 Characterization of LB films by AFM

The atomic force microscope is a powerful technique to measure surface topography with high lateral and vertical resolution. AFM was first introduced by Binnig, Quate and Gerber in 1986[31]. It was based on the scanning tunneling microscope (STM) to measure the topography of surfaces. The main advantage of AFM over STM is that it can be used to measure both conductive and non-conductive surfaces. AFM can characterize surfaces at length scales that vary from hundreds of microns down to the atomic level[26]. It has been used to measure films in ambient air, vacuum and fluid at different temperatures. AFM allows in situ measurements of monolayer adsorption[32] and real time observation of biological processes such as blood clotting[33]. AFM is generally considered to be a non-destructive technique. It can provide an insight into the mechanical properties of the film components such as friction and adhesion in addition to topographical information.

The atomic force microscope consists of four main parts: a probe that contains a cantilever with a tip on its end, a piezoelectric micropositioner, a laser beam and a photodiode[34] as shown in Figure 1-8. The piezoelectric micropositioner is made of an actuator material that allows very small mechanical movements upon applying a voltage. The cantilevers have different shapes such as rectangular or triangular. They also vary in length and thickness. The longest and the thinnest cantilevers are more flexible and have less spring constant than the shortest and the thickest ones. Spring constants can vary between 0.002-100 N/m. The tip at the end of the cantilever can be made with different shapes; the pyramidal shape is the most common. The tips are made of silicon, silicon nitride, or pure metals and can be metal coated

with elements such as gold or chromium depending on its use. Its size varies with an average radius of curvature of ~ 30 - 200 nm.

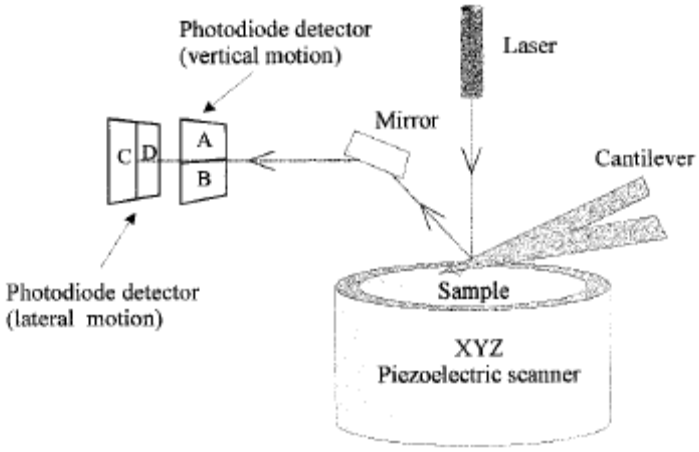

Figure 1-8. Schematic representation of an AFM [34] (Reproduced with permission from Chemical Reviews **1999,** 99, 2845. Copyright 1999 American Chemical Society).

The cantilever should be calibrated before doing any force measurement by finding its spring constant. The thermal tune method is the most practical and widely used. It depends on measuring the thermal noise of the cantilever which can be done by collecting time intervals of the deflection signal at thermal equilibrium while the cantilever is suspended away from the surface. Brownian motion of surrounding molecules (air) imparts random impulses to the cantilever during the sampling. The resulting function of time is Fourier transformed and the spring constant can be obtained[35].

There are different modes to measure the topography of the surface. The most widely used are: contact mode and tapping mode. In contact mode, the tip is in a direct contact with the surface keeping the vertical deflection of the cantilever constant. The tip is forced to move up and down following the topography of the surface. Thus, the laser bouncing off the backside of the tip changes its position on the photodiode detector. By transferring the position of the laser into x, y and z data, a 3D topographic image is obtained. In tapping mode, the cantilever is

oscillated at its resonance frequency. The tip taps the surface in small intervals during its oscillation period, and moves up and down following its topography by keeping the amplitude constant. The photodiode measures the difference in the laser position depending on the tip movement[36].

Friction is another parameter that can be measured by AFM. It can be detected by measuring the lateral deflection of the cantilever on the surface[34]. This type of measurement should be carried out by scanning at an angle of 90 º to the long axis of the cantilever. Friction usually depends linearly on the loading force on the cantilever[34].

Another type of useful AFM-based measurement is adhesion force. This is often measured by a force curve which is a plot showing the vertical deflection of the cantilever as a function of the distance between the tip and the surface (Figure 1-9). Each force curve is identified by regions that indicate the position of the tip on the sample surface. (A) represents a large tip – sample separation where no detectable interactions are present. As the tip is moving closer to the surface at some separation, the gradient of interaction energy exceeds the restoring force of the cantilever so the van der Waals attraction will pull the tip into contact with the surface. This is also called the jump into contact point (B). The deflection of the cantilever tracks the movement of the sample (C). In region (C), the interaction between the tip and the surface becomes repulsive at this short distance. As the tip is withdrawn from the sample, the same previous region is observed as both the tip and sample remain in contact (D).As the tip moves away from the sample, the restoring force exerted by the bending of the cantilever overcomes the adhesive force of the tip – sample microcontact and the tip breaks away from the sample (E). Then the cantilever returns to its non-interacting equilibrium position (F)[34, 36].

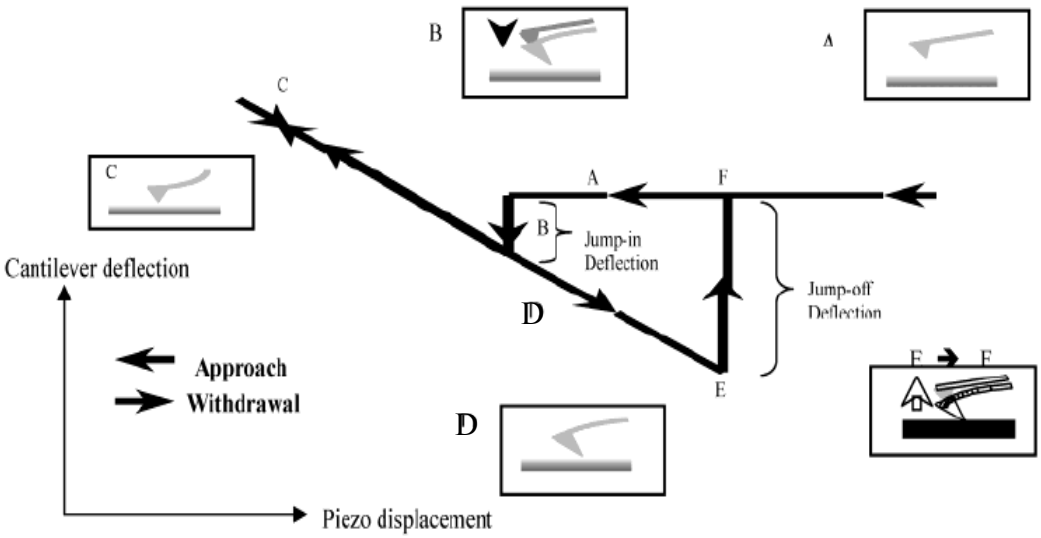

Figure 1-9. Force curve representing the vertical deflection of the cantilever as a function of the distance between the tip and the sample[37] (Reproduced with permission from Langmuir **2004,** 20, 2707. Copyright 2004 American Chemical Society).

The finite force necessary to pull the tip off the sample surface corresponds to the adhesive force between the tip and the sample. The force of adhesion is measured by analyzing the retrace curve[34]. The jump off of the cantilever is changed directly from deflection (in volts) into force (in nN) through the cantilever spring constant, the deflection sensitivity, and applying Hook's Law (equation 1-23). To get a statistically relevant value of the force of an interaction, a large number of force curves (≥200) are collected and analyzed[34].

$$F_{ad} = k\Delta z \qquad (1\text{-}23)$$

Force measurements are generally not carried out in ambient air as it is difficult to interpret them because of the presence of capillary forces which are usually 1-2 orders of magnitude larger than typical intermolecular forces (Figure 1-10). The capillary forces obscure the small differences between the interactions of different functional groups on the surface with the tip[36]. Force curves are usually measured in vacuum or in liquid to remove the influence of capillary forces.

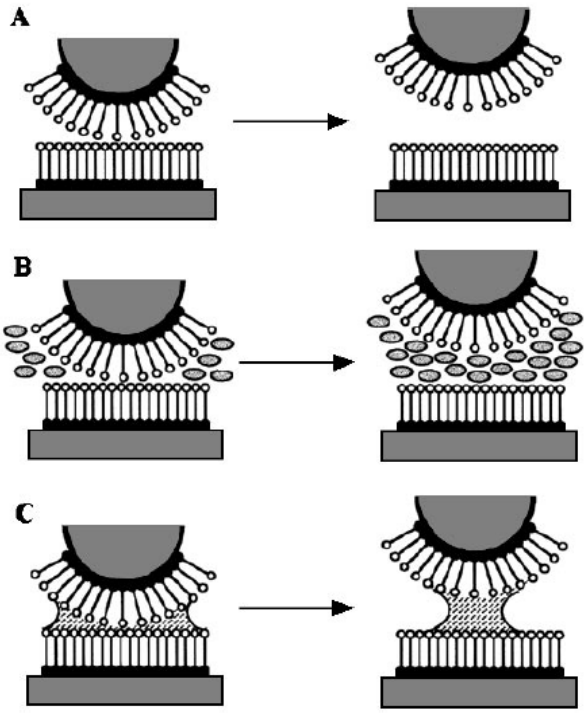

Figure 1-10. Comparison between force measurements in A, vacuum; B, liquid; and C, ambient air.[36] "Reprinted, with permission, from Annual Review of Materials Science**,** Volume 27 (c) 1997 by Annual Reviews www.annualreviews.org".

One of the limitations of basic AFM imaging is its lack of chemical information about the surface. Significant efforts have been made to make the AFM a chemical probe of the surface in addition of a topographic one. One approach to this has been the development of chemical force microscopy (CFM) to measure the force of adhesion and friction between different functional groups on the tip and on the surface. In this approach, AFM tips are chemically functionalized by the formation of self-assembled monolayers of thiols on gold plated tips[38] or of silane on silicon and silicon nitride tips[39]. By preparing LB films or self-assembled monolayers of different surfactants on the surface, interactions between different combinations of functional groups on the surfaces and the modified tips can be measured. For example, Noy et al. measured the forces between the combinations of $COOH/CH_3$, CH_3/CH_3 and COOH/COOH on gold-coated tip and gold substrates[38].

1.6 Hydrocarbon and fluorocarbon surfactants as monolayer materials in LB films

Different types of compounds have been used to prepare LB films, including saturated and unsaturated fatty acids, fatty alcohols, perfluoroalkyls, phospholipids, vitamins and proteins[6]. Mixed LB films have been widely studied as the mixed films can have more desirable properties than those of the pure components.

In the field of monolayers, fluorinated amphiphiles play an important role because of their applications in materials science and biomedicine[40, 41]. These applications originate from the improved thermal, chemical and physical properties of fluorinated surfaces in comparison with their nonfluorinated counterparts. These properties include low friction coefficients[18, 42, 43], high density, fluidity, compressibility and high dielectric constants[44].

Under appropriate conditions in monolayers, and because of the large difference in the cohesive force of the fluorinated surfactants and the hydrocarbon amphiphiles, the two types of molecules phase-separate[20]. If the interaction between the head groups of fluorinated and hydrogenated surfactants is strong enough, the two components become miscible and can deviate from ideal mixing[20, 45]. Fluorinated and hydrocarbon molecules form different patterns on the surface upon phase-separation. The significance of patterned surfaces arises from their wide applications in the field of biology as they have chemical and biological sensing properties[46].

Imae et al[25]. studied mixed LB films composed of chains of perfluorocarbon of different lengths and fatty acids by atomic force microscopy (AFM) and surface pressure –area isotherms. Phase – separation took place in all the systems and irregular islands were observed on the surface.

Iimura et al. carried out a systematic study on LB films of different fatty acid chains and perfluoroether[30]. Phase-separation took place in all the systems studied. A thorough analysis of

the properties of the isotherms was performed. They also studied the LB film under different temperatures and reported its effect on the pattern formed as discussed in the next section (1.8).

Different applications were introduced for the fluorocarbon/hydrocarbon films in the field of biochemistry. Frommer et al.[46] studied the adsorption of the tobacco mosaic virus on a phase-separated film of fluorocarbon and hydrocarbon. It was found that the virus adsorbs preferentially on the circular hydrocarbon domains. Fang and Knobler[47] used LB deposition to prepare a monolayer of alkyl silane on silicon, followed by exposure to perfluoroalkyl silane that chemisorbs in the voids between the alkyl groups. They used these films to study the interaction of bovine serum albumin that adsorbs preferentially on the methyl terminated regions on the film.

LB films of hydrocarbon and fluorocarbon were used to study the interactions between gold nanoparticles and amino acids. The silicon surface was patterned by washing out one of the components leaving the chemisorbed component on the surface by the use of an organic solvent. A compound containing an amino group is added in the voids on the surface. When the gold nanoparticles are introduced to the system, they bind preferentially on the amino groups[48].

Many studies were done on mixed LB films of fluorinated compounds and hydrocarbon chains mainly to investigate their miscibility[10, 20] and the structures formed[18, 25, 49]. However fewer studies were carried out to investigate the mechanism of phase – separation and domain formation.

1.7 Pattern formation in LB films

It is important to understand the mechanism of the formation of these films, and their stability in terms of kinetics, in order to ultimately control patterns on surfaces. LB films of different components produce different patterns on the monolayer. This depends mainly on the

materials used for deposition and their interactions and miscibility. Different studies suggested that the substrate, rate and direction of withdrawal, surface pressure of deposition, temperature and the spreading solvent have an effect on the shape and the size of the structures formed on the surface.

Iimura et al. reported that the structures of the domains obtained in LB films of fatty acids and perfluoroethers depend on the increase of the line tension[30]. The line tension is the energy needed to create unit length of the circumference of the domain. When the line tension increases, large circular domains form. They observed that when the perfluoroether compound is kept the same, and as the chain length of the acid increases, the domains take narrower and linear patterns compared to the large circular patterns at shorter chain lengths. This is explained by the decrease in line tension as the fatty acid chain length increases. They also noticed an increase in the domain size as temperature increases, they explained these domains as being a result of a change in mobility of the molecules[30].

Matsumoto et al. explained the different domains obtained in a system of fatty acids and perfluoroalkyl silane as a result of the difference between homo and hetero interactions which is proportional to the line tension[50, 51]. The homo interactions, w_{AA} and w_{BB} are the interactions between the molecules of the same type, whereas the hetero interactions, w_{AB} are those between different types of molecules, following the equation:

$$(w_{AA} + w_{BB})/2 < w_{AB} \qquad (1\text{-}24)$$

By increasing the length of the fatty acid chain keeping the perfluoroalkyl silane compound constant, the pattern changed from narrow linear domains into large circular domains[50]. The increase in the fatty acid chain length was explained by the decrease of the homo interactions energy (w_{AA} or w_{BB}) resulted from the increase in the dispersive interactions between the

molecules of the same type. As a result, an increase in line tension was observed. When the fluoroalkyl silane chain increases in length, the line tension decreases and the domains take narrow shapes since this chain remains shorter than the hydrocarbon chain[50].

In a different system of alkyl and perfluroalkyl chains, Matsumoto observed that by increasing the fluoroalkyl chain, the domain size decreases. This is explained by the stabilizing energy caused by the dispersive interactions. When the perfluoroalkyl chain increases, w_{AB} decreases because of the increase in the dispersive interactions between the alkyl and the perfluoroalkyl chains. The decrease in this hetero interaction is larger than that in the homo interaction, also the decrease in w_{BB} contributes only as half as w_{AB}. This increase in chain length decreases the contribution of line tension, resulting in the decrease of the domains size adopting narrower patterns[51].

McConell reported that the pattern formed in phospholipid bilayers is a result of the competition between line tension and dipole – dipole interactions. The line tension is defined as the free energy needed to create a unit length of domain boundary; it favors the formation of large or circular domains. The dipole interactions are the repulsive interactions in the monolayer as the molecules are aligned in a parallel manner. The dipole interactions favor the formation of narrow elongated domains[52] because of the repulsion between the molecules within the domains. Thus it is energetically costly for these molecules to interact with the same type. The molecules reduce the energy of interaction between them through the formation of narrow domains with lower interaction energy between the molecules within the domains. Depending on the dominant force of interaction between the molecules in a monolayer, the patterns vary from one system to another.

In addition to the dominant interactions, Sikes et al. observed that the substrate has a significant effect during the film preparation. They observed that the deposition of fatty acids on mica (pH=5.8) or negatively charged SiO_2 (pH =9.3) produces separate islands and dendritic patterns. When positively charged SiO_2 (at pH =5.8) was used, a featureless surface was obtained[53]. Hexadecanoic acid when deposited on mcia formed dendritic structures whereas it formed separated islands when deposited on negatively charged SiO_2. In a separate study, Sikes et al. suggested that the formation of monolayer of fatty acid is a first order phase transition governed by nucleation. As temperature increases, the number of domains formed increases.[54]

Because of the solid substrate roughness, the monolayer formed on the surface of the sub-phase might not be transformed as it is to the solid substrate, but defects might form. These defects are not only because of the solid substrate but also they are attributed to the monolayer being discontinuous on the sub-phase even before being transferred. This is explained by the weak interactions between the chains. However if the monolayer is continuous and stable on the liquid surface, it is transferred like a carpet on the solid substrate[6].

For phospholipid bilayers, the speed at which the withdrawal/dipping of the substrate take place affects both the periodicity of the linear pattern obtained and the line thickness. It was observed by Moreille and Badia[55] that by increasing the dipping speed, the number of lines per unit area increases and their thickness decreases. They also observed that deposition of the lipid film at higher surface pressure resulted in the formation of continuous lines rather than broken ones. They suggested that the stripes formed at high surface pressures are the result of the alignment and the coalescence of the circular domains observed at lower surface pressures. The stripe formation was explained by the depletion phase containing one of the components in the solid phase and the other is in the liquid expanded phase. Since the formation of the solid phase

is close to the contact line, the contact angle and the meniscus fluctuate. Another observation in this system is that the phospholipid stripes are perpendicular to the dipping direction. For anisotropic systems, the domains are organized by the flow and reorient themselves by it.

The choice of the spreading solvent used affects the surface pressure – area isotherms thus Langmuir films on the sub-phase. It also can affect the LB film formed on the solid substrate. The change of the solvent of fatty acids from chloroform[25] into a mixture of hexane:THF[18] changed the relative positions of the isotherms at different molar fractions and the additivity rule became valid to the system.

1.8 Ostwald ripening versus coalescence in monolayers

Another factor that affects the size of the domains formed and can explain the mechanism of their formation is Ostwald ripening. Ostwald ripening is the two-dimensional diffusion of molecules on the surface, from the larger domains into the smaller domains so that the larger domains become larger at the expense of the smaller domains. According to Gibbs-Thomson effect, the smaller domains decrease in size until they reach their critical nucleus size. They rapidly disappear because of the thermodynamic instability of subcritical clusters[56]. As a result, the particles' number density decreases and their size increases[57]. The driving force in Ostwald ripening is to reduce the total surface free energy[57]. It is considered to be the last stage in domain formation and condensation transition from gas to liquid or liquid to solid[56]. It takes place after nucleation of the islands[58].

The Lifshitz-Slyozov equation[59] defines the rate at which Ostwald ripening (domain coarsening) takes place. In a 2D system, the domains grow according to the following equation[60]:

$$< A >= kt^{2\alpha} \qquad (1\text{-}25)$$

where <A> is the average area of the domain, k is a constant that depends on the surface tension, diffusion constant of the molecules, and the degree of supersaturation[61], t is time, α is the growth exponent and is equal to 1/3 for diffusion-controlled processes[60]. The growth rate exponent, α might vary depending on the system and the stage of growth. It might range from 1/4 [62] to 1/2 [63] and even 1 at early stages of growth[64]. In these case when α does not equal 1/3, the mechanism of growth is affected by the hydrodynamic flow and the Brownian motion or coalescence becomes important as the mechanism of domain growth. Hydrodynamic flow in liquids is the flow of the material from narrow regions to wider regions because of concentration difference.

The surface diffusion coefficient (D) for the molecules can be obtained from the rate equation as follows[65]:

$$D = \frac{kT}{2\gamma a^4} \cdot \frac{\Delta R^3}{\Delta t} \qquad (1\text{-}26)$$

where k is Boltzmann constant, T is the temperature in K, γ is the surface energy, a is the lattice parameter of the material that diffuses, R is the radius of the domain formed and t is time.

Since Ostwald ripening is a diffusion controlled process, it is affected by changes in temperature. An increase in temperature increases the mobility of the molecules and as a result the diffusion rate increases. In a theoretical study, Madras and McCoy tried to control the domain growth via Ostwald ripening by changing the temperature[56]. This can give an insight into tailoring particles of specific size and shape which is an important part of surface patterning. It was also observed that in systems where Ostwald ripening is the dominant mechanism, the thermodynamic stability of the system is high[66].

Despite the in depth knowledge of Ostwald ripening, kinetic studies of diffusion and domain growth in LB films are not common. It was reported only for phospholipid bilayers[60, 67]. There have been studies on surface diffusion in other systems such as diblock copolymer[68], thin

polymer films such as polystyrene and diethyl oxalate[69], and atomic diffusion using copper on tantalum substrates[65].

Coalescence is another process that might take place during domain growth in 2D and 3D. It is the merging of smaller domains to form larger domains. This requires that the small domains come into contact with each other. It depends on the Brownian motion of the domains. In contrast with Ostwald ripening, coalescence does not depend on molecular diffusion but it depends on the movement of the domain as a whole unit. In Ostwald ripening, the final shape of the domains is retained which is in contrast to coalescence as shown in Figure 1-13. The difference between Ostwald ripening and coalescence in addition to the mechanism of formation as in Figure 1-13, is the rate law applied. For coalescence, the radius of the domain increases exponentially with time as in equation (1-36)[66], compared to the linear time dependence for Ostwald ripening as in equation (1-25).

$$a^3 = a_0^3 e^{kt} \qquad (1\text{-}27)$$

Coalescence was observed in self assembled monolayer formation. Shwartz et al. studied the kinetics of monolayer formation of octadecylphosphonic acid on mica[32]. They observed that nucleation takes place followed by the aggregation stage in which the islands grow from the deposited molecules without the formation of new nuclei. The last stage in their mechanism was coalescence which represented the growth of the domains accompanied by the decrease in the number of islands.

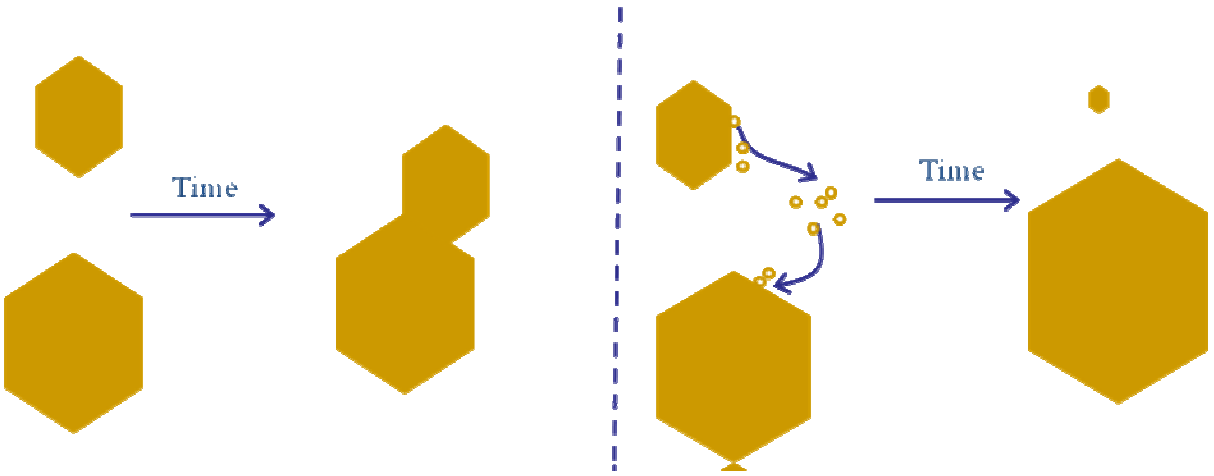

Figure 1-11. Sketch of left, coalescence mechanism; right, Ostwald ripening mechanism.

1.9 Research objectives

The goal of this research is to study phase-separation of mixed LB films containing hydrocarbon / fluorocarbon surfactants. Not much is known about mechanism and kinetics of phase-separation in these LB films. In this study, different hydrocarbon / fluorocarbon systems were investigated to determine the mechanism and kinetics of their phase-separation. In this project, the miscibility of these two components and the factors affecting phase-separation were investigated. Measurements were carried out to determine the factors affecting the pattern obtained on the surface. An investigation of the effect of chain length on the pattern obtained and the phase-separation and miscibility of the components in the mixed film was carried out.

Surface pressure – area isotherms in conjunction with the AFM imaging were the main measurements carried out to study the phase-separation of these systems. Other surface sensitive techniques were used in this project, including X-ray photoelectron emission microscopy (X-PEEM) and confocal fluorescent microscopy. These techniques in combination with the AFM were used to study the morphology of the surface and the chemical composition of the domains. The mechanism and kinetics of phase-separation were studied by changing experimental

conditions such as sub-phase temperature, solvent evaporation time, deposition pressure, and agitation of the solution mixture.

1.10 References

1. Langmuir, I., *Science* **1936,** 84, 379.
2. Ulman, A., *An Introduction to Ultrathin Organic Films from Langmuir-Blodgett to Self-Assembly*. Academic Press Inc.: San Diego, 1991.
3. Tadros, T. F., *Surfactants*. Academic Press Inc.: London, 1984.
4. Petty, M. C., *Langmuir - Blodgett Films an Introduction*. Cambridge University Press: Cambridge, 1996.
5. Evans, D. F.; Wennerstrom, H., *The Colloidal Domain Where Physics, Chemistry, Biology and Technology Meet*. VCH Publishers, Inc: New York, 1994.
6. Gaines, G., *Insoluble Monolayers at Liquid-Gas Interfaces*. Interscience Publishers: New York, 1966.
7. Adamson, A. W.; Gast, A. P., *Physical Chemistry of Surfaces*. Wiley: New York, 1997.
8. Langmuir, I., *J. Chem. Phys.* **1933,** 1, 756.
9. Rontu, N.; Vaida, V., *J. Phys. Chem. C* **2007,** 111 (27), 9975.
10. Broniatowski, M.; Romeu, N. V.; Dynarowicz-Latka, P., *J. Phys. Chem. B* **2006,** 110 (7), 3078.
11. Dervichian, D., *J. Chem. Phys.* **1939,** 7, 931.
12. Harkins, W.; Copeland, L., *J. Chem. Phys.* **1942,** 10, 272.
13. Stallberg-Stenhagen, S.; Stenhagen, E., *Nature* **1945,** 156, 239.
14. Goodrich, F., *Proc. Int. Cong. Surf. Activity* **1957,** 1, 85.
15. Korchoweic, B.; Paluch, M.; Corvis, Y.; Rogalska, E., *Chem. Phys. Lipids* **2006,** 144, 127.
16. Broniatowski, M.; Dynarowicz-Latka, P., *Langmuir* **2006,** 22 (6), 2691.
17. Atkins, P.; Paula, J. d., *Physical Chemistry*. W. H. Freeman and Company: New York, 2002.
18. Matsumoto, M.; Tanaka, K.; Azumi, R.; Kondo, Y.; Yoshino, N., *Langmuir* **2003,** 19 (7), 2802.
19. Castelli, F.; Sarpietro, M. G.; Rocco, F.; Ceruti, M.; Cattel, L., *J. Colloid Interface Sci.* **2007,** 313 (1), 363.
20. Shibata, O.; Yamamoto, S. K.; Lee, S.; Sugihara, G., *J. Colloid Interface Sci.* **1996,** 184 (1), 201.
21. Langmuir, I., *Trans. Faraday Soc.* **1920,** 15, 62.
22. Blodgett, K., *J. Am. Chem. Soc.* **1934,** 56, 495.
23. Langmuir, I.; Schaefer, V., *J. Am. Chem. Soc.* **1937,** 59, 2400.
24. Ksv Instruments. http://www.ksvltd.com/content/index/monolayertools (accessed December 2008)
25. Imae, T.; Takeshita, T.; Kato, M., *Langmuir* **2000,** 16 (2), 612.
26. Schwartz, D.; Garnaes, J.; Viswanathan, R.; Chirvolu, S.; Zasadzinski, J., *Phys. Rev. E* **1993,** 47 (1), 452.
27. Krasnikov, S.; Hanson, C.; Beggan, J.; Cafolla, A., *J. Phys.: Conference Series* **2008,** 100, 82041.

28. McKiernan, A. E.; Ratto, T. V.; Longo, M. L., *Biophys. J.* **2000,** 79 (5), 2605.
29. Lipp, M. M.; Lee, K. Y. C.; Waring, A.; Zasadzinski, J. A., *Biophys. J.* **1997,** 72 (6), 2783.
30. Iimura, K.; Shiraku, T.; Kato, T., *Langmuir* **2002,** 18 (26), 10183.
31. Binnig, G.; Quate, C. F.; Gerber, C., *Phys. Rev. Lett.* **1986,** 56 (9), 930.
32. Doudevski, I.; Hayes, W. A.; Schwartz, D. K., *Phys. Rev. Lett.* **1998,** 81 (22), 4927.
33. Baranauskas, V.; Fontana, M.; Guo, Z. J.; Ceragioli, H. J.; Peterlevitz, A. C., *Nanotechnology* **2004,** 15, 1661.
34. Takano, H.; Kenseth, J. R.; Wong, S. S.; O'Brien, J. C.; Porter, M. D., *Chem. Rev.* **1999,** 99 (10), 2845.
35. Kelley, V. *Support Note 398, Di Atomic Force Microscope Thermal Tune*; Veeco: 2004.
36. Noy, A.; Vezenov, D. V.; Lieber, C. M., *Annu. Rev. Mater. Sci.* **1997,** 27, 381.
37. Noel, O.; Brogly, M.; Castelein, G.; Schultz, J., *Langmuir* **2004,** 20 (7), 2707.
38. Noy, A.; Frisbie, C. D.; Rozsnyai, L. F.; Wrighton, M. S.; Lieber, C. M., *J. Am. Chem. Soc.* **1995,** 117 (30), 7943.
39. Nakagawa, T.; Ogawa, K.; Kurumizawa, T., *J. Vac. Sci. Technol., B* **1994,** 12 (3), 2215.
40. Kissa, E., *Fluorinated Surfactants and Repellents* Marcel Dekker Inc.: New York, 2001.
41. Krafft, M. P., *Adv. Drug Delivery Rev.* **2001,** 47, 209.
42. Overney, R. M.; Meyer, E.; Frommer, J.; Guntherodt, H. J.; Fujihira, M.; Takano, H.; Gotoh, Y., *Langmuir* **1994,** 10 (4), 1281.
43. Matos, L.; Ravey, J. C.; Serratrice, G., *J. Colloid Interface Sci.* **1989,** 128 (2), 341.
44. Lehmler, H. J.; Bummer, P. M., *J. Colloid Interface Sci.* **2002,** 249 (2), 381.
45. Sugihara, G.; Yamamoto, M.; Wada, Y.; Murata, Y.; Ikawa, Y., *J. Solution Chem.* **1988,** 17 (3), 225.
46. Frommer, J.; Luthi, R.; Meyer, E.; Anselmetti, D.; Dreier, M.; Overney, R.; Guntherodt, H. J.; Fujihira, M., *Nature* **1993,** 364 (6434), 198.
47. Fang, J. Y.; Knobler, C. M., *Langmuir* **1996,** 12 (5), 1368.
48. Abe, M.; Scamehorn, J. F., *Mixed Surfactant Systems*. Marcel Dekker: New York, 2005.
49. Matsumoto, M.; Tanaka, K.; Azumi, R.; Kondo, Y.; Yoshino, N., *Chem. Lett.* **2002,** (10), 970.
50. Mazaki, T.; Shibata, H.; Kondo, Y.; Yoshino, N.; Matsumoto, M., *Chem. Lett.* **2008,** 37 (4), 480.
51. Matsumoto, M.; Watanabe, S.; Tanaka, K.; Kimura, H.; Kasahara, M.; Shibata, H.; Azumi, R.; Sakai, H.; Abe, M.; Kondo, Y.; Yoshino, N., *Adv. Mater.* **2007,** 19 (21), 3668.
52. McConnell, H. M., *Annu. Rev. Phys. Chem.* **1991,** 42, 171.
53. Sikes, H. D.; Woodward, J. T.; Schwartz, D. K., *J. Phys. Chem.* **1996,** 100 (21), 9093.
54. Sikes, H. D.; Schwartz, D. K., *Langmuir* **1997,** 13 (17), 4704.
55. Moraille, P.; Badia, A., *Langmuir* **2002,** 18 (11), 4414.
56. Madras, G.; McCoy, B. J., *J. Chem. Phys.* **2003,** 119 (3), 1683.
57. Gratz, H., *J. Mater. Sci. Lett.* **1999,** 18 (20), 1637.
58. Ribic, P. R.; Bratina, G., *J. Phys. Chem. C* **2007,** 111 (50), 18558.
59. Lifshitz, I. M.; Slyozov, V. V., *J. Phys. Chem. Solids.* **1961,** 19 (1-2), 35.
60. Jensen, M. H.; Morris, E. J.; Simonsen, A. C., *Langmuir* **2007,** 23 (15), 8135.
61. Krichevsky, O.; Stavans, J., *Phys. Rev. E* **1995,** 52 (2), 1818.
62. Velasco, E.; Toxvaerd, S., *Phys. Rev. Lett.* **1993,** 71 (3), 388.
63. Leptoukh, G.; Strickland, B.; Roland, C., *Phys. Rev. Lett.* **1995,** 74 (18), 3636.

64. Siggia, E. D., *Phys. Rev. A* **1979,** 20 (2), 595.
65. Fillot, F.; Tokei, Z.; Beyer, G. P., *Surf. Sci.* **2007,** 601 (4), 986.
66. Sitnikova, N. L.; Sprik, R.; Wegdam, G.; Eiser, E., *Langmuir* **2005,** 21 (16), 7083.
67. Blanchette, C. D.; Orme, C. A.; Ratto, T. V.; Longo, M. L., *Langmuir* **2008,** 24 (4), 1219.
68. Bassereau, P.; Brodbreck, D.; Russell, T. P.; Brown, H. R.; Shull, K. R., *Phys. Rev. Lett.* **1993,** 71 (11), 1716.
69. Haas, C. K.; Torkelson, J. M., *Phys. Rev. E* **1997,** 55 (3), 3191.

CHAPTER 2
STRUCTURAL AND COMPOSITIONAL MAPPING OF A PHASE-SEPARATED LANGMUIR-BLODGETT MONOLAYER BY ATOMIC FORCE MICROSCOPY

This chapter is a slightly modified copy of an article published in *Langmuir* in November 2006. (Reproduced with permission from Langmuir **2007,** 23, 2582-2587.

Mixed LB films are objects of growing attention because of the improved properties that the mixed film has over films prepared from their pure, single components. Combinations of fluoroalkyl chains / alkyl chains were widely studied because they phase-separate under specific conditions. In this paper we studied an example of hydrocarbon / fluorocarbon mixed film to investigate their phase-separation and pattern formation. Langmuir and LB films of arachidic acid ($C_{19}H_{39}COOH$) (AA) and perfluorotetradecanoic acid ($C_{13}F_{27}COOH$) (PA) were characterized using surface pressure – area isotherms and atomic force microscopy measurements.

Analysis of the isotherms based on the additivity rule shows that the two film components are immiscible. Topography and tip-sample adhesion forces were measured to characterize the film morphology and the chemical composition of the domains. This chapter introduces the selective dissolution method that was developed and used for many other measurements that followed in this thesis. In selective dissolution, a specific solvent is chosen that preferentially dissolves one component of the mixed monolayer leaving the other component behind. The chemical composition of the film can then be determined by observing changes in the film topography. In conjunction, the force of adhesion between the AFM tip and sample can be

measured and chemical composition can be determined. We found that AA phase-separated from PA forming elevated hexagonal domains on the mica surface. We were able to identify the chemical composition of the domains in the film by the use of the AFM. We extended the typical uses of AFM from topographical information to chemical identification.

These mixed LB films of AA/PA were also characterized using x-ray photoelectron emission microscopy (X-PEEM). X-PEEM is a surface sensitive synchrotron-based technique with high lateral spatial resolution. The near edge x-ray absorption fine structure (NEXAFS) spectra were measured for the different domains in the film. The C-H and C-F peaks were identified from the NEXAFS spectra and the films were excited at the corresponding peak separately. Bright hexagonal domains were observed when the film was excited at the C-H peak indicating the presence of hydrocarbon (AA) in these domains. These measurements confirmed the previous composition of the mixed films inferred from AFM in Chapter 2. X-PEEM is a supportive technique to study the chemical composition of thin films. This work was published in *Journal of electron spectroscopy and related phenomena* in December 2007. (*Journal of electron spectroscopy and related phenomena* **2008**, 162 ,107-114). For this research paper, I prepared samples for AFM and X-PEEM measurements on silicon substrates, and assisted Stephen Christensen (the first author) to prepare additional samples. I assisted with AFM characterization of the films and I reviewed the paper in its various drafts. This paper is not included in the thesis.

For this current research paper[1], I prepared samples, performed the measurements, and played a major role in interpreting the results and the preparation of the paper. My supervisor provided guidance throughout the experimental work and was greatly involved in result interpretation and in writing this paper.

2. Structural and Compositional Mapping of a Phase-Separated Langmuir-Blodgett Monolayer by Atomic Force Microscopy

Shatha E. Qaqish and Matthew F. Paige

Department of Chemistry, University of Saskatchewan, 110 Science Place, Saskatoon, SK. Canada S7N 5C9

Received October 2, 2006. In Final Form: November 23, 2006

2.1 Abstract

The structure and composition of a phase-separated arachidic acid ($C_{19}H_{39}COOH$) (AA) and perfluorotetradecanoic acid ($C_{13}F_{27}COOH$) (PA) Langmuir-Blodgett monolayer film was characterized by several different types of Atomic Force Microscope (AFM) measurements. At the liquid-air interface, surface pressure-area isotherms show that mixtures of the two acids follow the additivity rule expected from ideal mixtures. Topographic images of the deposited monolayer indicate that the surfactants are oriented normal to the substrate surface, and that the acids undergo phase-separation to form a series of discontinuous, hexagonal domains separated by a continuous domain. A combination of lateral force (friction) imaging and adhesion force measurements show that the discontinuous domains are enriched in AA, whereas the surrounding continuous domain is a mixture of both AA and PA. This was further verified by selective, in-situ dissolution of AA by n-hexadecane, followed by high-resolution topographical imaging of the discontinuous domains.

2.2 Introduction

Fluorinated molecules have attracted considerable interest in part because of the desirable mechanical properties they can impart when tethered to solid surfaces. Surfaces modified with fluorinated molecules can show improved chemical and thermal properties, along with lower friction coefficients over their non-modified counterparts[2-4]. Langmuir and Langmuir-Blodgett (LB) films that contain fluorinated amphiphiles have proven to be particularly useful model systems for studies of fluorinated surfaces, as LB films tend to be highly ordered and relatively simple to prepare. These model systems have provided significant insight into friction and lubrication properties at nanometer length scales. Of particular recent interest have been mixed LB systems comprised of fluorinated and non-fluorinated amphiphiles[3, 5-8]. Because of weak intermolecular van der Waals attractions, perfluorinated compounds tend to show strong air-water interface activity as well as strong lipophobicity. When mixed with non-fluorinated amphiphiles, the two can be miscible or can phase-separate to form well-defined regions of different chemical composition.

The structure and composition of mixed amphiphilic systems have been investigated using a variety of analysis techniques, including surface pressure measurements, IR spectroscopy, and AFM measurements[2, 3, 5-9]. The latter is of particular interest because of its potential for simultaneous topographic and compositional surface mapping of LB films. Chemical mapping at nanometer length-scales is often problematic in surface studies, simply because most analysis techniques with spatial resolution on this length scale lack either sensitivity or chemical specificity. Since its inception, the atomic force microscope has become a fundamental research tool for characterizing the topography of surfaces at the nanometer length scale. Concurrent with its development as a tool for basic topographic imaging has been the

development of the AFM for compositional mapping of surfaces[10, 11]. Since the AFM makes use of tip-sample interaction forces for operation, effects such as friction, mechanical compliance, adhesive forces and others can be exploited in order to infer sample composition. There are a number of important approaches to AFM-based compositional mapping, including lateral force (friction) imaging, force modulation and force-volume imaging when the instrument uses contact mode feedback, and phase imaging, force modulation and electric / magnetic force imaging for intermittent contact feedback[11]. Considerable efforts have also been made to specifically tailor tip - substrate interaction forces via chemical modification of AFM tips, which can be used to obtain image contrast on the basis of specific chemical interactions between functional groups[10, 12]

In this work, the structure and composition of a phase-separated LB film comprised of arachidic acid (AA) and perfluorotetradecanoic acid (PA) deposited onto a mica substrate has been investigated. Several other authors have also carried out characterization studies on this system. Imae et al.[6] have investigated both Langmuir and LB films of a number of perfluorinated-hydrogenated amphiphile mixtures, including the AA-PA system, by surface pressure-area isotherms and AFM imaging. The authors reported phase-separation of the two components, and postulated, on the basis of changes in domain size as a function of AA content observed in AFM images, that at low surface pressures, deposited films consisted of isolated domains that were rich in AA, surrounded by a continuous domain rich in PA. However, definitive proof of this assignment by AFM imaging was challenging because of the film's high surface roughness and poorly defined domain edges. It is also worth noting that the pressure-area isotherms of amphiphile mixtures described by Imae did not obey a simple additivity rule, as might be anticipated for phase-separation.

Matsumoto et al.[2, 5] have reported somewhat different results from the same system. These authors observed from surface pressure-area isotherms that the additivity rule held for the AA / PA system, and from careful IR measurements that the molecular axes of AA and PA were almost perpendicular to the film surface. In addition, AFM topography and friction imaging revealed well-defined domains, with heights and frictional properties consistent with domains that were rich in AA. It was postulated that the differences observed between these two studies might be caused by differences in experimental conditions, including spreading solvent and other subtle factors.

In this work, the topography and chemical composition of a phase-separated AA and PA LB monolayer has been investigated through a series of AFM-based measurements, including topographic imaging, friction imaging and adhesive force measurements. Surface pressure-area isotherms were measured to compare with previous literature results, and LB films of different composition were deposited onto a mica substrate and analyzed in the AFM. In addition to these AFM approaches, which have been successful for compositional mapping in other systems, we have made use of a new approach for compositional mapping, that of in-situ selective dissolution of one component of the LB film. By incubating the film in a solvent that dissolves only one component of the mixed surfactants, the chemical composition of the film can be determined through changes in the topography of the sample. The general applicability of this novel approach for chemical mapping in a variety of systems is discussed.

2.3 Experimental Section

2.3.1 Chemicals

Arachidic acid (99%) and perfluorotetradecanoic acid (97%) were purchased from Sigma-Aldrich Corporation. The solvent n-hexadecane (99%) was purchased from Alfa Aesar, while hexanes (HPLC grade) and terahydrofuran were purchased from EMD and Merck EM

Science, respectively. Mica was purchased from SPI (Structure Probe Inc., West Chester, PA, USA) supplies, and was freshly cleaved with adhesive tape prior to use.

2.3.2 Langmuir-Blodgett Film Preparation

LB experiments were performed on a KSV 2000 Langmuir trough system (KSV Instruments, Helsinki, Finland), at room temperature and with ultrapure water (Millipore, pH 7.5) as a sub-phase. Before each measurement, the water surface was cleaned thoroughly by suction, and blank runs (compression of the clean surface) showed no appreciable change in surface pressure with compression. Stock solutions of AA and PA were prepared by dissolving the solid hydrocarbon or perfluorocarbon in a 9:1 volume ratio of hexane: THF to give final concentrations of 8.3×10^{-3} M and 5.0×10^{-3} M for AA and PA, respectively. Surface pressure-area isotherms were collected for pure AA, PA, and mixtures of the two in well-defined stoichiometric ratios. The stock solutions were mixed in appropriate volumes to give a range of AA:PA mole ratios (1:0, 3:1, 2:1, 1:1, 1:3 and 0:1).

For isotherm and deposition experiments, a 30 μL aliquot of the appropriate solution was placed on the sub-phase surface, and the solvent was allowed to evaporate for at least ten minutes. During isotherm measurements, a barrier compression rate of 20 mm min^{-1} was used. For film deposition, a compression rate of 10 mm min^{-1} was used until a deposition pressure of 20 mN m^{-1} was reached. After reaching the deposition pressure, the film was allowed to stabilize for ten minutes before the mica substrate was pulled upwards through the water-air interface in a single stroke. The film was left to dry at room temperature for several hours before measuring in the AFM.

2.3.3 Atomic force microscope measurements

AFM measurements were carried out in contact mode on a Dimension Hybrid Nanoscope system (Veeco Metrology Group, Santa Barbara, CA, USA). The microscope was mounted in an acoustic-vibration isolation system. Commercial Si_3N_4 AFM probes (Veeco Metrology Group, Santa Barbara, CA, USA), with nominal spring constants of 0.5 N/m and 0.01 N/m were used for measurements in air and in hexadecane, respectively. The manufacturer's values for cantilever spring constants were used. Measurements in n-hexadecane were carried out in a liquid cell, with samples being allowed to stabilize under hexadecane for ~3 hours prior to imaging. For lateral force (friction) imaging, the cantilever was scanned at an angle 90º to the main cantilever axis. Histograms of adhesion forces for the mixed surfactant films, as well as control samples of pure PA and AA films were produced by analyzing the retraction portion of force curves. Each histogram consisted of ~200 independent adhesion force measurements.

2.4 Results and Discussion

2.4.1 Surface pressure-area isotherms

Figure 2-1 shows pressure-area isotherms for a range of different AA-PA mixtures, including those collected for the pure amphiphiles alone. Film collapse pressures were typically around 50 mN m^{-1}, though slightly larger values were observed for the 3:1 and 1:1 mole ratio mixtures. The liquid phase transition at around ~22 mN m^{-1} became less pronounced as higher mole fractions of PA were used. The isotherms of the mixtures of AA and PA were located between the isotherms for the two pure acids (additivity rule), indicating that the two different components are phase-separated. These results are in excellent agreement with the results of Matsumoto[2, 5], though somewhat different from those described by Imae[6]. The spreading solvent we used for these experiments was identical to that used by Matsumoto (we found the

perfluorinated surfactant to be insoluble in chloroform, as was reported previously), which lends support to the importance of spreading solution composition in these experiments.

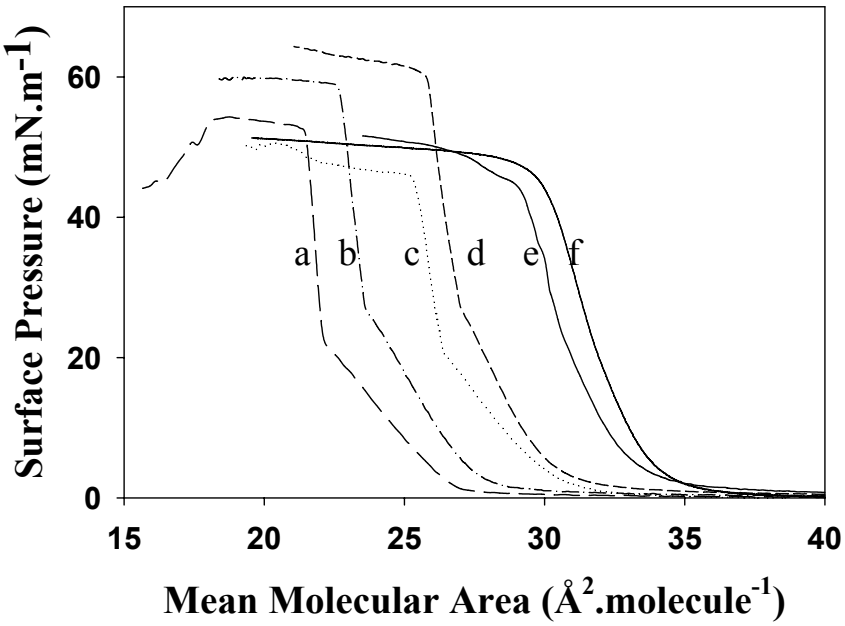

Figure 2-1. Surface pressure-area isotherms of AA, PA and their mixtures at room temperature on a water sub-phase (a represents pure AA, b represents 3:1, c represents 2:1, d represents 1:1, e represents 1:3, f represents pure PA).

2.4.2 AFM measurements

LB films of the mixed surfactants were prepared on mica substrates and were measured by contact mode AFM imaging in air. Figure 2-2A shows a typical topography (height mode) image and cross-section for an LB film deposited from a 2:1 mixture of AA and PA. The films formed well-defined domains that were approximately hexagonal in shape (herein referred to as 'discontinuous domains') and typically around 1-2 μm in diameter. These domains were surrounded by a continuous matrix (herein referred to as the 'continuous domain') that was lower in height than the discontinuous domains. Edges of the discontinuous domains were very clearly defined, and surface roughness in these samples was minimal. Cross-section analysis shows the average difference in height between the continuous domains and the discontinuous domain is ~6

Å which is very close to the expected 7 Å difference in length between AA (25 Å) and PA (18 Å) (lengths were calculated for molecules in vacuum using Spartan '04, MMFF). It is worth noting that perfluorinated molecules are shorter than alkanes containing the same number of carbon atoms since perfluorinated carbon chains often adopt a helical structure (for a recent discussion of this topic see the paper by Jang et al.[13]).

Similar film structures were observed for samples deposited at different AA / PA ratios. It was found that when the mole ratio of AA to PA increased, the area of the discontinuous domain increased compared to that of the continuous domain. The combination of these two results suggests that the discontinuous domains contain at least a significant proportion of AA, whereas the continuous domain is likely predominately PA. For the remainder of the experiments described here, LB films in a 2:1 AA:PA ratio were used.

In their investigations of mixed amphiphilic films, Imae et al. postulated that some of the rough surface features and poorly defined domain boundaries observed in their samples might be associated with the formation of bilayers and higher order structures resulting from piling-up of amphiphiles[6]. To eliminate the possibility that structures observed in our systems are the result of bilayer formation, we have carried out a "scratch test", in which an LB film was scraped off the mica surface by scanning the sample at the highest operating force accessible to our instrument and using a cantilever with a spring constant of 0.32 N/m. It should be noted that etching the sample with the tip required the use of very high imaging forces; under conditions used for normal topography imaging in air, the sample showed no observable tip-induced changes, and could be imaged repeatedly without damage. An image of a film after the scratch test is shown in Figure 2-2B, along with cross-sectional analysis. The height difference between the underlying mica surface and each of the continuous and the discontinuous domains was

measured to be 16 Å and 22 Å, respectively, which corresponds extremely well with the lengths expected for the individual amphiphiles. This clearly shows that under the deposition conditions used for these experiments, the films consist of a monolayer with the constituent molecules oriented perpendicular to the underlying substrate.

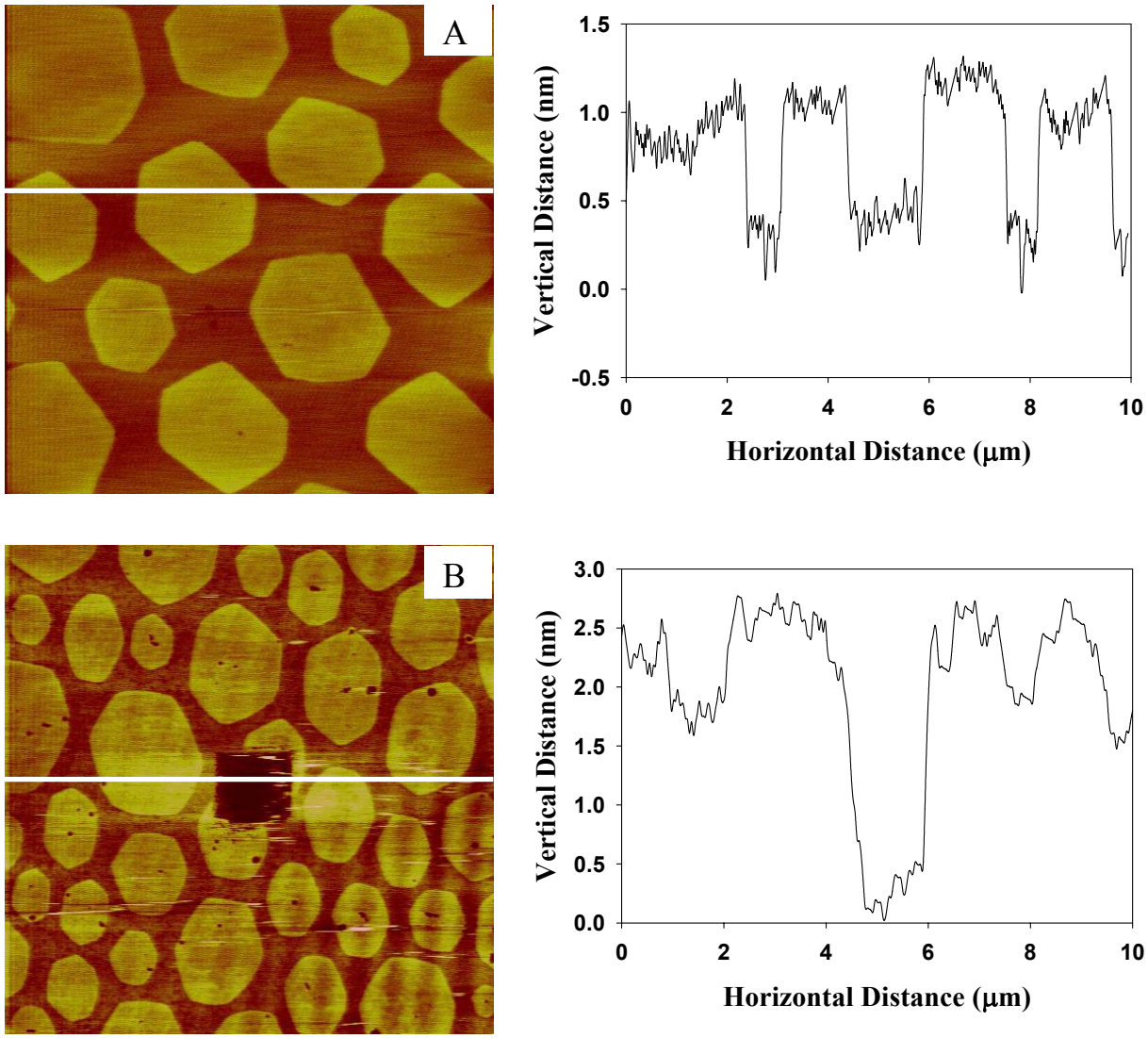

Figure 2-2. (A) AFM height mode image (10 μm x 10 μm) and corresponding cross-sectional analysis of 2:1 LB film deposited on mica. (B) Height mode image (10 μm x 10 μm) after scratching sample in air at high imaging force, and corresponding cross-sectional analysis of the scratched area. Images were measured in contact mode in air.

In addition to topographical imaging, the LB films were also analyzed via friction force imaging in air. Typical friction images (data collected from the forward 'trace' and backward 'retrace' portions of the scan) from an LB film are shown in Figure 2-3A, B. The difference in friction signal between the hexagonal domains and the surrounding continuous domain remains constant in the trace and the retrace image at ~30 mV. The image contrast reverses with the cantilever scan direction, indicating that the contrast can be attributed to friction differences between the two domains. In terms of overall contrast (Figure 2-3A represents the "true" friction contrast for our instrument's cantilever-detector configuration), the discontinuous domains show lower friction than the surrounding continuous domain. A number of other investigators have reported that hydrocarbon surfaces generally have lower friction than fluorocarbons[2, 3, 6, 8, 14]. On this basis, the friction measurements are entirely consistent with the topographical evidence that indicates the discontinuous domains are enriched in hydrocarbon. It is also worth noting that the friction images suggest the continuous domain is not entirely

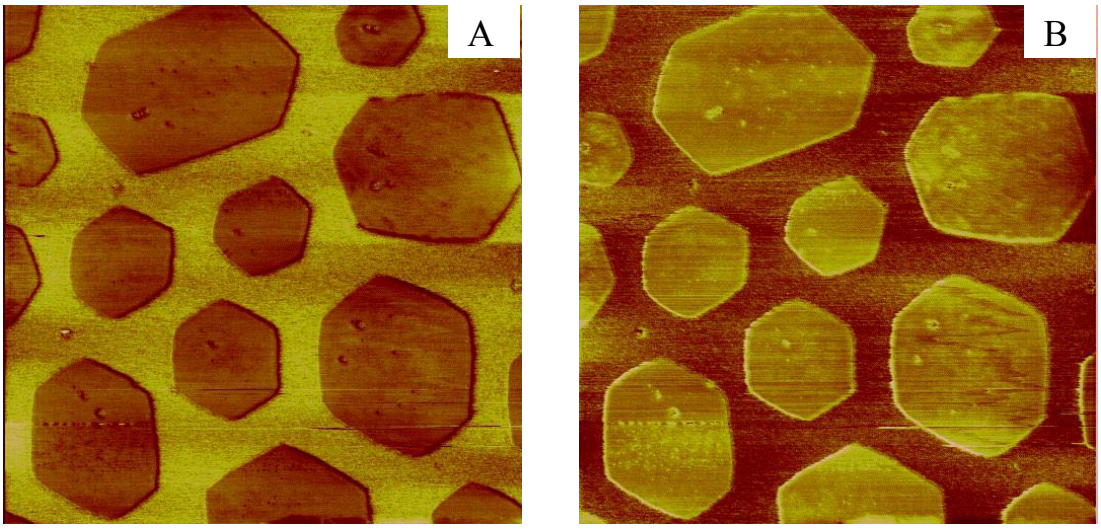

Figure 2-3. LFM friction image (10 μm x 10 μm) of 2:1 LB film measured in air (A) trace, (B) retrace.

homogeneous in composition. Closer inspection of the discontinuous domain in Figure 2-3A reveals contrast fluctuations that are not easily distinguished in the topographical images. Higher magnification images of these regions in air tended to result in smeared, poorly resolved images that were difficult to definitively analyze.

In order to gain greater insight into the composition of the continuous domain, as well as to definitively identify the composition of the discontinuous domain, a novel approach to compositional mapping in the AFM was devised. By incubating the LB film in a judiciously chosen solvent, it should be possible to preferentially dissolve one of the two amphiphilic components in the film, and by high-resolution topographic imaging in the solvent of choice, determine where the soluble component originated from. An additional benefit of this approach is that adhesion force measurements can also be used for chemical identification, as the capillary forces that make such measurements problematic in air will be negated by the presence of solvent. We note that while we have developed this approach independently, a similar methodology has previously been described by Ge et al.[15] to distinguish between physisorbed and chemisorbed organosilanes on a silicon substrate.

For the AA/PA system, we chose to incubate and image the film in n-hexadecane. From basic solubility studies, it was observed that solid PA was insoluble in n-hexadecane, and it seemed reasonable to expect AA to be at least partially soluble in an n-alkane solvent. After a three-hour incubation period in hexadecane contained inside the AFM fluid cell, samples were imaged using contact mode. An image of an LB film incubated and measured under n-hexadecane is shown in Figure 2-4, along with an appropriate cross-section. The basic film structure is still intact after incubation, that is, there are still well-defined discontinuous domains distributed uniformly over the sample. However, the discontinuous domains that were

previously higher than the continuous domain, have become lower after incubation. Cross-sectional analysis shows that the height difference between continuous and discontinuous domains in hexadecane is ~14 Å which is very close to the expected length of a PA molecule. In some experiments, the surface was imaged before the three-hour incubation period was over, and it was observed that the difference in height between the continuous and discontinuous domains increased with time until a constant height difference was reached. These combinations of results are consistent with the gradual desorption of AA from the film surface by the solvent. On the basis of these measurements, we can definitively identify the discontinuous domains as consisting almost entirely of AA.

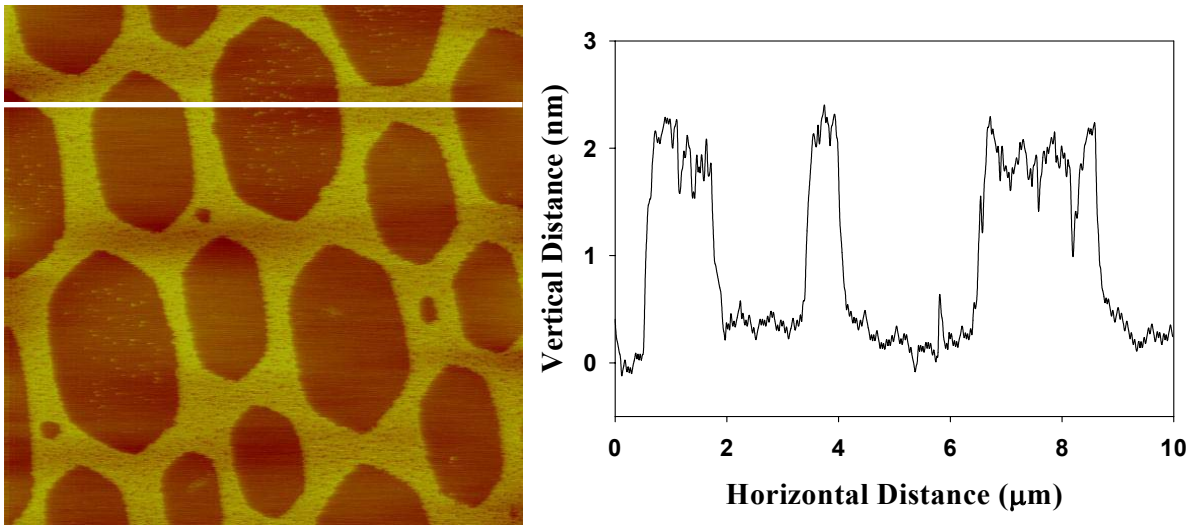

Figure 2-4. AFM height image (10 μm x 10 μm) of 2:1 LB film imaged in n-hexadecane and corresponding cross-sectional analysis.

Experiments were also carried out in which the same region of the sample was imaged before and after incubation in n-hexadecane (Figure 2-5), in order to detect if there was any significant re-ordering or spreading of the remaining PA into the voids left by the removal of AA. There was a negligible difference in the size of the original discontinuous domains and the void spaces after incubation, indicating that the remaining PA generally does not relax and "in-

fill" the new vacancies. Some small amount of re-ordering cannot entirely be ruled out, but extent to which it occurs is negligibly small.

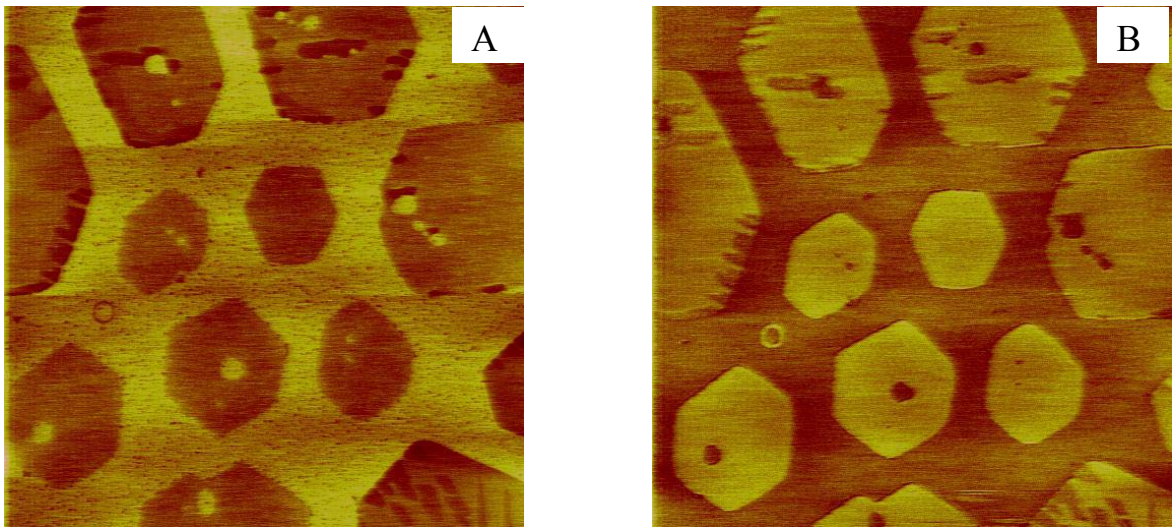

Figure 2-5. AFM height image (10 μm x 10 μm) of 2:1 LB film imaged in A, air; and its corresponding image B measured in n-hexadecane.

In addition to compositional identification of the discontinuous domains, these imaging experiments have also provided additional insight into the composition of the continuous domain. Imaging in n-hexadecane minimized much of the smearing and resolution loss that was encountered when imaging the continuous domain in air, allowing higher resolution topographic mapping of the surface. A high-resolution image of the continuous domain taken in n-hexadecane is shown in Figure 2-6. In these images, large numbers of nanometer-sized pits can be observed throughout the continuous domain. The depth of the pits is again comparable with the expected length of a PA molecule, indicating that the continuous domain, while predominately consisting of PA, also contains a substantial fraction of AA. By analyzing the relative area occupied by the nanometer-sized pits, we estimate that the continuous domain has a composition of ~13% AA and ~87% PA.

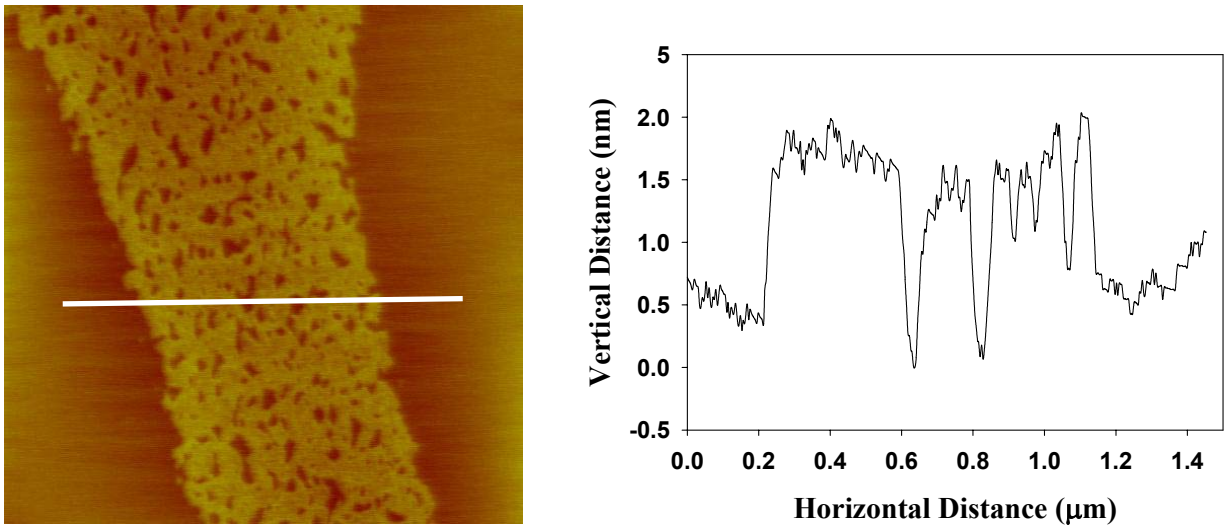

Figure 2-6. High resolution AFM height image (2μm x 2μm) of the continuous domain of 2:1 LB film imaged in n-hexadecane after a 3 hour incubation period, along with corresponding cross-sectional analysis.

As a final approach to mapping the composition of the LB film, adhesion force measurements between an unmodified Si_3N_4 probe tip and different regions of the sample were carried out. The tip-sample adhesion force was obtained from the retraction portion of an AFM force curve. Figure 2-7 shows a typical pair of retraction curves taken from both the discontinuous and continuous domains in n-hexadecane. The two different regions show markedly different adhesive forces, with the discontinuous domains exhibiting a very small force of adhesion compared to the continuous domain. As a calibration experiment, the force of adhesion for LB films of pure AA and PA on mica was measured after incubating in n-hexadecane for three hours, and these values were then compared with those measured for the different domains, including the nanometer-sized pits in the continuous domain. Adhesion force histograms for the pure films are shown in Figure 2-8A, B, and histograms for the different regions on the mixed films are shown in Figure 2-9A-C.

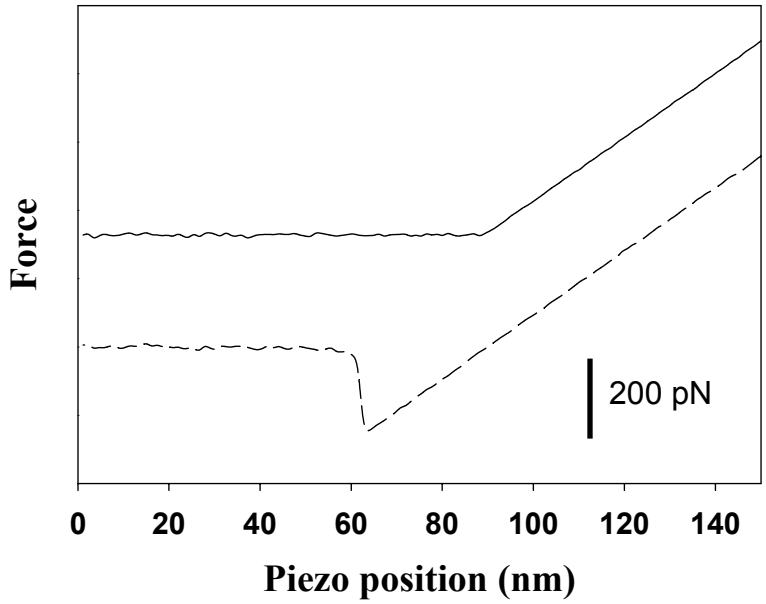

Figure 2-7. Tip retraction curves measured in n-hexadecane of 2:1 LB film. The dashed line shows a typical retraction curve collected for a pure PA film, and the solid line shows a retraction curve for the same tip with a pure AA film. The adhesion force (~200 pN) is given by the depth of the trough in the curve, as indicated by the vertical bar.

As seen in Figure 2-8, the surfaces prepared from pure AA and PA gave significantly different adhesion forces. For the pure AA film, the mean force of adhesion was 12±6 pN and for PA, approximately twenty times larger with a mean value of $2.4\pm0.8\times10^2$ pN (uncertainty ranges indicate the standard deviation of the measurements). Note, the lower limit of detection in our system is 3 pN, as determined by the standard deviation of the force signal measured at large tip-sample separations. We are reluctant to further interpret the shape of the histograms in too much detail - the AA histogram in particular does not follow simple Gaussian behavior- and will focus discussion on the mean values of adhesion force for this work. It is interesting to note, however, that while the mean adhesive force for the AA sample is quite different from that of the PA, it does not equal that for bare mica measured in n-hexadecane (measurements of freshly cleaved mica in n-hexadecane gave an average force of $2.4\pm0.9\times10^2$ pN). This is somewhat surprising, as the image data suggests that the solvent completely removes the AA from the mica

surface. The adhesion force measurements indicate that the situation is not so simple. It is possible that AA remains loosely associated with the surface, perhaps rapidly binding and unbinding during the course of the experiments. This effect might play a role in the unusual shape of the adhesion force histogram for pure AA.

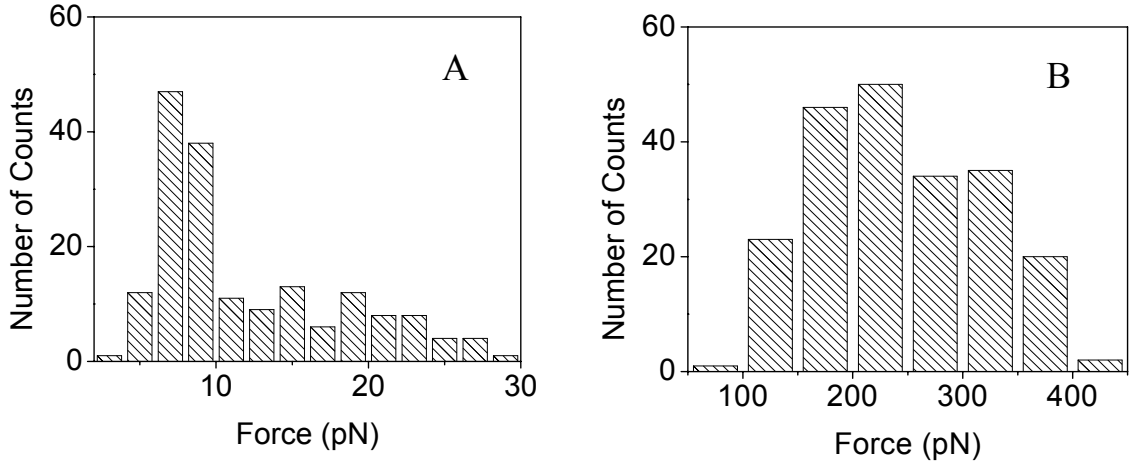

Figure 2-8. Histograms of tip-sample adhesion forces measured in n-hexadecane for (A) a pure AA film, and (B) a pure PA film.

Adhesion force measurements carried out on the discontinuous domains gave histogram shapes and mean adhesive forces that were comparable with those obtained for pure AA (Figure 2-8A). The mean adhesive force for the discontinuous domains was 10±4 pN, which is well within the uncertainty range determined for the pure AA sample. Measurements on the elevated regions of the continuous domain gave mean adhesive force of $2.0\pm0.5\times10^{2}$ pN, which again, compares well with value obtained from the pure film. Histogram shapes for the two were also comparable in terms of overall shape, indicating that the elevated regions consisted of PA. Measurements on the nanometer-sized pits in the continuous domain gave a value of $4\pm1\times10^{1}$ pN. This is approximately twice as large as the values measured for the pure AA sample, but this slightly higher value may be attributed to difficulties in the probe tip completely penetrating the

pits, or small fluctuations in tip position during the force curve collection process. In general, all of the adhesive force measurements agree with the topographic and friction force imaging, indicating that the discontinuous domains are composed of AA, and the continuous domains are primarily PA but with small deposits of AA inside.

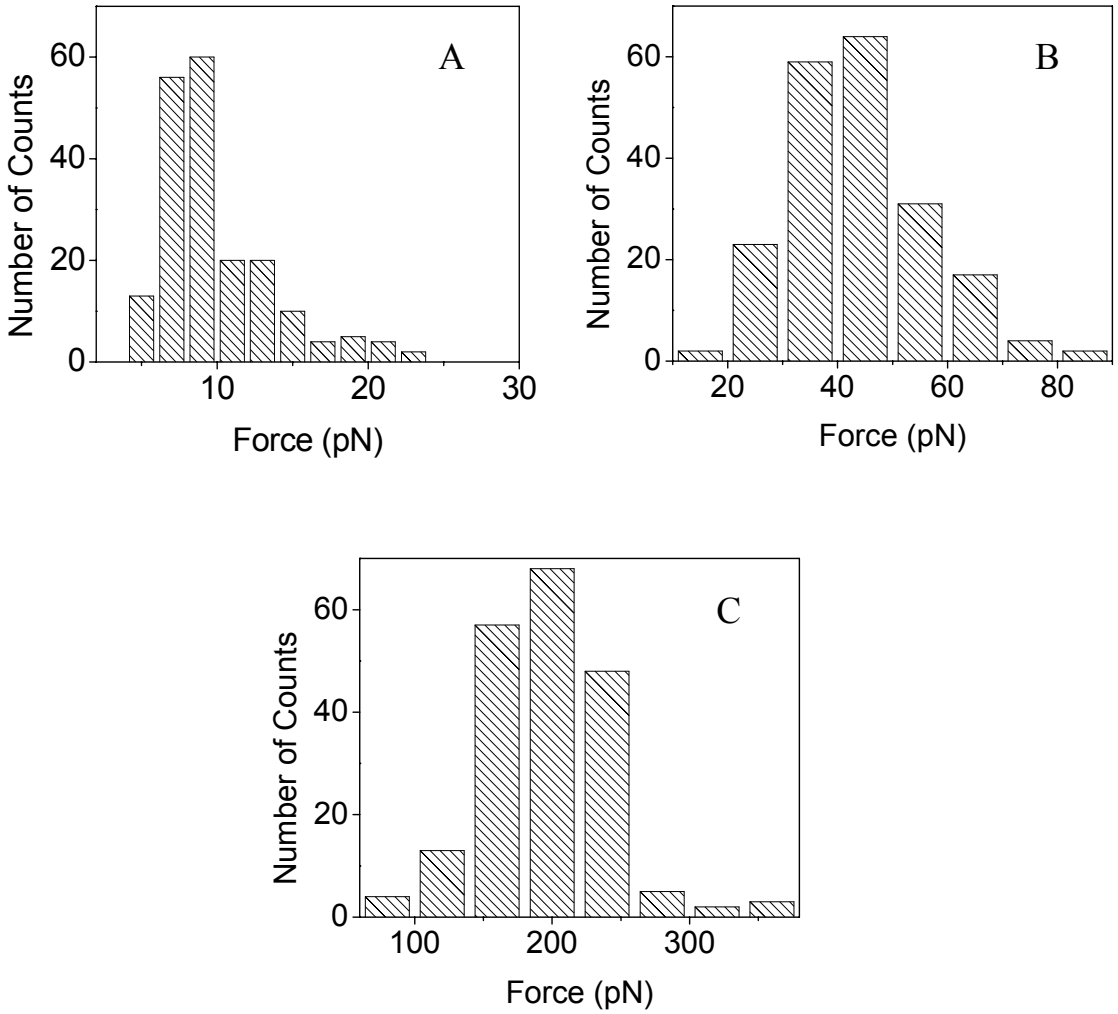

Figure 2-9. Histograms of tip-sample adhesion forces measured in n-hexadecane for different regions on a 2:1 LB film. (A) Discontinuous domains (B) Nanometer-size pits in continuous domain, (C) Elevated regions in the continuous domain.

While these measurements are, to our knowledge, the first reported values for the force of adhesion between a non-modified AFM tip and a perfluorinated surface in n-hexadecane, the

values for adhesive forces reported here are in good qualitative agreement for those obtained in a related system. Hayashi et al. have reported adhesion force measurements between a non-modified AFM tip and self-assembled monolayers terminated with CH_3 and CF_3 groups[16].

These authors reported that in both air and in vacuum, the force of adhesion between an AFM probe and a fluoroalkylsilane-treated Si substrate exceeded that for an alkylsilane treated surface. This difference was attributed to stronger electrostatic interactions between the highly electronegative fluorine atoms and the readily polarizable AFM tip. While the values observed by Hayashi (~40 nN and 26 nN for CF_3 and CH_3 terminated surfaces in air, respectively) are considerably larger than those observed in this work, the same general qualitative trend was observed. Differences in absolute values of adhesion forces can be attributed to the elimination of capillary forces because of the n-hexadecane solvent, as well as differences in the exact chemical nature of the groups used to functionalize the surface.

The approach of selective, in situ dissolution of one component of the mixed LB film has proven to be a useful one, and has great potential for use in AFM-based compositional mapping of a variety of systems. The main challenge to using this approach will be in selecting a solvent that will selectively remove one component over another. However, if this challenge can be met, then two of the major assets of AFM measurements, that of high-resolution imaging in liquids and high-sensitivity force measurements can be used with great facility.

2.5 Conclusions

In summary, this paper describes the structural and compositional mapping of a phase-separated LB monolayer film of perfluorotetradecanoic acid and arachidic acid. Under appropriate deposition conditions, the two amphiphiles phase-separate to form films consisting of hexagonal, discontinuous domains surrounded by a continuous domain. A combination of

high-resolution AFM topography imaging and friction imaging suggests that the discontinuous domains are rich in hydrocarbon, while the surrounding continuous domain is rich in perfluorocarbon. This has been verified by a new approach to compositional mapping in AFM, that of selective dissolution of one component through careful selection of solvent. High-resolution imaging of the sample after selective dissolution, followed by adhesive force measurements verify the composition of the film, though it was also found that the continuous domain contained nanometer-sized deposits of hydrocarbon in addition to perfluorocarbon.

2.6 Acknowledgements

Funding for this work was provided by the Natural Sciences and Engineering Research Council of Canada (NSERC), the Canada Foundation for Innovation (CFI), the Province of Saskatchewan and by the University of Saskatchewan. We also extend our gratitude to J. Valiani and Adam Leontowich for their useful comments and assistance.

2.7 References

1. Qaqish, S. E.; Paige, M. F., *Langmuir* **2007,** 23 (5), 2582-2587.
2. Matsumoto, M.; Tanaka, K.; Azumi, R.; Kondo, Y.; Yoshino, N., *Langmuir* **2003,** 19 (7), 2802-2807.
3. Overney, R. M.; Meyer, E.; Frommer, J.; Guntherodt, H. J.; Fujihira, M.; Takano, H.; Gotoh, Y., *Langmuir* **1994,** 10 (4), 1281-1286.
4. Matos, L.; Ravey, J. C.; Serratrice, G., *J. Colloid Interface Sci.* **1989,** 128 (2), 341-347.
5. Matsumoto, M.; Tanaka, K.; Azumi, R.; Kondo, Y.; Yoshino, N., *Chemistry Letters* **2002,** (10), 970-971.
6. Imae, T.; Takeshita, T.; Kato, M., *Langmuir* **2000,** 16 (2), 612-621.
7. Jacobi, S.; Chi, L. F.; Fuchs, H., *J. Vac. Sci. Technol. B* **1996,** 14 (2), 1503-1508.
8. Overney, R. M.; Meyer, E.; Frommer, J.; Brodbeck, D.; Luthi, R.; Howald, L.; Guntherodt, H. J.; Fujihira, M.; Takano, H.; Gotoh, Y., *Nature* **1992,** 359 (6391), 133-135.
9. Matsumoto, M.; Tanaka, M.; Azumi, R.; Manda, E.; Tachibana, H.; Kondo, Y.; Yoshino, N., *Molecular Crystals and Liquid Crystals Science and Technology Section a-Molecular Crystals and Liquid Crystals* **1997,** 294, 31-34.
10. Noy, A.; Vezenov, D. V.; Lieber, C. M., *Annu. Rev. Mat. Sci.* **1997,** 27, 381-421.

11. Takano, H.; Kenseth, J. R.; Wong, S. S.; O'Brien, J. C.; Porter, M. D., *Chemical Reviews* **1999,** 99 (10), 2845-2890.
12. Noy, A.; Frisbie, C. D.; Rozsnyai, L. F.; Wrighton, M. S.; Lieber, C. M., *Journal of the American Chemical Society* **1995,** 117 (30), 7943-7951.
13. Jang, S. S.; Blanco, M.; Goddard, W. A.; Caldwell, G.; Ross, R. B., *Macromolecules* **2003,** 36 (14), 5331-5341.
14. Fang, J. Y.; Knobler, C. M., *Langmuir* **1996,** 12 (5), 1368-1374.
15. Ge, S. R.; Takahara, A.; Kajiyama, T., *Langmuir* **1995,** 11 (4), 1341-1346.
16. Hayashi, K.; Sugimura, H.; Takai, O., *Applied Surface Science* **2002,** 188 (3-4), 513-518.

CHAPTER 3
DETERMINATION OF THE TWO-DIMENSIONAL CRYSTAL LATTICE OF ARACHIDIC ACID IN A PHASE-SEPARATED LANGMUIR-BLODGETT MONOLAYER BY ATOMIC FORCE MICROSCOPY

This is an unpublished work carried out to determine the molecular level organization of AA molecules in the micron scale hexagonal structures described in the previous Chapter (2). AA forms hexagonal domains that phase-separate from PA in the mixed films. It has previously been reported in the literature that the 2D crystals grow in a hexagonal shape on LB films when the amphiphiles organize in a hexagonal crystal lattice. The underlying molecular organization and packing in the monolayer is related to the structures formed on the solid substrate. This work is aimed at examining whether this is applicable to our system, where the micron sized hexagonal domains of AA are related to the AA molecular packing. This chapter describes molecular level AFM imaging measurements of the AA unit cell packing in the monolayer. A comparison between the molecular arrangement of AA and that of mica, the underlying substrate, has been carried out.

For this work, I prepared samples, performed the measurements, and played a major role in interpreting the results and the preparation of this chapter. My supervisor provided guidance throughout the experimental work and results interpretation and was involved in editing this chapter.

3. Determination of the two-dimensional crystal lattice of arachidic acid in a phase-separated Langmuir-Blodgett monolayer by atomic force microscopy

Shatha E. Qaqish and Matthew F. Paige

Department of Chemistry, University of Saskatchewan, 110 Science Place, Saskatoon, Saskatchewan, Canada S7N 5C9

3.1 Abstract

The two-dimensional (2D) unit cell of arachidic acid $C_{19}H_{39}COOH$ (AA) molecules in a phase-separated, mixed Langmuir-Blodgett (LB) monolayer of AA, and perfluorotetradecanoic acid $C_{13}F_{27}COOH$ (PA) was measured using atomic force microscopy (AFM) imaging in air. The molecular level measurements by AFM imaging of AA / PA mixed LB film show that AA molecules are packed in a 2D oblique lattice. The ordering of the AA molecules in this particular lattice is one of the factors that results in the formation of the hexagonal domains observed in the mixed AA / PA films. The 2D lattice parameters are (0.45 ± 0.04 nm and 0.59 ± 0.04 nm). This lattice structure is different from that of mica which has a 2D hexagonal lattice with lattice spacing of 0.55 ± 0.04 nm and 0.51 ± 0.06.

3.2 Introduction

LB films have numerous applications that arise from the molecular level organization of the amphiphiles and their perfect layering. These applications are in the field of optics[1], biological sensing[2], and membrane modeling[2]. LB films have been used as model systems to study 2D phenomena because of the arrangement of the molecules in a regular manner compared to micelles or random distribution in the bulk. It has been noted that the organization of these

films at molecular levels plays an important role in determining the structure obtained at the micron length scale[3].

A number of studies have focused on determining the degree of molecular order in Langmuir and LB films of fatty acids, because of the importance of the molecular level organization and its role in determining the surface structure. Several techniques have been used to investigate molecular ordering, including near edge x-ray absorption fine structure (NEXAFS)[4], x-ray diffraction[5] and polarization modulation infrared spectroscopy[6].

Recently, the atomic force microscope and the scanning tunneling microscope have been used to investigate the 2D lattice and the ordering in thin films through scanning at molecular resolution. Atomic force microscopy (AFM) has been widely used to measure monolayers and multilayers on different surfaces because of its advantage over scanning tunneling microscopy (STM) which is limited to measurements of conductive surfaces[7]. AFM is very surface sensitive; it measures only the atoms located at the interface with high lateral resolution < 0.1 nm[8]. Because of these properties, AFM has been used to measure the 2D lattice of different films and solid surfaces even in liquid, for example [9].

LB films of AA and its salts have been widely studied through molecular scale AFM imaging in order to determine their lattice parameters and their 2D unit cell. Bourdieu et al.[10] were the first to measure a bilayer of AA deposited from a 10^{-4} M $BaCl_2$ sub-phase using AFM. They observed a distorted hexagonal lattice of the bilayer. This distortion was explained to be either an intrinsic structural property of the bilayer or a tip induced structure. Several years later, Schwartz and co-workers[8] investigated by AFM imaging the structure of multilayers of cadmium arachidate salt deposited from a 10^{-4} M $CdCl_2$ sub-phase. They reported the formation of a 2D rectangular lattice of AA in these multilayers, and also investigated the reorganization of the

molecules of AA into multilayers[11]. They found that hexagonal packing geometry of AA molecules was dominant in a monolayer, whereas reorganization into a herringbone packing took place in multilayers. Evensen et al.[12] studied the effect of the deposition pressure on the molecular arrangement of AA multilayers in LB films. They reported a 2D oblique unit cell in these films and they found that the unit cell dimensions increased as the deposition pressure decreased. This was explained by an increase in the tilt of the alkyl chain with respect to the substrate as the deposition pressure decreases.

It has previously been reported in the literature that the 2D crystal growth yields 2D hexagonal structures on LB films when the amphiphiles take a hexagonal crystal lattice[3]. The underlying molecular organization and packing in the monolayer is related to the structures formed on the solid substrate. These micron sized hexagonal structures in LB films were observed in some mixed-surfactant monolayers including AA with the partially fluorinated compound heptadecafluorononadecanoic acid ($CF_3(CF_2)_7(CH_2)_{10}COOH$)[3], and octadecanesulfate ($SHCH_2(CH_2)_{16}COOH$) with perfluorononanoic acid ($CF_3(CF_2)_7COOH$)[13].

The purpose of this study is to investigate if the micron-sized hexagonal domains observed in the mixed AA / PA LB films have hexagonal packing at the molecular level, since this correlation was reported previously in other systems[3]. In this work, AFM measurements on a monolayer of 2AA:1PA at molecular resolution were performed. Analysis of the images showed that AA molecules are packed in a 2D oblique lattice with cell dimensions that agree with the previously reported values of the oblique lattice of AA in the literature[12]. As a control experiment, a comparison of the AA lattice structure with that of mica was performed, and revealed significant differences between the two (mica has a hexagonal lattice). This suggests that the unit cell observed of the mixed film of AA / PA is related to the molecular packing of

AA and not the underlying mica substrate and that the AA film was not removed from the substrate during imaging measurements.

3.3 Experimental

3.3.1 Chemicals

Arachidic acid (99%) and perfluorotetradecanoic acid (97%) were purchased from Sigma-Aldrich Corporation. Hexanes (HPLC grade) and tetrahydrofuran (THF) were purchased from EMD and Merck EM Science, respectively. Mica was purchased from SPI (Structure Probe Inc., West Chester, PA), and was freshly cleaved with adhesive tape prior to use.

3.3.2 Langmuir-Blodgett film deposition

LB films were prepared using a KSV 2000 Langmuir trough system (KSV Instruments, Helsinki, Finland), with ultrapure water (Millipore, resistivity 18.2 MΩ·cm) as a sub-phase. Stock solutions of 8.4×10^{-3} M of AA and 5.1×10^{-3} M of PA were prepared in a 9:1 volume ratio of hexanes:THF. The solutions were combined to give a 2:1 mole ratio mixture of AA and PA, respectively. Before each measurement the sub-phase surface was cleaned by vacuum suction and the platinum Wilhelmy plate was cleaned by flaming in a propane torch. The deposition experiments were performed as described previously[14] by spreading a 30 μL aliquot of the 2AA:1PA mixture on the sub-phase at 20.6 ºC and waiting 10 min for solvent evaporation. Film deposition was carried out at a surface pressure of 30 $mN.m^{-1}$ and at a rate of barrier compression of 10 $mm.min^{-1}$ until reaching the desired surface pressure, at which point it was changed to 5 mm min^{-1} to match the substrate withdrawal rate from the sub-phase. The sub-phase temperature was controlled by water circulation through the trough's external jacket from a Haake K F3 water bath (Haake, Berlin, Germany). Sub-phase surface temperature was monitored throughout the experiment with a thermocouple, and was kept constant to within ± 0.5 ^{o}C.

3.3.3 Atomic force microscope measurements

AFM measurements were carried out on a Multimode system equipped with an E scanner (Veeco Metrology Group, Santa Barbara, CA). Measurements were done in air in contact mode using commercial silicon nitride AFM probes (Veeco Metrology Group, Santa Barbara, CA) with nominal spring constant of 0.58 $N.m^{-1}$. Image analysis was carried out with either Nanoscope version 6.13 (Veeco Metrology Group, Santa Barbara, CA) or ImageJ[15]. As was noted in a previous publication, the samples could be imaged repeatedly (using either tapping or contact mode) without causing tip-induced damage.[14] The tip was engaged normally to the surface, and once a good large-scale (10 μm × 10 μm) image was obtained, the microscope was zoomed into the middle of one of the hexagonal domains. The final scan size was 5 nm × 5 nm and the scan rate was 30 Hz with an image resolution of 256 samples / line. The integral and the proportional gains were set to 2.5 and 2.0, respectively. Tapping mode AFM measurements were carried out on a Dimension Hybrid Nanoscope system (Veeco Metrology Group, Santa Barbara, CA). The microscope was mounted in an acoustic-vibration isolation system. Commercial silicon AFM probes with nominal spring constant of (12-130) N m^{-1} and nominal resonance frequency ~330 kHz were used for tapping mode measurements in air.

3.4 Results and discussion

Using molecular level AFM imaging, the 2D unit cell in which AA molecules are packed in the mixed AA / PA film was measured. Figure 3-1A shows an AFM height mode image (20 μm × 20 μm) of a 2AA:1PA LB film. A height mode image (5 nm × 5 nm) is shown in Figure 3-1B. A 2D periodic structure at molecular resolution was observed. Rows of molecules were observed at ~ 45 º to the horizontal and intersect with each other forming a 2D lattice. All measurements were directly extracted from the AFM image (Figure 3-1B) without digital

filtering beyond simple image flattening. The measurements of the distance between the elevated domains in Figure 3-1B agreed with what literature values for unit cell dimensions for closely related systems. This suggests that Figure 3-1B is a real molecular level image of the LB film. Before obtaining Figure 3-1B, a larger scale image (Figure 3-1A) was obtained to ensure that the tip was in contact with the surface during scanning and the image was real.

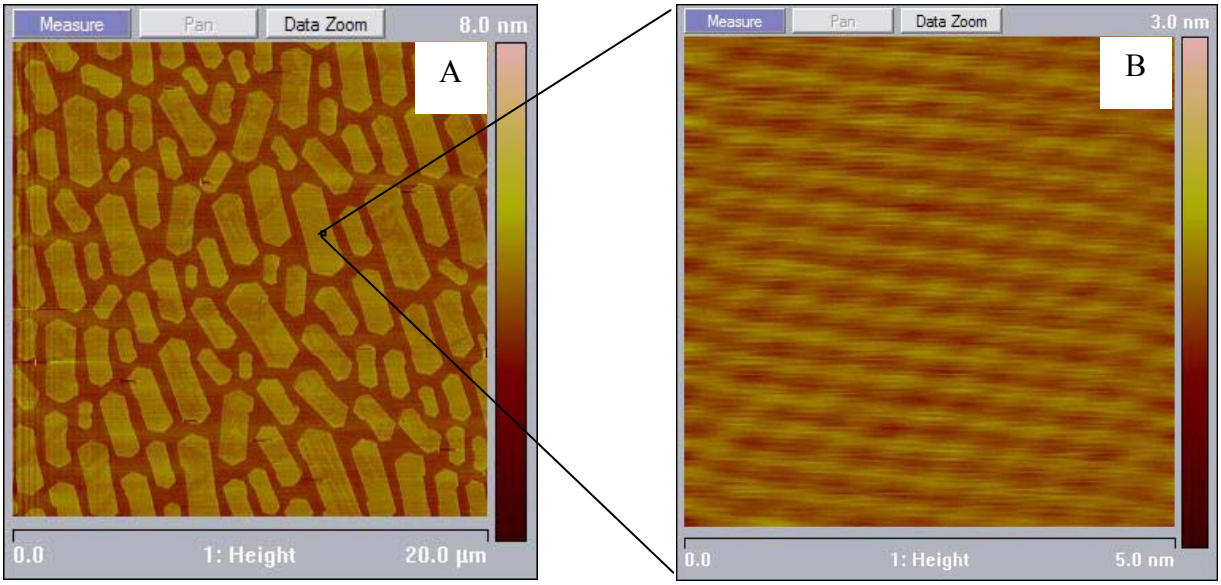

Figure 3-1. AFM height mode images of 2AA:1PA LB film in air. A, tapping mode with scan size 20 µm × 20 µm; B, contact mode with scan size 5 nm × 5 nm.

The distances between nearest-neighbor molecules X and Y in the unit cell, as shown in Figure 3-2, were measured for the AFM image of the AA molecules (Figure 3-1B). It was found that X = 0.59 ± 0.04 nm and Y = 0.45 ± 0.04 nm and $\gamma = 126 \pm 6^{\circ}$. Since $X \neq Y$ and $\gamma \neq 90^{\circ}$, this suggests that AA molecules are arranged in an oblique lattice[16]. The analysis was done by choosing three atoms for every measurement and connecting them by vectors whose lengths and the angle in between can be measured directly using ImageJ[15]. At least twenty different sets of atoms were analyzed and the error range cited above represents the standard deviation of these measurements. As shown in Figure 3-2, in the oblique lattice, $X \neq Y$ and $\gamma \neq 90^{\circ}$. For the

hexagonal lattice, X = Y and $\gamma = 120^{o}$ [16]. The difference in the relative values of X and Y and the angle γ are the main parameters that determine the structure of the 2D lattice and the unit cell.

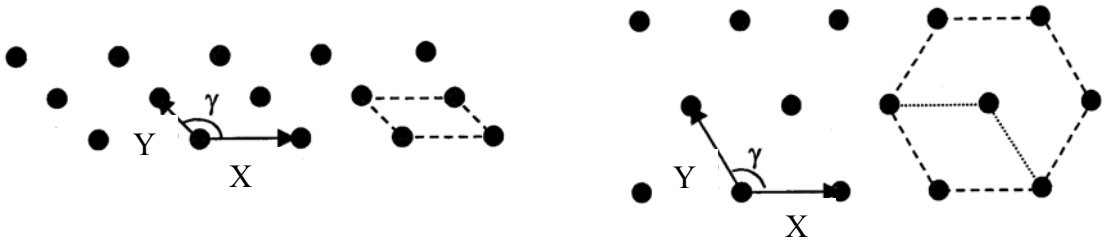

Figure 3-2. 2D arrangement of the molecules in the unit cell. Left, 2D oblique crystal lattice; right, 2D hexagonal crystal lattice. The parameters a and b and the angle γ are assigned.[16]

For comparison purposes, both a_0 and b_0 (the unit cell dimensions - Figure 3-3) were calculated: $a_0 = 0.46 \pm 0.04$ nm and $b_0 = 0.89 \pm 0.07$ nm. These values agree well with those obtained for a monolayer of cadmium arachidate deposited from water sub-phase of pH 7 (a_0 = 0.477 nm and b_0 = 0.826 nm)[17]. The authors suggested that AA molecules in the monolayer were organized in a hexagonal lattice. Iimura et al. showed that under appropriate pH, the floating cadimuim arachidate monolayer had an orthorhombic unit cell[6]. In a separate study, Evenson et al. studied 12-layer AA LB films and obtained an oblique structure with values of a_0 and b_0 that are close to the values measured here within experimental error ($a_0 = 0.58 \pm 0.07$ nm and b_0 = 0.79 ± 0.03 nm)[12]. The authors found that by changing the surface pressure of deposition ranging between 20 – 50 $mN.m^{-1}$, the crystal lattice did not change but the lattice parameters (a_0 and b_0) changed. This was attributed to the tilt in the AA chains on the substrate surface when the surface pressure decreases.

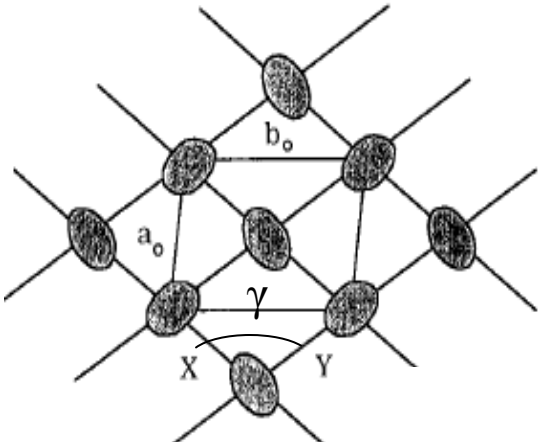

Figure 3-3. Schematic diagram of the LB film surface showing the oblique crystal lattice. The values a_0 and b_0 are indicated, as well as the distance between the nearest-neighbor molecules X and Y and the angle γ[12].

To ensure that what was measured in Figure 3-1 was the 2D lattice of AA and not the underlying substrate mica, an AFM image of mica measured at the molecular level (Figure 3-4) was obtained from Veeco (the manufacturer company of AFM in Santa Barbara, CA). The analysis of the 2D mica lattice shows that $a_0 = 0.50 \pm 0.05$ nm and $b_0 = 0.94 \pm 0.06$ nm. The values for both mica and AA are the same within the experimental error. This indicates that both mica and AA molecules are ordered in a similar 2D lattice. Whether the 2D crystal structure is hexagonal[17], rectangular[8] or oblique[12], there is no difference between a_0 and b_0 values within experimental error. The crystal lattice dimensions of mica are $X = 0.55 \pm 0.04$ nm and $Y = 0.51 \pm 0.06$ nm and $\gamma = 121 \pm 7^{\circ}$. These measurements suggest that mica has a 2D hexagonal lattice where X = Y and $\gamma = 120^{\circ}$ [16]. These values are in agreement with those previously reported of mica that every 0.52 nm the molecule is repeated[9]. The difference in the 2D lattice between mica and AA, in terms of X, Y and γ values, indicates that what was measured in the LB film was different than mica. AA molecules form a 2D oblique lattice whereas mica has a 2D hexagonal lattice.

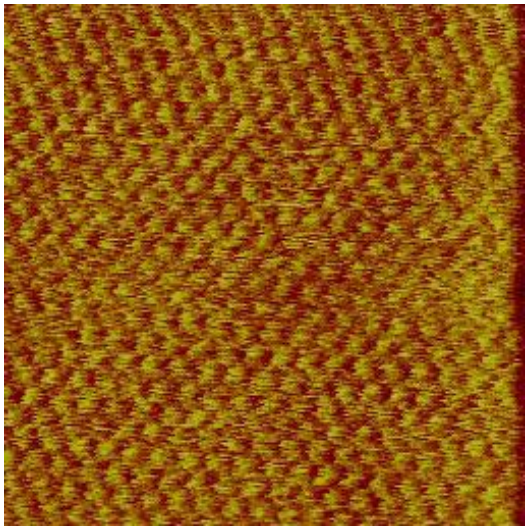

Figure 3-4. AFM deflection mode image of mica at molecular level. Scan size 10 nm × 10 nm. This image was obtained from Veeco (the manufacturer company of AFM in Santa Barbara, CA).

The molecular arrangement of AA, in the micron sized hexagonal domains, in an oblique crystal lattice agrees with what was suggested in the literature that the micron sized hexagonal domains sometimes had a hexagonal lattice[3]. The formation of micron scale hexagonal domains in mixed LB films is not unique to AA molecules[3]. Liu et el. observed these structures in a mixed film of octadecanesulfate ($SHCH_2(CH_2)_{16}COOH$) and perfluorononanoic acid ($CF_3(CF_2)_7COOH$)[13]. In the mixed LB film of palmitic acid $CH_3(CH_2)_{14}COOH$ and perfluorooctadecanoic acid $CF_3(CF_2)_{16}COOH$, hexagonal domains were formed on the surface as discussed in Chapter 7. These structures were observed in other hydrocarbon / fluorocarbon systems such as behenic acid ($CH_3(CH_2)_{18}COOH$) / PA mixed LB films and stearic acid ($CH_3(CH_2)_{16}COOH$) / perfluorooctadecanoic acid as discussed in Chapter 8.

The hexagonal domains that form on the surface of an LB film of AA / PA has an underlying oblique lattice arrangement of AA molecules. However, while there is a general correlation between having an oblique lattice and larger-scale hexagonal domains, additional factors affect the structure formed on the LB films. Some of these factors are discussed in

Chapter 4 of this thesis. Briefly, a major factor is competition between the forces of interaction between the molecules in terms of line tension and dipole interactions. In addition, the domains are affected by the flow of the water sub-phase and are oriented by it. Other factors include temperature, surface pressure, and annealing time (the time at which the monolayer spends on the sub-phase before compressing the film).

3.5 Conclusions

In this work, the lattice spacing and the unit cell of AA in the mixed LB films of AA / PA were measured. The 2D lattice of AA molecules was obtained by AFM measurements at the molecular level. Unit cell dimensions measurements showed that AA molecules adopted a 2D oblique lattice, which is different than that of mica, the underlying substrate, which has a hexagonal lattice of different dimensions. The micron size hexagonal domains have an oblique lattice of AA molecules.

3.6 Acknowledgements

Funding for this work was provided by the Natural Sciences and Engineering Research Council of Canada (NSERC), the Canada Foundation for Innovation (CFI), the Province of Saskatchewan and by the University of Saskatchewan. Professor P. Ming Huang and Dr. Ailsa Hardie in the department of soil science are acknowledged for access to use the multimode AFM.

3.7 References

1. Khanarian, G., *Thin Solid Films* **1987,** 152, 265.
2. Frommer, J.; Luthi, R.; Meyer, E.; Anselmetti, D.; Dreier, M.; Overney, R.; Guntherodt, H. J.; Fujihira, M., *Nature* **1993,** 364 (6434), 198.
3. Abe, M.; Scamehorn, J. F., *Mixed Surfactant Systems*. Marcel Dekker: New York, 2005.
4. Fujimori, A.; Sugita, Y.; Nakahara, H.; Ito, E.; Hara, M.; Matsuie, N.; Kanai, K.; Ouchi, Y.; Seki, K., *Chem. Phys. Lett.* **2004,** 387, 345.

5. Barton, S. W.; Thomas, B. N.; Flom, E. B.; Rice, S. A.; Lin, B.; Peng, J. B.; Ketterson, J. B.; Dutta, P., *J. Chem. Phys.* **1988,** 89 (4), 2257.
6. Ren, Y.; Iimura, K.; Kato, T., *J. Chem. Phys.* **2001,** 114, 6502.
7. Skoog, D.; Holler, F.; Nieman, T., *Principles of Instrumental Analysis*. Harcourt Brace & Company: Florida, 1998.
8. Schwartz, D.; Garnaes, J.; Viswanathan, R.; Chirvolu, S.; Zasadzinski, J., *Phys. Rev. E* **1993,** 47 (1), 452.
9. Fukuma, T.; Kobayashi, K.; Matsushige, K.; Yamada, H., *Appl. Phys. Lett.* **2005,** 87, 034101.
10. Bourdieu, L.; Silberzan, P.; Chatney, D., *Phys. Rev. Lett.* **1991,** 67 (15), 2029.
11. Schwartz, D. K., *Annu. Rev. Phys. Chem.* **2001,** 52, 107.
12. Evenson, S.; Badyal, J.; Pearson, C.; Petty, M., *J. Phys. Chem.* **1996,** 100, 11672.
13. Zhu, B.; Zhang, P.; Wang, L.; Liu, Z., *J. Colloid Interface Sci.* **1997,** 185, 551.
14. Qaqish, S. E.; Paige, M. F., *Langmuir* **2007,** 23 (5), 2582.
15. Rasband, W. S. *Imagej*, 1.37v; U.S. National Institute of Health: Bethesda, Maryland, USA, 1997-2005.
16. Peng, J. B.; Barnes, G. T.; Gentle, I. R., *Adv. Colloid Interface Sci.* **2001,** 91 (2), 163.
17. Takamoto, D.; Aydil, E.; Zasadzinski, J.; Ivanova, A.; Schwartz, D.; Yang, T.; Cremer, P., *Science* **2001,** 293, 1292.

CHAPTER 4
MECHANISTIC INSIGHT INTO DOMAIN FORMATION AND GROWTH IN A PHASE-SEPARATED LNAGMUIR-BLODGETT MONOLAYER

This chapter is a slightly modified copy of an article published in *Langmuir* in July 2007. (Reproduced with permission from *Langmuir* **2007**, 23, 10088-10094. Copyright 2007 American Chemical Society)

In the previous Chapters (2-3), the LB film of AA/PA was fully characterized as an example of a phase-separated, mixed monolayer of hydrocarbon / fluorocarbon. In addition to their wide applications as discussed previously, mixed LB films are good examples to study phase-separation. Little is known about the mechanism of phase-separation in these monolayers. In this chapter, the mechanism of phase-separation and domain growth and the factors affecting it in the LB film of AA/PA is determined through AFM imaging.

For this purpose, deposition conditions were varied in terms of sub-phase temperature, mechanical agitation of the surfactant solutions, surface pressure at which the deposition takes place, and incubation time (the time that the film spends on the sub-phase before compression). We found that Ostwald ripening is the mechanism by which the domains grow upon phase-separation. This chapter highlights the major deposition factors that control the pattern formation in these LB films.

For this research paper, I prepared samples, performed the measurements, and played a major role in interpreting the results and the preparation of the paper. My supervisor provided guidance throughout the experimental work and was involved in result interpretation and in editing this paper.

4. Mechanistic Insight into Domain Formation and Growth in a Phase-Separated Langmuir-Blodgett Monolayer

*Shatha E. Qaqish and Matthew F. Paige**

Department of Chemistry, University of Saskatchewan, 110 Science Place, Saskatoon, SK. Canada S7N 5C9

Received May 15, 2007. In final form: July 17, 2007

4.1 Abstract

The mechanism of formation and growth of phase-separated domains in mixed arachidic acid ($C_{19}H_{39}COOH$) (AA) and perfluorotetradecanoic acid ($C_{13}F_{27}COOH$) (PA) monolayer films was investigated through a combination of surface pressure-area isotherm measurements and Atomic Force Microscope (AFM) imaging. In the mixed AA-PA monolayer system, distinct discontinuous domains consisting primarily of AA form spontaneously in a surrounding continuous matrix enriched in PA. By varying monolayer deposition conditions, including temperature, surface pressure and mechanical agitation of sample solutions, it was determined that phase-separated nuclei are formed initially in the bulk sample solution, and further growth of domains proceeds on the sub-phase surface via an Ostwald ripening process involving diffusion of AA from the matrix to the discontinuous domains. In addition, selective dissolution of the arachidic acid followed by in situ AFM imaging has allowed visualization of the fusion of AA to the phase-separated domains and highlighted some unusual pattern formation that occurs at low sub-phase temperatures.

4.2 Introduction

Surface films and coatings that contain fluorinated molecules are of significant current interest and application in modern surface science. A host of desirable mechanical and chemical properties are associated with fluorinated surfaces, including low mechanical friction, as well as chemical and thermal inertness to name a few.[1-3] Of particular recent interest in this field has been the phase behavior of mixed perfluorocarbon and hydrocarbon amphiphiles at the air-water and solid-air interfaces.[1, 2, 4-10] Langmuir and Langmuir-Blodgett (LB) films of these mixtures can, under appropriate conditions, exhibit phase-separation between the two different types of amphiphiles. Phase-separation in these systems can generally be attributed to the weak intermolecular van der Waals attraction between perfluorinated molecules coupled with their highly lipophobic nature.

The majority of studies involving phase-separation in mixed perfluorocarbon-hydrocarbon systems have been directed towards determining the structure and chemical composition of the separated domains.[1, 2, 4-11] A good example of a phase-separating system that has been investigated in this way is the binary mixture of arachidic acid ($C_{19}H_{39}COOH$) (AA) and perfluorotetradecanoic acid ($C_{13}F_{27}COOH$) (PA). Langmuir and mica-supported LB films of the AA-PA mixture have been characterized by Imae[7] with a combination of surface pressure-area isotherms and AFM imaging. These authors reported phase-separation of the two components, and postulated that the deposited films consisted of domains that are rich in AA, surrounded by a continuous domain rich in PA. However, definitive proof of this assignment via AFM imaging was problematic because of very rough topographical features in their samples. For the same system, Matsumoto et al.[1] determined, through careful IR measurements, that the molecular axes of AA and PA were almost perpendicular to the film surface. In addition, AFM

topography and friction imaging allowed the authors to infer that the domains were enriched in hydrocarbon. Recently, Qaqish et al.[10] have definitively determined the composition of both the continuous and phase-separated domains in mica supported LB films through a combination of AFM-based measurements. Of particular note in this study was an experimental approach in which one component of the mixed LB film was dissolved in a solvent, leaving the other component behind (selective dissolution). This allowed high-resolution compositional mapping of the LB film to be carried out by observing voids left by the soluble component. Using this approach it was found that the discontinuous domains of the phase-separated LB films consisted almost entirely of AA whereas the surrounding continuous domain was mostly PA but contained many small deposits of hydrocarbon.

While significant effort has gone into structural and compositional mapping of these phase-separated systems, the detailed mechanisms by which the lateral structuring of domains takes place are less well understood. Understanding the mechanism of lateral domain formation is a desirable research goal, as it may ultimately lead to controllable patterning of fluorinated surfaces at the micrometer and nanometer length scales. Several authors have attempted to gain insight into this topic by observing the effect of various experimental parameters on domain structure. Iimura et al.[6] have examined the effect of different deposition (sub-phase) temperatures and alkyl chain length on domain structures for mixtures of the cadmium salts of n-alkyl fatty acids and perfluoropolyethers. It was observed that for these systems, the domain structures varied systematically over the parameter space explored. In particular for the cadmium salt of AA, Iimura observed a significant increase in the size of domains when the deposition temperature was increased above a boundary temperature, whose value depends on the surfactant used, along with a decreasing number of domains. The phenomena were explained in terms of

competition between line-tensions at the boundary between the different phases and repulsive forces that exist between the surfactants. In a related study, Matsumoto et al. have investigated the domain structures formed in phase-separated alkyl surfactant-perfluorosilane LB films.[5] They noted that for a mixture of arachidic acid and a C_{10} perfluorinated silane, an increase in sub-phase temperature gave rise to an increase in size of the discontinuous domains, and suggested that the temperature dependence might be related to an increased mobility of molecules on the sub-phase surface at elevated temperatures.

The goal of this study is to gain insight into the mechanism of domain formation and growth in the phase-separated AA-PA system. On the basis of the studies described previously, we postulate that the phase-transition occurs first through nucleation in the bulk solution, then further growth of the discontinuous domains can be described via an Ostwald ripening process, in which hydrocarbon molecules from smaller domains are transported via diffusion to larger domains. Experiments aimed at testing this hypothesis have been devised, which include preparing phase-separated films under a variety of conditions (temperature, surface pressure, mixing of sample solutions) and characterizing the film properties using a combination of surface pressure-area isotherm measurements and atomic force microscope imaging. In terms of the latter, extensive use of the in situ dissolution technique has been made in order to gain insight into both the morphology and chemical composition of the LB films.

4.3 Experimental Section

4.3.1 Chemicals

Arachidic acid (99%) and perfluorotetradecanoic acid (97%) were purchased from Sigma-Aldrich Corporation. Hexanes (HPLC grade) and tetrahydrofuran (THF) were purchased from EMD and Merck EM Science, respectively. n-Hexadecane (99%) was purchased from Alfa

Aesar. Mica was purchased from SPI (Structure Probe Inc., West Chester, PA), and was freshly cleaved with adhesive tape prior to use.

4.3.2 Isotherm measurements and Langmuir-Blodgett film deposition

Langmuir and LB films were prepared using a KSV 2000 Langmuir trough system (KSV Instruments, Helsinki, Finland), with ultrapure water (Millipore, resistivity 18.2 MΩ·cm) as a sub-phase. Stock solutions of 8.4×10^{-3} M of AA and 5.1×10^{-3} M of PA were prepared in a 9:1 volume ratio of hexanes:THF. The solutions were combined to give a 2:1 mole ratio mixture of AA and PA, respectively. Before each measurement the sub-phase surface was cleaned by vacuum suction and the platinum Wilhelmy plate was cleaned by flaming in a propane torch. The isotherm and deposition experiments were performed as described previously[10] by spreading a 30 μL aliquot of the 2AA:1PA mixture on the sub-phase at a specific temperature and waiting 10 min for solvent evaporation. All isotherm measurements were carried out at a rate of barrier compression of 20 mm min^{-1}.

Unless stated otherwise in the text, film deposition was carried out at a surface pressure of 20 mN m^{-1}. The barrier compression rate was kept at 10 mm min^{-1} until reaching the desired surface pressure, at which point it was changed to 5 mm min^{-1} to match the substrate withdrawal rate from the sub-phase. This took place after 10 min of sample stabilization. The sub-phase temperature was controlled by water circulation through the trough's external jacket from a Haake K F3 water bath (Haake, Berlin, Germany). Sub-phase surface temperature was monitored throughout the experiment with a thermocouple, and was kept constant to within ± 0.5 ^{o}C.

4.3.3 Atomic force microscope measurements

AFM measurements were carried out on a Dimension Hybrid Nanoscope system (Veeco Metrology Group, Santa Barbara, CA). The microscope was mounted in an acoustic-vibration

isolation system. Commercial silicon AFM probes with nominal spring constant of (12-130) N m^{-1} and nominal resonance frequency ~330 kHz were used for tapping mode measurements in air. Measurements in n-hexadecane were carried out in contact mode in a liquid cell using silicon nitride probes with nominal spring constant of 0.01 N m^{-1}. Samples were left to stabilize for ~3 h in n-hexadecane before imaging. All AFM probes were purchased from Veeco Metrology Group, Santa Barbara, CA. Image analysis was carried out with either Nanoscope version 6.13 (Veeco Metrology Group, Santa Barbara, CA) or ImageJ.[12] The analysis was carried out by saving the images as jpg file and changing it using the ImageJ software into a binary image. This was followed by either analyzing particles at size (pixel^2) of 0.5-infinity and circularity of 0.0-1.0, or by measuring the area manually through drawing a polygon around the domain and then measuring its area. This latter method of analysis was used for the images of low resolution. The area measured in pixel^2 was converted into μm^2 by using the suitable number of pixel per image. As was noted in a previous publication, the samples could be imaged repeatedly (using either tapping or contact mode) without causing tip-induced damage.[10] Samples were positioned in the microscope such that the vertical axis in the images is in the direction of withdrawal of the solid substrate from the water surface.

4.4 Results and discussion

4.4.1 Surface pressure measurements

Surface pressure-area isotherms for pure AA, pure PA and a 2AA:1PA mixture measured at sub-phase temperatures ranging from 5.7-30.1 ^oC are shown in Figure 4-1A-D. Over the temperature range explored, the isotherm for the mixed film fell between those of the pure surfactants, though closer to that of the pure AA as is expected based on the relative mole ratio of the mixture. This is in good agreement with our previously reported observations[10], and those

of Matsumoto[1], that the additivity rule is valid for this system and that phase-separation may be taking place. Also consistent with our previous measurements, a strong liquid phase transition (~25 mN m^{-1} at 5.7 ^{o}C) was observed for pure AA but a much less pronounced transition was found for the mixed film and the pure PA. The occupied area per molecule of PA in the solid phase (~26 Å $molecule^{-1}$ at 5.7 ^{o}C) was larger than the area occupied per molecule of AA in the solid phase (~19 Å $molecule^{-1}$ at 5.7 ^{o}C), which is the anticipated result based on the difference in cross-sectional areas of the two molecules.

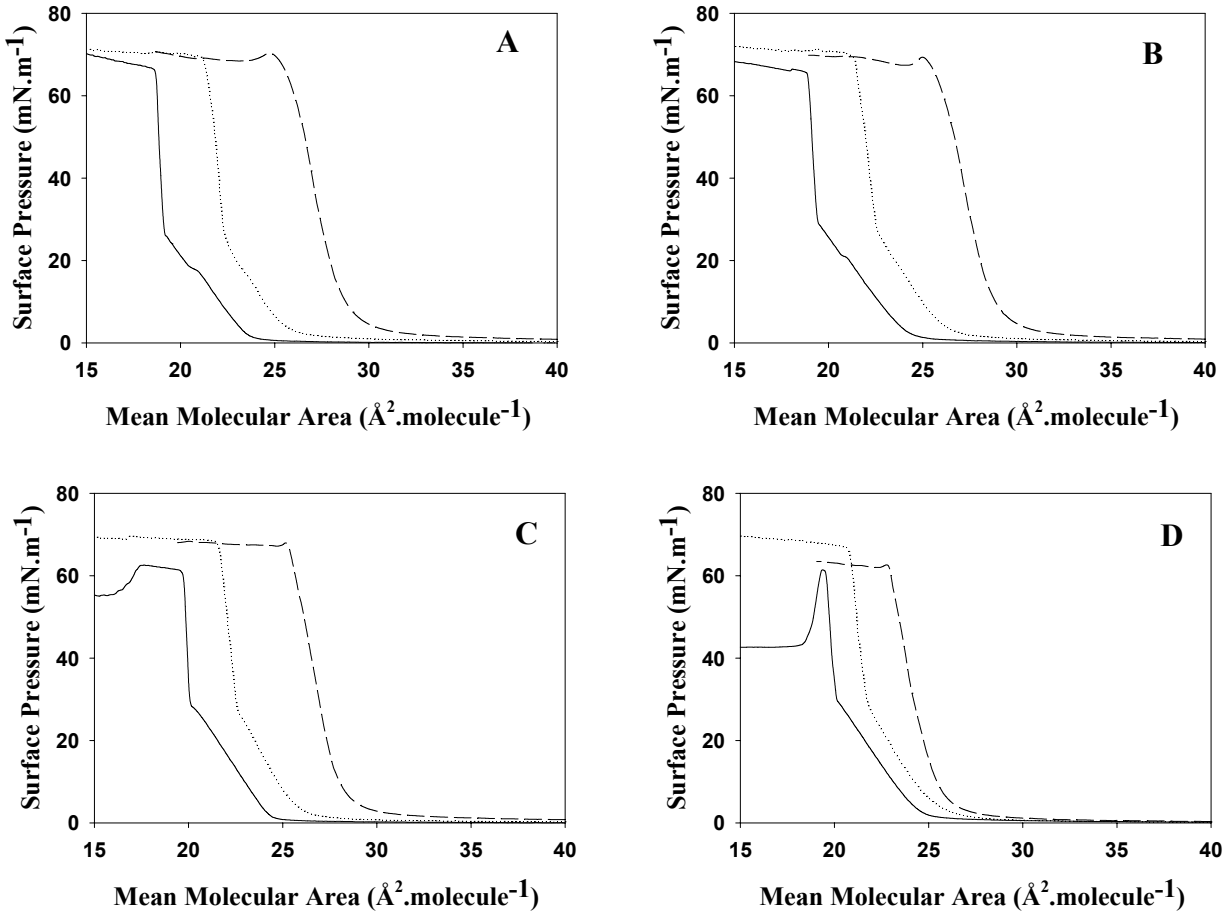

Figure 4-1. Surface pressure-area isotherms of surfactants on a water sub-phase, at water-air interface at A) 5.7 ºC, B) 10.7 ºC, C) 20.3 ºC, D) 30.1 ºC. The solid line corresponds to pure AA, the dotted line corresponds to 2AA:1PA (without shaking the solution mixture), and the dashed line corresponds to pure PA.

In terms of temperature dependence, it was generally observed that for pure AA, the isotherms were shifted to larger mean molecular areas with increasing temperature. For pure PA, increasing the sub-phase temperature generally caused the isotherms to be shifted to smaller mean molecular areas. The net result of these shifts was that the spacing between isotherms for the pure films decreased significantly at higher sub-phase temperatures. It should be noted that the shifts observed were irregular in size over the temperature range studied, and despite repeated, careful measurements, did not follow any recognizable trend. In a study of a mixed fatty-acid / perfluoropolyether, Iimura[6] observed a small expansion of the low-pressure phase for a pure C_{20} fatty acid, which they attributed to strengthened intermolecular interactions (film cohesion) because of the lower temperature, and it is likely a similar effect is taking place with AA. For the perfluorinated PA molecules, intermolecular interactions are expected to be very weak, and the temperature dependence can be rationalized in terms of thermal fluctuations and the affinity of the hydrophilic headgroup for the water surface.

4.4.2 Film morphology by atomic force microscopy

To gain insight into the mechanism of domain formation and growth in this system, LB films were deposited onto mica from the air-water interface and imaged using the atomic force microscope. To characterize the effect of sub-phase temperature on phase-separation, LB films were deposited at a surface pressure of 20 mN m^{-1} (in the region of liquid expanded phase), and at different temperatures in the range of 4.4-31.9 ºC. Figure 3-2A-F shows a series of AFM height mode images (20 μm × 20 μm) taken in tapping mode in air of LB films deposited as a function of increasing sub-phase temperature.

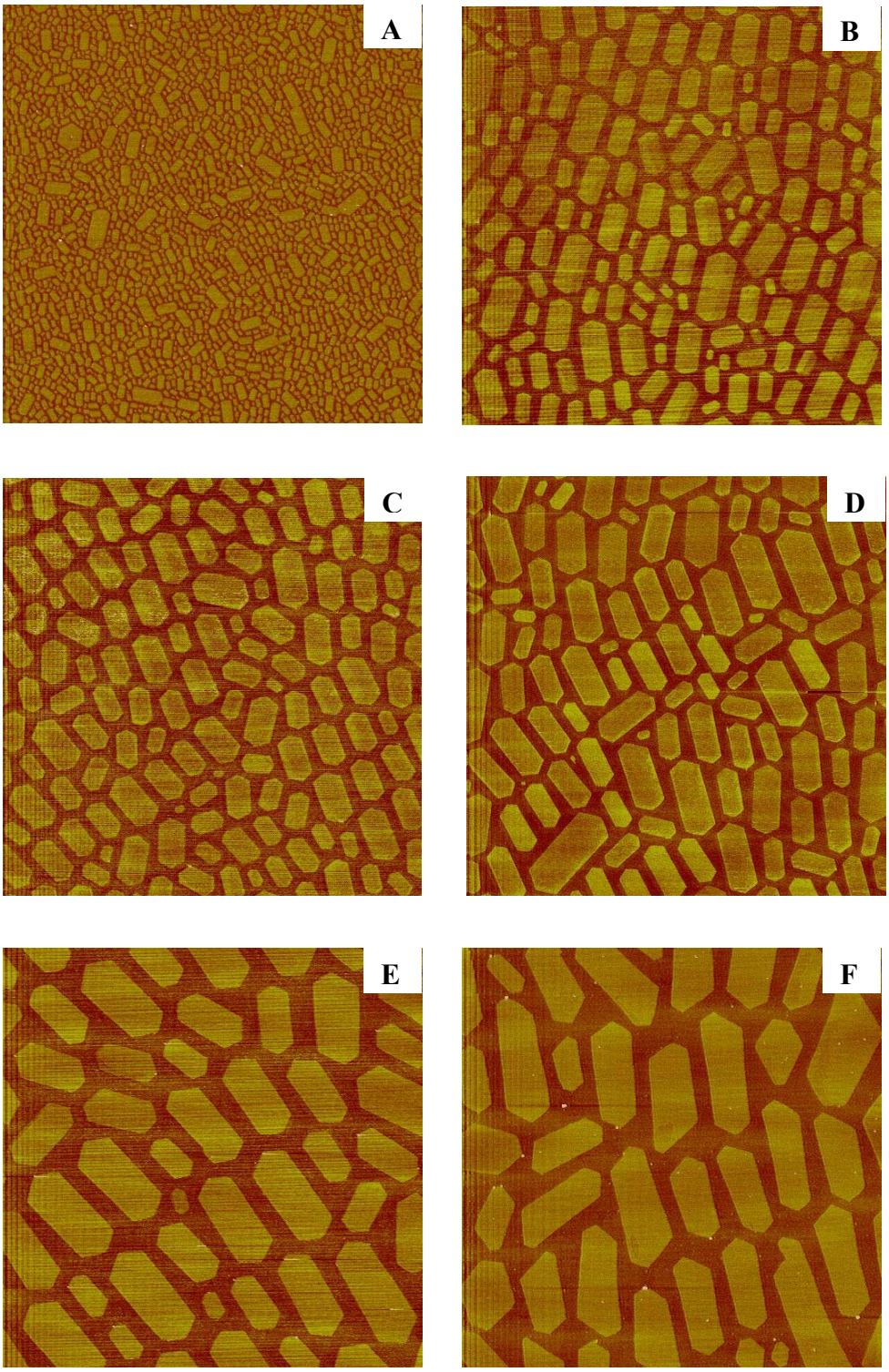

Figure 4-2. AFM height mode images (20 μm × 20 μm) obtained from a 2AA:1PA LB film deposited on mica, without shaking the solution mixture, at a surface pressure of 20 mN m^{-1} at A) T = 4.4 ºC, B) T = 10.1 ºC, C) T = 15.4 ºC, D) T = 21.4 ºC, E) T = 25.5 ºC, F) T = 31.9 ºC. Images were measured using tapping mode in air.

Under all deposition conditions studied, the LB films consisted of a series of discontinuous domains (the light-colored islands) which were elevated by ~6 Å over the surrounding (darker) continuous domain. We have previously identified the discontinuous domains as consisting primarily of AA oriented perpendicular to the substrate surface and the continuous domain as PA oriented perpendicular to the surface, with the difference in domain height due to the difference in molecular lengths of PA and AA (~7 Å as determined through molecular mechanics (MMFF, Spartan '06) modeling of the structures).

As is apparent from Figure 4-2A-F, both the size and the number of discontinuous domains are strongly dependent upon the sub-phase temperature. While the discontinuous domains were heterogeneous in size, some general trends can be extracted from the images in terms of mean domain area and the number of domains. At low temperatures, there are a large number of small domains, and as the temperature increases, the average domain size increases while the number decreases. A plot of mean domain size and mean number of domains per 20 μm × 20 μm region as a function of sub-phase temperature is shown in Figure 4-3. The mean domain size has a single-exponential (Arrhenius-like) temperature dependence, which one might reasonably expect for a process under kinetic control. These results are in qualitative agreement with those described by Matsumoto and Iimura[5, 6], but in contrast with that observed by Sikes in their investigation of domain formation in pure fatty-acid films deposited onto mica substrates.[13, 14] Sikes predicted that, for a system that undergoes a first-order phase transition in two-dimensions, the number of domains will have the same temperature dependence as the rate of nucleation. This gives a general qualitative prediction that the number of islands should increase in an approximately exponential fashion with temperature, which is the exact opposite of what we observe in our system. While caution should be taken in extending arguments from a single-

component film to the two-component film used in these measurements, the basic temperature dependence measured here clearly indicates that a simple nucleation-type mechanism cannot be used to describe domain formation in the AA-PA system.

As an alternative to a purely nucleation and growth style mechanism of formation, we propose that the discontinuous domains in the AA-PA system form through an initial nucleation step, and then grow via a two-dimensional Ostwald ripening process. In terms of the latter effect, Ostwald ripening can be considered part of a first-order phase transition for the condensation of a metastable phase.[15] This mechanism of phase growth, generally driven by minimization of the phase-boundary area, can be found in a wide variety of systems, including the formation of nanoparticles[16], quantum dots[17], rock formation[18] and superalloys[19] to name a few. At low sub-phase temperatures, a large number of small nuclei are initially formed.

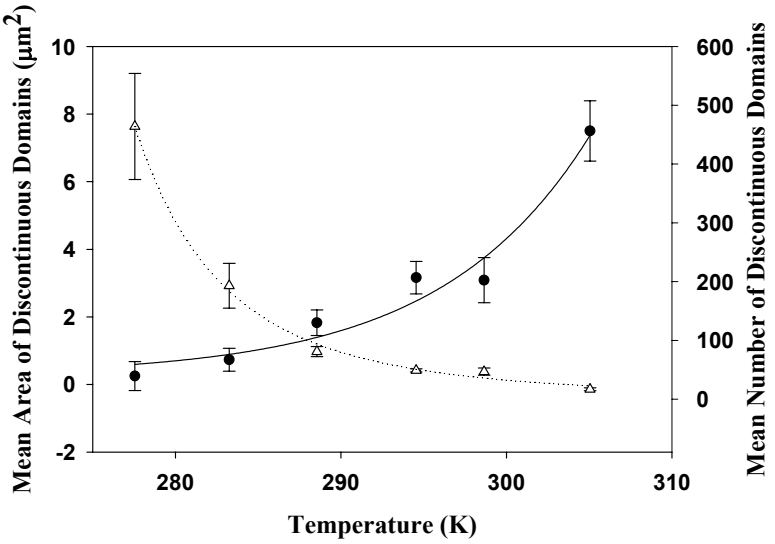

Figure 4-3. Plot showing the mean area of the discontinuous domains and the average number of discontinuous domains per 20 μm × 20 μm image as a function of sub-phase temperature. The LB films were deposited at a surface pressure of 20 mN m^{-1}. The circles correspond to the mean area of the discontinuous domains, and the triangles correspond to the mean number of domains. Image data was collected and analyzed from a minimum of 10 macroscopically separate areas on at least two different samples for each temperature. The lines are exponential functions added as a guide to the eye.

At higher temperatures, AA molecules will have a greater mobility on the water surface and will tend to diffuse from the smaller domains and the continuous domain into the larger domains. Growth of the larger domains will take place at the expense of the smaller domains, further decreasing their size and decreasing the net phase-boundary area. The ultimate result of this process would be an overall decrease in the number of small domains and an increase in the number of the large remaining domains, which is in excellent agreement with our AFM image data. In addition, domain growth rate will be controlled by the rate at which diffusion can take place on the sub-phase surface and if this is the case, the Arrhenius-like temperature dependence of domain size is the expected outcome. In effect, the images that are obtained in these experiments are "snapshots" of various stages of the Ostwald ripening process, and these are intermediate states that have not yet gained thermodynamic equilibrium. With time, when the domains' size are equal and there is no growth driven by the surface tension, diffusion of the molecules between the domains is equal, and the system is in thermodynamic equilibrium.

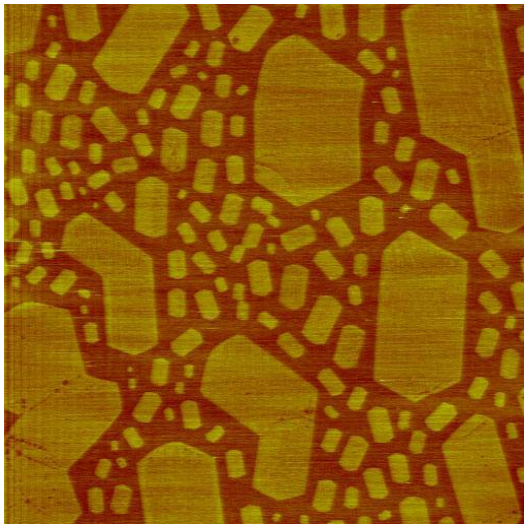

Figure 4-4. AFM height mode image (20 μm × 20 μm) of 2AA:1PA film deposited on mica, without shaking the solution mixture at a surface pressure of 20 mN m^{-1} and a temperature of 4.3 ºC. The solution mixture deposited on the water sub-phase was left for 3 hours before compressing to the indicated surface pressure. The image was measured in contact mode in air.

A detailed study of the domain growth kinetics has not been carried out here, and will be the topic of a future research project. However, a simple study of the effect of equilibration time on domain structure was carried out. If Ostwald ripening is indeed the main mechanism of domain growth in this system, then one would reasonably expect to observe larger discontinuous domains if the amount of time the Langmuir film was allowed to equilibrate on the sub-phase was increased. To test this hypothesis, a Langmuir film was prepared at 4.3 ^{o}C, equilibrated for 3 hours at the same temperature, then compressed to a surface pressure of 20 mN m^{-1} before deposition. As seen previously in Figure 4-2A, with an approximate equilibration time of 10 minutes, the resulting LB film consists of numerous, small domains. When the equilibration time is extended to 3 hours, one still observes small domains that are comparable in size (though fewer in number) to those observed previously, but also a significant number of larger domains as shown in Figure 4-4. This is exactly the anticipated result for an Ostwald ripening process preceded by an initial nucleation step.

In an attempt to gain additional insight into the mechanism of domain growth as well as to characterize any initial domain nucleation events, the influence of different deposition pressures (range of 1 to 30 mN m^{-1}) on the domain morphology was surveyed. Figure 4-5 shows a series of 20 μm × 20 μm images of 2AA:1PA, taken in tapping mode in air, of samples deposited at 20.6 ^{o}C and different surface pressures along with the corresponding cross-sectional analysis. Discontinuous domains were observed over the entire range of surface pressures examined. At low surface pressures, the domains were approximately circular, with diameters of an average of ~3 μm. The domains were relatively few in number and there was a considerable distance between adjacent discontinuous domains. As the surface pressure was increased, the typical domain size decreased, the number of domains per image increased and the distance

between adjacent domains decreased. Analysis of the average distance between domains (defined here as the distance between adjacent domain edges) gave values of 2.5 ± 1.6 μm at a surface pressure of 1 mN m^{-1}, a distance of 1.7 ± 1.2 μm at 5 mN m^{-1}, 1.5 ± 0.9 μm at 10 mN m^{-1}, and 0.6 ± 0.3 μm at 30 mN m^{-1}. Above surface pressures of 15 mN m^{-1}, the size of the domains remained essentially constant.

We interpret these results, particularly those observed at low surface pressures, as meaning the phase-separation process likely begins in the bulk solution before being constrained on the sub-phase surface. It is worth noting that the surfactant concentrations used in these experiments are comparable or greater than with typical critical micelle concentrations (CMC) observed for aqueous fatty acids and for perfluorinated fatty acids at room temperature[20], though these values will likely be different in non-aqueous solvents. We have carried out a preliminary measurement of the change in surface tension as a function of concentration of our AA-PA mixture (data not shown), and the results indicate the CMC is well below the surfactant concentrations used in this study. Thus, it is likely that the initial mixture of surfactants contains micelles and other multi-molecular aggregates that are enriched in AA. When placed on the sub-phase surface and solvent is allowed to evaporate, the aggregates will form 2-dimensional, AA-rich domains, which will grow via Ostwald ripening. At low surface pressures, the AA molecules will have a large diffusion coefficient, and large domains can form after a relatively short equilibration period. For higher surface pressures, the lateral diffusion coefficients are accordingly lowered (see for example [21, 22]) and an identical equilibration period results in comparably smaller domains. As an upper limit on the size of the initial multimolecular aggregates, a reasonable estimate can be obtained from the mean domain size from the LB film formed at 4.4 ^{o}C and short equilibration times (Figure 4-2A). Taking this value, 0.25 μm^2, and

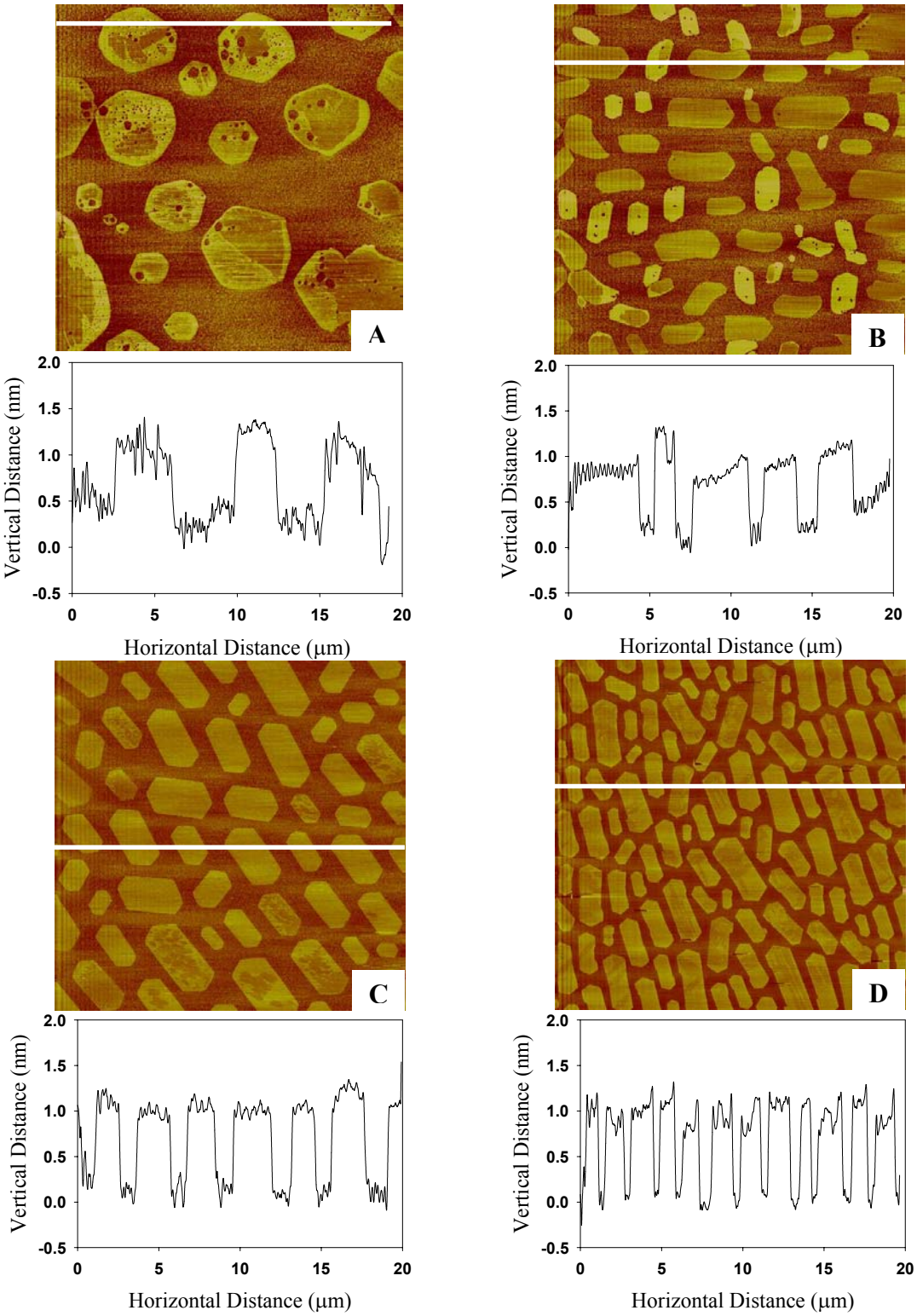

Figure 4-5. AFM height mode images (20 μm × 20 μm) and corresponding cross sectional analysis of 2AA:1PA LB film deposited on mica at T = 20.6 ºC without shaking the solution mixture and at a surface pressure of A) 1 $mN.m^{-1}$, B) 5 $mN.m^{-1}$, C) 10 $mN.m^{-1}$ and D)30 $mN.m^{-1}$. Images were measured using tapping mode in air, and were low pass filtered before analysis.

comparing it with the estimated cross-sectional area of an AA molecule (~$8x10^{-20}$ m^2), suggests that there should be on the order of 10^6 molecules per aggregate in solution.

Another factor that has been found to affect the overall morphology of the discontinuous domains in the LB monolayers is mechanical agitation of the surfactant solutions. For all of the studies described here so far, the stock solutions of surfactant, after initial preparation and mixing, were not mixed or shaken further before use and were allowed to settle for several days. If, in fact, phase-separation in this system first takes place in bulk solution through the formation of multimolecular aggregates, then vigorous mechanical mixing might reasonably be expected to disrupt the shape and number of initial nuclei, and hence the structures of the larger discontinuous domains. Figure 4-6A-F shows a series of AFM images taken for a series of samples deposited at different temperatures, after the surfactant solutions had been vigorously shaken then placed on the sub-phase. Comparing these images with those in Figure 4-2 shows that the morphology of the domains has been drastically altered by mechanical agitation. This likely results from fusing and mixing the aggregates that are already present in solution, essentially pushing the system even further away from its state of thermodynamic equilibrium. This is reinforced by the fact that the process was found to be reversible; well-defined hexagonal domains could be formed from the mechanically agitated solution by simply leaving the solution mixture to settle for several days.

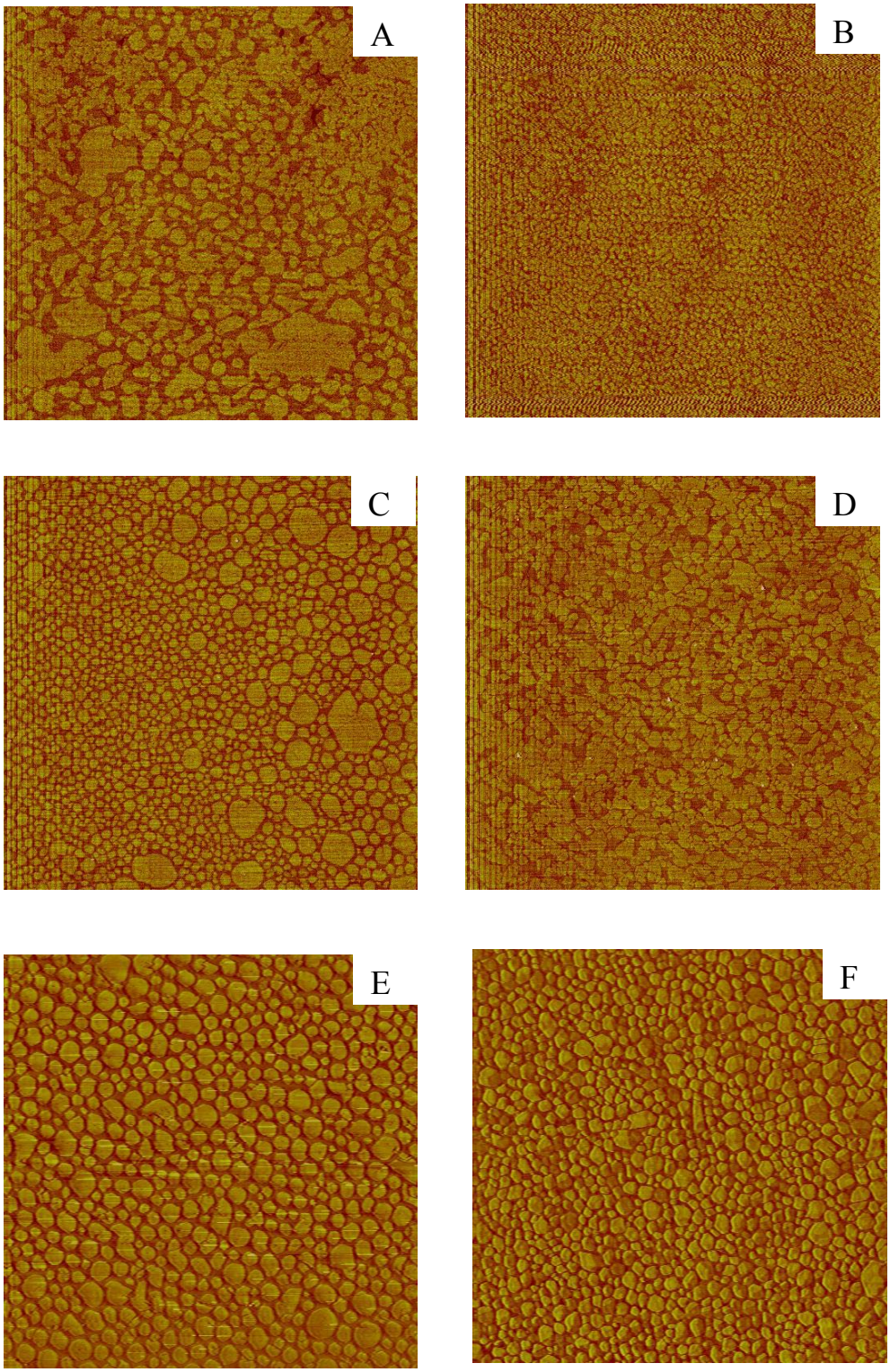

Figure 4-6. AFM height mode images (20 μm × 20 μm) of 2AA:1PA LB film deposited on mica at a surface pressure of 20 mN m^{-1}, with shaking the solution mixture, at temperature of A) T = 5.6 ºC, B) T = 10.7 ºC, C) T = 15.3 ºC, D) T = 20.1 ºC, E) T = 25.5 ºC, F) T = 30.3 ºC. Images were measured using tapping mode in air.

An additional point worth noting is that for the unmixed surfactant solutions, the overall morphology of the discontinuous domains is not controlled exclusively by the kinetics of the Ostwald ripening process. It is clear from Figure 4-5D and others taken under similar conditions that there is a preferred orientation of the discontinuous domains at higher surface pressures. In Figure 4-5D, the long axis of the discontinuous domains is, in fact, oriented in the direction of withdrawal of the substrate from the sub-phase (i.e. the long axis is normal to the sub-phase surface). This preferential orientation can be attributed to the hydrodynamic behavior of anisotropic structures under flow, as they move in the same direction of the flow and are oriented by it.[23, 24]

At lower pressures, the domains tend to be more circular and hence, the orienting effect is less pronounced. Another factor that might also influence the morphology of the domains is the chemical nature of the solid substrate. It has been shown that for some systems, domain morphology in deposited films can depend on the difference between the substrate-monolayer interfacial energy and the water-monolayer interfacial energy.[13] However, for this system we have carried out deposition on several different substrates (silicon oxide, Si_3N_4) and from preliminary observations, found no significant differences in domain morphology between substrates.

4.4.3 Compositional analysis of films by selective dissolution

In addition to basic topographical analysis of the deposited LB films, chemically selective in situ dissolution experiments were carried out in order to characterize the composition of the films. As described in a previous publication[10], incubation of the films in n-hexadecane results in preferential removal of the AA, leaving behind both the PA and voids that were originally occupied by AA. Imaging the resulting films in n-hexadecane is non-perturbative and

allows high-resolution, compositional mapping of the monolayer films. The basic principle of this approach is illustrated in Figure 4-7A,B in which AFM images of a film deposited at 20 mN m^{-1} and 31.9 ^{o}C have been collected before and after n-hexadecane incubation, along with an appropriate cross-sectional analysis. The region that was elevated when imaged in air (Figure 4-7A) becomes lower in height after incubation and imaging in n-hexadecane, indicating that the discontinuous domains (AA rich) have been dissolved. The height difference between the discontinuous domains and the surrounding area is comparable to the chain length of PA (18Å) as observed previously.[10] Similar results were observed at all deposition temperatures, as well as for samples that had been mechanically agitated, indicating that the composition of the domains was largely independent of different preparation conditions.

In Figure 4-8A,B, a higher-resolution image of several discontinuous domain edges is shown, along with the intervening continuous region between domains. The continuous domain contains a large number of pits formerly occupied by AA that, as described in our previous work, indicates a significant AA content in the continuous domain. By calculating the total area of the pits relative to the image area, it was found that the continuous domain was 7 ± 2 % and 5 ± 1 % arachidic acid, at 31.9 ºC and 4.4 ºC, respectively. Closer inspection of the discontinuous domain edges shows that they are not infinitely sharp, and that in places, the pits of the continuous domain merge with the discontinuous domain edge. This is strong further evidence for domain growth via the Ostwald mechanism, via fusion of molecules of AA in the continuous domain into the discontinuous domains.

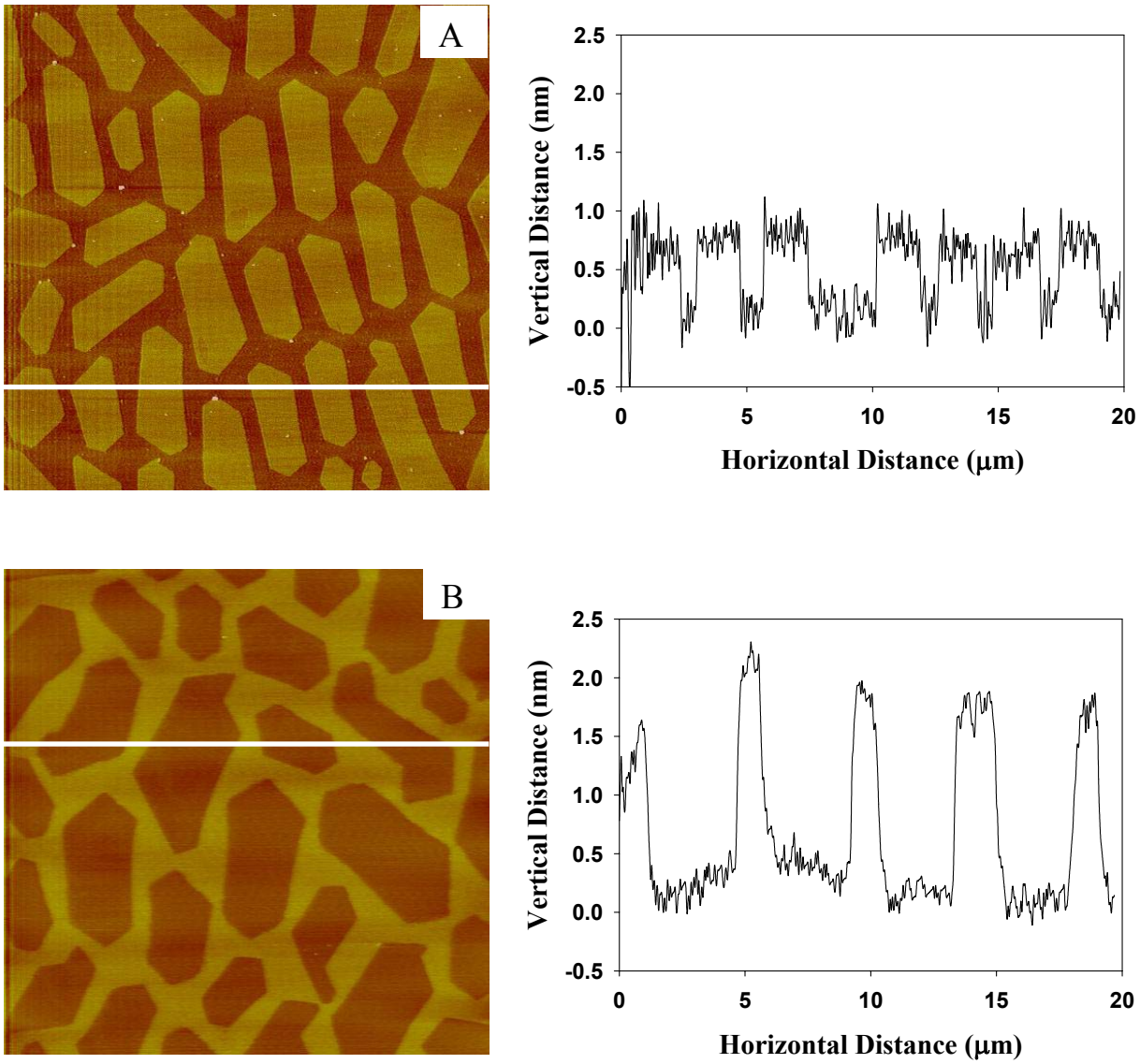

Figure 4-7. AFM height mode images (20 μm × 20 μm) and corresponding cross-sectional analysis of a 2AA:1PA LB film deposited on mica, at T = 31.9 ºC and surface pressure = 20 mN m^{-1} without shaking of the solution mixture. Images were measured A) in air using tapping mode, B) in n-hexadecane using contact mode.

For films deposited at lower temperatures similar effects can be seen, though there are some differences in the lateral ordering of the films. At higher deposition temperatures, the pits left by AA appear to be randomly distributed over the continuous domain. However, for the films deposited at lower temperatures, there was a tendency for the pits to order themselves and form long strands (Figure 4-8B), suggesting a propensity for the AA molecules to associate with each other at these temperatures. In classical nucleation theory involving simple fluids, it is generally assumed that nuclei form as compact spheres in order to minimize their surface-area to volume ratio [25] and as such these more complex structures are unexpected. It is certainly possible that these strand-like structures are formed as a consequence of the film deposition process. However, Frenkel et al.[26] have recently carried out numerical simulation studies of nucleation followed by Ostwald ripening in model polar fluids and found that in these systems, the initial nucleation step involved formation of chains of molecules, including both linear and branched chains, instead of simple spherical objects. Obviously one cannot directly extend Frenkel's model to the work here because of numerous factors including, but not limited to the length scale of phenomenon (Frenkel's work predicted collapse of the chains at length scales considerably smaller than those observed here) and the effect of spreading the molecules onto a polar sub-phase. However, it is conceivable that the structures observed in the AFM images are residuals of chains that form in an analogous fashion. This unusual pattern formation in the continuous domain will be explored in greater detail in future studies.

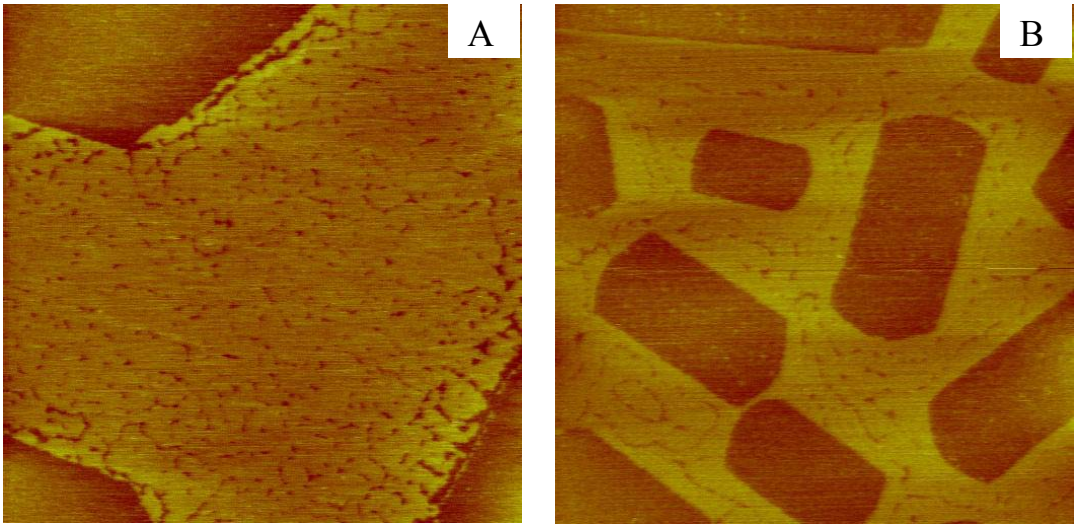

Figure 4-8. High resolution AFM height mode images (1.6 μm × 1.6μm) of 2AA:1PA LB film deposited on mica from air-water interface at surface pressure of 20 $mN.m^{-1}$, A) at T = 31.9 ºC and B) at T = 4.4 ºC without shaking the solution mixture. Images were measured using contact mode in n-hexadecane.

4.5 Conclusions

In this work, the mechanism of formation and growth of the hydrocarbon-rich domains in a phase-separated, mixed hydrocarbon-perfluorocarbon surfactant monolayer has been characterized using surface pressure-area isotherms and AFM topographic measurements. Mechanistic insight into the formation and growth process was gained by characterizing monolayer films at the air-liquid and the solid-air interface under a variety of experimental conditions. It was shown that the main steps in the formation and growth of the separated domains involved an initial nucleation process involving multimolecular aggregates, likely taking place in the bulk surfactant solution, followed by further growth of the domains on the sub-phase surface by Ostwald ripening. It was also observed that, at low sub-phase temperatures, unusual, ordered chains of AA can form in the continuous phase of the deposited

films, which might be a consequence of the deposition process or that nucleation occurs not through compact, spherical objects but rather through more extended structures.

4.6 Acknowledgements

Funding for this work was provided by the Natural Sciences and Engineering Research Council of Canada (NSERC), the Canada Foundation for Innovation (CFI), the Province of Saskatchewan and by the University of Saskatchewan. Professors Stephen Urquhart and Andrzej Baranski are acknowledged for useful discussions and comments.

4.7 References

1. Matsumoto, M.; Tanaka, K.; Azumi, R.; Kondo, Y.; Yoshino, N., *Langmuir* **2003,** 19 (7), 2802-2807.
2. Overney, R. M.; Meyer, E.; Frommer, J.; Guntherodt, H. J.; Fujihira, M.; Takano, H.; Gotoh, Y., *Langmuir* **1994,** 10 (4), 1281-1286.
3. Matos, L.; Ravey, J. C.; Serratrice, G., *J. Colloid Interface Sci.* **1989,** 128 (2), 341-347.
4. Matsumoto, M.; Tanaka, K.; Azumi, R.; Kondo, Y.; Yoshino, N., *Chemistry Letters* **2002,** (10), 970-971.
5. Matsumoto, M.; Tanaka, K.; Azumi, R.; Kondo, Y.; Yoshino, N., *Langmuir* **2004,** 20 (20), 8728-8734.
6. Iimura, K.; Shiraku, T.; Kato, T., *Langmuir* **2002,** 18 (26), 10183-10190.
7. Imae, T.; Takeshita, T.; Kato, M., *Langmuir* **2000,** 16 (2), 612-621.
8. Jacobi, S.; Chi, L. F.; Fuchs, H., *Journal of Vacuum Science & Technology B* **1996,** 14 (2), 1503-1508.
9. Overney, R. M.; Meyer, E.; Frommer, J.; Brodbeck, D.; Luthi, R.; Howald, L.; Guntherodt, H. J.; Fujihira, M.; Takano, H.; Gotoh, Y., *Nature* **1992,** 359 (6391), 133-135.
10. Qaqish, S. E.; Paige, M. F., *Langmuir* **2007,** 23 (5), 2582-2587.
11. Matsumoto, M.; Tanaka, M.; Azumi, R.; Manda, E.; Tachibana, H.; Kondo, Y.; Yoshino, N., *Molecular Crystals and Liquid Crystals Science and Technology Section a-Molecular Crystals and Liquid Crystals* **1997,** 294, 31-34.
12. Rasband, W. *Imagej*, 1.37v; Research Services Branch, National Institute of Mental Health: Bethesda, Maryland.
13. Sikes, H. D.; Woodward, J. T.; Schwartz, D. K., *Journal of Physical Chemistry* **1996,** 100 (21), 9093-9097.
14. Sikes, H. D.; Schwartz, D. K., *Langmuir* **1997,** 13 (17), 4704-4709.
15. Marqusee, J. A.; Ross, J., *Journal of Chemical Physics* **1983,** 79 (1), 373-378.
16. Liu, Y.; Kathan, K.; Saad, W.; Prud'homme, R. K., *Phys. Rev. Lett.* **2007,** 98 (3).
17. Vengrenovich, R. D.; Gudyma, Y. V.; Yarema, S. V., *Semiconductors* **2001,** 35 (12), 1378-1382.

18. Miyazaki, K., *Contributions to Mineralogy and Petrology* **1991,** 108 (1-2), 118-128.
19. Baldan, A., *Journal of Materials Science* **2002,** 37 (11), 2171-2202.
20. Steigman, J.; Shane, N., *Journal of Physical Chemistry* **1965,** 69 (3), 968-&.
21. Meller, P.; Peters, R.; Ringsdorf, H., *Colloid and Polymer Science* **1989,** 267 (2), 97-107.
22. Peters, R.; Beck, K., *Proceedings of the National Academy of Sciences of the United States of America-Biological Sciences* **1983,** 80 (23), 7183-7187.
23. Jeffery, G. B., *Proceedings of the Royal Society of London Series a-Containing Papers of a Mathematical and Physical Character* **1922,** 102 (715), 161-179.
24. Okagawa, A.; Cox, R. G.; Mason, S. G., *J. Colloid Interface Sci.* **1973,** 45 (2), 303-329.
25. Adamson, A. W.; Gast, A. P., *Physical Chemistry of Surfaces*. 6 ed.; Wiley: New York, 1997; 'Vol.' p.
26. ten Wolde, P. R.; Frenkel, D., *Physical Chemistry Chemical Physics* **1999,** 1 (9), 2191-2196.

CHAPTER 5
CHARACTERIZATION OF DOMAIN GROWTH KINETICS IN A MIXED PERFLUOROCARBON / HYDROCARBON LANGMUIR-BLODGETT MONOLAYER

The following chapter is a slightly modified copy of a communication published in *Journal of Colloid and Interface Science* in June 2008. (Reprinted from Journal of Colloid and Interface Science, 325, Shatha E. Qaqish and Matthew F. Paige, Characterization of domain growth kinetics in a mixed Langmuir-Blodgett monolayer, 290-293, copyright (2008), with permission from Elsevier).

For the mixed AA/PA system (Chapters 2-4), we investigated the kinetics of domain growth. Two-dimensional (2D) kinetic studies are not widespread in comparison with the three-dimensional (3D) studies, though important information can be extracted from 2D studies if the data are correctly analyzed.

This current chapter is one of the few examples on understanding the kinetics of domain growth (coarsening) of an LB film. This was achieved by varying the time that the film spends on the sub-phase before compression. We used the Lifshitz-Slyozov equation to model the kinetics of this system where the area of the domain increases linearly as a function of time to the power 2/3. Also, we were able to differentiate between Ostwald ripening and coalescence of the domains as a function of time and temperature as described in details in this chapter.

For this research paper, I prepared samples, performed the measurements, and played a major role in interpreting the results and the preparation of the paper. My supervisor provided guidance throughout the experimental work and was involved in result interpretation and in editing this paper.

5. Characterization of domain growth kinetics in a mixed perfluorocarbon-hydrocarbon Langmuir-Blodgett monolayer

Shatha E. Qaqish and Matthew F. Paige*

Department of Chemistry, University of Saskatchewan, 110 Science Place, Saskatoon, Saskatchewan, Canada S7N 5C9

Received 9 May 2008, Accepted 10 June 2008

5.1 Abstract

The rate of domain growth in phase-separated, mixed Langmuir-Blodgett (LB) monolayers of arachidic acid, $C_{19}H_{39}COOH$ (AA) and perfluorotetradecanoic acid $C_{13}F_{27}COOH$ (PA) was tracked via atomic force microscope measurements. The growth rate of domains comprised of phase-separated AA was consistent with that predicted by the Lifshitz–Slyozov model for diffusion-limited Ostwald ripening. In addition to Ostwald ripening, some evidence for domain coalescence was also observed when LB films were deposited under conditions of low temperature and short incubation times, though this tendency disappeared at higher deposition temperatures.

5.2 Introduction

Fluorinated molecules are technologically important because of their numerous biomedical and materials science applications [1, 2]. Many of these applications originate from the improved thermal, chemical and physical properties of fluorine-terminated surfaces in comparison with their non-fluorinated counterparts, including low friction coefficients, chemical inertness [3-5] and high dielectric constant [6]. Of particular recent interest is the ability of fluorinated surfactants to phase-separate from hydrocarbon surfactants at the air-water and solid-air

interface. Under appropriate conditions, fluorinated surfactants can phase-separate from hydrocarbon amphiphiles, forming monolayer films with well-defined surface domains [3, 7-9]. We believe that the controlled patterning of solid surfaces with fluorinated molecules has important technological applications in the field of chemical and biological sensing [10], and wish to both understand and control the mechanism of phase-separation in these mixed systems.

In our previous work on the mixed arachidic acid (AA) - perfluorotetradecanoic acid (PA) system, it was observed that AA phase-separated from PA to form hexagonal domains when deposited onto solid mica substrates from the air-water interface [9]. Further measurements indicated that domain formation took place through an initial nucleation event in solution, followed by domain growth on the water surface [9]. It was noted that for fixed incubation time on the sub-phase surface, the average number of domains decreased as a function of increasing sub-phase temperature, while the average domain area increased. Similarly, increasing the incubation time at fixed temperature also resulted in a decrease in number of domains, while the average domain area increased.

The results obtained for the AA/PA system were consistent with domain growth via Ostwald ripening. Two primary mechanisms by which domain growth can occur during phase-separation are coalescence and Ostwald ripening (domain coarsening) [11, 12]. Coalescence is the merging of smaller domains to form a larger domain whereas Ostwald ripening is the growth of domains that have reached a critical size while smaller domains simultaneously decrease in size. The material that is lost from the smaller domains is taken up by the larger, growing domains. This process minimizes the interfacial energy between the two phases [12] and generally requires molecular diffusion from the smaller domains to the larger domains. The rate of Ostwald ripening in 2D systems has been described using the Lifshitz – Slyozov (LS) [13] relation:

$$\langle A \rangle = kt^{2\alpha} \quad (5\text{-}1)$$

where $\langle A \rangle$ is the average domain area, t is time, α is the growth-rate exponent which is equal to 1/3 for a diffusion governed processes [14], and k is a proportionality constant that depends upon a variety of factors including diffusion coefficient, temperature and others. This theory has been used to describe a diverse range of domain coarsening events in 2D systems, including phase-separation in films of diblock copolymers [15], Cu cluster formation on tantalum films [16] and domain formation in supported lipid bilayers [17], to name a few.

In this study, the detailed kinetics of domain growth in a mixed LB film of AA/PA have been investigated by tracking the time-evolution of domain size with AFM imaging under different film deposition conditions. Domain growth is modeled using the LS relationship, and the importance of domain coalescence in this system is also explored through inspection of domain morphology.

5.3 Materials and methods

5.3.1 Chemicals

Arachidic acid (99%) and perfluorotetradecanoic acid (97%) were purchased from Sigma-Aldrich Corporation. Tetrahydrofuran (THF) and hexanes (HPLC grade) were purchased from Merck EM Science and EMD, respectively. Mica was purchased from SPI (Structure Probe Inc., West Chester, PA), and was freshly cleaved with adhesive tape prior to use.

5.3.2 Langmuir-Blodgett film deposition

LB films were prepared using a KSV 2000 Langmuir trough system (KSV Instruments, Helsinki, Finland), with ultrapure water (Millipore, resistivity 18.2 MΩ·cm) as a sub-phase. The sub-phase temperature was controlled by water circulation through the trough's external jacket and monitored with a thermocouple.

Stock solutions of 8.9×10^{-3} M of AA and 5.0×10^{-3} M of PA were prepared separately in a 9:1 volume ratio of hexanes:THF. The solutions were mixed to give a 2:1 mole ratio mixture of AA:PA, respectively. Before each measurement the sub-phase surface was cleaned by vacuum suction and the platinum Wilhelmy plate was cleaned by flaming in a propane torch. Following our previous procedure [9], film deposition was carried out at a surface pressure of 20 $mN.m^{-1}$ and a barrier compression rate of 10 $mm.min^{-1}$. Mica was immersed in the sub-phase before spreading a 30 μL aliquot of the surfactant mixture onto the sub-phase. The spreading solvent was allowed to evaporate for different time intervals prior to compression. Upon reaching the desired surface pressure, the film was left to stabilize for 10 min. After stabilization, the mica was withdrawn at a rate of 5 $mm.min^{-1}$, and the compression rate was set equal to the withdrawal rate. Experiments were carried out over a range of sub-phase temperatures, as described in the text.

5.3.3 Atomic force microscope measurements

AFM measurements were carried out on a Dimension Hybrid Nanoscope system (Veeco Metrology Group, Santa Barbara, CA). Measurements were performed in either tapping or contact mode in air at a scan rate of 1.99 Hz. Commercial silicon nitride AFM probes with nominal spring constant of ~0.1 $N.m^{-1}$ and silicon probes with resonance frequency ~330 kHz were used for contact and tapping modes measurements, respectively. All probes were purchased from Veeco Metrology Group, Santa Barbara, CA. Image analysis was carried out with the software package ImageJ as described in details in Chapter 4[18].

5.4 Results and discussion

The rate of domain growth in 2AA:1PA LB films were investigated by characterizing and quantifying domain morphology as a function of the time allowed for the solvent to evaporate on

the sub-phase prior to film compression. Figures 5-1A-D show a series of images of 2AA:1PA LB films deposited at 10 ^{o}C and at evaporation times ranging from 10 min up to 62 hr. The films consisted of large numbers of hexagonal domains that were elevated above a flat, continuous domain. Cross-sectional analysis of a typical film (Figure 5-1E) shows that the height difference between the elevated hexagonal domains and the surrounding continuous domain is ~6 Å, which is comparable to what was observed previously [9]. This height corresponds to the difference between the molecular lengths of PA and AA (~7 Å as calculated through molecular mechanics modeling of the structures MMFF, Spartan ˋ06) which, in conjunction with a series of other measurements (including compositionally-sensitive AFM imaging), allowed unambiguous assignment of the hexagonal domain composition as primarily AA and the surrounding area as primarily PA [9].

The mean area per AA domain increased as a function of evaporation time whereas the total number of domains decreased with evaporation time. These are the anticipated results for domain growth that occurs via Ostwald ripening. To explore this further, a systematic survey of the effect of evaporation time and sub-phase temperature on mean AA domain size was carried out. The mean domain size of AA was measured using ImageJ software as described in details in Chapter 4. In Figure 5-2, the mean area per domain is plotted as a function of evaporation time (taken to the 2/3 power) for a series of different sub-phase temperatures. Plotted in this way, the mean domain area increased linearly, with the growth-rate increasing as a function of sub-phase temperature. Linear-regression analysis of the measured data indicates that it is well-represented by the LS model (equation **(5-1)**) in which a growth-rate factor of α = 1/3 (diffusion-controlled growth) is applied.

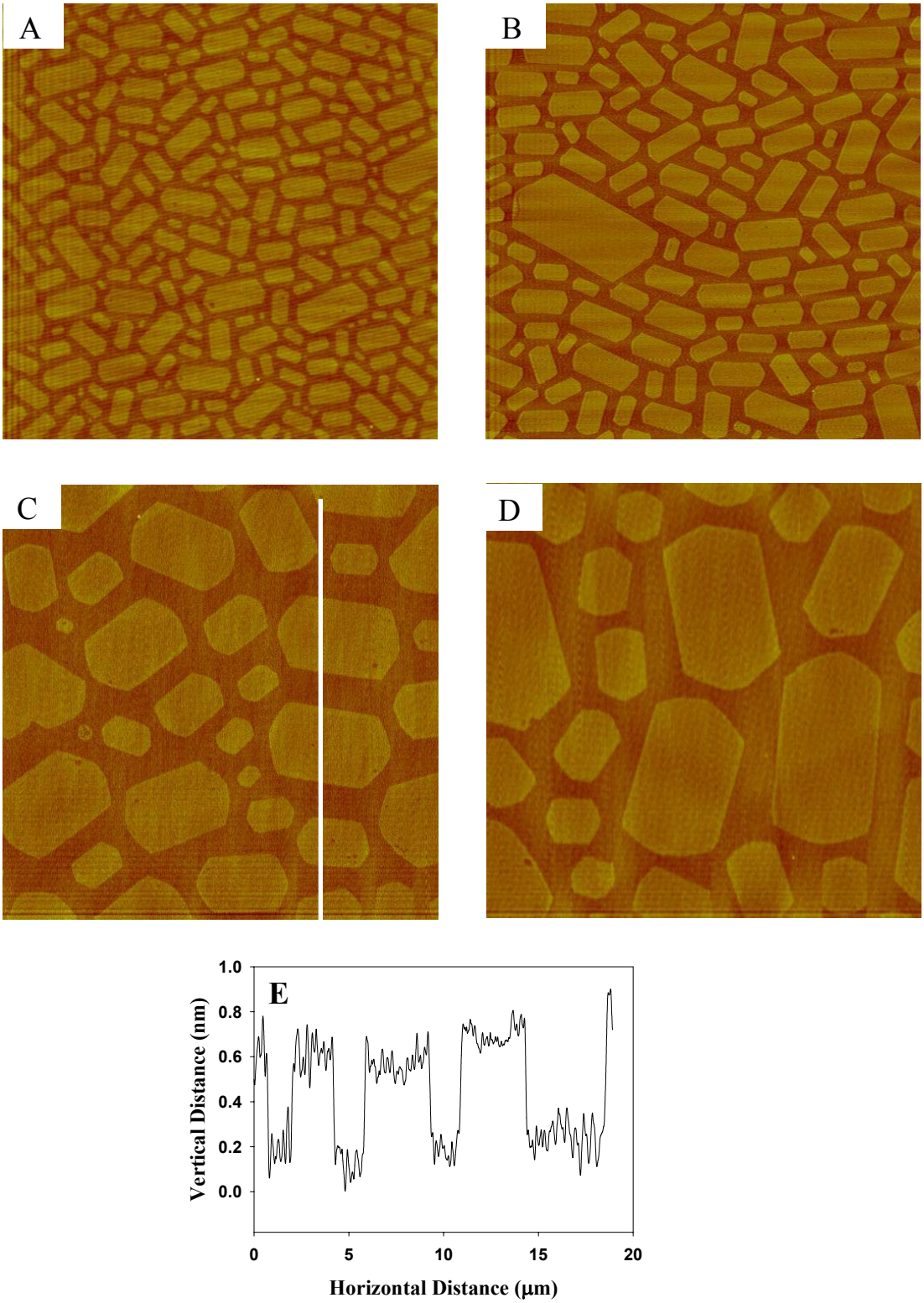

Figure 5-1. AFM height images (20 μm × 20 μm) of 2AA:1PA deposited at 10.1 ± 0.5 ^{o}C and at surface pressure of 20 mN.m^{-1} at different evaporation times; A, 10 min; B, 5 hr; C, 14 hr; D, 62 hr. E is a height cross section of image C.

These results are similar to those described for binary mixtures of phospholipid / cholesterol [19] and phospholipid bilayers [17] in which 2D domain growth was also controlled by Ostwald ripening. We also note that the rate of domain growth has an Arrhenius-like dependence on the sub-phase temperature as shown in the inset of Figure 5-2. While we are presently cautious at interpreting this result in a quantitative fashion (there is a significant amount of scatter in this data), we note that the general behaviour is consistent with the functional dependence of the proportionality constant k described in equation (5-1).

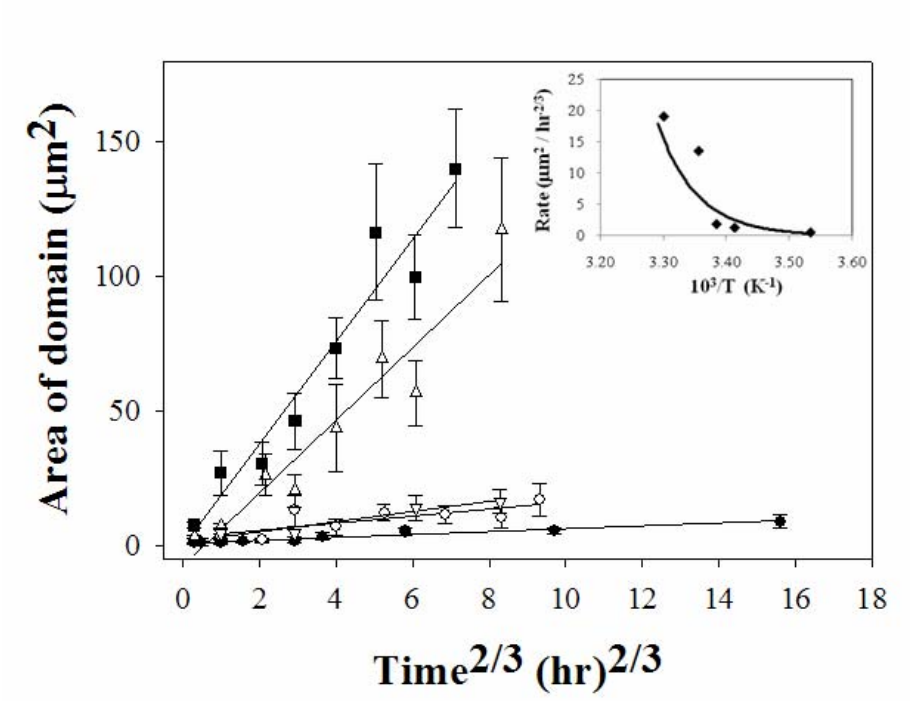

Figure 5-2. Average domain area as a function of time at different temperatures. Dark circles, 10.1 ± 0.5 °C; white circles, 20.4 ± 0.4 °C; triangles down, 22.5 ± 0.5 °C; triangles up, 25.2 ± 0.5 °C; squares, 30 ± 1 °C. Samples deposited at 20 mN.m^{-1}. Each point is the average of at least 200 individual domains, and error bars are standard errors. Inset: The growth rate as a function of temperature.

T (ºC)	R^2
10	0.95
20	0.58
22.5	0.93
25	0.93
30	0.94

Table5-1. Statistical analysis including R^2 value of the linear regression at every temperature of Figure 5-2.

Further insight into the mechanism of domain formation can be gained by comparing domain morphologies for samples prepared at different temperatures. Figure 6-3A,B compares surface domains that were deposited at 20^{o}C with those formed at 4^{o}C. At higher temperatures, the domains formed discrete, well-defined hexagons, but at lower temperatures, a significant fraction of large, irregular shaped domains were observed. These irregular-shaped domains still contain vestiges of hexagonal shapes and appear to consist of multiple, smaller hexagonal domains that have merged together. Similar reasoning has been used by Bassereau et al. in their investigation of domain formation in block copolymer thin films, in which the uniformity of domain shape as a function of time was used to exclude domain growth via coalescence [15]. While there are a number of effects that might cause these irregular structures to form, we tentatively interpret these images as indicating that coalescence is occurring to at least some degree at lower temperatures. There are several possible explanations why fewer coalesced domains are observed at elevated temperatures. Coalescence might still be taking place, followed by re-arrangement of the domains into hexagonal shapes to minimize the line tension between the phases. At elevated temperatures, domain re-arrangement may take place very rapidly after coalescence, and as such

the larger structures are almost never observed. Another explanation is that coalescence simply may not occur at elevated temperatures; at high temperatures, the domains will grow rapidly, and there will be a substantial activation energy barrier for the large domains to diffuse across the sub-phase surface and coalesce.

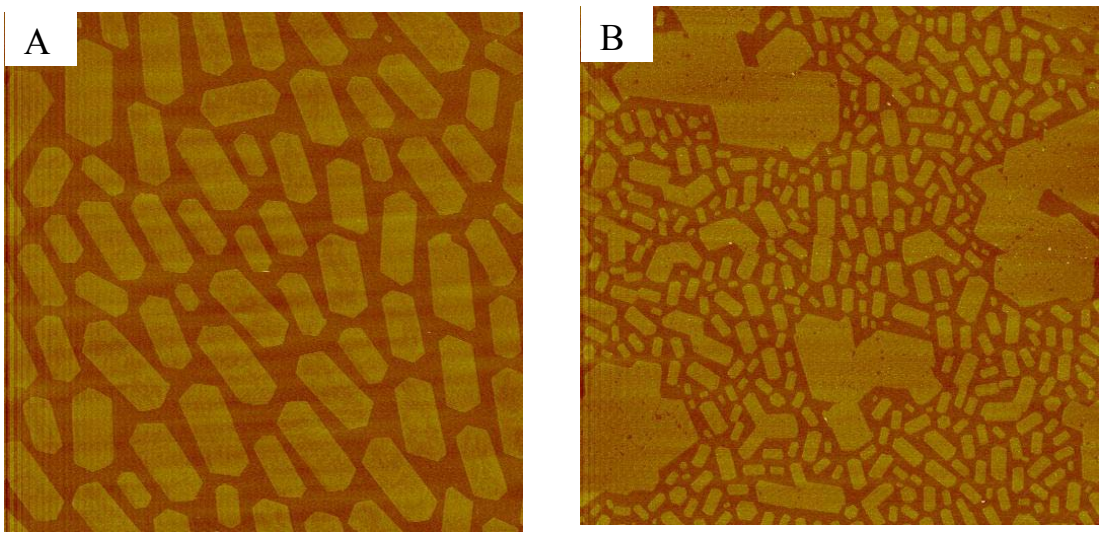

Figure 5-3. AFM height images (20 μm × 20 μm) of 2AA:1PA deposited at A, 20 ºC; B, 4 ºC; after 10 min of solvent evaporation time.

5.5 Summary

In this study we have investigated the rate of domain growth in a mixed LB monolayer of fatty acid and perflurocarboxylic acid. The change in area was followed as a function of time and temperature using AFM imaging. Ostwald ripening was found to be the dominant mechanism of the domain growth, and the process could be modeled using the LS model of domain growth. Some evidence of domain coalescence was observed at low temperatures but this disappeared when the sub-phase temperature was increased.

5.6 Acknowledgements

The Natural Sciences and Engineering Research Council of Canada (NSERC), the Canada Foundation for Innovation (CFI), the Province of Saskatchewan and the University of Saskatchewan are acknowledged for the funding of this work.

5.7 References

1. Krafft, M. P., *Advanced Drug Delivery Reviews* **2001,** 47, 209.
2. Kissa, E., *Fluorinated Surfactants and Repellents* Marcel Dekker Inc.: New York, 2001.
3. Matsumoto, M.; Tanaka, K.; Azumi, R.; Kondo, Y.; Yoshino, N., *Langmuir* **2003,** 19 (7), 2802.
4. Overney, R. M.; Meyer, E.; Frommer, J.; Guntherodt, H. J.; Fujihira, M.; Takano, H.; Gotoh, Y., *Langmuir* **1994,** 10 (4), 1281.
5. Matos, L.; Ravey, J. C.; Serratrice, G., *Journal of Colloid and Interface Science* **1989,** 128 (2), 341.
6. Lehmler, H. J.; Bummer, P. M., *Journal of Colloid and Interface Science* **2002,** 249 (2), 381.
7. Iimura, K.; Shiraku, T.; Kato, T., *Langmuir* **2002,** 18 (26), 10183.
8. Imae, T.; Takeshita, T.; Kato, M., *Langmuir* **2000,** 16 (2), 612.
9. Qaqish, S. E.; Paige, M. F., *Langmuir* **2007,** 23 (5), 2582.
10. Frommer, J.; Luthi, R.; Meyer, E.; Anselmetti, D.; Dreier, M.; Overney, R.; Guntherodt, H. J.; Fujihira, M., *Nature* **1993,** 364 (6434), 198.
11. Ribic, P. R.; Bratina, G., *Journal of Physical Chemistry C* **2007,** 111 (50), 18558.
12. Taylor, P., *Colloids and Surfaces a-Physicochemical and Engineering Aspects* **1995,** 99 (2-3), 175.
13. Lifshitz, I. M.; Slyozov, V. V., *Journal of Physics and Chemistry of Solids* **1961,** 19 (1-2), 35.
14. Haas, C. K.; Torkelson, J. M., *Physical Review E* **1997,** 55 (3), 3191.
15. Bassereau, P.; Brodbreck, D.; Russell, T. P.; Brown, H. R.; Shull, K. R., *Physical Review Letters* **1993,** 71 (11), 1716.
16. Fillot, F.; Tokei, Z.; Beyer, G. P., *Surface Science* **2007,** 601 (4), 986.
17. Jensen, M. H.; Morris, E. J.; Simonsen, A. C., *Langmuir* **2007,** 23 (15), 8135.
18. Rasband, W. S. *Imagej*, 1.37v; U.S. National Institute of Health: Bethesda, Maryland, USA, 1997-2005.
19. Seul, M.; Morgan, N. Y.; Sire, C., *Physical Review Letters* **1994,** 73 (17), 2284.

CHAPTER 6
RIPPLED DOMAIN FORMATION IN PHASE-SEPARATED MIXED LANGMUIR-BLODGETT FILMS

This chapter is a slightly modified copy of an article published in *Langmuir* in March 2008. (Reproduced with permission from *Langmuir* **2008**, 24, 6146-6153. Copyright 2008 American Chemical Society).

The work in this chapter focuses on the study of a mixed LB film of stearic acid ($C_{17}H_{35}COOH$), (SA) and perfluorotetradecanoic acid as a second example of perfluorocarbon / hydrocarbon mixed films. The reason for choosing this system was to investigate the effect of using a shorter hydrocarbon chain (SA instead of AA) on the pattern formed and the mechanism of phase-separation in thin films.

Structural and compositional mapping of the film was carried out by AFM imaging. Selective dissolution and force of adhesion measurements were performed to probe the film composition. The components phase-separated into a linear pattern which was different from the previous hexagonal pattern observed in the AA/PA system (Chapters 2-5). Films were prepared at different surface pressures in order to study the mechanism of phase-separation. This revealed that the components form hexagonal domains at low surface pressure that unwind into a linear rippled pattern at higher deposition pressures. The hexagonal domains and the lines are made of hydrocarbon molecules that force the fluorocarbon molecules in between.

For this research paper, I prepared samples, performed the measurements, and played a major role in interpreting the results and the preparation of the paper. My supervisor provided guidance throughout the experimental work, result interpretation and editing this paper.

6. Rippled domain formation in phase-separated mixed Langmuir-Blodgett films

*Shatha E. Qaqish and Matthew F. Paige**

Department of Chemistry, University of Saskatchewan, 110 Science Place, Saskatoon, Saskatchewan, Canada S7N 5C9

Received January 22, 2008. In Final Form: March 26, 2008

6.1 Abstract

The morphology and composition of phase-separated Langmuir and Langmuir-Blodgett films of stearic acid ($C_{17}H_{35}COOH$) (SA) mixed with perfluorotetradecanoic acid ($C_{13}F_{27}COOH$) (PA) have been investigated using a combination of atomic force microscopy (AFM) measurements and surface pressure-area isotherms. At elevated surface pressures, the mixed film phase-separated to form a distinct series of lines (ripples), as opposed to the hexagons that have previously been observed with mixed films with longer alkyl chain fatty acids. At low surface pressures, phase-separation is still observed, though a range of different domain structures were formed. The chemical composition of the phase-separated domains has been investigated by AFM-based compositional mapping, which has allowed unambiguous identification of the chemical composition of the domains. A simple mechanistic model describing how domain formation takes place in this system is presented.

6.2 Introduction

Under appropriate conditions, surfactant monolayers (Langmuir films) at the air-water interface can phase-segregate to form distinct domains. This phenomenon has been particularly well studied for lipid monolayer systems, for which it has been observed that domain shape depends heavily on factors such as film pressure, temperature and chemical composition. The

driving force for formation of different domain shapes in these systems is believed to be a subtle interplay of line tensions between phases in conjunction with long-range repulsive dipole interactions; line tensions tend to favor formation of circular domains, whereas dipole-dipole interactions tend to force domains into more complex, elongated shapes[1]. In addition, the kinetics of domain growth and surfactant mobility on the sub-phase can also affect domain shape[2]. Even for simple lipid systems, a wide range of shapes has been reported, including circles, stripes, spirals, ripples and more exotic 'dog-bones'[1]. A similar diversity of structures has also been reported for films deposited onto solid supports (Langmuir-Blodgett - LB films)[3-7].

Our group and others have been investigating the composition and morphology of LB films prepared from phase-separated mixtures of fatty acids and perfluorinated fatty acids, with an ultimate goal of understanding and controlling surface patterning in these systems[2, 8-10]. Industrially, fluorinated molecules have been used to modify solid surfaces and can impart desirable physical and chemical properties, including resistance to mechanical and chemical attack, reduction of friction and others. Perfluorinated surfactants are of particular interest in regards to surface patterning as they are both hydrophobic and lipophobic. This combination of properties causes many perfluorinated surfactants to phase-separate when mixed with hydrocarbons, with domain shapes presumably a function of at least some of the parameters described above.

Of particular interest to several groups have been LB films deposited from phase-separated mixtures of arachidic acid ($C_{19}H_{39}COOH$) (AA) and perfluorotetradecanoic acid ($C_{13}F_{27}COOH$) (PA)[2, 8-10]. We have recently observed, through compositionally sensitive AFM imaging, that mixed AA/PA films deposited onto hydrophilic mica substrates form micron-sized, hexagonal domains that are comprised almost entirely of AA, whereas the surrounding matrix is

primarily comprised of PA but contains many nanometer-sized deposits of AA[2]. Surfactant molecules in both types of domains are oriented normal to the substrate surface. It was also observed that the shapes and sizes of these domains depend strongly on film preparation conditions including temperature and deposition pressure. This was ultimately correlated to the mechanism of domain formation and growth, which proceeds first via aggregation of AA in the bulk deposition solution, followed by 2D Ostwald-ripening on the sub-phase surface[2].

As noted previously, a key factor that affects domain shape in phase-separating systems is the chemical composition of the film constituents. For phase-separation to take place in binary mixtures of saturated phospholipid monolayers, for example, it is generally necessary for the constituent phospholipids to differ in chain length by a minimum of four carbons, as well as having one of the components in a gel-phase[4, 7]. In an important study of binary mixtures involving fluorinated surfactants, Iimura et al.[11] have systematically investigated the effect of fatty-acid chain length on domain structure for binary mixtures of perfluoroethers and n-alkyl fatty acids. LB films deposited on silicon were found to phase-separate into circular domains for short alkyl chain lengths, whereas narrower, branched domains were observed at higher chain lengths. While these shape effects were correlated with line-tensions and dipole-dipole interactions, Iimura also noted the importance of mobility of the alkyl-fatty acid on the water surface in controlling pattern formation, and noted that the structures were likely trapped non-equilibrium shapes that were a consequence of the kinetics of domain growth.

In this work we have attempted to characterize the effect of chemical composition on domain structure for the mixed fatty acid / PA system. It was observed that by reducing the length of the fatty acid from $C_{19}H_{39}COOH$ (AA) to $C_{17}H_{35}COOH$ (stearic acid, SA), domains in the LB films are converted from elongated hexagons to a series of narrow, extended lines

(ripples). We have characterized the phase behavior of domain formation via surface pressure-area isotherms and probed both domain structure and composition through a series of AFM measurements (imaging and adhesion force measurements). In addition to providing invaluable insight into the mechanism of phase-separation and domain formation, this system has also allowed us to expand and further refine the compositional AFM mapping approaches that we have developed in previous experiments.

6.3 Experimental section

6.3.1 Chemicals

Stearic acid (99%) was purchased from BDH, perfluorotetradecanoic acid (97%) was purchased from Sigma-Aldrich Corporation. Hexanes (HPLC grade) and tetrahydrofuran (THF) were purchased from EMD and Merck EM Science, respectively. n-Hexadecane (99%) was purchased from Alfa Aesar. Stock solutions of 5.7×10^{-3} M of each of SA and PA were prepared separately in a 9:1 volume ratio of hexanes:THF. The solutions were mixed in appropriate volumes to give a range of SA:PA mole ratios (1:0, 3:1, 2:1, 1:1, 1:2, 1:3 and 0:1). Muscovite mica (Structure Probe Inc., West Chester, PA) was cut into ~1 cm^2 pieces and was freshly cleaved with adhesive tape prior to use.

6.3.2 Isotherm measurements and Langmuir-Blodgett film deposition

Langmuir and LB films were prepared using a KSV Langmuir trough system (KSV Instruments, Helsinki, Finland), with ultrapure water (Millipore, resistivity 18.2 MΩ.cm) as a sub-phase. Experiments were carried out at a temperature of 21 ± 1 ^{o}C, with the temperature controlled by water circulation through the trough's external jacket from a VWR 1157P water bath (VWR International, West Chester, PA). The temperature was monitored by a thermocouple immersed in the sub-phase surface.

Before each measurement, the sub-phase surface was cleaned by vacuum suction and the platinum Wilhelmy plate was cleaned by flaming with a propane torch. For isotherms, a 35 μL aliquot of the appropriate surfactant solution was spread on the sub-phase and the solvent was allowed to evaporate for a minimum of 10 minutes before compression. Surface pressure-area isotherms were collected for pure SA, PA, and their mixtures using a barrier compression rate of 20 $mm \cdot min^{-1}$. For deposition, a 30 μL aliquot of solution was spread and films were compressed at a rate of 10 $mm \cdot min^{-1}$ until reaching the desired surface pressure (values ranged from 1-30 $mN \cdot m^{-1}$). After waiting 10 minutes for film stabilization, the mica substrate, which had been immersed into the sub-phase prior to surfactant addition, was withdrawn at a rate of 5 $mm \cdot min^{-1}$. The mica was allowed to dry in a clean environment prior to imaging in the AFM.

6.3.3 Atomic Force Microscope Measurements

AFM imaging measurements were carried out on a Dimension Hybrid Nanoscope system (Veeco Metrology Group, Santa Barbara, CA) operating in contact mode. The microscope was mounted in an acoustic-vibration isolation system. Experiments were performed using silicon nitride AFM probes (Veeco Metrology Group, Santa Barbara, CA). Measurements in air were performed using probes with nominal spring constant of ~0.1 $N \cdot m^{-1}$ whereas in n-hexadecane, measurements were carried out in a commercial liquid cell using probes with spring constant of ~0.01 $N \cdot m^{-1}$. Samples were positioned in the microscope such that the vertical axis of the sample was in the direction of withdrawal of the solid substrate from the water surface. Correspondingly, the vertical axis in the image data corresponds to the sample withdrawal direction. Unless otherwise stated, samples could be imaged repeatedly without observable tip-induced damage. Histograms of tip-sample adhesion forces were generated by measuring the retraction portion of ~200 independent AFM force curves (analysis performed with Scanning Probe Image Processing software, version 4.3.1.0, Image Metrology, Hørsholm, Denmark). The manufacturer's value for

cantilever spring constants were used for adhesion force calculations, and all cantilevers were taken from the same batch to minimize potential variations in spring constant between different cantilevers.

6.4 Results and discussion

6.4.1 Surface pressure – area isotherms

Surface pressure–area isotherms were collected for pure PA and SA films at the air-water interface, as well as for mixtures of the two surfactants at a series of different mole fractions (Figure 6-1A). Isotherms for pure SA consisted of three distinct regions, a gaseous (disordered) region, a liquid-expanded region and a liquid-condensed region, which is consistent with other isotherm measurements in the literature (see for example, [12]). For the pure film at 21^{o}C, the transition between the liquid-expanded region to the liquid-condensed was observed at ~24 mN·m^{-1}, and a collapse pressure of ~60 mN·m^{-1} was observed. A molecular footprint for SA was estimated by fitting a linear function to the liquid-condensed region of the isotherm and extrapolating to zero surface pressure. This gave a value of 20 Å^{2}· molecule^{-1} which agrees well with other values in the literature[12]. Isotherms for pure films of PA consisted of a single, smooth curve which increased with compression until reaching a steady plateau. A molecular footprint of 29 Å^{2}· molecule^{-1} was determined for PA, which is comparable with our previous measurements[2] and larger than that for pure SA. The latter is an expected result, as the perfluorinated molecules tend to adopt a helical structure[13] as opposed to the simple zig-zag of n-alkyl chains. In terms of the mixed films, the transition between liquid regions shifted to larger mean-molecular areas as the mole fraction of PA increased, with the transition becoming increasingly difficult to resolve as the mole-fraction progressed towards that of pure perfluorocarbon. The isotherms of the mixtures fell between those of the two pure films. In

general, for mixed systems in which the two components are either completely immiscible or behave like an ideal mixture and are completely miscible, the following relationship (additivity rule) is valid:

$$A_{12} = A_1\chi_1 + A_2\chi_2 \qquad (6\text{-}1)$$

where A_{12} is the mean molecular area of the mixed monolayer for a given surface pressure, A_1 and A_2 are the mean molecular areas of the pure components and χ_1, χ_2 are the mole fractions of the pure components in the film. Positive and negative deviations from the additivity rule indicate intermolecular interactions between the constituents (repulsions or attractions, respectively).

To explore the validity of the additivity rule for these mixtures, a plot of mean molecular area as a function of mole-fraction was generated for four different surface pressures (5 $mN \cdot m^{-1}$, 10 $mN \cdot m^{-1}$, 20 $mN \cdot m^{-1}$ and 30 $mN \cdot m^{-1}$) on the isotherms (Figure 6-1B). No significant deviations from linearity were observed, and the slopes and intercepts of the lines agree with the predicted values from equation (6-1), which we take in conjunction with our AFM imaging experiments described in the following section to mean that the two components are immiscible and phase-segregate into different domains. The squares, the dots and the triangles in Figure 6-1B represent the values obtained from the experimental isotherms. The lines passing through them represent the theoretical values obtained from applying equation (6-1). It is clear from Figure 6-1B that the lines pass throughout all the points suggesting that the experimental values of the mean molecular areas and the theoretical values match. This results in no deviation from ideality.

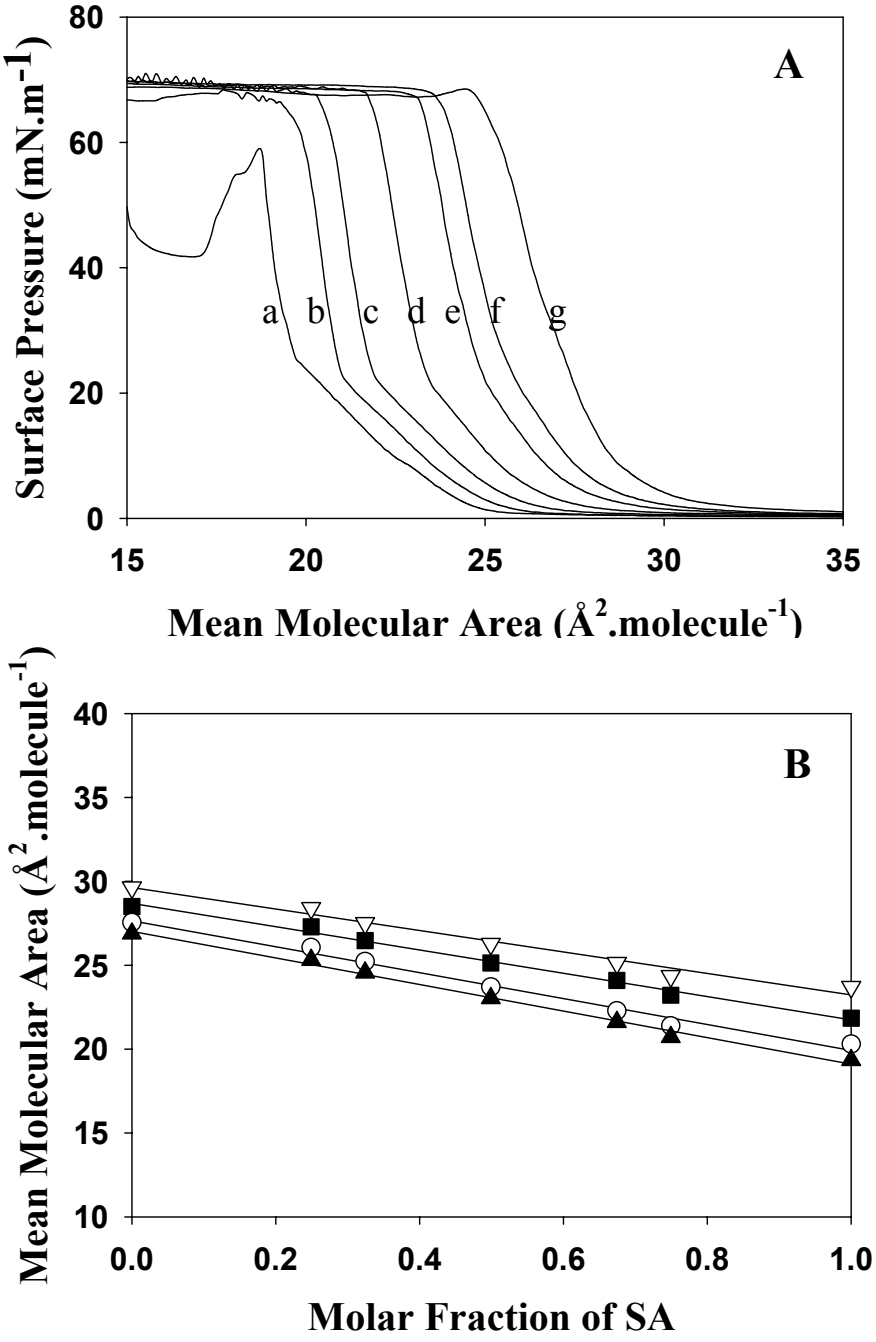

Figure 6-1. A) Surface pressure-area isotherms of SA, PA and their mixtures on a water subphase (a, pure SA; b, 3:1; c, 2:1; d, 1:1; e, 1:2; f, 1:3; g, pure PA). B) Mean molecular area as a function of the mole fraction of SA; white triangles down, 5 $mN \cdot m^{-1}$; black squares, 10 $mN \cdot m^{-1}$; white circles, 20 $mN \cdot m^{-1}$; black triangles up, 30 $mN \cdot m^{-1}$. The line through the data represents the ideal behavior.

It is worth noting that not every mixed hydrocarbon-perfluorocarbon system displays this type of behavior, and that relatively minor changes in the chemical nature of a component can significantly alter miscibility. In their study of mixed films of perfluorododecanoic acid ($CF_3(CF_2)_{10}COOH$) and stearic (or lauric) acid, Rontu et al[12] found significant miscibility between the two components and a positive deviation from ideal mixing. In a closely related study, Shibata[14] surveyed the miscibility of tetradecanoic acid ($CH_3(CH_2)_{12}COOH$) with a series of different length perfluorocarboxylic acids ($C_nF_{2n+1}COOH$), and found that the components were miscible (n=10, 12), immiscible (n=14) and a combination of both (n=16, 18), with the latter depending on whether the film was in the condensed or expanded state. In terms of general behavior, the results obtained in our measurements are entirely consistent with those of Rontu and Shibata; at fixed n-alkyl chain length, short chain perfluorocarboxylic acids generally give rise to miscible mixtures, while longer chains result in immiscibility. Shibata's system of n=14 resulted in an immiscible system with the hydrocarbon which is the case in our system of PA and SA. Comparing the results obtained in our measurements with those by Rontu, it is found that extending the perfluorcarboxylic acid by only two carbons completely switches the miscibility of the components. In Rontu's study, SA was miscible with ($C_{11}F_{23}COOH$) whereas in our study, SA was immiscible with PA which is only two carbon atoms longer than the compound Rontu used.

6.4.2 AFM measurements

The morphology of LB films deposited under a variety of conditions was characterized by contact mode AFM imaging. To be consistent and to allow comparison with previous measurements in the AA/PA system, all samples were prepared with a 2:1 mole ratio of SA: PA. Films deposited at surface pressures between 5-30 $mN \cdot m^{-1}$ consisted of a series of well-defined,

generally parallel lines (ripples) that were elevated above a flat region, with lines extending, in some cases, to more than 20 μm in length. Allowing the surfactants to equilibrate on the water sub-phase for longer periods of time prior to deposition did not significantly alter the film morphology. A typical image of a film prepared at deposition pressure of 10 $mN \cdot m^{-1}$ is shown in Figure 6-2A, B along with an image of a film that was deposited under identical conditions but using a mixture of AA and PA (Figure 6-2C, D). For the SA-based films, the average height difference between the top of the features and the underlying flat region was 0.9 ± 0.2 nm, while their widths were in the range of 0.1-0.3 μm, with significant variation in these values; the width of lines was found to decrease as a function of increasing deposition pressure. Note, these values are also widened above their "true" size because of tip-convolution effects. In comparison with the SA-based films, the AA/PA system forms hexagonal islands which are surrounded by a continuous matrix. For AA/PA, the height difference between the hexagonal islands and the surrounding matrix corresponds to the difference in molecular lengths of the two different surfactants, which has been used previously, in conjunction with other data, to assign chemical identities to the different regions[2]. While the topography measurements provide strong evidence of phase-separation, one cannot definitively identify the chemical composition of the domains based on the height data alone for the SA / PA system. The estimated lengths of SA and PA (calculated for molecules in vacuum using Spartan '04, MMFF) are 2.3 nm and 1.8 nm, respectively. A simple test in which the film was scratched off from the mica substrate by repeatedly imaging it at very high operating force was carried out, and the height difference between the bare substrate and the tops of the ripples was 1.6 ± 0.2 nm. This measured height by AFM is less than the calculated length of SA chain by Spartan. These data in combination suggest that the films consist of a single monolayer only, with the surfactant molecules oriented

at a considerable tilt-angle relative to the normal substrate axis, but it is also not unambiguous. Furthermore, one notes that the height differences observed in these systems are approaching the vertical resolution of our microscope, which further complicates chemical identification based on height differences alone.

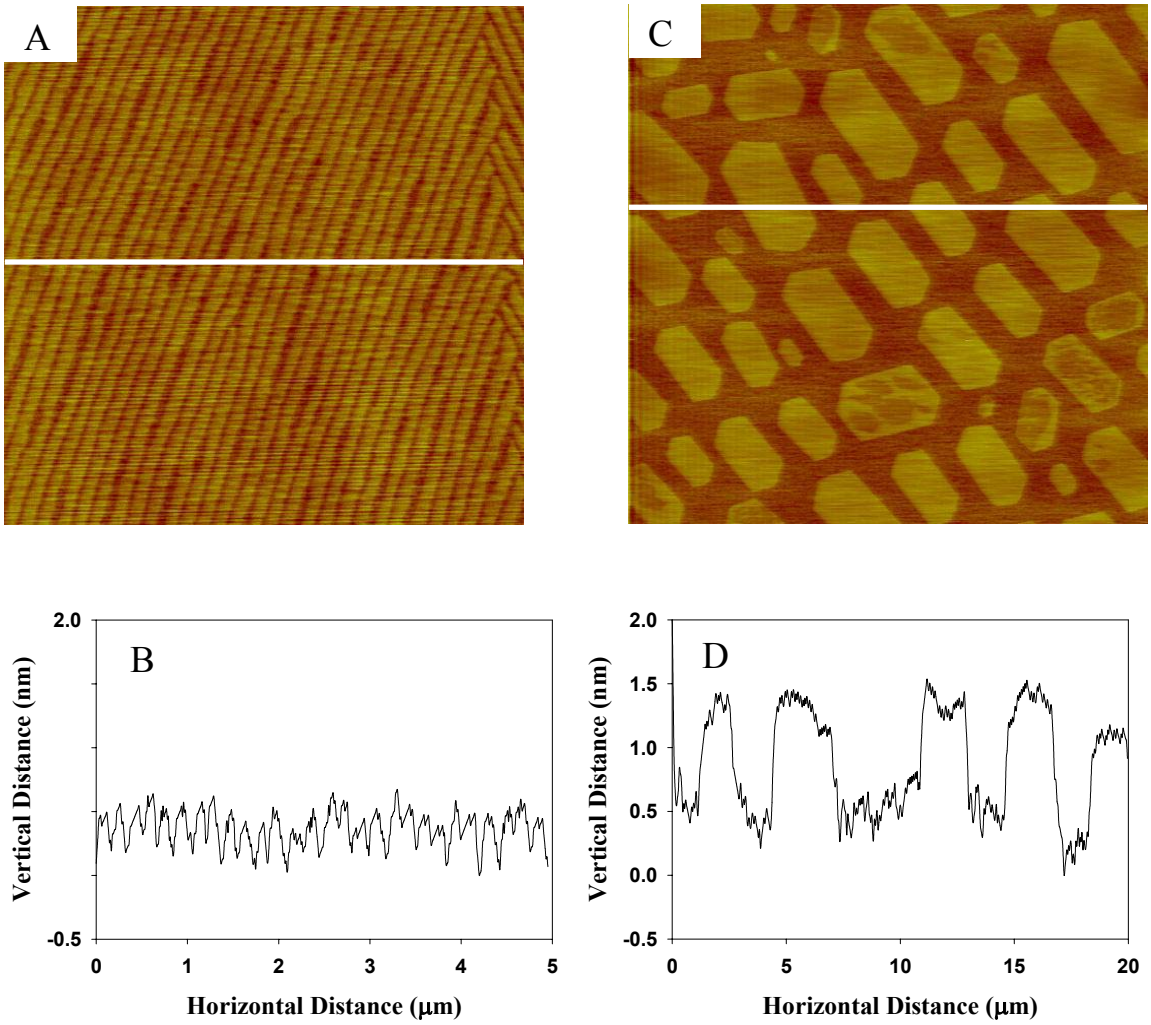

Figure 6-2. AFM height mode images and cross-sectional analysis of A), B) 2SA:1PA and C), D) 2AA:1PA LB films deposited at a surface pressure of 10 $mN \cdot m^{-1}$. A) 5 μm × 5 μm C) 20 μm × 20 μm. Images were taken in air.

There are some structural similarities between the film morphology that is observed in the mixed SA/PA films and so-called "ripple phases" that have been described in phospholipid bilayer and stacked bilayer systems[3-5, 7]. Mou et al. have reported the formation of comparable structures in supported lipid bilayers of 1,2-dipentadecanoyl-sn-glycero-3-phosphatidylcholine on mica, with the ripples being induced by the addition of tris-(hydroxymethy1)aminomethane (Tris) to the bilayers[5]. The underlying cause of ripple formation was not particularly well-understood in this system, though the extent of hydration of the headgroup and the influence of Tris on hydration was believed to play an important role. Tardieu[15] and others have also observed ripple formation for multilayer lecithin systems below the chain melting temperatures for the film. However, these previous studies were of simple one-component films, and for the SA/PA films, local composition plays a crucial role in dictating film morphology; control samples, consisting of the pure individual surfactants were deposited onto mica and imaged in the AFM, and these samples (deposited at several surface pressures, including the liquid expanded / condensed coexistence regions) formed featureless, homogeneous films. In subsequent parts of this paper, we describe further experiments aimed at determining the chemical composition of these phase-separated films.

To gain insight into the chemical composition of the LB films, samples were prepared at a variety of deposition pressures (1-30 $mN \cdot m^{-1}$) and imaged in the AFM. Under all conditions, distinct domains were observed, though the domain morphology varied significantly across this pressure range. Representative images for the different deposition pressures are shown in Figure 6-3A-H. At surface pressures of 1-2 $mN \cdot m^{-1}$ (Figure 6-3A, B), the films consist of large circular domains that were ~4 μm in diameter, elevated by a height of ~1.5 ± 0.3 nm and surrounded by a large number of smaller, discontinuous domains (~0.3 μm diameter, height ~0.9 ± 0.3 nm).

Again, none of the domain heights correspond to the lengths of individual SA or PA molecules, suggesting molecules are lying flat on the mica substrate. This is not surprising, given that at these pressures, the mixed films are in the gaseous state. It was also observed that the circular domains often contained point defects, which is again not unexpected given that the films were not highly compressed. Similar domains and defects have been observed for films prepared at low (1 $mN \cdot m^{-1}$) deposition pressures in our previous study of AA/PA phase-separation, in which it was found that the discontinuous domains were primarily composed of the hydrocarbon AA[2]. On this basis, the larger discontinuous domains will tentatively be assigned as hydrocarbon (SA), with this assignment to be verified later in this paper using alternative approaches.

At deposition pressures of 3 $mN \cdot m^{-1}$, domains consisting of short, branched line fragments were observed, which were intermingled with hexagonal domains (Figure 6-3C). In some cases, the hexagonal domains had line fragments extending from them, suggesting that the hexagonal domains might be breaking apart to form the lines. As the surface pressure was increased to 4-5 $mN \cdot m^{-1}$, the hexagonal domains were no longer observed, and the films consisted entirely of ripple patterns. There was, within our ability to measure, no obvious trend in ripple periodicity as a function of deposition pressure, though quantifying this exactly was problematic because the ripples often contained defects and bends which made exact quantification difficult. Based on these static images, it is reasonable to postulate that the circular domains observed at 1 and 2 $mN \cdot m^{-1}$ tend to convert into hexagonal structures at higher pressures, which in turn 'uncoil' into linear chains upon additional compression. It was observed that at pressures of ~20 $mN \cdot m^{-1}$, the ripples were somewhat less well-ordered than at pressures above and below this value. Again, while difficult to quantify, this result was quite reproducible and was observed in a number of different samples.

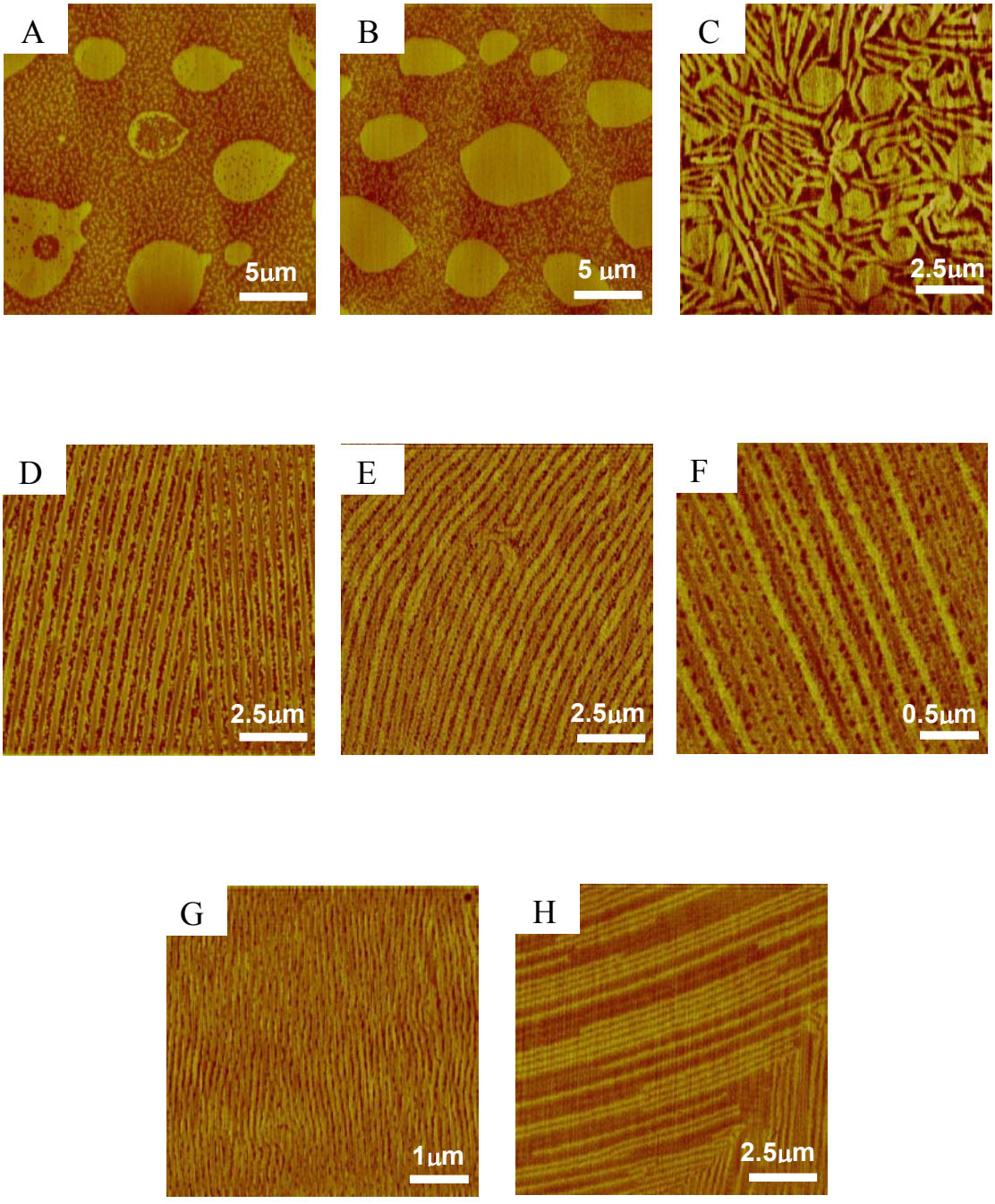

Figure 6-3. AFM height mode images of 2SA:1PA LB film on mica, deposited at a surface pressure of A) 1mN·m^{-1} B) 2 mN·m^{-1} C) 3 mN·m^{-1} D) 4 mN·m^{-1} E) 5 mN·m^{-1} F) 10 mN·m^{-1} G) 20 mN·m^{-1} H) 30 mN·m^{-1}. Images were taken in air.

We note that this pressure is close to the transition pressure between the liquid-expanded and the liquid-condensed regions of SA and postulate that there might be a relationship between the proximity to the transition and the extent of film order, but at present any relationship between the two remains unclear.

While not directly related to the determination of film composition, it is of interest to describe several additional features of the film morphology here. The ripples in the films can extend for many tens of microns in length, but they do have well-defined ends. For example in Figure 6-2A, there are several lines that end abruptly and meet a second line to form a "herringbone" pattern. This pattern can be observed in a number of other images taken at different deposition pressures (for example, Figure 6-3D,H), and appears to be a fairly common feature of the rippled films. We have also noted that for some samples, there are regions of the film that contain a significant number of bent ripples. Figure 6-4A, B shows one such region for a film deposited at 30 $mN \cdot m^{-1}$. While the films still contain many linear, parallel lines, the lines often undergo several ~45^{o} turns, and closer inspection of Figure 6-4B shows that the film retains vestiges of the hexagonal shapes that were observed at 3 $mN \cdot m^{-1}$. This lends further support to the idea that ripple formation proceeds through the formation of hexagons at lower surface pressures, followed by the decomposition of these hexagons. The formation of hexagons appears to be a common theme in the mixed hydrocarbon-perfluorocarbon surfactant films. As reported previously for the AA/PA system[2] (and shown in Figure 6-2C), phase-separation gives rise to well-defined hexagons of hydrocarbon in a PA matrix, and again hexagons are observed in the SA/PA system. Again, the precise explanation for this remains unclear, though it reinforces the concept that simple line-tension arguments are not sufficient to explain domain morphology in these systems, as one would simply expect the minimum energy domain shape to be circular.

McConnell has noted that elongated or elliptical domains are often observed in lipid systems when line tension effects are dominated by long-range electrostatic repulsions [1], and a similar effect may be at work in these systems.

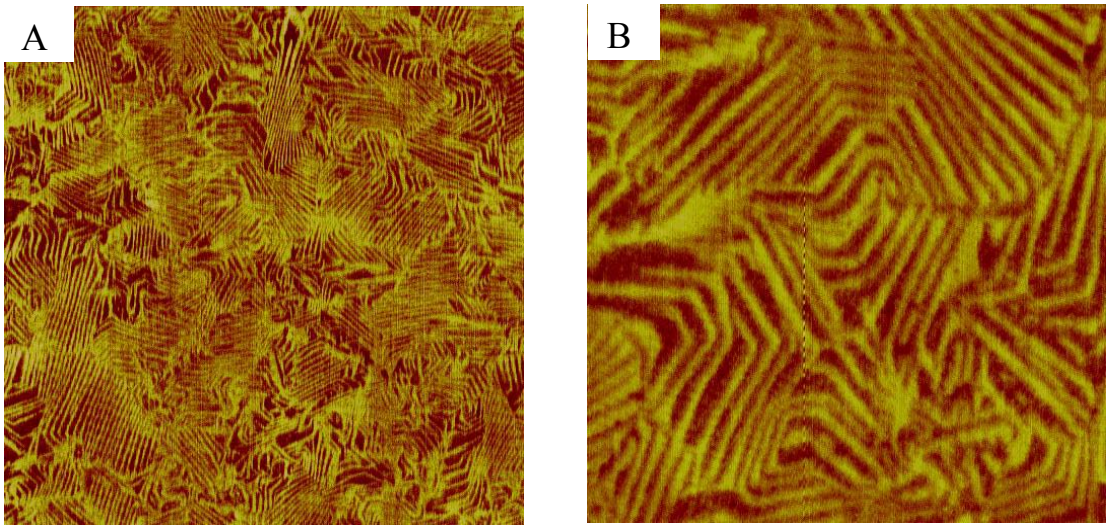

Figure 6-4. AFM height mode images of 2SA:1PA LB film on mica deposited at a surface pressure of 30 $mN \cdot m^{-1}$. A) 10 μm × 10 μm B) 2.5 μm × 2.5 μm. Images were taken in air.

A point that must be considered is the influence of the deposition process itself on the film surface morphology. It has been shown by several groups (see for example [3, 4, 7]) that ripple formation in LB systems can be strongly influenced by substrate mediated condensation near a phase transition, and that for some systems, ripple formation will always take place perpendicular to the direction of withdrawal of the substrate from the air-water interface. Since the onset of ripple formation was observed at pressures that were quite far away from a phase transition for the SA/PA system, we do not believe that substrate mediated condensation plays a major role. Furthermore, the rippled domains could also be deposited onto silicon oxide surfaces, indicating that the nature of the solid substrate plays a minimal role in controlling these features. There does appear to be some influence of the withdrawal process on film morphology.

For example, in Figure 6-3A-H, many (but not all) of the stripes are oriented parallel with the withdrawal direction of the substrate. However, we have also observed samples in which there is no obvious correlation between stripe orientation and withdrawal direction, and even within the same sample there are often multiple orientations of stripes. In general, it appears that the deposition process may influence the ripple patterns but if so, the effect is likely fairly subtle and is quite different from those described by previous groups.

To further probe the chemical composition of the rippled films, two approaches were taken: selective-dissolution/desorption of film components followed by AFM imaging, and adhesion force measurements. In terms of the former, films that were deposited at 1 $mN \cdot m^{-1}$ and 5 $mN \cdot m^{-1}$ were incubated in n-hexadecane for 5-10 minutes, as it has previously been observed that this treatment desorbs the hydrocarbon component, leaving behind the fluorocarbon and voids previously occupied by hydrocarbon[2]. It should be noted that there are several advantages to selective-dissolution for AFM-based chemical mapping over other approaches described in the literature. The samples are imaged in AFM "height" mode as opposed to phase or friction imaging, and hence mechanical properties of the sample should play a negligible role in image contrast. Also, our approach does not require chemical modification of AFM probe tips (so-called "chemical force microscopy"), which can sometimes be problematic. Images of the samples imaged using this approach are shown in Figure 6-5A, B. As compared to the samples imaged in air, the circular domains that had previously been elevated (Figure 6-3A) dissolved to the point of being level with the underlying substrate, except for a thin (~0.1 μm width) ring around the domain edge. This confirms the original postulate that the circular domains consist primarily of SA. Further comparison of Figure 6-3A and Figure 6-5A reveals that the smaller discontinuous domains surrounding the circular domains were not removed by n-hexadecane

incubation, indicating these smaller domains have an entirely different composition from the circular domains. This indicates that the small discontinuous domains are comprised of PA. The heights of these domains was ~0.6 ± 0.1 nm in n-hexadecane, which is comparable to their height in air, indicating that solvent incubation does not significantly perturb their structure.

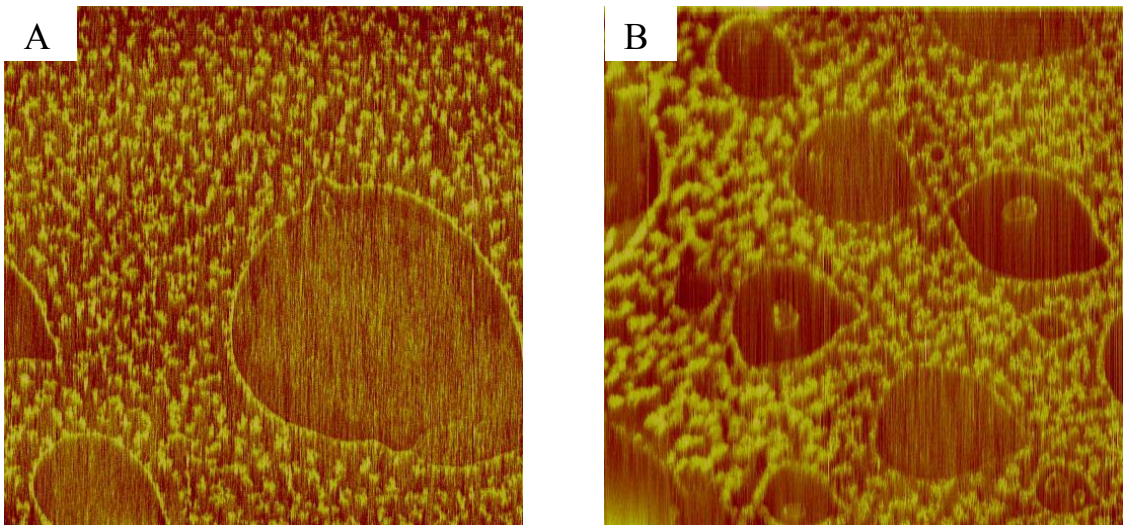

Figure 6-5. AFM height mode images of a 2SA:1PA LB film on mica deposited at a surface pressure of 1 $mN \cdot m^{-1}$ after incubation in n-hexadecane. A) 10 μm × 10 μm; B) 20 μm × 20 μm. Images were taken in n-hexadecane.

As an additional confirmation of the chemical identity of the different domains in the low surface pressure samples, histograms of the adhesion force between a standard silicon nitride AFM tip and the different regions in the sample deposited at 1 $mN.m^{-1}$ in n-hexadecane were produced and compared to those of a pure SA LB film control sample. Histograms are shown in Figure 6-6A-D. We note that care must be taken in placing too much weight on the absolute force values measured, since the forces will be affected by small variations in force constants between cantilevers (for these experiments, we have attempted to minimize this by using only cantilevers from the same batch, and whenever possible, the same cantilever). For this work, we

consider both the mean force values, their associated uncertainties and the overall shape of the histograms to make composition assignments.

Measurements of the adhesion force for the "vacant" regions inside of the circular domains in n-hexadecane gave a mean value of 40 ± 2 pN, for the smaller discontinuous domains the force of adhesion was $1.0 \pm 0.5 \times 10^2$ pN, and for the dark areas in the continuous domain the force of adhesion was 38 ± 3 pN. For the pure SA film control sample, a value of $0.4 \pm 0.1 \times 10^2$ pN was obtained. The uncertainty ranges in these measurements represent the standard deviation for the ~200 independent force measurements. We note that the uncertainty associated with the small discontinuous domains is large in comparison with the other values, which may be attributed to difficulties in precisely positioning the probe tip over these small regions. The adhesion force values for the circular domains (previously assigned as SA), the dark areas in the continuous domain and the pure SA film were, within error, the same, as was the general shape of the adhesion force histograms. In addition, a control sample consisting of freshly cleaved mica alone gave a value of $0.5 \pm 0.1 \times 10^2$ pN (data not shown), indicating that the void regions are likely bare mica. The adhesion forces for the small domains, however, were more than twice as large. These results in combination are entirely consistent with the small domains being comprised of PA, as suggested in the imaging experiments. In general, stronger tip-sample adhesion forces should be observed between PA and the tip as compared to those between the AA and the tip because of the strong interaction between the polarized tip and the highly electronegative fluorine atoms[2]. However there is a difference in the magnitude of the force of adhesion of PA from our previous work (240 ± 80 pN).

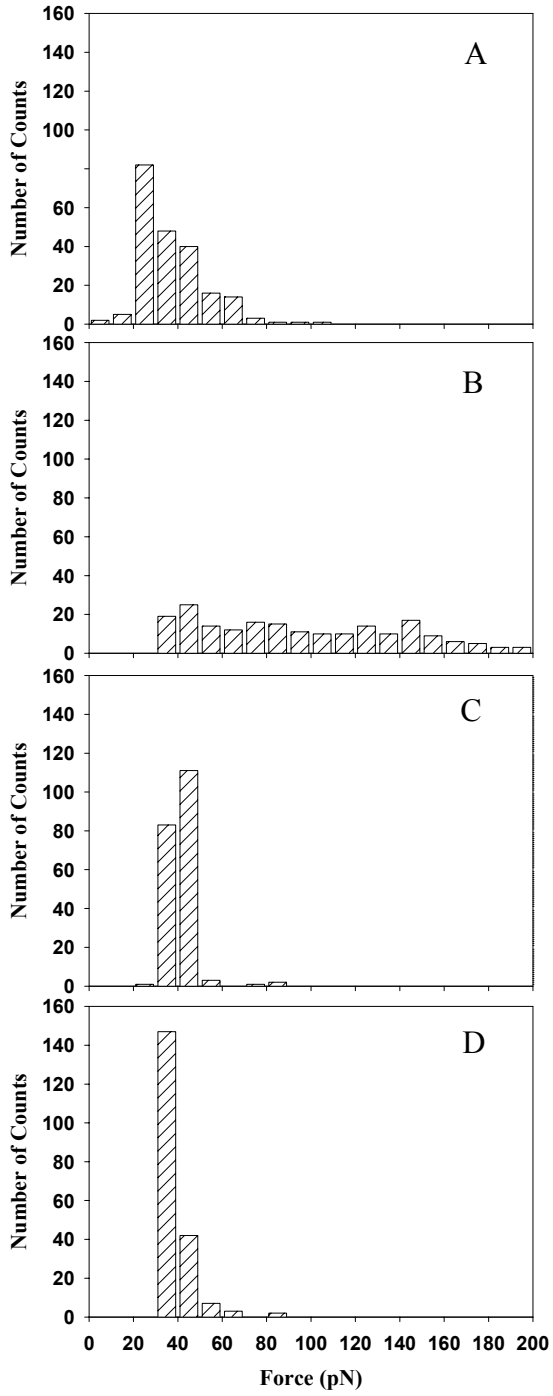

Figure 6-6. Histograms of adhesion force between a silicon nitride tip and the different regions on an LB film deposited at 1 $mN \cdot m^{-1}$. Forces were measured in n-hexadecane. A) pure stearic acid film on mica B) discontinuous domains for 2SA:1PA LB film C) circular domains D) dark regions in the continuous domain.

While there is likely some variation in the absolute values of measured adhesion forces because of small variations in cantilever spring constants between different probes, these are likely to be relatively small and the most probable source of this difference is the alignment of PA molecules on the substrate; for the previous study of the AA/PA film systems, PA molecules were aligned normal to the surface and were densely packed. For the films measured here, the molecular alignment is not normal to the surface and packing density is much lower. It is reasonable to assume this will shift the measured adhesion forces closer to those of the underlying substrate (smaller values).

As a final set of measurements, the composition of the rippled domains formed at higher surface pressure was probed via the selective dissolution imaging approach. Because the rippled domains were both small and highly homogeneous over large areas, it was very difficult to observe changes in the film topography after solvent incubation. To make any changes in the film topography more obvious, a film prepared at 5 $mN \cdot m^{-1}$ first had a 1 μm × 1 μm reference mark mechanically scratched into it by repeated imaging at high operating force. After scratching, a 5 μm × 5 μm image containing the reference mark and large regions of undamaged film was measured both in air and after n-hexadecane incubation. AFM images and cross-sections from such an experiment are shown in Figure 6-7A-D. The central result from these experiments is that there is a complete inversion of film topography after incubation in n-hexadecane. Ripples that were elevated above the background in air correspond to the lower regions in the n-hexadecane image. This is highlighted by the cross-sectional analysis of the same region of the image, before and after solvent incubation (Figure 6-7B,D). On this basis, one can assign the elevated regions for the samples imaged in air as consisting almost entirely of SA, with the space between adjacent elevated regions being filled with loosely packed PA.

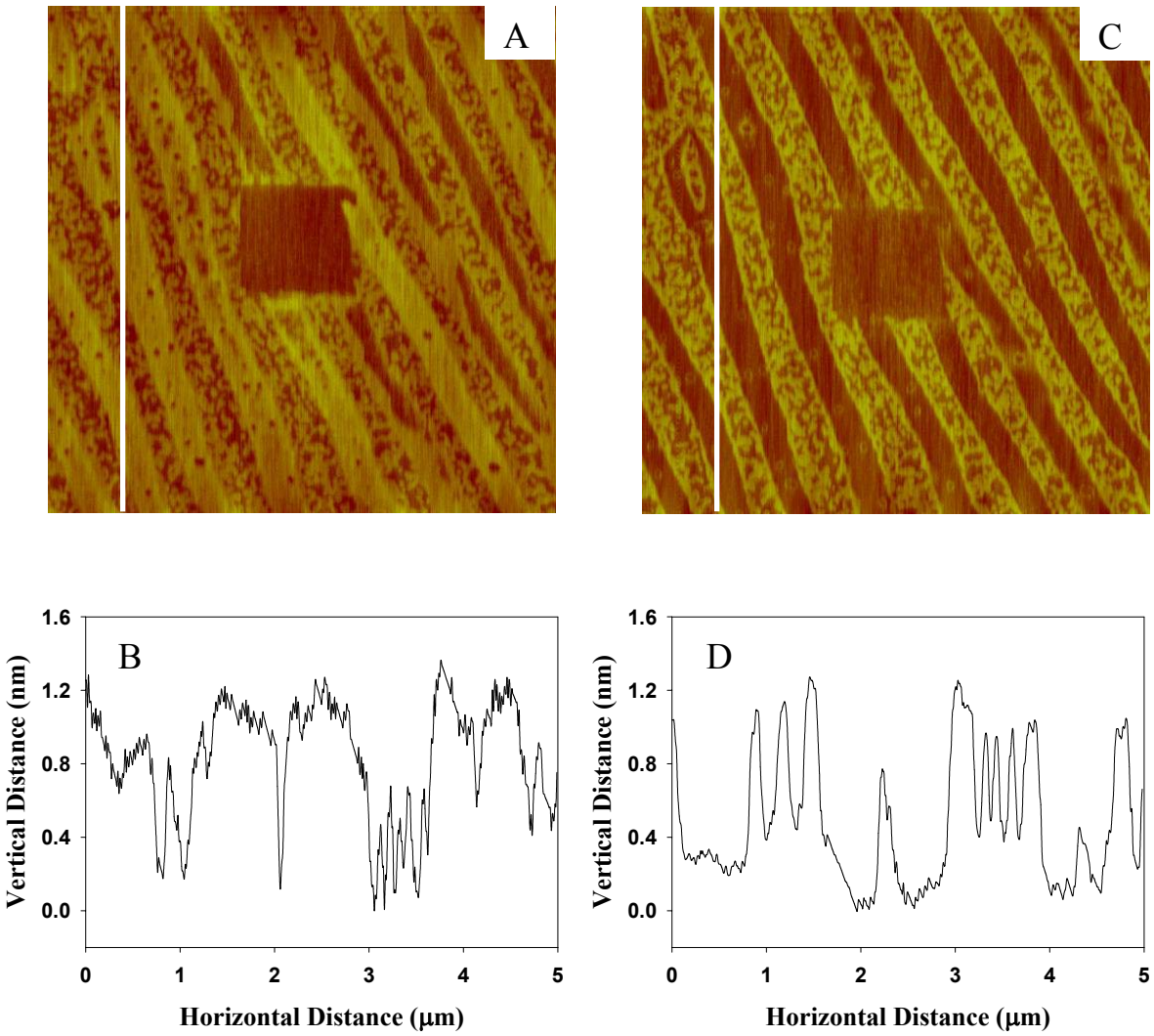

Figure 6-7. AFM height mode images and cross-sectional analysis of A), B) 2SA:1PA imaged in air, and C), D) 2SA:1PA imaged in n-hexadecane. LB films were deposited at a surface pressure of 5 $mN \cdot m^{-1}$. Image sizes are 5 μm × 5 μm. The bare region in the centre of the image has been scraped free of surfactant by repeated imaging at a high operating force.

After incubation, the elevated domains have a height of ~1.0 ± 0.1 nm which, again, is less than the full length of an individual PA molecule, adding further support that PA is not adsorbed normal to the mica substrate. Furthermore, the regions that are occupied by PA contain a significant number of voids. Closer inspection of Figure 6-7A reveals that these regions

contained many voids even before incubation, indicating that they were bare mica. This is quite reasonable, given that the deposition pressure chosen for this film was relatively low.

Using the combined topographic and compositional information collected in this work, one may speculate on the mechanism of formation of the rippled domains. From the low-pressure deposition films, it is clear that even before the film is compressed, phase-separation of the two components has already taken place in the bulk. The SA forms circular, micron-sized domains, which are surrounded by numerous small (~0.9 ± 0.3 nm) deposits that are enriched in PA. As the film at the air-water interface is compressed, the circular SA domains take on more complex, linear and hexagonal structures, which, because of compression, become densely packed on the sub-phase surface. Presumably, the PA deposits are compressed between the densely packed structures and begin to form a continuous film in the intervening space. As compression increases, the circular and hexagonal structures uncoil into linear chains to produce extended linear regions of SA with PA packed in between adjacent lines. Again, while speculative, this mechanism is strongly supported by the numerous observations made here. Further experiments aimed at confirming this mechanism are underway, with particular emphasis being placed on the role of kinetics of surfactant diffusion on formation of these novel domain structures.

6.5 Conclusions

In this work, the phase behavior, structure and composition of mixed Langmuir and Langmuir-Blodgett films of stearic acid and perfluorotetradecanoic acid was investigated. A combination of pressure-area isotherm and compositionally-sensitive AFM imaging experiments indicate that this system undergoes phase-separation, with the structure and chemical nature of the domains depending strongly upon the deposition pressure of the LB films. At deposition

pressures below 4 $mN \cdot m^{-1}$, the film consists of circular or branched domains of hydrocarbon, surrounded by smaller deposits of perfluorocarbon. At higher deposition pressures, the films consist of a series of parallel lines (ripples) that are composed almost entirely of hydrocarbon, with the intervening space between lines occupied by perfluorocarbon. A simple mechanism for the formation of the rippled domains was proposed, and discussed in context of the AFM imaging data.

6.6 Acknowledgements

Funding for this work was provided by the Natural Sciences and Engineering Research Council of Canada (NSERC), the Canada Foundation for Innovation (CFI), the Province of Saskatchewan and by the University of Saskatchewan.

6.7 References

1. McConnell, H. M., *Annual Review of Physical Chemistry* 1991, 42, 171-195.
2. Qaqish, S. E.; Paige, M. F., *Langmuir* 2007, 23 (5), 2582-2587.
3. Moraille, P.; Badia, A., *Langmuir* 2003, 19 (19), 8041-8049.
4. Moraille, P.; Badia, A., *Langmuir* 2002, 18 (11), 4414-4419.
5. Mou, J. X.; Yang, J.; Shao, Z. F., *Biochemistry* 1994, 33 (15), 4439-4443.
6. Brasseur, R.; Braun, N.; El Kirat, K.; Deleu, M.; Mingeot-Leclercq, M. P.; Dufrene, Y. F., *Langmuir* 2007, 23 (19), 9769-9772.
7. Gleiche, M.; Chi, L. F.; Fuchs, H., *Nature* 2000, 403 (6766), 173-175.
8. Matsumoto, M.; Tanaka, K.; Azumi, R.; Kondo, Y.; Yoshino, N., *Langmuir* 2003, 19 (7), 2802-2807.
9. Matsumoto, M.; Tanaka, K.; Azumi, R.; Kondo, Y.; Yoshino, N., *Chemistry Letters* 2002, (10), 970-971.
10. Imae, T.; Takeshita, T.; Kato, M., *Langmuir* 2000, 16 (2), 612-621.
11. Iimura, K.; Shiraku, T.; Kato, T., *Langmuir* 2002, 18 (26), 10183-10190.
12. Rontu, N.; Vaida, V., *Journal of Physical Chemistry C* 2007, 111 (27), 9975-9980.
13. Jang, S. S.; Blanco, M.; Goddard, W. A.; Caldwell, G.; Ross, R. B., *Macromolecules* 2003, 36 (14), 5331-5341.
14. Shibata, O.; Yamamoto, S. K.; Lee, S.; Sugihara, G., *Journal of Colloid and Interface Science* 1996, 184 (1), 201-208.
15. Tardieu, A.; Luzzati, V., *Journal of molecular biology* 1973, 75, 711-733.

CHAPTER 7
MONOLAYER BEHAVIOR OF PHASE-SEPARATED LANGMUIR-BLODGETT FILMS OF MIXED PALMITIC ACID AND PERFLUOROOCTADECANOIC ACID

This chapter is a modified copy of a manuscript submitted to Langmuir in January 2009.

The work in this chapter focuses on the study of an LB film of palmitic acid ($C_{15}H_{31}COOH$) and perfluorooctadecanoic acid ($C_{17}F_{35}COOH$) as a third example of perfluorocarbon / hydrocarbon mixed films. The purpose of investigating this system was to determine the effect of having a shorter hydrocarbon chain, and a longer fluorinated chain on the pattern formed and the mechanism of phase-separation in thin films. This example of mixed monolayer represents the opposite of what we studied in the previous two systems (Chapters 2 and 6) where the hydrocarbon chain was longer than the fluorocarbon compound.

Structural and compositional mapping of the film was performed by AFM, X-PEEM and confocal fluorescent microscopy measurements. The change in the molar ratios of the components of the film altered the structure obtained. We observed a loss of palmitic acid with time into the sub-phase, which is unique to this system. Deposition was done at different temperatures and different surface pressures in order to help in determining the underlying mechanism. A simple mechanistic model of phase-separation and domain formation in this system is described in this chapter.

For this research paper, I prepared samples, performed the isotherms and the atomic force microscopy measurements, and played a major role in interpreting the results and the preparation of the paper. Stephen Urquhart and Uday Lanke carried out X-PEEM measurements and data

analysis. Sophie Brunet carried out confocal fluorescent microscopy measurements. Matthew Paige is my supervisor who provided guidance throughout the experimental work and was involved in result interpretation and in editing this paper.

7. Monolayer behavior of phase-separated Langmuir-Blodgett films of mixed palmitic acid and perfluorooctadecanoic acid

*Shatha E. Qaqish, Stephen G. Urquhart, Uday Lanke, Sophie M.K. Brunet[†] and Matthew F. Paige**

Department of Chemistry, University of Saskatchewan, 110 Science Place, Saskatoon, Saskatchewan, Canada S7N 5C9

[†]Saskatchewan Structural Sciences Centre, University of Saskatchewan, 110 Science Place, Saskatoon, Saskatchewan, Canada S7N 5C9

7. 1 Abstract

The morphology and the chemical composition of mixed Langmuir and Langmuir-Blodgett (LB) films of palmitic acid ($C_{15}H_{31}COOH$) and perfluorooctadecanoic acid ($C_{17}F_{35}COOH$) have been investigated using a combination of atomic force microscopy (AFM), X-ray photoelectron emission microscopy (X-PEEM) and confocal fluorescent microscopy measurements. Surface pressure – area isotherms indicated the immiscibility of the two components of the monolayer at all molar fractions. The two surfactants phase-separated into hexagonal domains with short "hairy" extensions radiating from the domains. Measurements showed that the hexagonal domains and the hairy extensions were made of fluorocarbon and the hydrocarbon existed between the hairy extensions and in the area surrounding them. Phase-separation was observed at low surface pressure indicating that the molecules phase-separated in the bulk. The change in the molar fractions of the components in the mixed film lead to a change in the ratio between the hairy extensions and the hexagonal domains. An important factor took

place in this system that was not observed in all the previous systems, which was the preferential solubility of the palmitic acid in the sub-phase. The underlying forces responsible for phase-separation were investigated. A simple mechanism of the domain formation and growth was proposed.

7.2 Introduction

Mixed Langmuir and Langmuir-Blodgett (LB) films of two or more components show different and superior properties in comparison with those of the individual components. These films have been extensively studied as they can provide an insight into the interactions between the film-forming molecules[1]. Mixed films containing perfluorinated compounds are subjects of continuously growing interest as they have improved chemical and physical properties compared to their non-fluorinated counterparts[2-4]. As an example of these systems, mixtures of fatty acids and perfluorinated fatty acids were studied in terms of composition and morphology[2, 5-8]. However not much is known about the mechanism[6, 9] of domain formation in these films in order to control surface patterning which is of importance in chemical and biological sensing[10].

Mixed films of saturated fatty acids have been widely studied[11-13] because of their applications in pharmaceutical and food industry. The preferential dissolution of one component into the sub-phase is an important process that has been studied to understand the mechanism of how fatty acid microspheres function in releasing the drug from dosage[11].

The LB technique is an important method to fabricate nanothin films of controlled patterns of phase-separated mixtures. The structure of the phase-separated components in the LB films is affected by different parameters such as temperature, surface pressure and chemical composition. The pattern formed is a result of the competition of two forces; the dipole-dipole interactions and line tension[14]. Dipole-dipole interactions are repulsive forces resulting from the

parallel alignment of the molecules in the monolayer and favor the formation of elongated domains, whereas line tension favors the formation of large circular domains[14]. By manipulating the dominant interactions between the components, surface patterns can be controlled.

The chemical composition has a significant effect on the shape of the domains formed in perfluorinated mixed LB films. In our previous studies[7, 9, 15] of arachidic acid, $C_{19}H_{39}COOH$ (AA) and perfluorotetradecanoic acid, $C_{13}F_{27}COOH$ (PA); elevated hexagonal domains of hydrocarbon surrounded by a lower continuous domain of fluorocarbon with some deposits of hydrocarbon were observed. These hexagonal domains grow via Ostwald ripening[9] following the Lifshitz-Slyozov kinetic model of two-dimensional growth[16]. However when the hydrocarbon chain length was reduced to stearic acid $C_{17}H_{35}COOH$ (SA) and the fluorocarbon chain was kept constant, elevated linear domains of SA were observed with the space between them being filled with PA. This pattern was attributed to the change in line tension. Iimura et al. observed a change in the domains shape from circular into linear upon increasing the hydrocarbon chain length keeping a constant perflurooxaacid[17]. This was attributed to the change in the line tension and the mobility of the molecules[17]. The same trend was observed when the length of the fluorinated chains was increased keeping the alkyl chains constant[18]. Variations in the chain length affect mainly the line tension in terms of dispersive interactions between the chains, and do not alter the vertical dipole component which is only affected by the change in the head groups[18]. In theory, line tension should increase by increasing the chain length.[17] Thus domains of longer chain lengths adopt more circular structures. This trend was observed when the alkyl chain increases in length, keeping the perfluoroalkyl silane chain length constant.[19]

In this work we tried to characterize and understand the phase-separation in mixed LB films of palmitic acid, $C_{15}H_{31}COOH$ (C16) and perfluorooctadecanoic acid, $C_{17}F_{35}COOH$ (F18)

using different techniques. This study focuses on the mechanism of phase-separation as a function of the molar fraction in the system. Another important aspect of this study is the preferential dissolution of one component in the sub-phase and how it is inferred from the phase rule and the isotherm data.

It was observed that C16 and F18 phase-separated into hexagonal domains with hairy extensions irradiating from them. As the hydrocarbon content increased in the system, an increase in the length of these hairy extensions was observed. This property of the dependence of shape on the molar fraction was not dominant in other fatty acids mixed LB films.[2, 17] However, this property was previously observed in a film of fluorinated fatty acid and fluorinated silane[20]. This current system seems to combine the properties of the domains formed from the previous two systems; AA/PA[7, 9] and SA/PA[8] which are the hexagons and the linear patterns. Since the head groups were similar in all the systems, the hydrophobic interactions of the chains were the determining factor of the phase-separation mechanism. The phase-separation of the current system was investigated by surface pressure-area isotherms. The structure and the chemical composition of the phase-separated domains were studied by atomic force microscopy (AFM) measurements including selective dissolution[7, 8], X-ray photoelectron emission microscopy (X-PEEM) and confocal fluorescent microscopy. Detailed insight into the mechanism of phase-separation of this system is discussed.

7.3 Experimental section

7.3.1 Chemicals.

Palmitic acid, (C16) (90%) was purchased from Sigma-Aldrich Corporation, while perfluorooctadecanoic acid (F18) (97%) was purchased from Alfa Aesar. The fluorescent probe 4,4-difluoro-5,7-dimethyl-4-bora-3a,4a-diaza-s-indacene-3-hexadecanoic acid (BODIPY FL

C16) was purchased from Invitrogen Corp. (Carlsbad, CA). The solvents hexanes (HPLC grade), acetone (HPLC grade) and chloroform (HPLC grde) were purchased from EMD Chemicals Inc., whereas tetrahydrofuran (THF), toluene, methanol and trichloroethylene were purchased from Merck EM Science. Absolute ethanol was purchased from Commercial Alcohols Inc. Stock solutions of 2.7×10^{-3} M of each of C16 and F18 were prepared separately in a 9:1 volume ratio of hexanes:THF for C16, and hexanes:ethanol for F18. The solutions were mixed in appropriate volumes to give a range of C16:F18 mole ratios (1:0, 3:1, 2:1, 1:1, 1:2, 1:3 and 0:1). No precipitation was observed upon mixing.

A solution of 2.1×10^{-3} M of BODIPY FL was prepared in 8:2 volume ratio of hexanes:THF. A 6.5 μL aliquot of the probe was added to a 2 mL mixture of 1C16:1F18 to prepare a 0.25% molar ratio doped solution.

The different substrates used for the deposition experiments were prepared and cleaned as follows: Muscovite mica (Structure Probe Inc., West Chester, PA) was cut into ~ 1 cm^2 pieces and was freshly cleaved with adhesive tape prior to use. Phosphorus-doped silicon (Silicon Inc. Boise, ID) was cut into ~ 1 cm^2 pieces and was cleaned by sequentially sonicating in trichloroethylene, acetone and ethanol for 20 min each. The silicon was dried under nitrogen gas and then exposed to a short wavelength UV light Hg arc lamp (Ultra-violet Products Inc., San Gabriel, CA) for ~ 1 hr. Microscope cover glasses (1 ounce, 22 x 22 mm, No 1.5, VWR International, West Chester, PA) were cleaned by sonicating in methanol for 2 min, then were rinsed thoroughly by ethanol and were dried under nitrogen gas. The slides were then placed in a plasma cleaner PDC-32G (Harrick Plasma, Ithaca, NY) for ~ 20 min at high power to remove any residual contaminants.

7.3.2 Isotherm measurements and Langmuir-Blodgett film deposition.

Langmuir and Langmuir-Blodgett (LB) films were prepared using a KSV Langmuir trough system (KSV Instruments, Helsinki, Finland), with ultrapure water (Millipore, resistivity 18.2 MΩ.cm) as a sub-phase. Experiments were carried out at a temperature of 20.5 $\pm$ 0.6 ^{o}C unless otherwise stated. The temperature was controlled by water circulation through the trough's external jacket from a VWR 1157P water bath (VWR International, West Chester, PA) and was monitored by a thermocouple immersed in the sub-phase close to the surface.

Before each measurement, the sub-phase surface was cleaned by vacuum suction and the platinum Wilhelmy plate was cleaned by rinsing with chloroform then flaming with a propane torch. A 70 μL aliquot of the appropriate surfactant solution was spread on the sub-phase and the solvent was allowed to evaporate for a minimum of 10 minutes before compression unless otherwise stated. Surface pressure-area isotherms were collected for pure C16, F18, and their mixtures using a barrier compression rate of 20 mm/min. For deposition, the films were compressed at a rate of 10 mm·min^{-1} until reaching the desired surface pressure (20 mN/m). After waiting 10 minutes for film stabilization, the substrate, which had been immersed into the sub-phase prior to the surfactant addition, was withdrawn at a rate of 5 mm·min^{-1}, and the barrier rate was changed to match the withdrawal rate. The substrate was allowed to dry in a clean environment prior to imaging in the AFM. A mica substrate was used for the AFM measurements, phosphorus-doped silicon was used for X-PEEM measurements, and glass for fluorescence microscopy measurements. For fluorescent film deposition, two pieces of microscope coverglass were placed back-to-back on the dipper to minimize the contamination of the backside of each slide with fluorescent dye. To ensure there was no dye on the backside of

the cover glass, the surface was swabbed with hexanes prior to imaging in the fluorescence microscope.

7.3.3 Atomic force microscope measurements

AFM imaging measurements were carried out on a Dimension Hybrid Nanoscope system (Veeco Metrology Group, Santa Barbara, CA) operating in contact mode. The microscope was mounted in an acoustic-vibration isolation system. Experiments were performed using silicon nitride AFM probes (Veeco Metrology Group, Santa Barbara, CA). Measurements in air were performed using probes with nominal spring constant of ~ 0.1 or ~ 0.58 N/m whereas in toluene, measurements were carried out in a commercial liquid cell using probes with spring constant of ~ 0.58 N/m. Samples were positioned in the microscope such that the vertical axis of the sample was in the direction of withdrawal of the solid substrate from the water surface. Correspondingly, the vertical axis in the image data corresponds to the sample withdrawal direction. Samples could be imaged repeatedly without observable tip-induced damage.

7.3.4 X-ray photoelectron emission microscopy measurements.

X-PEEM measurements were performed with the PEEM-2 microscope at the Advanced Light Source (ALS, Berkley, CA) on the beamline 7.3.1.1.[21] with a linear polarization of ~ 85% and a Ti filter. The X-PEEM images were acquired as described previously[15] at a sequence of photon energies in order to establish a three-dimensional dataset that includes energy, x-coordinate and y-coordinate which is translated into an image. A photon shutter was used to reduce the radiation exposure between the data points and between the scans. Carbon 1s NEXAFS spectra were corrected by normalizing to an I_o spectrum collected for a freshly Ar^+ sputtered silicon wafer, measured under the same conditions as the LB film spectra. X-PEEM

images were collected separately at two different energies; 286.9 eV and 290.8 eV corresponding to the C 1s → σ^*_{C-H} and the C 1s → σ^*_{C-F}, respectively.

7.3.5 Confocal fluorescent microscopy measurements

The BODIPY FL doped LB films on glass were imaged using an LSM 410, Carl Zeiss inverted confocal fluorescence microscope (LSM Tech, USA) with 40X / 1.3 NA Plan – Neofluar objective. Samples were excited with 488 nm laser light from a multiline argon-ion laser and the emission was passed through a 510-560 nm bandpass filter. Image analysis and adjustment (contrast, brightness and gamma value (0.6)) was carried out using the software ImageJ [22].

7.4 Results and discussion

7.4.1 Surface pressure – area isotherms

Surface pressure – area isotherms were collected at the air-water interface at 20.5 ± 0.6 ºC for the pure C16 and F18 surfactants, and for a series of mixtures of different mole fractions of the two surfactants (Figure 7-1A). Isotherms for pure C16 consisted of three distinct regions, including a gaseous (disordered) region, a liquid-expanded region and a liquid-condensed region. The molecular footprint for C16 was calculated by fitting a linear function to the liquid-condensed region of the isotherm and extrapolating to zero surface pressure. The value obtained was 22-23 $Å^2$/molecule at 20 ºC which is consistent with reported literature values[23, 24]. Note, the molecular footprint for C16 is slightly larger than that for longer chain fatty acids such as stearic acid ($C_{17}H_{35}COOH$, 20 $Å^2$/molecule[8]) and arachidic acid ($C_{19}H_{39}COOH$, 20 $Å^2$/molecule[9]) at the same temperature, which can be attributed to the shorter chain-length compounds tendency to form expanded monolayers[25]. The transition between the liquid-

expanded to the liquid-condensed regions was at ~ 25 mN/m and a collapse pressure of ~ 50 mN/m was observed, which are again consistent with literature values[23, 26].

Surface pressure - area isotherms for a pure film of F18 consisted of a single, smooth curve which increased with compression until reaching a steady plateau with a collapse pressure at ~ 65 mN/m. A molecular footprint of 28-29 $Å^2$/molecule was determined for F18, which is slightly smaller than that reported by Shibata et al. (~ 35 $Å^2$/molecule) [27], though this difference can likely be attributed to the use of a substantially lower sub-phase pH (1.0) in those studies. The larger footprint of the perfluorinated compounds compared with the hydrocarbon is reasonable, given that the perfluorinated surfactants tend to adopt a helical structure[28] in contrast with the simple zig-zag of n-alkyl chains.

The isotherms of the mixtures fell between those of the pure films. For all of the mixed films, two collapse pressures were observed, with a collapse at ~ 50 mN/m and a second at ~ 65 mN/m, corresponding to the collapse pressures of the C16 and F18 components, respectively. The collapse pressures showed minimal variation as a function of film composition (Figure 7-1B). Invariance of the collapse pressures of individual components as a function of film composition in a surfactant mixture is a typical characteristic of immiscible film components[29, 30]. According to the two-dimensional phase rule, two completely immiscible components constrained to a monolayer will, if one of the film components is present in the bulk, have two degrees of freedom[25]. For fixed film temperature and external pressure, the film components should then be forced out of the monolayer at their equilibrium spreading pressures (surface pressure at which the monolayer is in equilibrium with the bulk phase), which is constant regardless of the initial composition of the spreading solution. These results strongly suggest that the two film components are immiscible.

To provide further insight into the degree of immiscibility of the two surfactants, the isotherms were analyzed in terms of the mean molecular area as a function of the molar fraction of C16 (Figure 7-1C). For a fully immiscible, two-component system, one expects the average area per molecule to scale as a function of the relative amounts of the individual film components, as shown in equation (7-1) [2]:

$$A_{12} = \chi_1 A_1 + \chi_2 A_2 \qquad (7\text{-}1)$$

where A_{12} is the average area per molecule in the mixed film, A_1, A_2 are the molecular areas for the pure components and χ_n is the molar fraction of the component. Deviations from the above equation indicates some degree of miscibility and intermolecular interaction between the film components[31].

Figure 7-1C shows experimentally measured values of A_{12} for four different surface pressures plotted as a function of molar fraction of C16, with the ideal linear behaviour anticipated from equation (1) included. In general, the measurements were well-represented by the simple linear fit, with any deviations from linearity simply caused by random scatter in the data (as determined through inspection of residuals from multiple repeats of these experiments). While desirable and potentially quite useful, we have not yet been able to develop a simple method of predicting miscibility of film components based on their chemical structure alone.

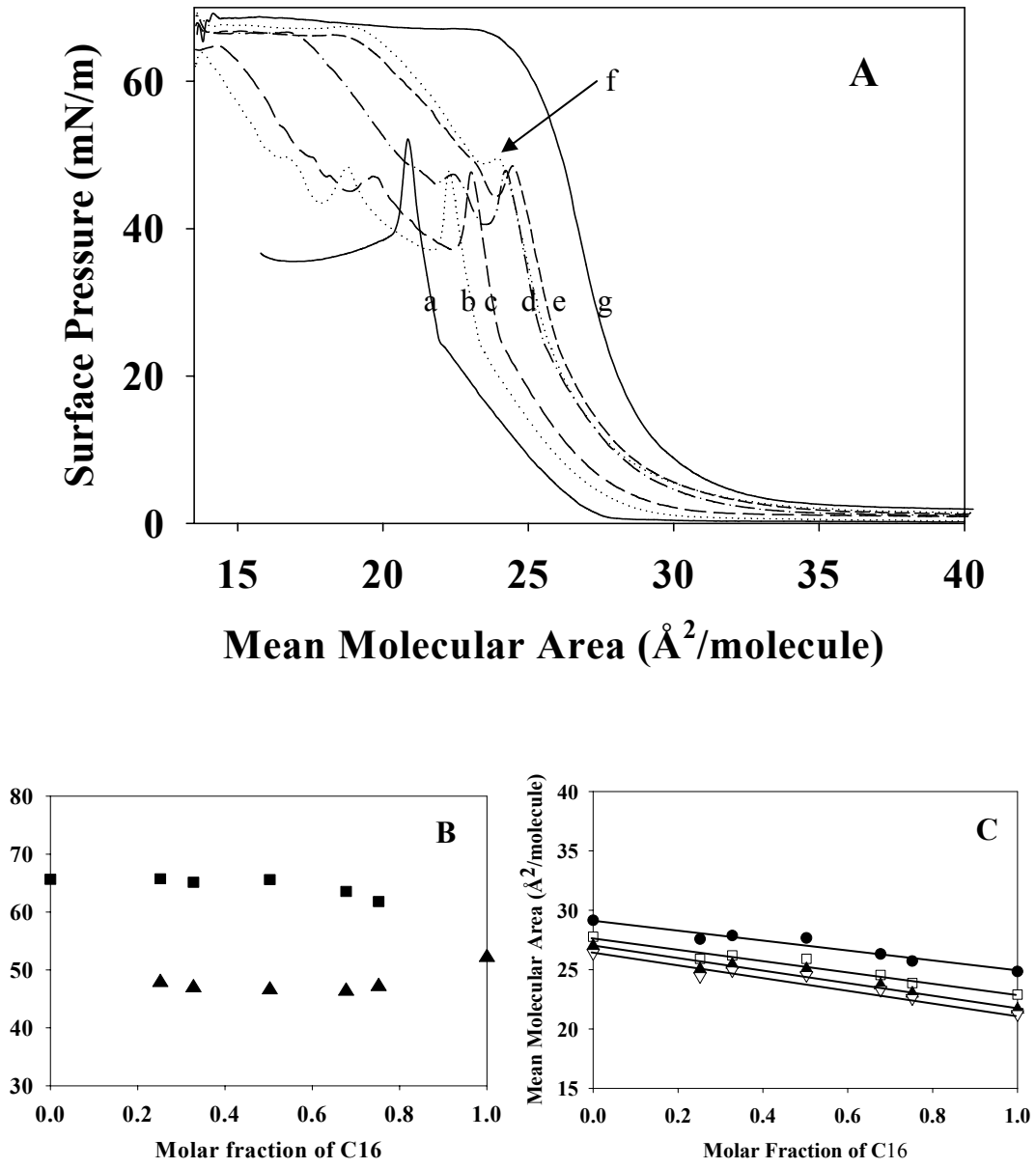

Figure 7-1. (A) Surface Pressure-area isotherms of C16, F18 and their mixtures on water subphase: a, pure C16; b, 3:1; c, 2:1, d, 1:1; e, 1:2; f, 1:3; g, F18. B, Collapse pressure as a function of the molar fraction of C16. Triangles, first collapse pressure; squares, second collapse pressure. C, Mean molecular area as a function of molar fraction of C16 at various surface pressure; dark circles, 10 mN/m; white squares, 20 mN/m; white triangles up, 30 mN/m; black triangles down, 40 mN/m. The dotted lines represent the ideal behavior.

For mixtures of C18 and perfluorinated fatty acids measured using sub-phase conditions comparable to those used here, extending the fluorocarbon chain from F12 to F14 switches the system from being miscible to immiscible[8, 32]. Shibata[27] has reported that C14 surfactants were miscible with shorter (F11-F13) perfluorocarbons, but not with F15. While moving to higher chain-length perfluorcarbons at a fixed length hydrocarbon increases miscibility, no obvious empirical relationship can be extracted from the literature that predict miscibility. This is not entirely surprising, since the extent of miscibility in these systems is expected to be a function of dipole-dipole interactions, dispersion forces and surface tension, making a priori predictions of miscibility challenging.

7.4.2 Film composition.

To probe the structure and composition of these films, as well as to gain insight into the mechanism of pattern formation, LB films were characterized using a variety of measurement techniques including AFM imaging, X-PEEM and confocal microscopy. Figure 7-2A-G shows a series of AFM images taken for pure and mixed-composition films deposited on mica at 20.5 ± 0.6 ºC and at a surface pressure of 20 mN/m. Pure F18 films (Figure 7-2A) consisted of multiple circular domains with diameters that varied between ~ 0.3 – 4.2 μm. These circular domains agree with the domains obtained by Imae et al. when studied the F18 system[6]. The domain heights (0.9 ± 0.2 nm) were less than the expected length of an F18 molecule (~ 2.3 nm), suggesting that the molecules are aligned with a considerable tilt angle with respect to the substrate surface. Upon the addition of C16 to the films, elevated hexagonal domains (heights of 1.2 ± 0.3 nm above the surrounding flat region) with multiple, short “hairy” extensions radiating out from the domains were observed.

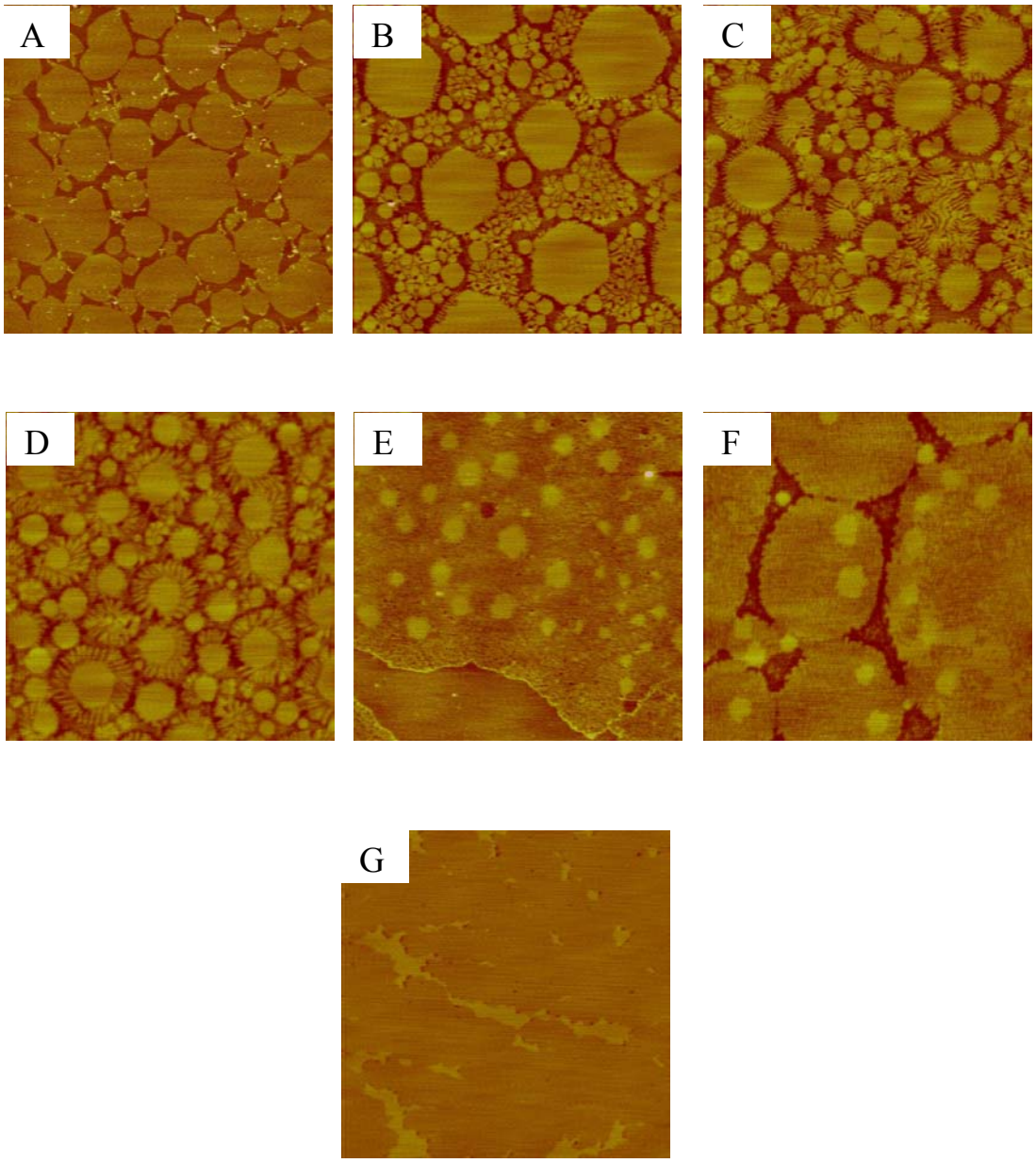

Figure 7-2. AFM height mode images of LB films on mica of pure C16 and F18 and their mixtures. A, pure F18; B, 3:1; C, 2:1, D, 1:1; E, 1:2; F, 1:3; G, C16. Films deposited at 20 mN/m, and 20 ºC. Scan size 5 μm × 5 μm.

As the molar fraction of the hydrocarbon in the mixture increased, the hexagonal domains became smaller and the extensions became longer (Figure 7-2B-F). The hairy extensions overlapped together at high molar ratios of C16 and formed a close-packed layer surrounding the hexagonal domains (Figure 7-2E, F). At sufficiently high fractions of C16 (see, for example, Figure 7-2F), the hairy extensions formed elliptical structures that encased several hexagons. The pure film of C16 appeared as a continuous monolayer, with occasional defects (Figure 7-2G).

In a number of previous studies of mixed LB films, AFM height information alone has been used to chemically identify the domains. In some film systems, for example mixed arachidic - perfluorotetradecanoic acid[7], this can be done in an unambiguous way because domain heights correspond to the difference in lengths of the constituent molecules. However, for this system, unambiguous identification is not so easy. To identify the chemical composition of the domains in the mixed films, the selective dissolution approach that has been described previously[7-9] was employed. Briefly, in this approach the mixed films are incubated in an organic solvent for ~ 5 min to dissolve and desorb the C16 component, while leaving the fluorocarbon behind. This approach has previously been shown to exclusively remove the hydrocarbon component in mixed hydrocarbon/perfluorocarbon LB films, allowing compositional mapping of the sample by observing void regions in the film. For the samples imaged here, samples were incubated in toluene; previous experiments made use of n-hexadecane for dissolution, but for the C16 containing films, it was found that toluene was slightly more efficient than n-hexadecane at removing the hydrocarbon component and so was used for all experiments.

Figure 7-3 A and C show height mode images of the same region of a film measured first in air and then after incubation in toluene. Comparison of these two figures shows that neither the hexagonal domains nor the hairy extensions were removed by incubation in toluene, which we interpret as meaning both the hexagons and the hairy extensions are primarily comprised of F18. Incubation in toluene results in a small but detectable change in sample morphology, with an average height difference between the elevated hexagonal domains and the underlying substrate of 1.2 ± 0.3 nm in air (Figure 7-3 B) and 1.8 ± 0.2 nm after toluene incubation (Figure 7-3 D). The hairy extensions showed height differences that were comparable to those for the hexagonal domains, again supporting that these parts of the sample have the same composition. We note that the observed difference in domain height in air is much larger than the difference in length between a chain of C16 and F18 (~ 0.2 nm). The difference in height between measurements in toluene and those in air can be attributed either to the removal of the hydrocarbon from the space surrounding the hexagonal domains, or to some alteration of the F18 (extension of the perfluorocarbon chain, change in tilt angle relative to the substrate surface) molecules upon immersion in toluene. To test the former, the film was measured in air after allowing the toluene to evaporate. A height difference similar to that measured in toluene was observed, suggesting that either the hydrocarbon dissolved or the F18 changed its tilt angle in the film when immersed in toluene and retains this arrangement even after the evaporation of toluene. While this approach has allowed unambiguous identification of the perfluorocarbon domains, further experiments are clearly required to definitively map the chemical nature of the surface.

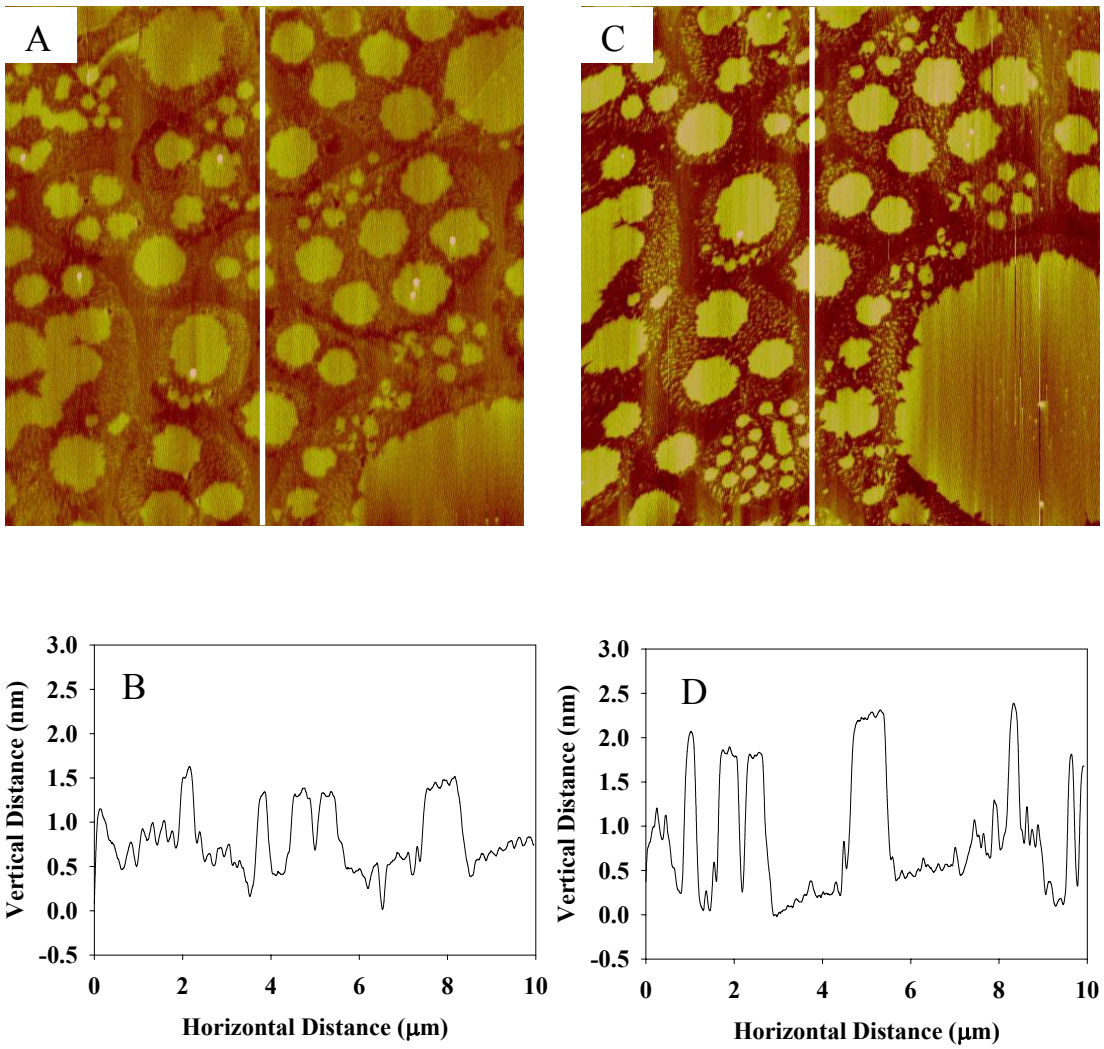

Figure 7-3. AFM height mode images of 1:1 LB films on mica deposited at 20 mN/m, and 20 ºC.A, in air; B, its cross section; C, in toluene; D, its cross section. Scan size 10 μm × 10 μm.

To unambiguously determine the location of C16 molecules in the mixed films, X-PEEM measurements were carried out on a 1:1 LB film deposited on silicon at 20 mN / m and 20.5 ± 0.6 ºC. Figure 7-4A shows the C1s NEXAFS spectra of the LB film. Strong peaks at 286.9 eV and at 290.8 eV were observed, which correspond to the C 1s → σ^*_{C-H} transition and the C 1s → σ^*_{C-F} transition, respectively[15]. Figure 7-4B shows an X-PEEM image of the LB film excited at 286.9 eV (C 1s → σ^*_{C-H} transition). At this energy, the hexagonal domains gave low signals and were surrounded by some bright domains indicating that these bright domains were composed of hydrocarbon. A grey region surrounding the above matrix whose brightness was lower than that surrounding the hexagons was observed. This indicates that there is hydrocarbon content in this region as well. The lower signal from the hydrocarbon in this grey region is because of the different packing of the hydrocarbon chains on the surface. In the area between the hairy extensions surrounding the hexagons, the C16 chains are either perpendicular or tilted with an angle on the surface, whereas in the grey region the C16 chains are parallel to the surface. Because of the interactions between C16 and F18 chains in the area close to the hexagons, the F18 chains force the C16 chains to be in an angle on the surface and not parallel to the surface. However in the grey region there are no F18 chains to interact with the C16 chains so they are parallel to the surface. When the hydrocarbon is parallel to the surface, the collected signal is from the excitation of one C-H bond at a time. In the case of the perpendicular or the tilted hydrocarbon, the signal is stronger as it is the outcome of a number of C-H excitations added together. Figure 7-4C represents the same above region excited at 290.8 eV corresponding to the C 1s → σ^*_{C-F} transition to detect the fluorocarbon. The bright regions consisted of hexagonal domains and hairy extensions in addition to some irregular smaller domains corresponded to the F18 chains. This result supports the previous AFM images that the hexagonal and the hairy

domains are composed of F18 molecules. It also shows that C16 is present between the hairy extensions and in the surrounding area and reveals its different packing on the surface.

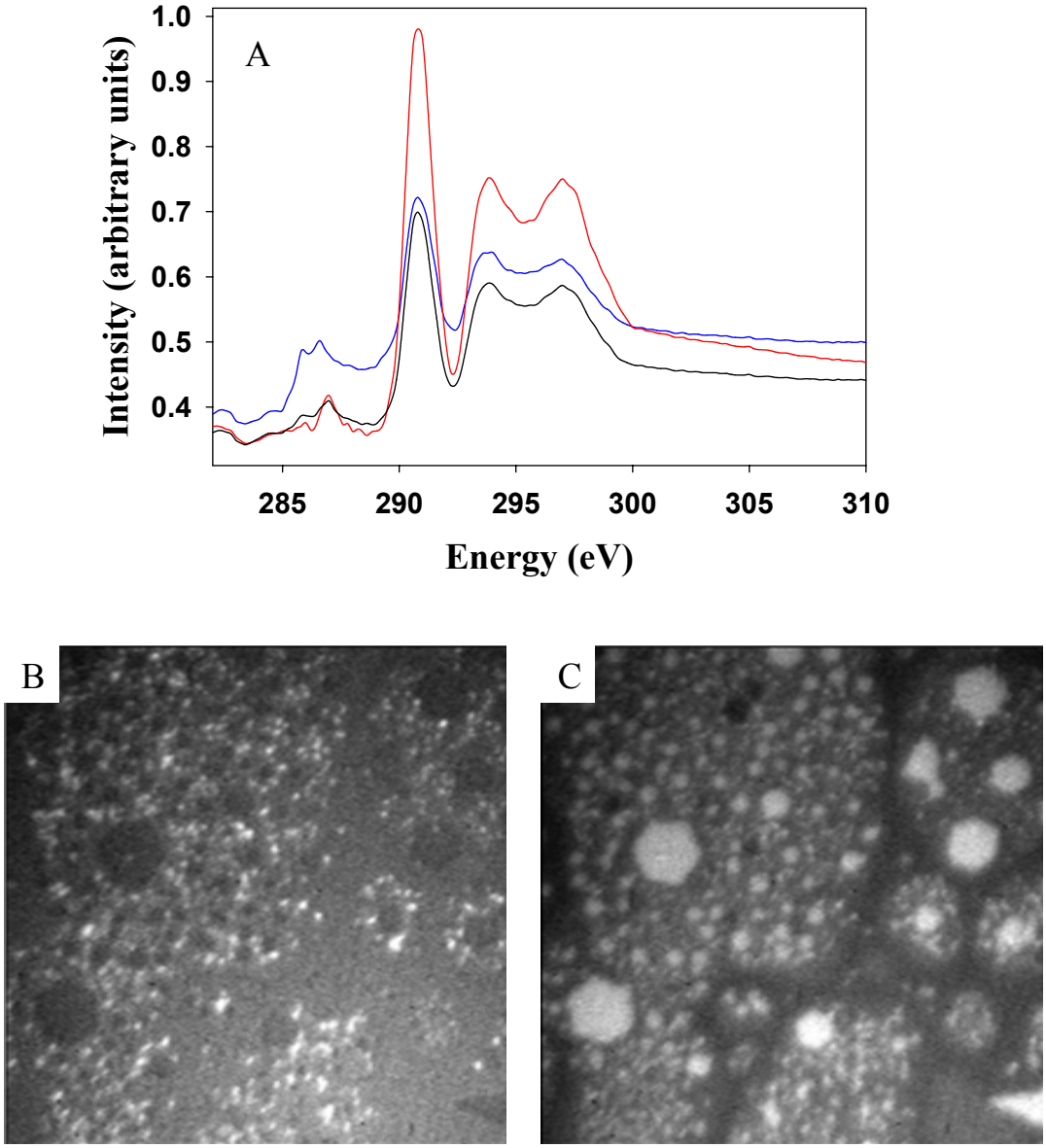

Figure 7-4. A, C 1s NEXAFS spectra for the different domains in 1:1 LB film deposited on silicon at 20 ºC and 20 mN/m. Red, hexagonal domains; blue, between the hexagonal domains; black, continuous domain. X-PEEM images of the 1:1 film measured at B, C-H edge; C, C-F edge. Scan size 28 μm × 28 μm.

For additional verification of the film composition, samples that had been doped with BODIPY FL C16, a fluorescently labeled palmitic acid analogue were deposited and imaged using confocal fluorescence microscopy. As control samples, films doped with different amounts (0.0% - 2.5% molar ratio) of fluorescent dye were deposited onto microscope coverglass and imaged in the AFM. It was observed that neither the use of coverglass as a deposition substrate nor the doping concentration alters the film morphology or the characteristics of the isotherms as long as the doping concentration is < 1.0%. Figure 7-5A shows an AFM image of the 0.25% doped 1:1 film on glass deposited at 20 mN/m and 20.5 ± 0.6 ºC. This image shows the same characteristic surface patterns observed previously for the non-doped samples (Figure 7-3A) where the hexagonal domains and the hairy extensions are elevated above the surface. In the doped film, the height difference between the hexagonal domains and the surrounding area is ~ 1.6 ± 0.3 nm in air, and ~ 2.3 ± 0.3 nm after incubation in toluene. These height differences are comparable with, though marginally larger than those obtained for the non-doped films, likely because of the presence of the bulky BODIPY FL group.

Figure 7-5B and C shows a fluorescence image and the corresponding AFM image of a 0.25% doped 1:1 film. The hexagonal domains, believed to be perfluorocarbon on the basis of the dissolution experiments, were dark in the fluorescence images, indicating the absence of fluorescent analogue. Between the hairy extensions and in the surrounding area, bright regions were observed, indicating the presence of the dye. These measurements provide final, unambiguous confirmation of the composition of the film that was suggested by the AFM and X-PEEM measurements.

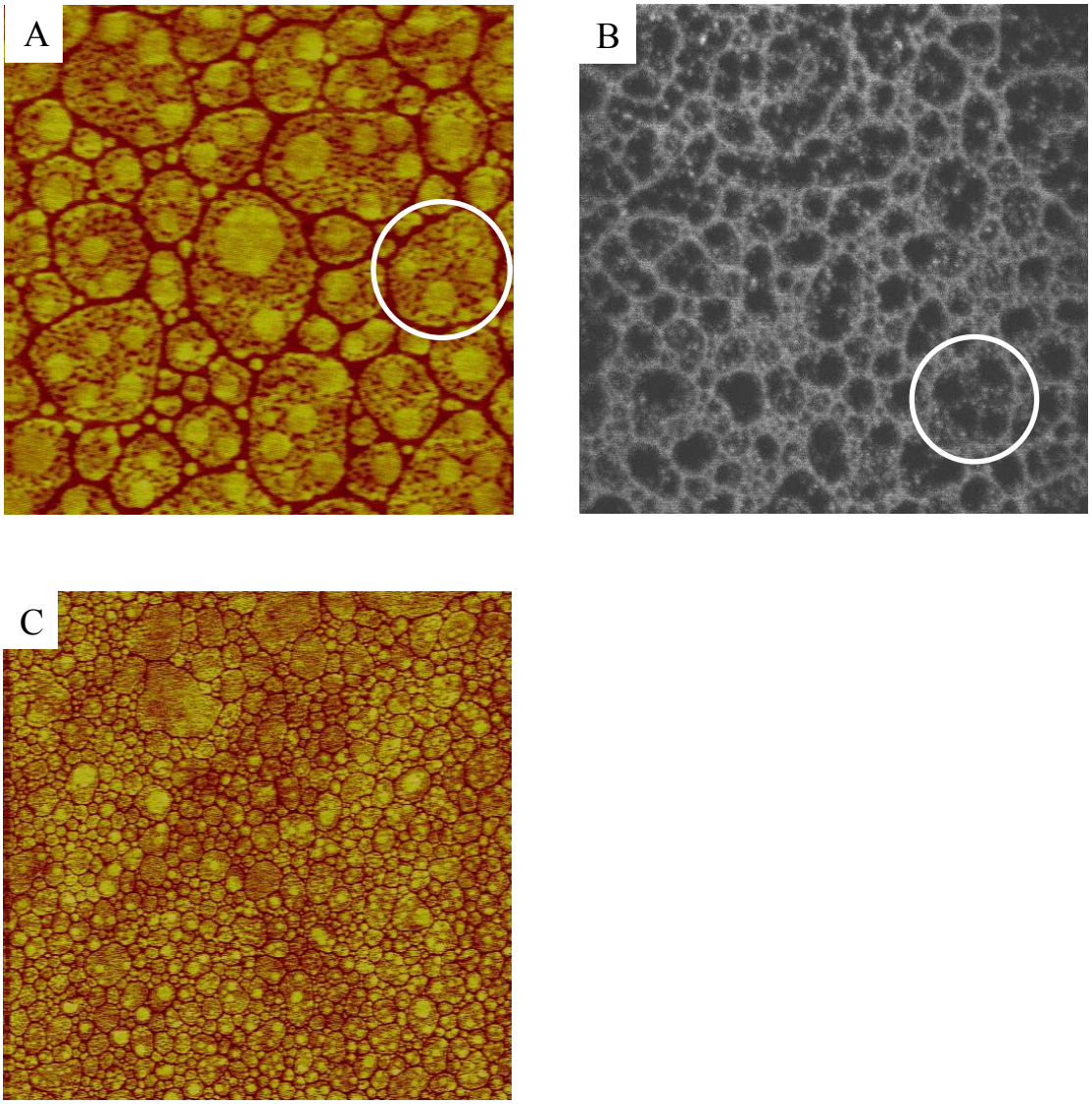

Figure 7-5. A, AFM height mode image; B, fluorescent image; C, AFM height mode image of 0.25% doped 1:1 LB films on glass at 20 ºC and 20 mN/m. Scan size 10 μm × 10 μm for A; and 40 μm × 40 μm for B and C

7.4.3 Phase - separation mechanism.

Understanding the mechanism by which these patterns form in a monolayer has always been a challenge. Imura et al. reported that the patterns obtained in LB films of fatty acids and perfluoroethers depend on the increase in the line tension[17]. When the line tension increases, large circular domains form. However the above theory did not explain all the changes in patterns observed in their system, so they mainly related pattern formation to change in mobility of the molecules[17]. Matsumoto et al. explained the different patterns obtained in a system of fatty acids and perfluoroalkyl silane as a result of the difference between homo and hetero interactions which is proportional to the line tension[18, 19]. In our previous systems of AA/PA[9] and SA/PA[8] we proved that Ostwald ripening was the mechanism by which the domains form and grow. A competition between line tension and dipole interactions leads to the formation of different patterns; the linear pattern in the SA/PA system compared to the large hexagonal pattern in the AA/PA system. However in this current system, no simple mechanism can explain the formation of this type of domains. As previously concluded from the phase rule supported by the analysis of the isotherms, an additional factor is taking place in this system that was not observed previously, which is the solubility of the palmitic acid in the water sub-phase. This behavior of palmitic acid in the monolayer was observed previously in a study of stearic acid and palmitic acid film[11]. Thus, it is important to explore the effect of the solubility on the pattern formed in order to get a better understanding of the mechanism of pattern formation.

To get an insight about the mechanism of this phase-separation and domain formation, 1:1 LB films were deposited on mica at different surface pressures starting at as low as 0.5 mN/m and up to 30 mN/m. These results (data in supporting material) showed the same pattern (hexagonal and hairy extensions surrounded by a continuous domain) throughout the different

surface pressures of deposition. This indicates that the phase-separation takes place in the bulk and does not depend on compressing the film. This is the result of strong phobic interactions between the different components that they phase – separate at a very low surface pressure[33].

In our previous systems of AA/PA[7] and SA/PA[8], at a fixed fluorocarbon chain, line tension increases upon the increase of the length of the hydrocarbon chains arising from the increase in the dispersive forces between the longer alkyl chains. This results in a decrease in the homo interactions (between similar chains). Thus the hydrocarbon content adopts larger domains for longer alkyl chains to decrease the line tension, whereas elongated narrower domains are adopted for shorter alkyl chains where the line tension is low and the dipole interactions play the major role. However in the above two systems, the hetero interactions (between different chains) stay constant because the hydrocarbon forms elevated regions in the mixed LB film[19]. This is similar to what was observed by Mazaki et al. upon mixing alkyl chains of different lengths with a fixed length perfluoroalkyl silane [19].

In this current system, the formation of narrow hairy extensions in this film arises from the decrease in line tension accompanied by the decrease in the hydrocarbon chain length. However the hetero interactions do not remain constant as in the previous systems because the hydrocarbon chains do not form the elevated regions in this film because the perfluorinated chains are longer. Thus both the homo and hetero interactions decrease[19]. The decrease in the former is more than that in the latter because of the tilt in the C16 chains and their parallel arrangement to the surface in some regions of the film as shown above by AFM and X-PEEM. This increases the line tension and the perfluorinated domains (higher domains) take large hexagonal shapes which is a common structure in mixed hydrocarbon/fluorocarbon LB films[7, 8]. In the C16 / F18 system, one force cannot be the dominant as it is clear in the AFM images.

Narrow lines and large hexagonal domains are present at all molar fractions and all surface pressures. This means that the system has each of the two forces (line tension and dipole interactions) being dominant in different regions of the film. The hetero interactions are lower in the hairy regions because of the interaction with the tilted hydrocarbon chain whereas the homo interactions are lower in the hexagonal domains because of the stronger dispersive interactions because of the absence of the hetero interactions as the C16 is lying parallel to the surface.

To fully explore the factors dominating phase-separation, 1:1 LB films were deposited at different temperatures. At lower temperatures 10.5 ± 0.5 ºC and at a surface pressure of 20 mN / m, the hexagonal domains became smaller and the hairy extensions were shorter compared to those at higher temperatures 20.5 ± 0.6 ºC (Figure 7-6A and B). This is expected since the dominant mechanism for domain growth is Ostwald ripening as proved previously in similar systems[9]. At higher temperatures the molecules have more mobility so they can diffuse faster from the smaller domains into the bigger domains. Thus the smaller domains become smaller until they disappear and the larger domains become larger.

However, at 30.5 ± 0.6 ºC and a surface pressure of 20 mN / m (Figure 7-6C), the film loses its distinct regions and no hexagons or hairy extensions were observed. These domains combine together to form one homogeneous monolayer with voids containing hydrocarbon. The height difference between this monolayer and the voids is similar to that between the hexagons and the surrounding area in air. This indicates that there is a tilt in the chains at higher temperatures. The assignment of the composition of these domains was confirmed by measuring the film in toluene. The elevated monolayer did not dissolve in toluene indicating that it is composed of fluorocarbon and the voids are filled with hydrocarbon.

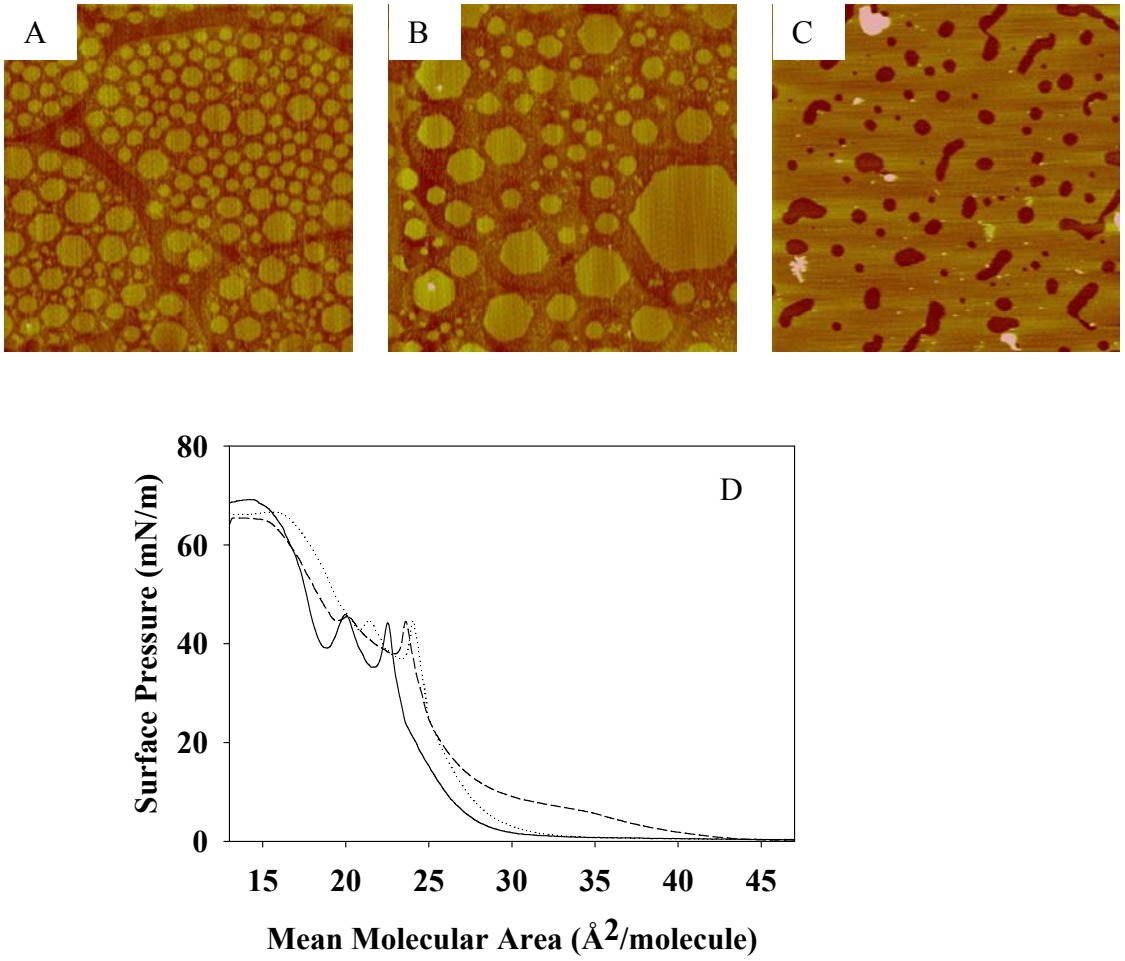

Figure 7-6. AFM height mode images of 1:1 LB films on mica deposited at 20 mN/m after 10 min of incubation time, and at a temperature of A, 10 ºC; B, 20 ºC; C, 30 ºC. Scan size 10 µm × 10 µm. D, surface pressure area isotherms of 1:1 solution at different temperatures; solid line at 10 ºC; dotted line at 20 ºC; dashed line at 30 ºC. All isotherms were collected after 10 min of incubation time.

The height of these domains in toluene is comparable to that in air. This suggests that the hydrocarbon chains in these voids are packed parallel to the surface and that the fluorocarbon does not extend in toluene. The content of the hydrocarbon is lower than that of the fluorocarbon as the area occupied by the voids is not equal to the elevated area. This is because of the slight

solubility of C16 in the water sub-phase. At higher temperatures there is more loss of C16 in the film because of their increasing solubility in the sub-phase. The solubility of C16 in water is 8.3 $\times 10^{-3}$ mg / g, which is around triple the solubility of stearic acid in water. This confirms the above mechanism suggesting less interaction between the hydrocarbon and the perfluorocarbon chains as they are packed parallel to the water surface. This parallel packing in addition to temperature plays a role in the loss of the hydrocarbon in the sub-phase.

The distinct pattern observed in the above film at 30.5 ± 0.6 ºC is explained by the formation of a new phase which appeared at 6 -7 mN/m as a small plateau (Figure 7-6D). The plateau represents the transition from the liquid expanded phase to the liquid condensed phase. This means that at any surface pressure higher than the plateau and at the point when the isotherm rises sharply, the deposition happens in the liquid condensed phase compared to the liquid expanded phase at which all the other films were deposited. This indicates that at the liquid expanded phase, the monolayer consists of hexagonal domains and hairy extensions; whereas at the liquid condensed phase, the monolayer is compact. This plateau was observed previously for other C16 monolayers[34]. When a film was deposited at 30.5 ± 0.6 ºC and at 15 mN/m instead of 20 mN/m; the morphology of the sample showed hexagonal and hairy extensions. The surface pressure of 15 mN/m is close to the plateau and below the sharp rise in the isotherm. This indicates that this surface pressure (15 mN/m) is part of the liquid expanded phase.

To verify the solubility of the C16 chains in the sub-phase, a 1:1 LB film was prepared at 20.5 ± 0.6 ºC, 20 mN/m and after 18 hr of incubation (solvent evaporation time on the sub-phase). Figure 7-7A shows circular domains with no branches but some small connectors between the domains. They look similar to those in the film of pure F18 in Figure 7-2A but these

domains are larger with some edges. This film lacks the presence of significant amounts of hydrocarbon that interacts with the F18 lowering the line tension and forming branched domains. However the domains are larger, which is another confirmation of Ostwald ripening taking place in the system after phase - separation. Longer evaporation times at low surface pressure gives the molecules more time to diffuse freely, thus the domains become larger. This was observed with the increase in temperature as well (Figure 7-6A and B).

The loss of the C16 from the film in the sub-phase with time was confirmed by measuring isotherms for 1:1 film at 20.5 ± 0.6 ºC, after 18 hr of incubation. The isotherm after long incubation time interval showed that the corresponding collapse pressure to the C16 almost disappeared (Figure 7-7B). This corresponding collapse pressure was still observed for the isotherm after 10 min of incubation time. The isotherm after 18 hr of incubation started to have a smooth curve that increased without distinct regions of phase transition, which is similar to that of pure F18.

As a final proof of the solubility of the C16 in the sub-phase, a 0.25% doped BODIPY FL 1:1 LB films were prepared under the same above conditions (18 hr and 30 hr of incubation) and then measured by AFM and confocal fluorescence. AFM showed the same structure of the doped film after 30 hr as that for the non-doped film after 18 hrs. After 18 hr of incubation, the domains of the doped film are more connected than those after 30 hr. This suggests that BODIPY FL dissolves in the sub-phase but it needs more time to completely dissolve compared to the C16 chains. This is because BODIPY FL is bulkier and more hydrophobic than C16 chains. The fluorescence images showed a very weak signal and it is different from the one expected for BODIPY FL even at a single molecule level. This signal was present in a 1:1 LB film prepared under the same above conditions but without the dye. This proves that the dye is not in the film

under both incubation times. This fluorescent signal is related to some contaminants present during deposition.

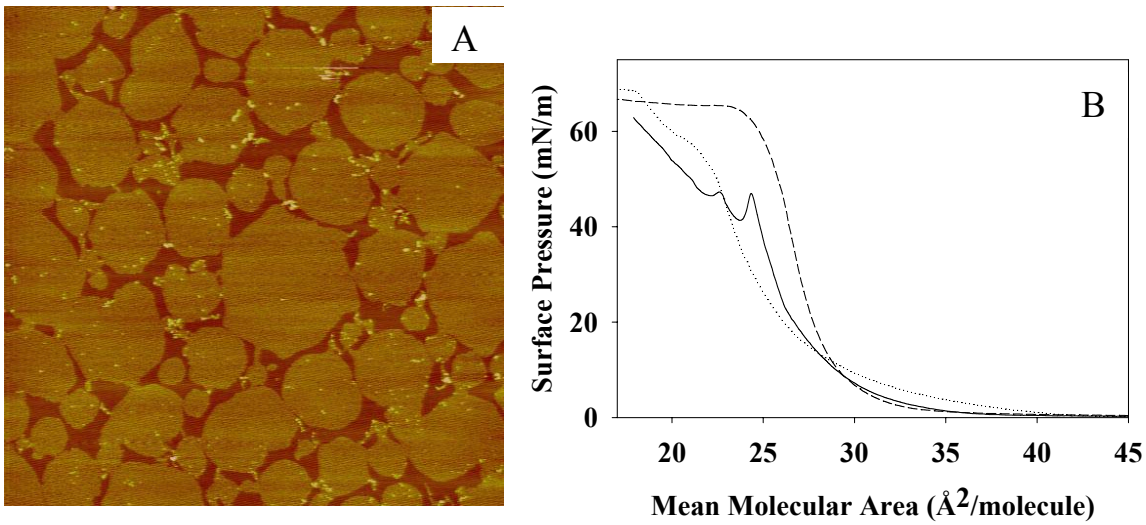

Figure 7-7. AFM height mode image of 1:1 LB film on mica deposited at 20 mN/m, at 20 ºC, after 18 hrs of incubation. Scan size 30 µm × 30 µm. B, surface pressure area isotherms of 1:1 film at 20 ºC. Solid line, after 10min; dotted line, after 18 hr; dashed line, pure F18 after 10 min.

This supports the previous hypothesis that the C16 is slightly soluble in the sub-phase and its solubility increases as a function of temperature and incubation time. This solubility arises from the packing of the C16 molecules parallel to the water surface which facilitates its solubility in addition to the relatively high sub-phase pH (6 for Millipore water) which makes the acid in the ionized form (fatty acids ionized at pH > 4)[35]. The solubility factor was expected from the phase rule explained previously and confirmed by the above measurements. The solubility of palmitic acid in the sub-phase was also observed in a mixed monolayer of SA/C16 as it was shown that the C16 chains escaped from the monolayer into the water[11]. This process was found

to be larger for the mixed palmitic acid monolayers than the pure palmitic acid as it is facilitated by disruption of the bonding between the palmitic acid chains[11]. This solubility was found to regulate drug release from the fatty acid microspheres into the body[11]. In the previous systems, no solubility of the hydrocarbon chains in the sub-phase was observed under the experimental conditions because of the longer alkyl chains used in the previous systems (AA/PA and SA/PA)[7, 8] and the perpendicular packing of the chains on the water surface. The increasing solubility of the C16 from the monolayer in the sub-phase was observed to increase at pH $\geq$ 6 [36] which is similar to the pH in our current system. This solubility has many applications in selective dissolution of the mixed components in drug delivery[11].

7.5 Conclusions

In this work, the structure and the chemical composition of mixed films of C16 / F18 were investigated using AFM, X-PEEM and confocal fluorescent microscopy measurements. Surface pressure – area isotherms indicated the immiscibility of the components in the system. The two surfactants phase – separated into elevated hexagonal domains with short hairy extensions surrounding them. The dipole interaction / line tension were the forces that controls phase – separation and the pattern obtained. Ostwald ripening was found to be the mechanism by which the domains form and grow. Preferential solubility of C16 into the water sub-phase was observed. This is a unique characteristic of C16 to control the pattern obtained on the surface which was not observed in any of the previous systems.

7.6 Acknowledgements

Funding for this work was provided by the Natural Sciences and Engineering Research Council of Canada (NSERC), the Canada Foundation for Innovation (CFI), the Province of Saskatchewan and by the University of Saskatchewan.

7.7 References

1. Dynarowicz-Latka, P.; Kita, K., *Advances in Colloid and Interface Science* **1999,** 79 (1), 1.
2. Matsumoto, M.; Tanaka, K.; Azumi, R.; Kondo, Y.; Yoshino, N., *Langmuir* **2003,** 19 (7), 2802.
3. Overney, R. M.; Meyer, E.; Frommer, J.; Guntherodt, H. J.; Fujihira, M.; Takano, H.; Gotoh, Y., *Langmuir* **1994,** 10 (4), 1281.
4. Matos, L.; Ravey, J. C.; Serratrice, G., *Journal of Colloid and Interface Science* **1989,** 128 (2), 341.
5. Matsumoto, M.; Tanaka, K.; Azumi, R.; Kondo, Y.; Yoshino, N., *Chemistry Letters* **2002,** (10), 970.
6. Imae, T.; Takeshita, T.; Kato, M., *Langmuir* **2000,** 16 (2), 612.
7. Qaqish, S. E.; Paige, M. F., *Langmuir* **2007,** 23 (5), 2582.
8. Qaqish, S. E.; Paige, M. F., *Langmuir* **2008,** 24 (12), 6146.
9. Qaqish, S. E.; Paige, M. F., *Langmuir* **2007,** 23 (20), 10088.
10. Frommer, J.; Luthi, R.; Meyer, E.; Anselmetti, D.; Dreier, M.; Overney, R.; Guntherodt, H. J.; Fujihira, M., *Nature* **1993,** 364 (6434), 198.
11. Qi, S.; Roser, S. J.; Deutsch, D.; Barker, S. A.; Craig, D. Q. M., *Journal of Pharmaceutical Sciences* **2008,** 97 (5), 1864.
12. Peng, J. B.; Barnes, G. T.; Gentle, I. R., *Advances in Colloid and Interface Science* **2001,** 91 (2), 163.
13. Tomoaiacotisel, M.; Zsako, J.; Mocanu, A.; Lupea, M.; Chifu, E., *Journal of Colloid and Interface Science* **1987,** 117 (2), 464.
14. McConnell, H. M., *Annual Review of Physical Chemistry* **1991,** 42, 171.
15. Christensen, S.; Lanke, U. D.; Haines, B.; Qaqish, S. E.; Paige, M. F.; Urquhart, S. G., *Journal of Electron Spectroscopy and Related Phenomena* **2008,** 162 (3), 107.
16. Qaqish, S.; Paige, M., *Journal of Colloid and Interface Science* **2008,** 325, 290.
17. Iimura, K.; Shiraku, T.; Kato, T., *Langmuir* **2002,** 18 (26), 10183.
18. Matsumoto, M.; Watanabe, S.; Tanaka, K.; Kimura, H.; Kasahara, M.; Shibata, H.; Azumi, R.; Sakai, H.; Abe, M.; Kondo, Y.; Yoshino, N., *Advanced Materials* **2007,** 19 (21), 3668.
19. Mazaki, T.; Shibata, H.; Kondo, Y.; Yoshino, N.; Matsumoto, M., *Chemistry Letters* **2008,** 37 (4), 480.
20. Matsumoto, M.; Tanaka, K.; Azumi, R.; Kondo, Y.; Yoshino, N., *Langmuir* **2004,** 20 (20), 8728.
21. Anders, S.; Padmore, H. A.; Duarte, R. M.; Renner, T.; Stammler, T.; Scholl, A.; Scheinfein, M. R.; Stohr, J.; Seve, L.; Sinkovic, B., *Review of Scientific Instruments* **1999,** 70 (10), 3973.
22. Rasband, W. S. *Imagej*, 1.37v; U.S. National Institute of Health: Bethesda, Maryland, USA, 1997-2005.
23. Ekelund, K.; Sparr, E.; Engblom, J.; Wennerstrom, H.; Engstrom, S., *Langmuir* **1999,** 15 (20), 6946.
24. Bibo, A. M.; Peterson, I. R., *Advanced Materials* **1990,** 2 (6-7), 309.
25. Gaines, G., *Insoluble Monolayers at Liquid-Gas Interfaces*. Interscience Publishers: New York, 1966.

26. Wojciechowski, K.; Grigoriev, D.; Ferdani, R.; Gokel, G. W., *Langmuir* **2006,** 22 (20), 8409.
27. Shibata, O.; Yamamoto, S. K.; Lee, S.; Sugihara, G., *Journal of Colloid and Interface Science* **1996,** 184 (1), 201.
28. Jang, S. S.; Blanco, M.; Goddard, W. A.; Caldwell, G.; Ross, R. B., *Macromolecules* **2003,** 36 (14), 5331.
29. Broniatowski, M.; Dynarowicz-Latka, P., *Langmuir* **2006,** 22 (6), 2691.
30. Petty, M. C., *Langmuir-BlodgettFilms an Introduction*. Cambridge University Press: Cambridge, 1996.
31. Castelli, F.; Sarpietro, M. G.; Rocco, F.; Ceruti, M.; Cattel, L., *Journal of Colloid and Interface Science* **2007,** 313 (1), 363.
32. Rontu, N.; Vaida, V., *Journal of Physical Chemistry C* **2007,** 111 (27), 9975.
33. Kissa, E., *Fluorinated Surfactants and Repellents* Marcel Dekker Inc.: New York, 2001.
34. Albrecht, O.; Matsuda, H.; Eguchi, K.; Nakagiri, T., *Thin Solid FIlms* **1999,** 338, 252.
35. Rosano, H.; Breindel, K.; Schulman, A.; Eydt, J., *Journal of Colloid and Interface Science* **1968,** 22, 58.
36. Brzozowska, I.; Figaszewski, Z. A., *Colloids and Surfaces B-Biointerfaces* **2003,** 30 (3), 187.

7.8 Supporting material

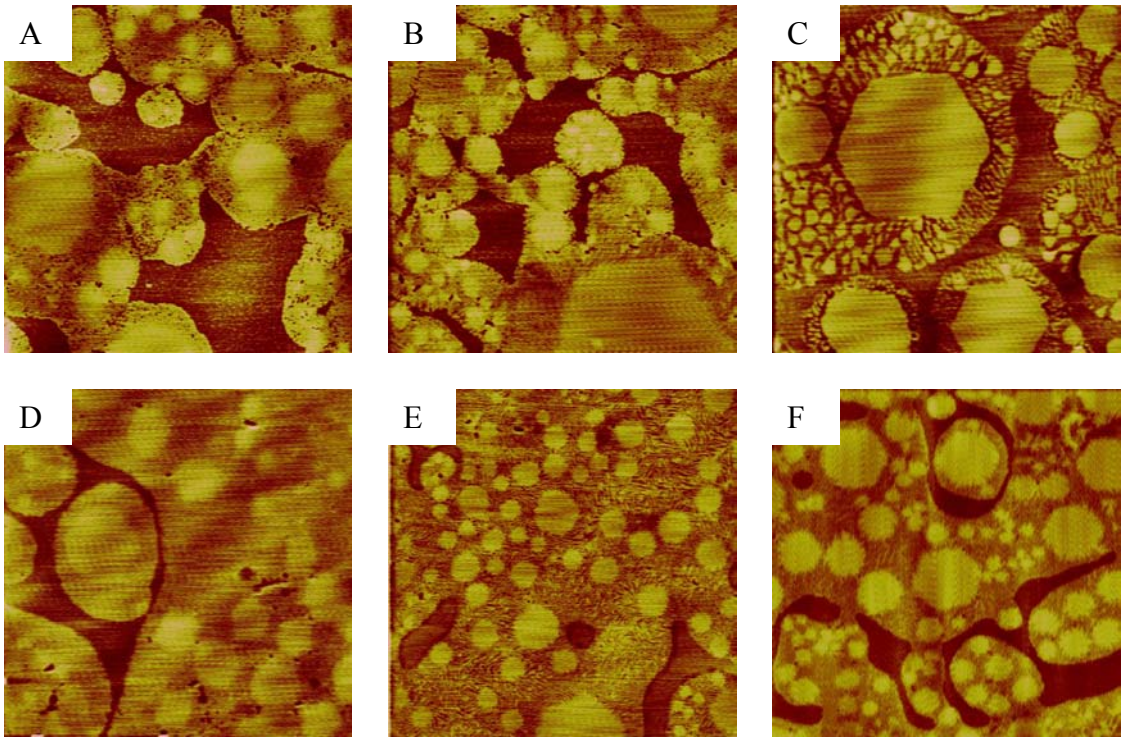

Figure 7-8. AFM height mode images of 1:1 LB films deposited at 20 ºC and at a surface pressure of A, 0.5 mN/m; B, 1 mN/m; C, 5 mN/m, D, 10 mN/m; E, 20 mN/m; F, 30mN/m. Scan size 5 μm × 5 μm.

CHAPTER 8
AN INVESTIGATION OF TWO-DIMENSIONAL MISCIBILITY BETWEEN PERFLUOROCARBOXYLIC ACID AND FATTY ACID SURFACTANTS AS A FUNCTION OF SURFACTANT CHAIN LENGTH

This chapter describes unpublished work aimed at determining the effect of surfactant chain length on the miscibility of the hydrocarbon and the perfluorocarbon compounds in mixed LB films. As observed in the previous chapters (2, 6, 7), the surfactant chain length plays a role in determining the pattern obtained in mixed LB films and the miscibility of its components. To gain a better understanding of the effect of chain length in these systems, we systematically studied the miscibility of two different perfluorinated surfactants (perfluorotetradecanoic acid ($C_{13}F_{27}COOH$) (F14) and perfluorooctadecanoic acid ($C_{17}F_{35}COOH$) (F18)) with a series of homologous fatty acids of varying length; behenic acid ($C_{21}H_{43}COOH$) (C22), arachidic acid ($C_{19}H_{39}COOH$) (C20), stearic acid ($C_{17}H_{35}COOH$) (C18), palmitic acid ($C_{15}H_{31}COOH$) (C16) and myristic acid ($C_{13}H_{27}COOH$) (C14). The increase in chain length (number of C atoms in the molecule) affects directly the dispersive forces between the chains, resulting in differences in miscibility and domain shapes in LB films of different components. This effect is discussed in detail, as well as the other factors affecting the domain shapes such as the competition between line tension and dipole interactions of the head groups.

Surface pressure – area isotherms and AFM measurements were carried out in order to analyze the relationship between chain length and miscibility. F18 was found to be immiscible when added to any of the fatty acids studied. For fatty acids with chains shorter or equivalent to that of F18, C18, C16 and C14, it was found that the monolayer components were immiscible.

When fatty acid chains become longer (C20 and C22) than F18, they become miscible. The intermolecular forces responsible for the miscibility of the components are discussed in detail.

For this work, I prepared samples, performed the measurements, and played a major role in interpreting the results and the preparation of this chapter. My supervisor provided guidance throughout the experimental work and was involved in result interpretation and in editing this chapter.

8. An investigation of two-dimensional miscibility between perfluorocarboxylic acid and fatty acid surfactants as a function of surfactant chain length

Shatha E. Qaqish and Matthew F. Paige

Department of Chemistry, University of Saskatchewan, 110 Science Place, Saskatoon, SK.

Canada S7N 5C9

8.1 Abstract

A systematic study was carried out to determine the two-dimensional (2D) miscibility of hydrocarbon and perfluorocarbon fatty acids in mixed LB films. Two different perfluorocarbon fatty acids were selected for investigation: F14 and F18. Five different hydrocarbon fatty acids of various chain lengths, including C22, C20, C18, C16, C14 were mixed separately with each of the two perfluorocarbon fatty acids. From surface pressure-area isotherm measurements, the additivity rule was valid for all the different combinations studied except for the C16 / F14 and C14 / F14 systems, where a negative deviation was observed. Isotherm analysis in conjunction with AFM imaging showed that all fatty acid / F14 systems were immiscible at all molar fractions examined. The fatty acid / F18 systems were immiscible for short chains of fatty acids (C14, C16, C18), whereas at longer fatty acid chains (C20, C22) the components of the mixed system became miscible. In general, when perfluorocarboxylic acid chain combined with fatty acids, the domains formed changed from large hexagonal domains into linear patterns as the fatty acid chain decreased in length. Some general conclusions regarding phase-separation and pattern formation in the mixed systems were drawn.

8.2 Introduction

Mixed Langmuir and LB films of two or more components have been extensively studied, as properties of these films provide information on the interactions between the molecules in the film. Studies of Langmuir and LB films are important tools to understand miscibility, pattern formation, phase-separation, and ideal mixing behavior or deviation from ideality between the molecules forming the film. Hydrocarbon and fluorocarbon compounds do not mix well and phase-separate because of the difference in cohesive forces between them. However if the dipole-dipole interactions between head groups are strong enough, the two components in the mixed films can be miscible[1].

There have been a number of studies of phase-separation in mixed hydrocarbon / fluorocarbon 2D systems. In their study of mixed films of perfluorododecanoic acid ($CF_3(CF_2)_{10}COOH$) and stearic or lauric acid ($CH_3(CH_2)_{10}COOH$), Rontu et al[2] found that the two components are miscible with a positive deviation from ideal mixing. This is related to the attractive interactions between the different components. In a closely related study, Shibata et al.[1] studied the miscibility of tetradecanoic acid ($CH_3(CH_2)_{12}COOH$) with a series of different length perfluorocarboxylic acids ($C_nF_{2n+1}COOH$), and found that the components were miscible (n=10, 12), immiscible (n=14) and a combination of both (n=16, 18), with the latter depending on whether the film was in the condensed or expanded state. This was explained by the interactions between the pure components as compared to those between the different components. Broniatowski et al[3]. studied the miscibility of mixed films containing the semifluorinated alkane, ($CH_3(CF_2)_{10}(CH_2)_{18}COOH$) F10H20. They found that this compound was completely miscible with the hydrogenated alcohol octadecanol ($C_{17}H_{35}CH_2OH$) and was fully immiscible with the alcohol perfluorinated analogue. They also found that ($CH_3(CF_2)_{10}(CH_2)_8COOH$) F10H10 had

partial miscibility with the semifluorinated analogues of the alcohol, which was dependent on the molar fraction of the components; as the alcohol content increased, the two components de-mixed. This is explained by the favorable interactions between the components of the same type; CH_2-CH_2 and CF_2-CF_2 groups, compared to the less attractive interactions between the CF_2 and CH_2 groups, which leads to phase-separation. In the case of the partially fluorinated alcohols, the switch from miscibility to immiscibility is related to molecular packing in which disorder increases as F10H20 is introduced, leading to the miscibility of the two components[3]. At larger molar faction of F10H20, phase-separation takes place. In a separate work, Broniatowski et al.[4] carried out a systematic study to investigate the effect of the fluorinated chain length on the 2D miscibility of hydrocarbon / fluorocarbon systems. This was studied by eliminating the head group interactions through the choice of simple fluorocarbons without head groups and by keeping the hydrocarbon chain length constant in the semifluorinated compounds. They found that surfactants with long perfluorinated segments (F10H20 and F9H20) mixed better with hydrogenated alcohols in comparison with the shorter semifluorinated compounds (F4H20 and F3H20). The longer alcohol chain ($C_{21}H_{43}CH_2OH$) (C22OH) mixed better with the semifluorinated chains as compared to the shorter alcohol chain ($C_{13}H_{27}CH_2OH$) (C14OH). This is attributed to the van der Waals forces that increase between the hydrocarbon part of F10H20 and the hydrocarbon chains as the hydrocarbon chain increases in length. As these interactions increase, the mutual miscibility of the components increases[4]. By increasing the fluorocarbon part of the semifluorinated compound, the CF_2-CF_2 van der Waals interactions between the adjacent chains increase.

The miscibility relationships determined from the above studies are mainly applicable to the systems studied and might not be extendable to other systems. It was previously observed

that by slightly changing the chemical composition of the system, whether it was the head group or the chain length, the miscibility rules changed dramatically [5].

The effect of component miscibility on LB film surface structures has also been investigated in some detail. Mazaki and co-workers studied the effect of chain lengths of fatty acids $CH_3(CH_2)_{n-2}COOH$ (where n=16, 18) on the structures of mixed films with perfluorosilanes, $CF_3(CF_2)_{m-1}C_2H_4SiCl$ (where m=4, 6, 10, 12).[6] They found that by decreasing the length of the hydrocarbon chain from n=18 to n=16, with a constant perfluorosilane compound, the domains shapes in the mixed LB films changed from large circular into narrow linear structures. This was attributed to the increase in the Van der Waals interactions between the hydrocarbon chains upon increasing the chain length. In a separate study, Iimura et al.[7] investigated the phase-separation of mixed films of perfluoropolyethers and different length fatty acid molecules ($CH_3(CH_2)_{n-2}COOH$ where n =18, 20, 22, 24). They found that phase-separation took place in all mixed LB films studied, and as the number of C atoms in the fatty acid chain decreased, the domains of the phase-separated films changed from narrow linear into large circular domains. The same trend was observed by Matsumoto et al.[8] in their mixed systems of semifluorinated carboxylic acids and stearic acid, upon the increase in the number of C atoms in the fluorocarbon chain. This disagreement of trend in the size and shapes of the domains formed in Mazaki's[6] study and those in Iimura's[7] and Matsumoto's[8] studies shows that for this type of studies, a simple change in the chemical composition affects the overall miscibility and phase-separation resulting in the formation of different domain structures.

The shapes of domains formed in phase-separated LB films is controlled by the competition between line tension and dipole interactions[9]. By adjusting the intermolecular force of attraction between the molecules, the shape of the domains forming the film is modified[8]. Line

tension is the free energy necessary to create a unit length of domain and favors the formation of large and or circular domains in order to reduce the total domain length[6]. This dominates when the hydrophobic interactions between the chains are attractive. Zhu et al.[10] explained line tension in terms of a mutual-phobicity between the hydrocarbon and the fluorocarbon chains. This phobicity is responsible for the higher overall energy of the uniform mixture which forces hydrocarbon / fluorocarbon mixtures to phase-separate. Dipole interactions originate from the polar head groups of the chains; they are repulsive forces because of the parallel arrangement of the dipoles[11]. They favor the formation of narrow linear domains. By changing the length of the hydrocarbon or fluorocarbon (the hydrophobic moiety) used in the mixed LB film, the line tension is only affected, with minimal affect on the net dipole interaction[8].

In this study, we carried out a systematic investigation of the miscibility and phase-separation of series of fatty acids and perfluorocarbon mixed Langmuir and LB films. F18 and F14 were the perfluorocarbxylic acids that combined with different chains of fatty acids, separately (C22, C20, C18, C16, C14). Surface pressure-area isotherms in conjunction with AFM measurements made it possible to study the miscibility of the components and the domains formed upon phase-separation. F14 was found to be immiscible with the fatty acids at all chain lengths. F18 was immiscible at shorter chain lengths (C18, C16 and C14) and miscible at longer chain lengths (C22 and C20). F14 when mixed with long fatty acid chains (C22 and C20) phase-separated into large hexagonal domains, whereas with shorter fatty acids, the domains had narrow linear pattern. F18 formed large hexagonal domains when combined with long fatty acid molecules (C18 and C16) and narrow linear fragments with short fatty acid molecules (C14), and was miscible with C20 and C22.

8.3 Experimental Section

8.3.1 Chemicals

Behenic acid (99%), arachidic acid (99%), palmitic acid (90%), myristic acid (99-100%) and perfluorotetradecanoic acid (97%) were purchased from Sigma-Aldrich Corporation. Stearic acid (99%) was purchased from BDH. Perfluorooctadecanoic acid (97%) was purchased from Alfa Aesar. Hexanes (HPLC grade) and tetrahydrofuran (THF) were purchased from EMD and Merck EM Science, respectively. Mica was purchased from SPI (Structure Probe Inc., West Chester, F14), and was freshly cleaved with adhesive tape prior to use.

8.3.2 Isotherm measurements and Langmuir-Blodgett film deposition

Langmuir and LB films were prepared using a KSV 2000 Langmuir trough system (KSV Instruments, Helsinki, Finland), with ultrapure water (Millipore, resistivity 18.2 MΩ·cm) as a sub-phase. Stock solutions of 5.7×10^{-3} M of fatty acids and F14 were prepared in 9:1 hexanes:THF. Solutions of 2.7×10^{-3} M of fatty acids and F18 were prepared in a 9:1 volume ratio of hexanes:THF and hexanes:EtOH for the fatty acids and F18, respectively. This concentration was restricted by the F18 solubility. The solutions of each of the acids were combined with F14 or F18 in appropriate volumes to give a range of hydrocarbon:flurocarbon mole ratios (1:0, 3:1, 2:1, 1:1, 1:2, 1:3 and 0:1). Before each measurement, the sub-phase surface was cleaned by vacuum suction and the platinum Wilhelmy plate was cleaned by flaming in a propane torch. The isotherm and deposition experiments were performed as described previously[12] by spreading a 30 μL aliquot of the fatty acid / F14 mixture and 70 μL aliquot of the fatty acid / F18 mixture on the sub-phase at 20.5 ± 0.5 ºC and waiting 10 min for solvent evaporation. All isotherm measurements were carried out at a rate of barrier compression of 20 mm min^{-1}.

Film deposition was carried out only for 2:1 mixed films at a surface pressure of 20 mN m^{-1}. The barrier compression rate was kept at 10 mm min^{-1} until reaching the desired surface pressure, at which point it was changed to 5 mm min^{-1} to match the substrate withdrawal rate from the sub-phase. This took place after 10 min of sample stabilization. The sub-phase temperature was controlled by water circulation through the trough's external jacket from a Haake K F3 water bath (Haake, Berlin, Germany). The sub-phase surface temperature was monitored throughout the experiment with a thermocouple.

8.3.3 Atomic force microscope measurements

AFM measurements were carried out on a Dimension Hybrid Nanoscope system (Veeco Metrology Group, Santa Barbara, CA). The microscope was mounted in an acoustic-vibration isolation system. All AFM measurements were carried out in contact mode in air using commercial silicon nitride AFM probes with nominal spring constant of ~ 0.58 $N.m^{-1}$. AFM probes were purchased from Veeco Metrology Group, Santa Barbara, CA. Samples were positioned in the microscope such that the vertical axis in the images is in the direction of withdrawal of the solid substrate from the water surface.

8.4 Results and discussion

8.4.1 Surface pressure measurements

Surface pressure-area isotherms for the pure acid films measured at the air-water interface are shown in Figures 8-1 and 8-2. Isotherms for all of the pure fatty acids consisted of three distinct regions, a gaseous (disordered) region, a liquid-expanded region and a liquid-condensed region.

For C14, the liquid expanded state had a long region of constant surface pressure at ~ 15-17 $mN.m^{-1}$ in the shape of a plateau before it moved up slightly towards the liquid-condensed

state. This was followed by a short liquid-condensed state after which the surface pressure increased sharply starting at ~ 20 $mN.m^{-1}$ where the solid state or super liquid existed. This behavior of C14 monolayer was previously observed by Bibo et al.[13] and Albrecht et al.[14] In both studies the isotherms of C14 showed four different phases similar to those reported in this study. The plateau reported by Bibo et al.[13] was at ~ 7 $mN.m^{-1}$ which was lower than what was observed in this work. The main reason for this is the difference in temperature as the isotherms were measured at 13.2 ºC by Bibo et al.[13] The effect of sub-phase temperature on the isotherm measured was studied by Albrecht et al.[14] where they observed an increase in the transition pressure as temperature increased. They reported a plateau value at ~ 15 $mN.m^{-1}$ at 20 ºC using hexane as a solvent which is similar to what was observed here. A similar horizontal plateau was observed for C16 at 30 ºC as shown in Chapter 7. This agrees with the reported phase behavior of C16 in the above two studies[13, 14]. This plateau of C16 was not observed in this study as the measurements were carried out at 20 ºC.

For the pure fatty acid films, the transition between the liquid-expanded state to the liquid-condensed state took place at higher surface pressures as the chain length of the acid increased (Table 8-1). The collapse pressure followed the same trend as the transition pressure. It has been previously reported in the literature that the film stability increases as a function of chain length[15]. The increase of the collapse pressure observed here indicates the stability of the film formed with longer chain lengths[15]. Films of longer chain lengths (more C atoms per molecule) have larger dispersive interactions so greater attraction between the chains results in the formation of more condensed films compared to the shorter chains. This is illustrated by the following equation (8-1)[16, 17]:

$$\Pi_s = -\frac{400m}{a^{3/2}} \qquad (8\text{-}1)$$

Where Π_s is the cohesive force which represents the energy of interaction between the CH_2 groups in the acid chain, m is the number of CH_2 groups per chain and a is the molecular area. Applying the above equation, the dispersive energy between C22 chains is ~ 80 dyne.cm^{-1} compared to ~ 51 dyne.cm^{-1} between C14 chains. The main factor that caused this difference in the energy calculated is the number of CH_2 groups in the chains, considering that the difference in molecular area between the two molecules is minimal ~21.5 Å^2 and ~ 20.8 Å^2 for C22 and C14, respectively. This molecular area is derived from the pure isotherms of each of the acids as discussed later in the text.

Fatty acid	#C atoms / chain	Collapse pressure	Transition pressure
Behenic acid	22	~ 70 mN.m^{-1}	~ 33 mN.m^{-1}
Arachidic acid	20	~ 65 mN.m^{-1}	~ 30 mN.m^{-1}
Stearic acid	18	~ 60 mN.m^{-1}	~ 25 mN.m^{-1}
Palmitic acid	16	~ 60 mN.m^{-1}	~ 26 mN.m^{-1}
Myristic acid*	14	~ 40 mN.m^{-1}	~ 22 mN.m^{-1}

***** The transition pressure was the main transition, which was between the liquid condensed-state and the solid state

Table 8-1. Trends in collapse pressure and the transition pressure from the liquid expanded state to the liquid condensed state as a function of fatty acid chain length.

In terms of the mixed films (Figures 8-1, 8-2), the transition between liquid regions becomes difficult to resolve as the mole-fraction progressed towards that of pure perfluorocarbon. A slight increase in the collapse pressure of the mixtures with some fluctuations was observed as the molar fractions of the perfluorocarbon increased in the C20 / F14, C16 / F14 and C14 / F14 systems.

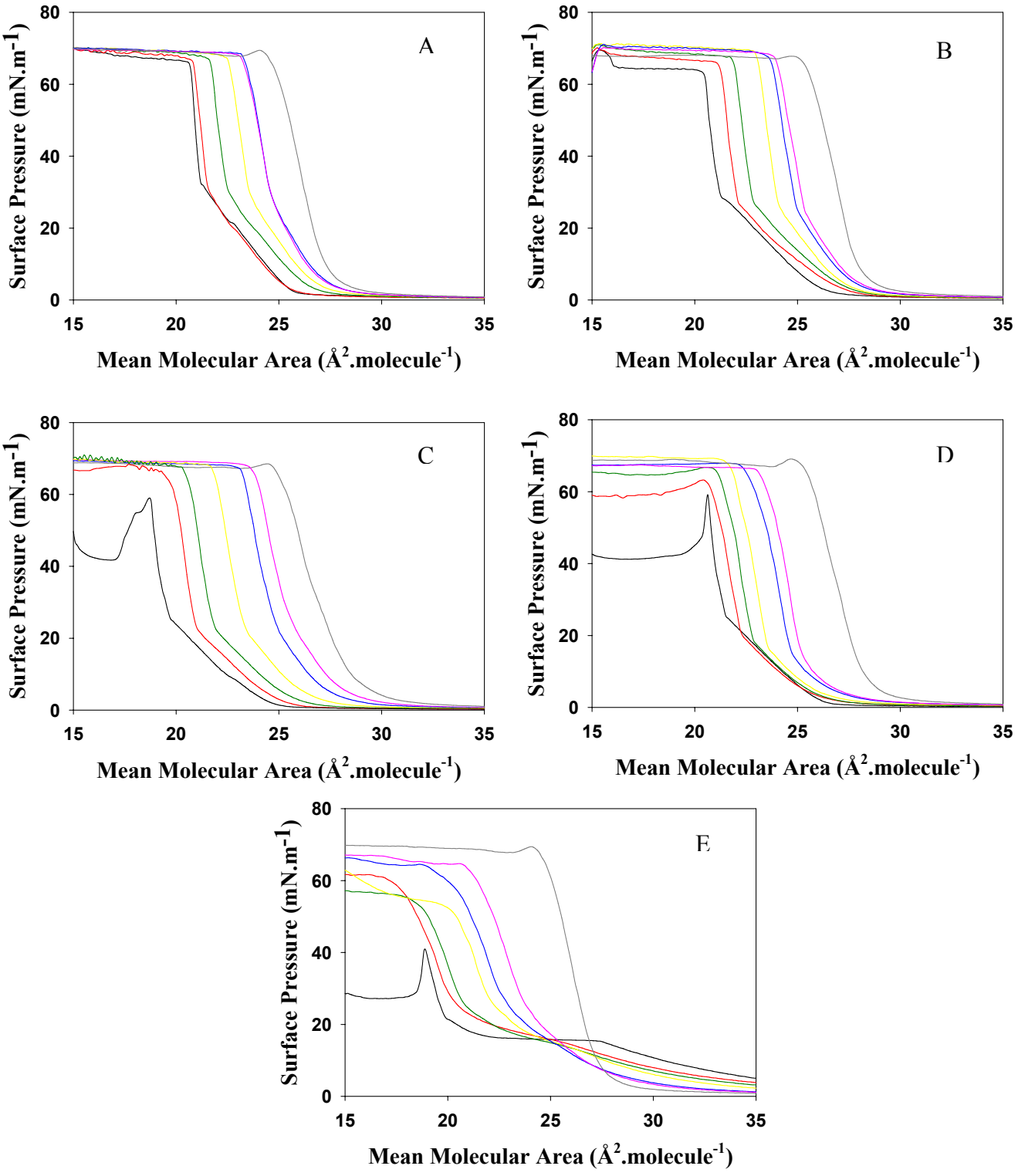

Figure 8-1. Surface pressure – area isotherms and the corresponding mole fractions versus mean molecular area analysis of A, C22:F14; B, C20:F14; C, C18:F14; D, C16:F14; E, C14:F14; at different mole fractions of each, black, pure hydrocarbon; red, 3:1; green, 2:1; yellow, 1:1; blue, 1:2; pink, 1:3; grey, pure F14.

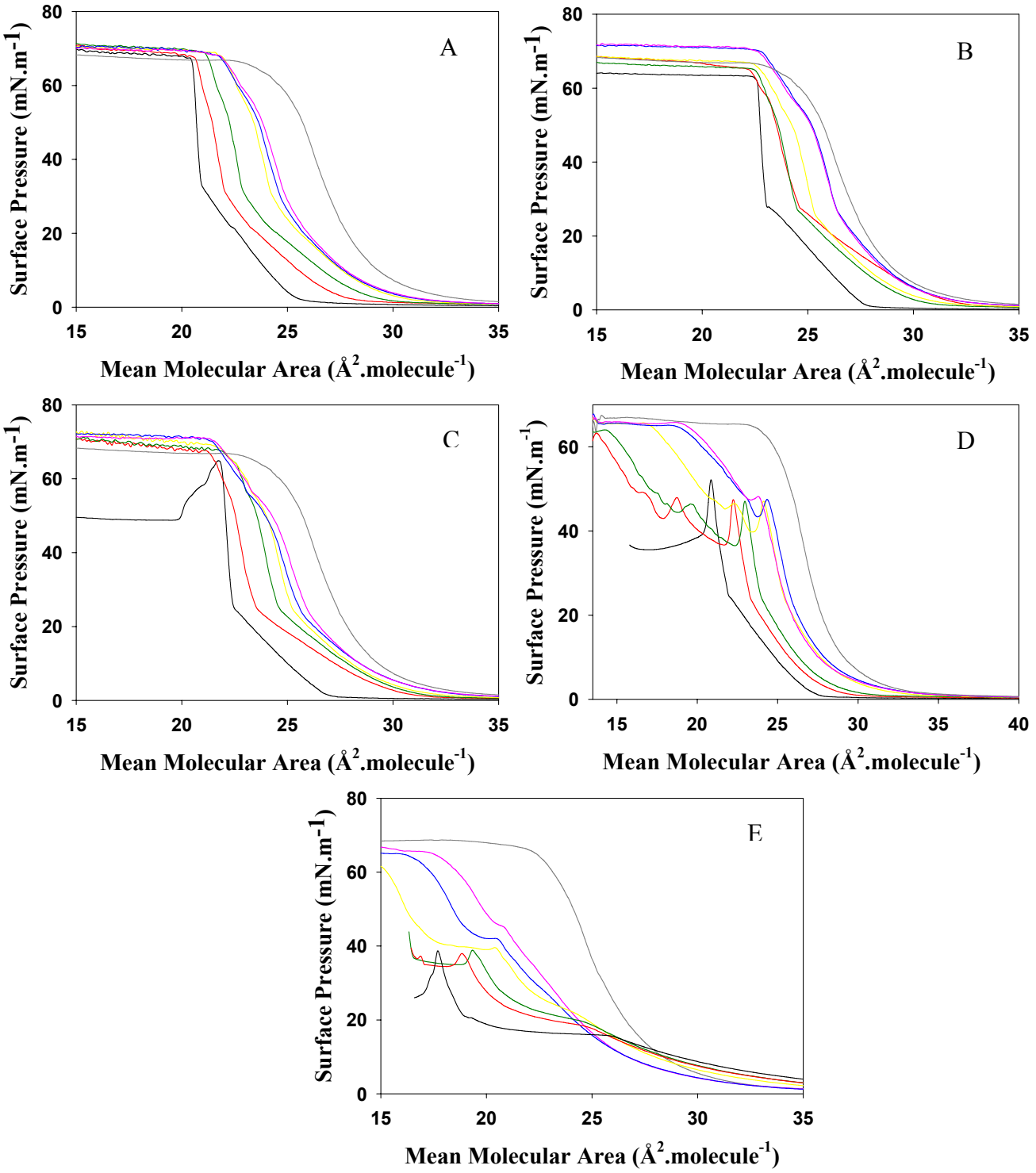

Figure 8-2 Surface pressure – area isotherms and the corresponding mole fractions versus mean molecular area analysis of A, C22:F18; B, C20:F18; C, C18:F18; D, C16:F18; E, C14:F18; at different mole fractions of each, black, pure hydrocarbon; red, 3:1; green, 2:1; yellow, 1:1; blue, 1:2; pink, 1:3; grey, pure F18.

This indicates some degree of miscibility or interaction between different components in the mixed films[18], which helps in the diffusion of molecules through the medium and facilitates Ostwald ripening (Chapters 4 and 6). In the case of C16 / F18 and C14 / F18 systems, two collapse pressures were observed, with each corresponding to the collapse pressure of the individual components. The presence of two collapse pressures suggests that each component kept its main characteristics and it indicates the immiscibility of the components[18]. The collapse pressure should be carefully interpreted, as in some cases the film might not be at true thermodynamic equilibrium when the collapse takes place[18].

For pure fatty acids, the mean area occupied by a molecule (molecular footprint) in the solid phase was estimated by fitting a linear function to the liquid-condensed region of the isotherm and extrapolating to zero surface pressure. This gave a value of 20-23 $Å^2 \cdot molecule^{-1}$. It has been observed that fatty acids with lower melting points form more expanded monolayers than those with higher melting point[19]. Broniatowski et al. observed an increase in the molecular footprint when the length of the fatty alcohol decreased so a more expanded film formed[4]. However, we did not observe this effect in our data. Isotherms for pure films of the fluorinated compounds F14 and F18 consisted of a single smooth curve that increased upon compression until it reached a plateau. A molecular footprint of ~ 29 $Å^2 \cdot$ $molecule^{-1}$ was determined for F14 and F18, which is comparable with our previous measurements[12] and larger than that for all the pure fatty acid chains. The perfluorinated molecules adopt a helical structure[20] as opposed to the simple zig-zag of the hydrocarbon chains, so they are expected to have a larger molecular footprint. The collapse pressure of F14 and F18 was ~ 70 $mN.m^{-1}$.

The isotherms of the mixtures fell between those of the two pure films in all the systems studied. In general, for mixed systems that follow the additivity rule (equation 8-2), the two components are either completely immiscible or are completely miscible.

$$A_{12} = A_1\chi_1 + A_2\chi_2 \qquad (8\text{-}2)$$

where A_{12} is the mean molecular area of the molecule in the mixed monolayer at a certain surface pressure, A_1 and A_2 are the mean molecular areas of the molecule in its pure film and χ_1, χ_2 are the mole fractions of the pure components in the mixed film. Positive and negative deviations from the additivity rule indicate intermolecular interactions between the constituents (repulsions or attractions, respectively). To explore the validity of the additivity rule for these mixtures, the mean molecular area as a function of mole-fraction of each of the fatty acids studied was analyzed for three different surface pressures (10 $mN{\cdot}m^{-1}$, 20 $mN{\cdot}m^{-1}$ and 30 $mN{\cdot}m^{-1}$) as shown in Figures 8-3 and 8-4. The lines across the points represent the ideal behavior. No significant deviations from linearity were observed in most of the systems studied. For the C16 / F14 and C14 / F14 systems a negative deviation was observed at all mole fractions and at all surface pressures analyzed. This deviation from ideality indicates a decrease in the mean molecular area occupied by the molecule in the mixture. This is attributed to the strong intermolecular forces of attraction in terms of dispersive forces between the chains of the two components in the mixed film. This is explained by the close chain lengths of the hydrocarbon and F14. This is supported by the trend in collapse pressure as discussed earlier. The same negative trend was observed for C14 / F18 film only at 10 $mN.m^{-1}$ at all mole fractions. This can be explained by the increase in the CF_2-CF_2 interactions because of the short hydrocarbon chain that does not obscure these interactions at a low surface pressure.

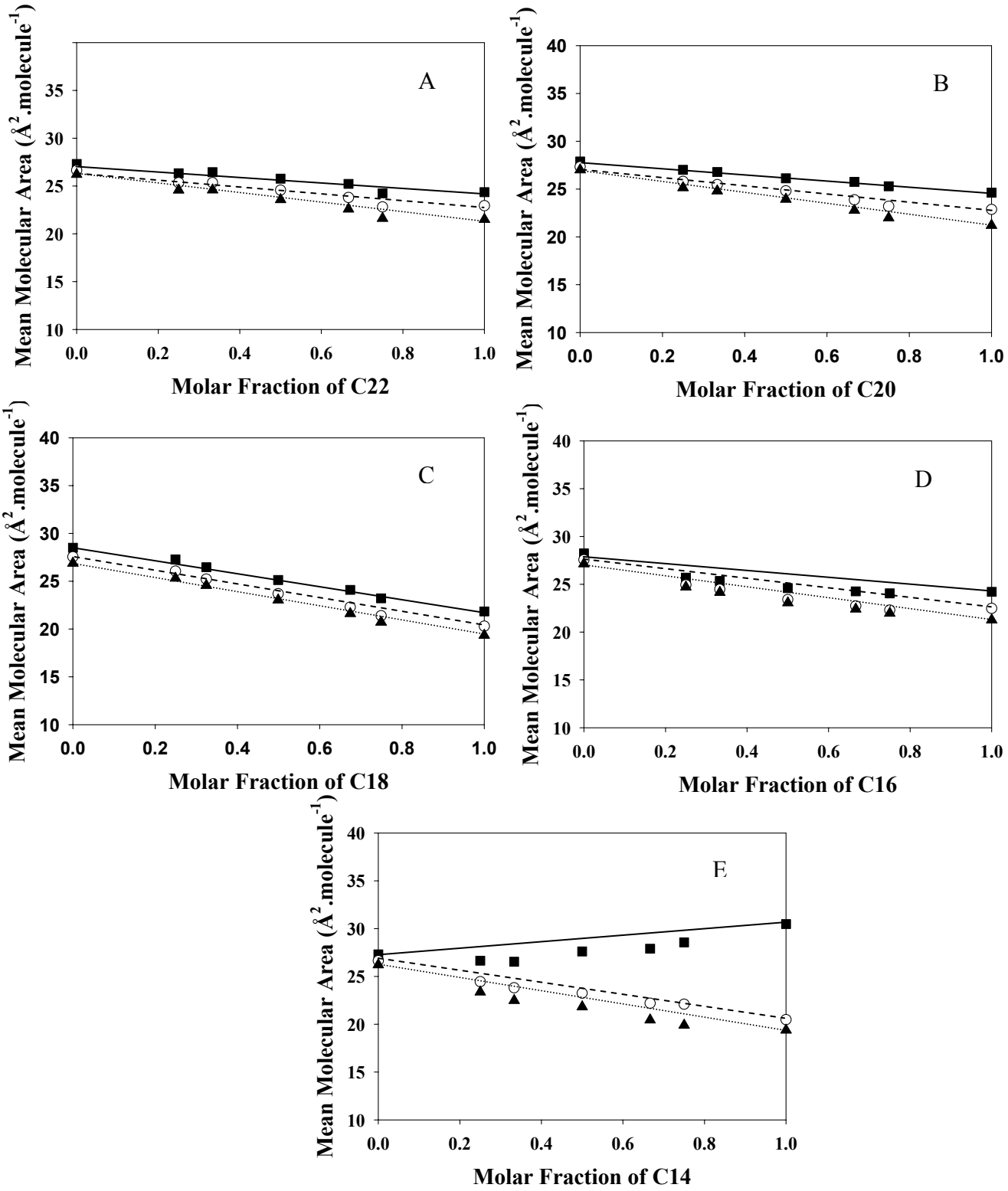

Figure 8-3. Analysis of mean molecular area versus molar fraction of A, C22; B, C20; C, C18; D, C16; E, C14; at different mole fractions of each for the mixed films containing F14. Black squares, 10 $mN.m^{-1}$; white circles, 20 $mN.m^{-1}$; black triangles, 30 $mN.m^{-1}$.

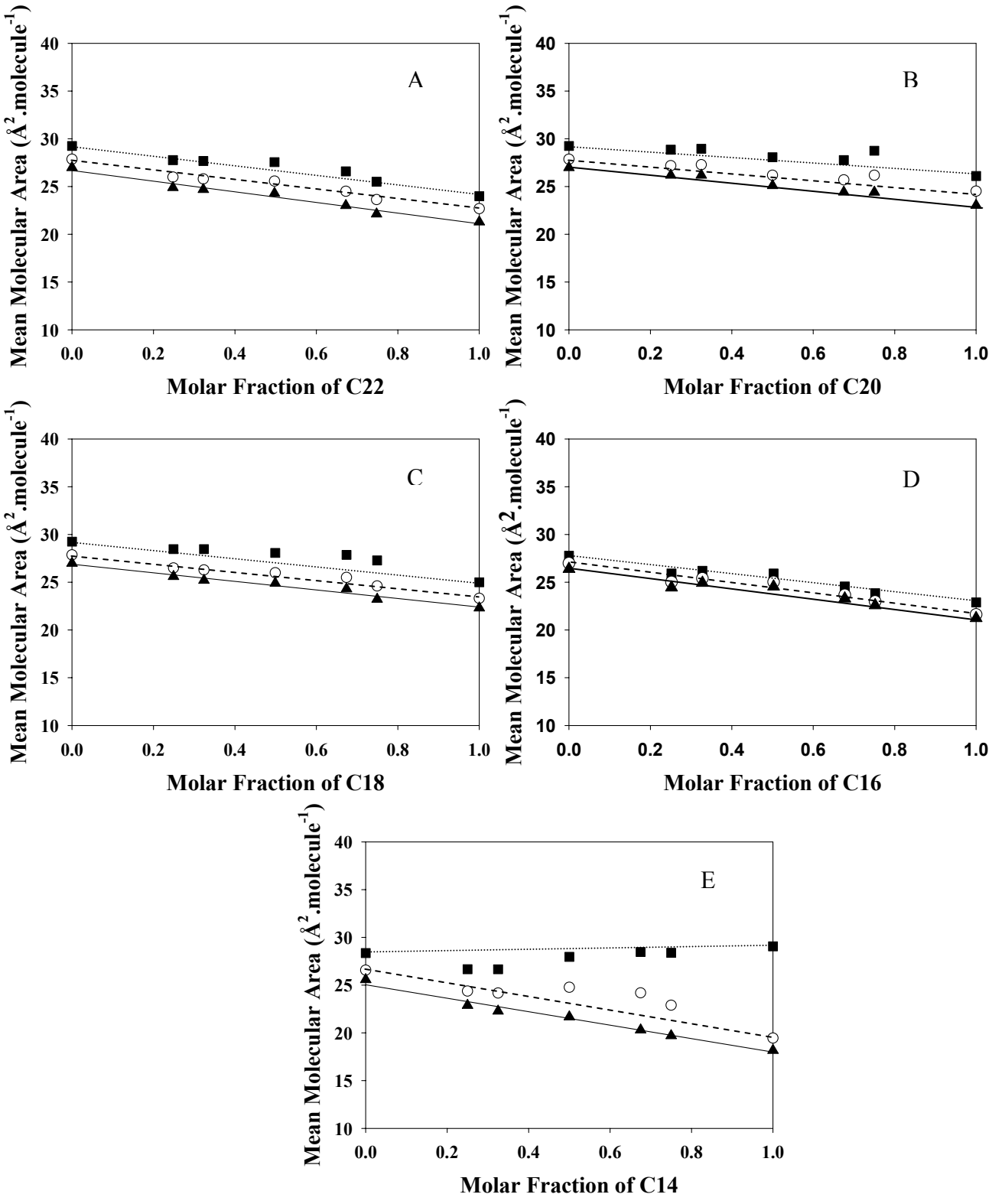

Figure 8-4. Analysis of mean molecular area versus molar fraction of A, C22; B, C20; C, C18; D, C16:; E, C14; at different mole fractions of each for the mixed films containing F18. Black squares, 10 mN.m^{-1}; white circles, 20 mN.m^{-1}; black triangles, 30 mN.m^{-1}.

This deviation of C14 in both systems indicates the formation of a less stable more compact film because of its short chain length which decreases the dispersive interactions energy between the chains. The validity of the additivity rule in most of the mixed films indicates that the two components of the film are either completely immiscible or ideally mixed. In conjunction with AFM measurements, the components are classified to be either miscible or immiscible and phase-segregate.

8.4.2 AFM measurements

The morphology of the LB films for each of the mixed systems was characterized by contact mode AFM imaging. To be consistent with and to allow comparison with previous measurements, all samples were prepared with a 2:1 mole ratio of hydrocarbon : fluorocarbon. Films of different fatty acids combined separately with F14 are shown in Figure 8-5. C22 / F14 in the mixed film phase-separated into hexagonal domains of 3.4 ± 1.8 μm in width and ~ 0.6 – 0.9 nm in height. These domains are similar to those observed for C20 / F14 system in terms of height (~ 0.7 nm), but larger in width (2.1 ± 0.9 μm) . In the mixed film of C18 / F14, the components phase-separated into a narrow linear pattern elevated by 0.9 ± 0.2 nm with a width of 0.1 - 0.3 μm. The linear diagonal structure can be observed in Figure 8-5C. For C16 / F14 system, the film forms a homogeneous monolayer with some small circular domains of ~ 1.1 nm height and width of ~ 0.2 - 1.6 μm. For C14 / F14 system, the film shows small discontinuous light domains on the mica surface with a height difference of ~ 0.5 – 0.8 nm. Taking into account the chain length difference between the two components and the molar ratio, it is reasonable to assign that the hexagonal domains in C22 / F14, C20 / F14, the lighter lines in C18/F14 and the lighter regions in C16 / F14 and C14 / F14 are made of hydrocarbon because all the hydrocarbon chains are longer than the F14 chains.

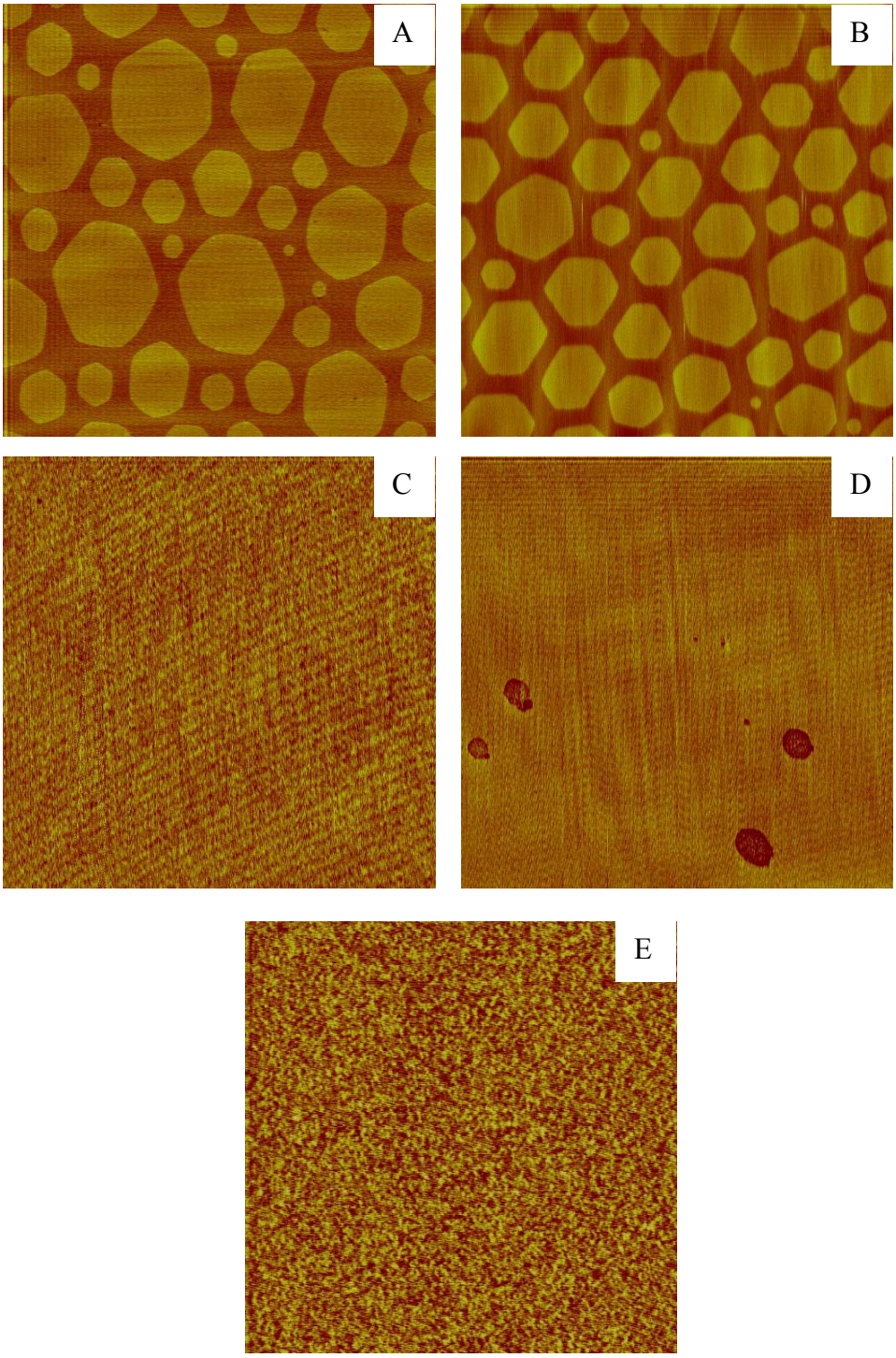

Figure 8-5. AFM height mode images in air of 2:1, A, C22:F14; B, C20:F14; C, C18:F14; D, C16:F14; E, C14/F14 deposited at 20 ºC and at a surface pressure of 20 $mN.m^{-1}$. Image size 20 µm × 20 µm for A, B and D, 5 µm × 5 µm for C and E.

In the case of the C16 / F14 system, the isotherm data confirmed by the AFM images suggested attractive interactions between the molecules of different components which resulted in deviation from ideality. The isotherms data showed a negative deviation and the AFM images showed a homogeneous monolayer with some circular domains. The negative deviation indicates that the interactions between the different components are more favorable than those between the same components. To confirm whether the domains observed in the AFM image of this mixed film are deposits of fluorocarbon or just holes in the film, an LB film was prepared from a solution of higher molar fraction of F14 as shown in Figure 8-6. This film shows that as the F14 content increased, more small circular domains were observed. This supports that these domains are made of F14. The area occupied by F14 in this film is not equal to that occupied by C16 although the molar ratio in this film is 1:1. This suggests that F14 is not completely immiscible with C16 in the film. This can be attributed to a degree of miscibility due to some attractive interactions between the components as shown in the isotherm analysis (Figure 8-3).

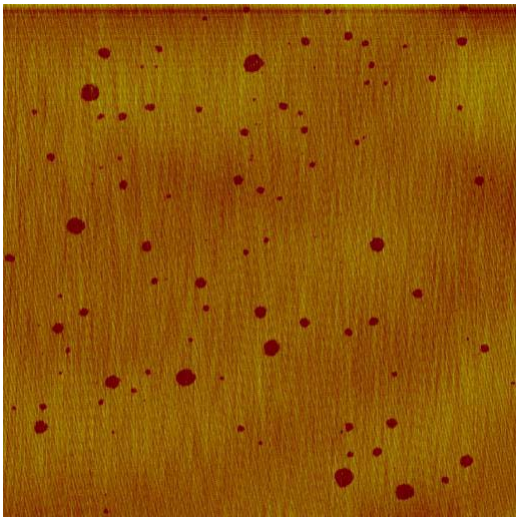

Figure 8-6. AFM height mode images in air of 1C16:1F14 deposited at 20 ºC and at a surface pressure of 20 $mN.m^{-1}$. Image size 20 μm × 20 μm.

AFM in conjunction with isotherm measurements shows that all of the fatty acids used in this study, when combined with F14, phase-separated into different domains. It has been previously reported in literature that the shape of the domains obtained upon phase-separation is controlled by the forces of interactions between the chains of the components in the mixed films[6, 8]. In this work, it was observed that for long fatty acids, C22 / F14 and C20 / F14, the components phase-separated into large hexagonal domains. This is attributed to the high line tension between the different components in the mixed films that arises from strong dispersive interactions between the long hydrocarbon chains. For long hydrocarbon chains, stronger dispersive interactions are observed, as more CH_2 groups in the chain are involved in these van der waals interactions (equation 8-1). The line tension favors the formation of large circular domains in order to minimize the border length of the domain where no sufficient interactions between the same type of chains exist. When the hydrocarbon chain was reduced in length, the polar head group became more significant and the electrostatic force of interaction in terms of repulsion dominated over line tension. In this case the components of the mixed film phase-separated into narrower domains. This can be seen in the case of C18 / F14 where stearic acid molecules formed a linear pattern forcing the F14 molecules in between as shown previously[5] in Chapter 6. These dipole interactions dominated in the C14 / F14 system as well. The molecules of C14 phase-separated into vey small domains surrounded by those of F14.

From these observations of hydrocarbon / F14 systems, one can conclude that the hydrocarbon phase-separated from F14 at all chain lengths. At longer hydrocarbon chains (C22, C20), the line tension was the dominant force which decreased as the hydrocarbon chain length decreased until the dipole interaction dominated (C18, C14). C16 represents an example of a system with some degree of miscibility.

AFM images of mixed LB films of hydrocarbon / F18 are shown in Figure 8-7. For larger fatty acid surfactants (C22 and C20), the two components were completely miscible. The images show circular domains pushing into each other with some vacant areas in between. These AFM images agree well with what was reported previously by Imae et al. when studied the C20 / F18 system[21]. No phase-separation observed in these images. In conjunction with isotherm data, the two components are found to be miscible. This miscibility arises from the strong dispersive interactions between the different components. This is because of the presence of long chains of both the hydrocarbon and the fluorocarbon. These van der Waals interactions become stronger as the number of the groups participating increases[4]. Having a long hydrocarbon chain in this system, helps in preventing the repulsion between the fluorocarbon chains, thus favoring the miscibility of the system and increasing its entropy. With shorter fatty acid chains (C18, C16), phase-separation took place and the domains had circular / hexagonal structures. This is explained by the line tension being the dominant force in this system and favors the formation of large circular domains. In the C14 / F18 mixed film, the components phase-separated into narrow worm-like domains, with height difference ~ 1.2 nm. The brighter domains might be made of F18, since it is longer than C14. Similar to the case of F14, at shorter chain lengths, the dipole interaction dominates in terms of repulsion favoring the formation of small narrow domains.

It can be inferred that the formation of the hexagonal domains and the linear fragments in the mixed LB films of C16 / F18 are just an intermediate between the shape of the domains formed at the longer chain (C18) and that at the shorter chain (C14). This is because of the competition between line tension and dipole interaction so both patterns can be seen; large hexagonal and narrow linear structures.

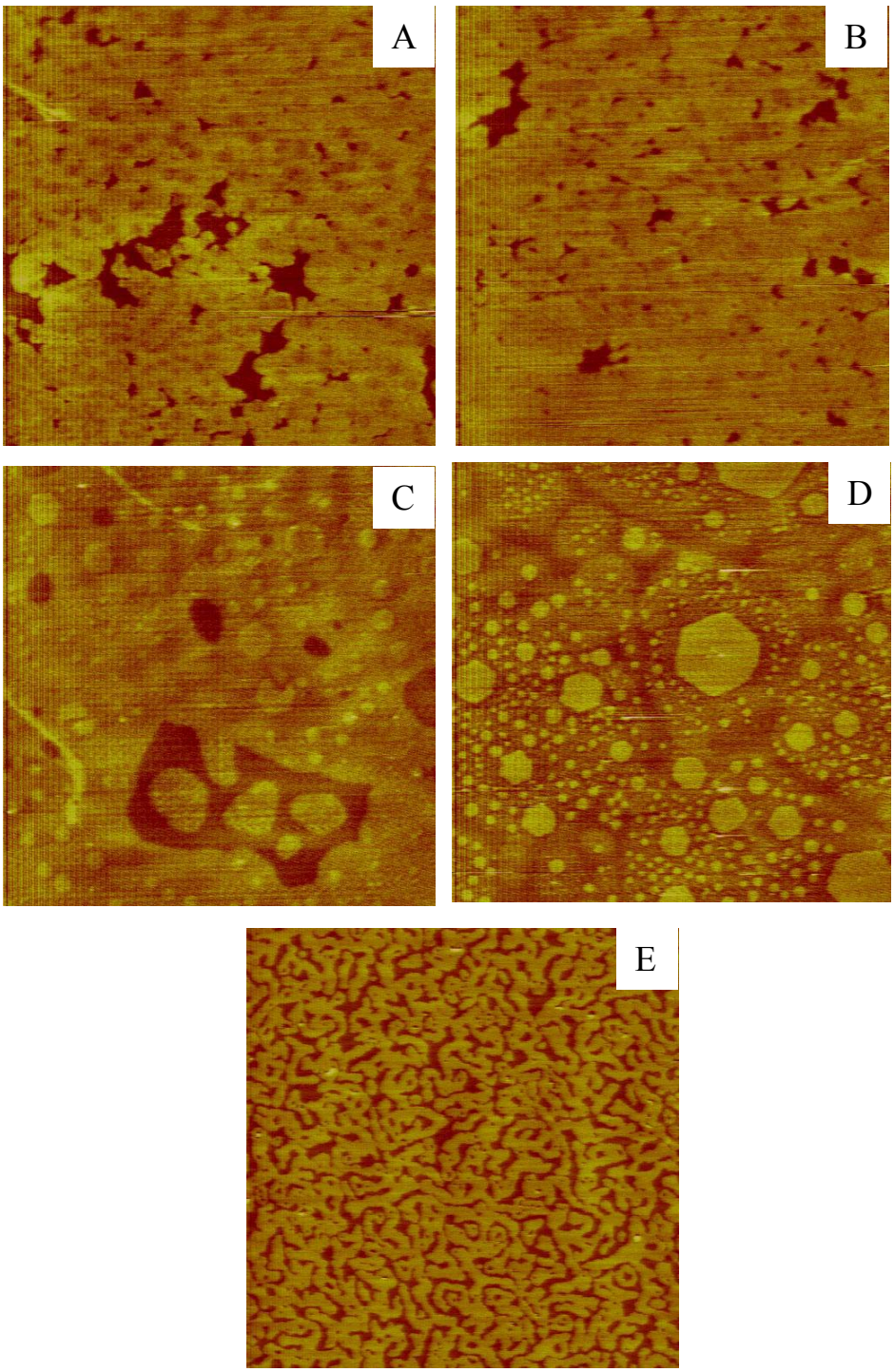

Figure 8-7. AFM height mode images in air of 2:1, A, C22:F18; B, AA:F18; C, C18:F18; D, C16:F18; E, C14:F18 deposited at 20 ºC and at a surface pressure of 20 $mN.m^{-1}$. Image size 20 µm × 20 µm for all except E 10 µm × 10 µm.

Generally, it was found that F18 was miscible with longer hydrocarbon chains (C22, C20). When the hydrocarbon chain length became comparable (C18) or shorter (C16, C14) than that of F18, the film components became immiscible and phase-separation took place. Line tension was responsible for phase-separation and the shapes of the domains obtained with longer chain fatty acids. Once the hydrocarbon chains become shorter, dipole interactions started to dominate.

What was observed in this systematic study in the case of F18 with all the other hydrocarbon chains agrees with Shibata's study[1]. Shibata and co-workers found that when the hydrocarbon chain was longer than that of the fluorocarbon, the components were miscible. At equal lengths of the chains, the components are immiscible and at longer fluorocarbon and shorter hydrocarbon chains, the components are miscible and immiscible depending on the molar fraction. This agrees with what was observed in the case of fatty acid / F18 systems. In their study of mixed films of perfluorododecanoic acid ($CF_3(CF_2)_{10}COOH$) and stearic or lauric acid, Rontu et al[2] found that the two components are miscible and have a positive deviation from ideal mixing. Comparing our results with Rontu's, it can be concluded that by changing the fluorocarbon chain by just two carbon atoms, the miscibility is inverted in the system. In the case of the F14 system that was studied here, the results obtained agree with Shibata's results for C14 / F14. The general trend of the hydrocarbon / F14 mixed films agrees with the trend observed by Mazaki et al.[6] in their study of fluoroalkylsilane / fatty acids. At a short and constant fluoralkylsilane chain and a longer hydrocarbon chain the components phase-separate and the domains formed have large circular structures. When the hydrocarbon chain is reduced by just two carbon atoms, the domains adopt narrow linear shapes. In a separate study, Broniatowski et al.[4] observed that as the perfluorinated segment became longer in the perfluoroalcohols, the

compound mixed well with the alcohols compared to those with shorter perfluorinated segment. This supports our observations in comparison of F14 and F18 where F18 was miscible with some fatty acids in contrary to F14 which was immiscible with all the range of fatty acids. However, not every mixed hydrocarbon / perfluorocarbon system displays this type of behavior, and that minor changes in the any of the components can significantly affect their miscibility. Comparing the results obtained in these measurements for the two systems (F14 and F18), it was found that extending the perfluorcarboxylic acid by four carbons switches the miscibility of some components and changes the pattern obtained in the mixed films.

8.5 Conclusions

In this work, a systematic study was carried out to investigate the 2D miscibility of series of hydrocarbon chains (C22, C20, C18, C16, C14) combined separately with F14 and F18. The isotherms analysis in conjunction with AFM imaging showed that F14 was immiscible with all the hydrocarbon chains with some slight miscibility with C16. F18 was miscible with longer hydrocarbon chains (C22 and C20) and immiscible with chains that are shorter or of the same length as F18 (C18, C16, C14). Different patterns were observed in the mixed LB films which are attributed to the line tension at longer chain lengths and dipole interactions at shorter chain lengths. This general rule is applicable for these compounds in this study. As has been previously discussed, simple changes in the compounds used can alter the miscibility rules of the system.

8.6 Acknowledgements

Funding for this work was provided by the Natural Sciences and Engineering Research Council of Canada (NSERC), the Canada Foundation for Innovation (CFI), the Province of Saskatchewan and by the University of Saskatchewan.

8.7 References

1. Shibata, O.; Yamamoto, S. K.; Lee, S.; Sugihara, G., *Journal of Colloid and Interface Science* **1996,** 184 (1), 201.
2. Rontu, N.; Vaida, V., *Journal of Physical Chemistry C* **2007,** 111 (27), 9975.
3. Broniatowski, M.; Dynarowicz-Latka, P., *Langmuir* **2006,** 22 (6), 2691.
4. Broniatowski, M.; Romeu, N. V.; Dynarowicz-Latka, P., *Journal of Physical Chemistry B* **2006,** 110 (7), 3078.
5. Qaqish, S. E.; Paige, M. F., *Langmuir* **2008,** 24 (12), 6146.
6. Mazaki, T.; Shibata, H.; Kondo, Y.; Yoshino, N.; Matsumoto, M., *Chemistry Letters* **2008,** 37 (4), 480.
7. Iimura, K.; Shiraku, T.; Kato, T., *Langmuir* **2002,** 18 (26), 10183.
8. Matsumoto, M.; Watanabe, S.; Tanaka, K.; Kimura, H.; Kasahara, M.; Shibata, H.; Azumi, R.; Sakai, H.; Abe, M.; Kondo, Y.; Yoshino, N., *Advanced Materials* **2007,** 19 (21), 3668.
9. McConnell, H. M., *Annual Review of Physical Chemistry* **1991,** 42, 171.
10. Zhu, B.; Zhang, P.; Wang, L.; Liu, Z., *Journal of Colloid and Interface Science* **1997,** 185, 551.
11. Ishikawa, T.; Ejaz, M.; Tsujii, Y.; Shibata, H.; Matsumoto, M., *Colloids and Surfaces a-Physicochemical and Engineering Aspects* **2008,** 321 (1-3), 76.
12. Qaqish, S. E.; Paige, M. F., *Langmuir* **2007,** 23 (5), 2582.
13. Bibo, A. M.; Peterson, I. R., *Advanced Materials* **1990,** 2 (6-7), 309.
14. Albrecht, O.; Matsuda, H.; Eguchi, K.; Nakagiri, T., *Thin Solid FIlms* **1999,** 338, 252.
15. Gaines, G., *Insoluble Monolayers at Liquid-Gas Interfaces*. Interscience Publishers: New York, 1966.
16. Davies, J., *Journal of colloid Science* **1956,** 11, 337.
17. Chatterjee, B.; Ghosh, K., *Kolloid-Z. u. Z. Polymere* **1971,** 250, 615.
18. Petty, M. C., *Langmuir-BlodgettFilms an Introduction*. Cambridge University Press: Cambridge, 1996.
19. Ries, H. E.; Kimball, W. A., *Journal of Physical Chemistry* **1955,** 59 (1), 94.
20. Jang, S. S.; Blanco, M.; Goddard, W. A.; Caldwell, G.; Ross, R. B., *Macromolecules* **2003,** 36 (14), 5331.
21. Imae, T.; Takeshita, T.; Kato, M., *Langmuir* **2000,** 16 (2), 612.

CHAPTER 9
CONCLUSIONS AND FUTURE WORK

9.1 Conclusions

In this PhD thesis, phase–separation in different hydrocarbon / fluorocarbon LB films was studied through surface characterization of Langmuir and LB films. The films were deposited under different experimental conditions to explore the factors affecting miscibility and phase–separation in the system. This has provided insight into the mechanism and kinetics of phase – separation and domain growth.

In this thesis, the factors affecting miscibility of different hydrocarbon / fluorocarbon surfactant systems have been investigated. These systems have not been studied previously. Understanding the miscibility of the components in LB films gives insight about interactions of molecules in 2D, as well as help in controlling surface patterning . This study completes and adds to the previous work done on the miscibility in mixed Langmuir and LB films[1-4].

In the past, a limited number of studies has been carried out to reveal the mechanism and the kinetics of phase–separation and domain growth in mixed LB films of hydrocarbon / fluorocarbon. The mechanism of phase–separation was associated with homo and hetero interactions[5, 6] as well as the competition between line tension and dipole interactions and the mobility of the molecules[7].

However, in this study, Ostwald ripening was found to be the mechanism by which domains form and grow upon phase–separation. Diffusion of molecules in 2D was

found to be a major factor in determining domain growth. This is the first study in the literature to report and to introduce Ostwald ripening as one of the mechanisms of domain formation and growth in mixed LB films. This helps in better understanding the mechanism of phase–separation and domain formation of other systems where a simple line tension / repulsion model is not entirely sufficient to describe all the important properties of the system.

In terms of kinetic studies, there is a lack of information about the kinetics of domain growth in LB films in general[8], and mixed hydrocarbon / fluorocarbon LB films in particular. In this work, the kinetics of domain growth in hydrocarbon / fluorocarbon LB films were studied for the first time. The system was found to follow Lifshitz – Slyozov model of domain growth in 2D. This work is the only example in the literature that discusses and models the kinetics of domain growth in mixed LB films of hydrocarbon / fluorocarbon. This provides a better understanding of film stability.

The mixed LB films of AA / PA were investigated as an example of a hydrocarbon / fluorocarbon mixed system. Surface pressure–area isotherms of the pure components and their mixtures showed that the additivity rule was applicable to the system, and the components were completely immiscible. This was supported by the AFM data that revealed the morphology and the chemical composition of the mixed LB films. Selective dissolution and force curves measurements by AFM were successfully used to determine the chemical composition of the domains. In the AA / PA mixed films, hexagonal domains made of AA were surrounded by a sea of PA with some deposits of AA (~ 7 %) (Chapter 2). In this chapter, the chemical composition of the film was revealed solely by AFM measurements. Matsumoto et al. used IR spectroscopy to

identify the chemical composition of the domains obtained in the same system, but failed to observe the nanometer-size deposits of AA[9, 10]. The authors used AFM data simply to obtain information about the morphology of the surface and not to obtain chemical information. Imae et al.[11] studied the same system and identified the surface morphology only using AFM. X-PEEM imaging when carried out confirmed our AFM data in determining the chemical composition of the domains. Thus the film was fully characterized in terms of morphology and chemical composition by AFM and X-PEEM.

Once the film was characterized, molecular level imaging using AFM was carried out to investigate the underlying 2D molecular packing inside the hexagonal domains. Measurements showed that AA molecules in the hexagonal domains are organized in an oblique crystal lattice (Chapter 3). This packing was observed in other LB systems containing AA or its salts[12-14]. Imae et al. observed a specific ordering of the AA molecules in the mixed AA / F18 film, but without identifying its molecular packing[11]. This is the first study to report the molecular packing of AA in the mixed system of AA / PA. The oblique molecular packing in this study might have contributed to the formation of micron size hexagonal domains of AA in these films. It is the first study to relate the molecular ordering to the micron size domains.

For the previously characterized system (AA / PA), mechanism and kinetics of phase–separation and the factors affecting the domain shape in the films were investigated. It was observed that as the sub-phase temperature increases, the domain size increases. Surface pressure, at which the deposition takes place, was found to have an effect on the shapes of the domains formed. At a low surface pressure, the domains have large circular shapes, they are few in number with large distance separating the adjacent

domains. When the surface pressure increases, the domains take a narrow hexagonal shape and the distance separating them becomes smaller. Agitation of the stock solution was found to have a major effect on the domains formed. The hexagonal domains formed in the LB films are not equilibrium structures so by shaking the solution mixture, this pushed them even further from equilibrium. The new domains formed have small circular shapes that are not affected by change in temperature. The flow of the water in the sub-phase organizes the domains and reorients them towards it. Incubation time, at which the solvent is left to evaporate on the sub-phase, is a significant factor in determining the domains shape and size. At longer times, the domains increase in size (Chapter 4).

Some of these factors were previously reported in literature to play a role in the shape of the domains in different LB films, such as temperature[7], surface pressure[11] and the substrate[15]. In this work, the different factors affecting domain shapes were used to investigate the mechanism of phase–separation and domain formation. The effect of temperature and time on the system indicates that a diffusion based mechanism takes place in the system in comparison with other systems[7]. The system does not depend on the substrate or the withdrawal rate. The agitation effect on the mixture is first reported in this study.

In terms of mechanism of phase-separation and domain formation, AA was found to phase-separate from PA in the bulk and before the spreading and the compression of the monolayer. Upon phase-separation the domains grow as a function of time and temperature via Ostwald ripening (Chapter 4). Coalescence was found to take place in the mixed AA / PA LB films mainly at low temperatures (Chapter 5). Ostwald ripening was found to be the mechanism of domain growth in this system upon phase-separation. This

suggests a new mechanism to be introduced in the field of domain formation and growth in thin films. The underlying force that drives phase-separation in this films was reported previously in literature in terms of line tension / dipole interactions[7] and homo / hetero interactions[5]. Ostwald ripening explains the mechanism of domain formation in other systems in this study where a simple line tension / dipole interaction theory is not enough to explain all of the observed phenomena. This also explains other systems reported in literature where the mechanism of formation of specific domains was not understood[7].

The kinetics of the domain growth in the mixed AA / PA LB films was modeled by Lifshitz-Slyozov equation in which the domains area is directly proportional to the time to the power 2/3, for diffusion controlled processes. This was accomplished by depositing the films at different incubation times. As the incubation time increases, more molecules diffuse from the smaller domains into the larger domains that increase in size on the expense of the smaller domains. Increasing the temperature resulted in more mobility of the molecules so more diffusion and larger domains observed (Chapter 5). This process occurs via Ostwald ripening as proven in Chapter 4. This is the first time to report a comprehensive study of domain growth kinetics in 2D and to model it. This gives insight into better understanding the 2D kinetics of molecules on surfaces and in thin films.

To further explore the factors affecting the domain shapes, the effect of changing the length of the hydrocarbon or fluorocarbon chain on the domain shape and miscibility was investigated. The first system studied was a mixture of SA and PA. The components phase – separate as observed by AFM and isotherm data. It was found that the shape of the domains formed in the mixed LB film of SA / PA changed dramatically. The domains

take a linear shape made of SA molecules that force the PA molecules in between (Chapter 6). This particular change of pattern on the surface as a function of chain length was observed previously in literature in a study of alkyl silane and perfluoroalkyl silane[6]. However, this is the first study reported on SA / perfluorocarbon mixed monolayers. It also explains in detail the mechanism of domain formation, unlike previous studies[6]. Understanding the mechanism of phase-separation and domain formation provides valuable information to the field of surfaces.

Another mixed system was studied where the perfluorocarbon chain is longer than the hydrocarbon chain. The system of choice was C16 / F18. Phase-separation still takes place in the system according to AFM and surface pressure-area isotherm data. The mixed film has hexagonal domains with hairy extensions irradiating from them. These domains are made of fluorocarbon with some deposits of hydrocarbon in between. For this system, X-PEEM and confocal measurements were carried out to resolve the chemical composition of the features in the film. The loss of C16 with time in the sub-phase is an important and unique behavior of C16. This property results in changing the domains shape obtained in the monolayer (Chapter 7). Imae et al.[11] studied the same system, however their isotherm data are different which might be related to the difference in the solvent used. The AFM images of Imae do not reveal the fine features obtained in our study. No mechanism of domain formation was discussed, nor was the influence of C16 solubility on the pattern formation. C16 is one of the few fatty acids that dissolves in the sub-phase with time. This adds another factor, in addition to those previously studied (Chapters 5-7) and previously reported in the literature[5-7, 15], which affects the shape of the domains obtained on surfaces and controls it. This is the first study to report the

control of patterns on surfaces through controlling the solubility of one of the film components. The driving force of domain formation in this system showed clearly, in addition to all the previous studies in this work, that simple line tension model is not enough and Ostwald ripening plays an important role in domain formation. This provides a better understanding to phase-separation mechanism in mixed LB films.

The chain length of the molecules studied in this project played an important role in determining the shapes of the domains obtained as observed in Chapters 2,5 and 6. This arises from the difference in the intermolecular interactions between the different chains. The difference in the number of CH_2 groups plays an important role in determining the strength of the van der Waals interactions between molecules. This affects the competition between line tension and dipole interactions since they are the dominant forces affecting domain shape. To obtain a better understanding of the effect of chain length, a systematic study was carried out. F14 and F18 were studied separately in mixed LB films in combination with different chains of hydrocarbon (C14, C16, C18, C20, C22) in Chapter 8. It is the first time that such a systematic study on these systems was carried out. This systematic study provides an important foundation for understanding the miscibility of different systems and the pattern formed on surfaces as a function of chain length. This completes the other studies of miscibility in mixed Langmuir and LB films that were carried out on other hydrocarbon / fluorocarbon systems.[1-4] This study also explains in details the mechanism of the pattern formation on surfaces in terms of line tension / dipole interactions and homo / hetero interactions. It discusses the conditions under which one force dominates and controls the pattern formed.

F14 was found to be immiscible and phase-separated with all the hydrocarbons studied. This agrees with what was obtained by Shibata et al.[4] With longer chains of hydrocarbon (C22 and C20), the line tension is dominant and the interactions between the chains of the same type are strong. The line tension prefers the formation of large / circular domains. When the hydrocarbon chains become shorter (C18, C16 and C14), the dipole interactions between the head groups in terms of repulsion play an increasingly important role where it favors the formation of narrow domains (Chapter 8). This agrees with what was previously observed by Mazaki et al in terms of chain length effect[6].

When a longer fluorocarbon chain (F18) was used in the mixed films with different hydrocarbon chain lengths (C14, C16, C18, C20, C22), F18 was found to be immiscible with shorter hydrocarbon chains (C14, C16, C18) and miscible with longer chains (C20 and C22). At longer chains of hydrocarbon, the interactions between the different types of chains are strong enough that it made it difficult for the components to phase-separate.

For C18 / F18 mixed film, line tension dominates and the dispersive interactions between the chains of the same type are strong resulting in the formation of large hexagonal domains in the mixed film. As the hydrocarbon chain becomes shorter, the dipole interactions between the head groups start to dominate over line tension favoring the formation of narrow domains (C16). For C16 / F18 system, both large hexagonal domains and narrow linear domains exist. For C14 / F18 mixed films dipole interactions dominate and narrow worm-like domains formed on the surface. The dipole interactions of the head groups dominate at shorter hydrocarbon chains as there are not enough methyl groups to strengthen the interactions between the chains (Chapter 8).

In Chapter 8, a comprehensive study of the different systems was carried out using AFM and surface pressure – area isotherms measurements. Some studies in literature reported miscibility[1-4] and the patterns obtained[5-7, 11] in different Langmuir and LB systems. The results of these studies are applicable to the investigated systems only and cannot be extended to other systems. Because of that, some of these studies do not explain the observations in these current systems and might contradict them.

In this research project, we were able to reveal the structure and the chemical composition of mixed hydrocarbon / fluorocarbon LB films. The mechanism of phase-separation of the different components was successfully investigated. The different factors affecting the miscibility, phase-separation and domain formation were studied. The miscibility rules of these systems were deduced.

9.2 Future work

Investigation of the effect of the head group on the interactions between the chains and their effect on miscibility and phase-separation is an important direction to which this study can be taken. Comparison between different chains used where the only difference is the head group will lead to and reveal more fundamental issues in phase-separation and miscibility. By keeping the hydrocarbon part of the chain fixed, the head group can be alcohol, amine, carboxylic acid, aldehyde, methyl group.

A comprehensive study of the effect of semifluorinated compounds in comparison with perfluorinated compounds is an asset that helps in understanding the mechanism of phase-separation. Rules of miscibility can be deduced from these studies as well as the factors affecting it.

Other types of phase diagrams can be extracted from isotherm measurements like transition pressure as a function of molar fraction and transition pressure as a function of

temperature. This helps in explaining the structures obtained on the surface. Changing the pressure at which deposition takes place, might change the shape of domains obtained depending on which part of the phase diagram the deposition takes place at. Analyzing phase diagrams in terms of mean molecular area as a function of mole fraction and the calculation of the free energy of mixing are important tools to study miscibility of mixed LB films.

These above studies can be extended to phospholipid systems in combination with fluorinated or semi fluorinated fatty acids. Phase diagrams can be generated and miscibility studies can be carried out.

9.3 References

1. Rontu, N.; Vaida, V., *J. Phys. Chem. C* **2007,** 111 (27), 9975.
2. Broniatowski, M.; Dynarowicz-Latka, P., *Langmuir* **2006,** 22 (6), 2691.
3. Broniatowski, M.; Romeu, N. V.; Dynarowicz-Latka, P., *J. Phys. Chem. B* **2006,** 110 (7), 3078.
4. Shibata, O.; Yamamoto, S. K.; Lee, S.; Sugihara, G., *J. Colloid Interface Sci.* **1996,** 184 (1), 201.
5. Matsumoto, M.; Watanabe, S.; Tanaka, K.; Kimura, H.; Kasahara, M.; Shibata, H.; Azumi, R.; Sakai, H.; Abe, M.; Kondo, Y.; Yoshino, N., *Adv. Mater.* **2007,** 19 (21), 3668.
6. Mazaki, T.; Shibata, H.; Kondo, Y.; Yoshino, N.; Matsumoto, M., *Chem. Lett.* **2008,** 37 (4), 480.
7. Iimura, K.; Shiraku, T.; Kato, T., *Langmuir* **2002,** 18 (26), 10183.
8. Jensen, M. H.; Morris, E. J.; Simonsen, A. C., *Langmuir* **2007,** 23 (15), 8135.
9. Matsumoto, M.; Tanaka, K.; Azumi, R.; Kondo, Y.; Yoshino, N., *Chem. Lett.* **2002,** (10), 970.
10. Matsumoto, M.; Tanaka, K.; Azumi, R.; Kondo, Y.; Yoshino, N., *Langmuir* **2003,** 19 (7), 2802.
11. Imae, T.; Takeshita, T.; Kato, M., *Langmuir* **2000,** 16 (2), 612.
12. Evenson, S.; Badyal, J.; Pearson, C.; Petty, M., *J. Phys. Chem.* **1996,** 100, 11672.
13. Takamoto, D.; Aydil, E.; Zasadzinski, J.; Ivanova, A.; Schwartz, D.; Yang, T.; Cremer, P., *Science* **2001,** 293, 1292.
14. Schwartz, D. K., *Annu. Rev. Phys. Chem.* **2001,** 52, 107.
15. Sikes, H. D.; Woodward, J. T.; Schwartz, D. K., *J. Phys. Chem.* **1996,** 100 (21), 9093.